

University of Southern Queensland

Faculty of Health, Engineering & Sciences

**STABILITY ANALYSIS OF SHALLOW  
UNDRAINED TUNNEL HEADING USING  
FINITE ELEMENT LIMIT ANALYSIS**

A dissertation submitted by

**Mr. Alexander Bell**

In fulfilment of the requirements of

**Bachelor of Engineering (Civil)**

**October, 2016**

# ABSTRACT

This dissertation investigated the undrained stability of shallow tunnel heading problems subjected to varying loading conditions by performing a two-dimensional plane strain analysis. Failure due to the blowout mechanism was highlighted as a major focus area, due to the lack of previous research on the topic. Finite element limit analysis (FELA), employed through the geotechnical software analysis package, Optum G2, was used to determine lower and upper bound factor of safety ( $FoS$ ) values for a range of various scenarios. The factor of safety values were calculated using the gravity multiplier method (GMM) and the strength reduction method (SRM). These methods were directly compared and the strength reduction method was found to be the most suitable method for analysing scenarios with either a surcharge or internal tunnel pressure applied. The results obtained in this study were validated by comparing a sample to results published by Augarde, Lyamin and Sloan (2003). This comparison found a very good level of agreement.

The factor of safety is a function of three dimensionless parameters; the pressure ratio ( $PR$ ), strength ratio ( $SR$ ) and depth ratio ( $DR$ ). The relationship between the factor of safety and these parameters was investigated. A number of plots and displacement vector fields were created to better assist in understanding these relationships and the specific failure mechanism related to each scenario. This process reinforced the need to not only design tunnels for failure due to collapse but to also check for failure due to blowout.

The stability of tunnels has historically been expressed in the form of a stability number, similar to the approach adopted by Taylor (1937). This dissertation presents results by applying the factor of safety approach, allowing for direct and clear interpretation of results and any practical implications. The research culminated in the development of a variety of tunnel heading stability design charts. These design charts have been designed for use by practicing engineers in the preliminary stages of tunnel design. A number of select examples are provided to outline some of the potential uses of the design charts. One particularly useful practical application of the design charts is the ability to determine a safe operating range for the pressure that can be applied to the tunnel excavation face by a tunnel boring machine during construction.

# **DISCLAIMER PAGE**

**University of Southern Queensland**

**Faculty of Health, Engineering and Sciences**

**ENG411/ENG4112 Research Project**

## **Limitations of Use**

The Council of the University of Southern Queensland, its Faculty of Health, Engineering & Sciences, and the staff of the University of Southern Queensland, do not accept any responsibility for the truth, accuracy, or completeness of material contained within or associated with this dissertation.

Persons using all or any part of this material do so at their own risk, and not at the risk of the Council of the University of Southern Queensland, its Faculty of Health, Engineering & Sciences or the staff of the University of Southern Queensland.

This dissertation reports an educational exercise and has no purpose or validity beyond this exercise. The sole purpose of the course pair entitled “Research Project” is to contribute to the overall education within the student’s chosen degree program. This document, the associated hardware, software, drawings and other material set out in the associated appendices should not be used for any other purpose: if they are used, it is entirely at the risk of the user.

# **CANDIDATE'S CERTIFICATION**

**University of Southern Queensland**

**Faculty of Health, Engineering & Sciences**

**ENG4111/ENG4112 Research Project**

## **Certification of Dissertation**

I certify that the ideas, designs and experimental work, results, analyses and conclusions set out in this dissertation are entirely my own effort except where otherwise indicated and acknowledged.

I further certify that the work is original and has not been previously submitted for assessment in any other course or institution, except where specifically stated.



Alexander Bell

0061056627

# **ACKNOWLEDGEMENTS**

This research project was conducted under the close supervision of Dr Jim Shiau, whose time, interest, guidance, feedback and knowledge in the field of geotechnical engineering has been greatly appreciated throughout. Further acknowledgment must be extended to all members of the USQ tunnelling research group for all of the accumulated knowledge they have contributed to this topic, forming a strong learning foundation. An additional thanks must be extended to my parents, Tim and Vicki, and my partner, Rosa, for their continuous support throughout this challenging learning experience.

# TABLE OF CONTENTS

<b>ABSTRACT</b> .....	<b>i</b>
<b>DISCLAIMER PAGE</b> .....	<b>ii</b>
<b>CANDIDATE’S CERTIFICATION</b> .....	<b>iii</b>
<b>ACKNOWLEDGEMENTS</b> .....	<b>iv</b>
<b>TABLE OF FIGURES</b> .....	<b>viii</b>
<b>TABLE OF TABLES</b> .....	<b>xiii</b>
<b>CHAPTER 1: INTRODUCTION</b> .....	<b>1</b>
1.1    Outline of Study .....	1
1.2    Methodology .....	2
1.3    Research Objectives .....	3
1.4    Organisation of Thesis .....	3
<b>CHAPTER 2: GENERAL REVIEW</b> .....	<b>6</b>
2.1    Introduction .....	6
2.2    Significance of Tunnels.....	6
2.3    Tunnelling Terminology .....	7
2.4    History of Tunnels .....	7
2.5    Tunnel Construction Methods.....	11
2.6    Design Criteria .....	15
2.7    Tunnel Stability Review.....	16
2.8    Factor of Safety Approach .....	20
<b>CHAPTER 3: NUMERICAL MODELLING REVIEW</b> .....	<b>23</b>
3.1    Optum G2 Introduction .....	23
3.2    Finite Element Limit Analysis .....	23
3.3    Gravity Multiplier Method.....	24
3.4    Strength Reduction Method .....	25
3.5    Optum G2 Modelling .....	26

3.6	Optum G2 Slope Example .....	30
3.7	Optum G2 Tunnel Heading Example.....	34
<b>CHAPTER 4: TUNNEL HEADING ANALYSIS: COLLAPSE .....</b>		<b>41</b>
4.1	Introduction .....	41
4.2	Problem Statement .....	41
4.3	2D Tunnel Heading Numerical Modelling.....	45
4.4	Factor of Safety Bounds.....	46
4.5	Internal Comparison of Collapse Results.....	48
4.6	External Comparison of Collapse Results.....	55
4.7	Optum G2 Tunnel Heading Collapse Results and Discussion.....	57
4.8	Conclusion .....	66
<b>CHAPTER 5: TUNNEL HEADING ANALYSIS: BLOWOUT.....</b>		<b>68</b>
5.1	Introduction .....	68
5.2	Problem Statement .....	68
5.3	Significance of the Blowout Failure Mechanism.....	72
5.4	2D Tunnel heading Numerical Modelling .....	73
5.5	Factor of Safety Bounds.....	75
5.6	Internal Comparison of Blowout Results .....	76
5.7	Optum G2 Tunnel Heading Blowout Results and Discussion .....	82
5.8	Conclusion .....	91
<b>CHAPTER 6: TUNNEL HEADING ANALYSIS: STABILITY DESIGN</b>		
<b>CHARTS.....</b>		<b>93</b>
6.1	Introduction .....	93
6.2	Problem Statement .....	93
6.3	2D Tunnel Heading Numerical Modelling.....	96
6.4	Factor of Safety Bounds.....	98
6.5	Optum G2 Tunnel Heading Results and Discussion.....	99
6.6	Tunnel Heading Stability Design Charts.....	103
6.7	Tunnel Heading Stability Design Examples .....	110

6.8	Conclusion .....	112
<b>CHAPTER 7: CONCLUSION.....</b>		<b>114</b>
7.1	Summary .....	114
7.2	Future Research.....	116
<b>REFERENCES.....</b>		<b>117</b>
<b>APPENDIX A – PROJECT SPECIFICATION.....</b>		<b>121</b>
<b>APPENDIX B – INITIAL RESULTS AND PLOTS.....</b>		<b>122</b>
<b>APPENDIX C – EXTERNAL COMPARISON .....</b>		<b>131</b>
<b>APPENDIX D – FINAL RESULTS AND PLOTS.....</b>		<b>132</b>

# TABLE OF FIGURES

Figure 2.1: Terminology relevant to tunnel cross section and longitudinal section (Chapman, Metje & Stärk 2010).....	7
Figure 2.2: Brunel’s shield, a diagram showing a longitudinal section and one of the twelve frames (Guglielmetti et al. 2007). .....	8
Figure 2.3: Hudson River Tunnel. Excavation utilising Greathead’s shield, cast iron lining and compressed air (Megaw & Bartlett 1981). .....	9
Figure 2.4: Illustration of English and Beaumont’s tunnel boring machine (Maidl, Maidl & Thewes 2013). .....	10
Figure 2.5: Typical face drilling rig used in drill and blast tunnelling (Atlas Copco 2014). .....	12
Figure 2.6: Diagram of typical tunnel boring machine with shield (Maidl, Maidl & Thewes 2013). .....	13
Figure 2.7: Example of bottom-up cut and cover tunnelling (Wallis 2002). .....	14
Figure 2.8: Design stability chart for square tunnel, H/B=2 (Wilson et al. 2013). .....	19
Figure 2.9: (a) Midpoint circle diagram outlining parameters; (b) Stability number plotted against slope angle (Das 2010). .....	21
Figure 3.1: Optum G2 opening screen (Optum Computational Engineering 2016). .....	26
Figure 3.2: Geometrical model demonstrating the different tools available (Optum Computational Engineering 2016). .....	27
Figure 3.3: Model showing a number of different material layers (Optum Computational Engineering 2016). .....	28
Figure 3.4: Mesh view of a model with boundary conditions and a fixed distributed pressure (Optum Computational Engineering 2016). .....	28
Figure 3.5: Stage manager window displaying the options for a limit analysis (Optum Computational Engineering 2016). .....	29
Figure 3.6: Solved model with deformation scale at eighty percent & plastic multiplier shown (Optum Computational Engineering 2016). .....	30

Figure 3.7: Geometrical model of slope stability problem (Optum Computational Engineering 2016).....	31
Figure 3.8: Full restraints applied to the geometrical model (Optum Computational Engineering 2016).....	31
Figure 3.9: Material types assigned to layers (Optum Computational Engineering 2016). .....	32
Figure 3.10: 10kPa surcharge pressure applied to model (Optum Computational Engineering 2016).....	32
Figure 3.11: Stage Manager for upper and lower bound SRM (Optum Computational Engineering 2016).....	33
Figure 3.12: Results log displaying upper bound FoS calculation (Optum Computational Engineering 2016).....	33
Figure 3.13: Results of slope stability analysis showing fifty percent deformation and the plastic multiplier (Optum Computational Engineering 2016).....	34
Figure 3.14: Geometrical model for tunnel heading problem with depth ratio equals two (Optum Computational Engineering 2016).....	35
Figure 3.15: Tunnel heading stability model restraints (Optum Computational Engineering 2016). .....	35
Figure 3.16: Material type assigned to tunnel heading example (Optum Computational Engineering 2016).....	36
Figure 3.17: 50kPa surcharge and internal tunnel pressure applied to tunnel heading model example (Optum Computational Engineering 2016). .....	36
Figure 3.18: Stage manager for upper and lower bound SRM and GMM (Optum Computational Engineering 2016). .....	37
Figure 3.19: Results log showing upper and lower bound GMM results (Optum Computational Engineering 2016). .....	37
Figure 3.20: Upper bound SRM results of tunnel heading example showing fifty percent deformation with mesh overlay (Optum Computational Engineering 2016).....	38
Figure 3.21: Upper bound SRM results of tunnel heading example showing displacement vectors (Optum Computational Engineering 2016). .....	38
Figure 3.22: Upper bound SRM results of tunnel heading example showing shear strain (Optum Computational Engineering 2016).....	39

Figure 3.23: Upper bound SRM results of tunnel heading example showing $\sigma_1$ , $\sigma_2$ vectors (Optum Computational Engineering 2016).....	39
Figure 3.24: Upper bound SRM results of tunnel heading example showing plastic multiplier (Optum Computational Engineering 2016). .....	40
Figure 4.1: Tunnel heading stability problem statement.....	42
Figure 4.2: Example of collapse failure mechanism produced in Optum G2 showing plastic multiplier and 60% deformation scale. DR = 2, SR = 1.10, PR = +10. ....	45
Figure 4.3: Tunnel heading finite element mesh with mesh adaptivity. ....	46
Figure 4.4: Graphical comparison of upper and lower bound results obtained through SRM for PR = 0.....	49
Figure 4.5: Graphical comparison of upper and lower bound results obtained through GMM for PR = 0.....	49
Figure 4.6: Graphical comparison of upper and lower bound results obtained through SRM for PR = +5.....	54
Figure 4.7: Comparison of collapse results to external publication. [1] Denotes data obtained from Augarde, Lyamin and Sloan (2003).....	56
Figure 4.8: Tunnel heading failure by collapse showing displacement vector field and mesh overlay. PR=0, DR=2 & SR=1.50.....	58
Figure 4.9: Plot of factor of safety verse pressure ratio for tunnel heading problem, DR = 2 and SR = 1.50.....	59
Figure 4.10: Displacement vector field. PR = +10, DR = 2, SR = 1.50.....	60
Figure 4.11: Displacement vector field. PR = +5, DR = 2, SR = 1.50.....	60
Figure 4.12: Displacement vector field. PR = +3, DR = 2, SR = 1.50.....	60
Figure 4.13: Displacement vector field. PR = +1, DR = 2, SR = 1.50.....	61
Figure 4.14: Displacement vector field. PR = 0, DR = 2, SR = 1.50.....	61
Figure 4.15: Displacement vector field. PR = -1, DR = 2, SR = 1.50.....	61
Figure 4.16: Displacement vector field. PR = -1.5, DR = 2, SR = 1.50.....	62
Figure 4.17: Factor of safety vs. strength ratio for all positive pressure ratios. DR = 1. .	63
Figure 4.18: Factor of safety vs. strength ratio for all positive pressure ratios. DR = 2. .	63
Figure 4.19: Factor of safety vs. strength ratio for all positive pressure ratios. DR = 3. .	64

Figure 5.1: Tunnel heading stability problem statement.....	69
Figure 5.2: Example of blowout failure mechanism produced in Optum G2 showing plastic multiplier and 60% deformation scale. DR = 2, SR = 1.10, PR = -16.....	72
Figure 5.3: Docklands blowout failure diagram (Institution of Civil Engineers 1998). ...	73
Figure 5.4: Sinkhole caused by blowout (Institution of Civil Engineers 1998).....	73
Figure 5.5: Tunnel heading finite element mesh with mesh adaptivity. ....	74
Figure 5.6: Displacement vector field showing failure mechanism for SRM upper bound. DR = 1, SR = 2.00, PR = -8 and corresponding FoS = 0.604. ....	80
Figure 5.7: Displacement vector field showing failure mechanism for GMM upper bound. DR = 1, SR = 2.00, PR = -8 and corresponding FoS = 15.43. ....	80
Figure 5.8: Graphical comparison of upper and lower bound results obtained through SRM for PR = -8. ....	81
Figure 5.9: Tunnel heading failure by blowout showing displacement vector field. PR = -5, DR = 2 & SR = 1.50.....	83
Figure 5.10: Plot of factor of safety verse pressure ratio for tunnel heading problem, DR = 2 and SR = 1.50.....	84
Figure 5.11: Displacement vector field. PR = -16, DR = 2, SR = 1.50.....	85
Figure 5.12: Displacement vector field. PR = -8, DR = 2, SR = 1.50.....	85
Figure 5.13: Displacement vector field. PR = -5, DR = 2, SR = 1.50.....	86
Figure 5.14: Displacement vector field. PR = -3, DR = 2, SR = 1.50.....	86
Figure 5.15: Displacement vector field. PR = -2, DR = 2, SR = 1.50.....	86
Figure 5.16: Factor of safety vs. strength ratio for all negative pressure ratios. DR = 1.	87
Figure 5.17: Factor of safety vs. strength ratio for all negative pressure ratios. DR = 2.	88
Figure 5.18: Factor of safety vs. strength ratio for all negative pressure ratios. DR = 3.	88
Figure 5.19: Factor of safety vs. strength ratio for DR = 2, PR = -3.....	90
Figure 6.1: Tunnel heading stability problem statement.....	94
Figure 6.2: Tunnel heading finite element mesh with mesh adaptivity. ....	97
Figure 6.3: Factor of safety variation with pressure ratio for model with DR = 2 and SR = 1.50.....	100

Figure 6.4: Displacement vector field for intermediate weightless scenario, DR = 2, SR = 1.50, PR = -1.75, corresponding FoS =13.09.....	101
Figure 6.5: Factor of safety variation with pressure ratio for all strength ratios. DR = 2. ....	102
Figure 6.6: Tunnel heading stability design chart for DR = 1.....	103
Figure 6.7: Tunnel heading stability design chart for DR = 2.....	104
Figure 6.8: Tunnel heading stability design chart for DR = 3.....	104
Figure 6.9: Tunnel heading stability design chart for SR = 0.10. ....	105
Figure 6.10: Tunnel heading stability design chart for SR = 0.30. ....	106
Figure 6.11: Tunnel heading stability design chart for SR = 0.50. ....	106
Figure 6.12: Tunnel heading stability design chart for SR = 0.70. ....	107
Figure 6.13: Tunnel heading stability design chart for SR = 0.90. ....	107
Figure 6.14: Tunnel Heading Stability Design Chart for SR = 1.10.....	108
Figure 6.15: Tunnel heading stability design chart for SR = 1.30. ....	108
Figure 6.16: Tunnel heading stability design chart for SR = 1.50. ....	109
Figure 6.17: Tunnel heading stability design chart for SR = 2.00. ....	109

# TABLE OF TABLES

Table 4.1: SRM and GMM results obtained for PR = 0 with comparison of upper bound and lower bound.....	48
Table 4.2: Comparison of SRM and GMM results for PR = 0. ....	50
Table 4.3: CPU run time comparison for various collapse scenarios. ....	51
Table 4.4: SRM and GMM results obtained for PR = +5 with comparison of upper bound and lower bound.....	52
Table 4.5: Comparison of SRM and GMM results for PR = +5. ....	53
Table 4.6: Comparison of collapse results to external publication. ....	56
Table 4.7: Factor of safety results for collapse failure related to model with DR = 2 and SR =1.50. ....	58
Table 4.8: Upper bound factor of safety results for all positive pressure ratios.....	65
Table 5.1: Comparison of upper and lower bound factor of safety results for PR = -8. ....	77
Table 5.2: CPU run time comparison for various blowout scenarios. ....	78
Table 5.3: Comparison of GMM and SRM results for PR = -8. ....	79
Table 5.4: Factor of safety results for collapse failure related to model with DR = 2 and SR =1.50. ....	83
Table 5.5: Upper bound factor of safety results for all negative pressure ratios.....	89
Table 6.1: Factor of safety results for model with C/D = 2 and SR =1.50.....	100

# CHAPTER 1:

## INTRODUCTION

### 1.1 Outline of Study

This paper is focused on investigating tunnel heading stability for various cases of shallow tunnelling in undrained clay. A two-dimensional tunnel analysis was conducted for various scenarios where the load parameter, or pressure ratio as it will be referred to in this paper, was equal to zero, greater than zero and less than zero. Varying the pressure ratio allowed for the investigation of tunnel heading failure related to both the collapse and blowout mechanisms, with additional focus on the blowout failure mechanism due to the lack of previous research in this area. Ultimately, the factor of safety method was used to establish new safety design charts to assist engineers in the preliminary stages of tunnel design. Prior to this, a full understanding of tunnel heading stability must be obtained by reviewing and studying previous literature. Taylor (1937) applied the factor of safety approach to slope stability to develop Taylor's slope stability design charts. The tunnel stability literature indicated that the stability of a tunnel is determined by predicting the limiting load that a tunnel can withstand prior to collapse. Broms and Bennermark (1967) were the first to develop this theory and apply it to tunnelling by deriving an initial stability number. By combining knowledge gained from Broms and Bennermark (1967) and Taylor (1937) it was possible to apply the factor of safety approach to tunnel heading stability.

The geotechnical analysis software package, Optum G2, developed by the University of Newcastle, was the program selected to model the tunnel heading stability problems for this project. Optum G2 is a powerful, yet user-friendly, finite element limit analysis (FELA) software program used for the two-dimensional analysis of a broad range of geotechnical problems. Before modelling the tunnel heading problems it was necessary to gain a full understanding of the software, this was done by reading the user's manual provided by the manufacturer and performing a number of selected examples. Previous literature has utilised FELA modelling by applying the load multiplier method, meaning a unit load is applied and amplified until a state of failure is induced. However, to apply the factor of safety approach, this project focused on the gravity multiplier and strength reduction methods. As the name suggests, the gravity multiplier method amplifies the gravity ( $g$ ) until a state of failure is reached while the strength reduction method reduces the cohesive strength of the soil ( $C_u$ ) until a state of failure is induced. The factor by which

the gravity is increased, or the strength is reduced, can be taken directly as the factor of safety. Results obtained from both methods were compared to each other and to external results obtained from a notable publication.

The failure mechanism of any scenario could be defined as either collapse, a downward soil movement, or blowout, an upward soil movement. The failure mechanism of each scenario was determined and discussed along with the relationship between the varying model input parameters. All results obtained from the Optum G2 analysis were presented in various stability design charts, which will possibly be useful to practicing engineers while in the preliminary stages of tunnel design. A number of select design examples were presented so the reader can better understand the application and usefulness of the design charts.

## **1.2 Methodology**

The methodology for this research project was formulated in accordance with Appendix A – ‘Project Specification’ and is presented below in a number of basic steps.

1. Research literature relevant to tunnelling and in particular, tunnel heading stability.
2. Research literature related to the factor of safety approach and FELA.
3. Learn how to use Optum G2 by reading the manual and completing example problems.
4. Develop 2D models for shallow tunnel heading stability by varying the pressure ratio, depth ratio and strength ratio.
5. Perform an internal comparison of results obtained from the strength reduction and gravity multiplier methods, where applicable.
6. Compare Optum G2 shallow tunnel heading results with previously published results.
7. Discuss the failure mechanism for varying pressure ratios and the relationships between factor of safety, pressure ratio, strength ratio and depth ratio.
8. Develop stability design charts by applying the factor of safety approach.
9. Present and discuss a number of examples developed from the design stability charts.
10. Conclude research and introduce future work that could be performed on the topic.

### 1.3 Research Objectives

This study aimed to achieve a number of research objectives. The first, and broadest, objective was to gain a general knowledge of tunnel engineering with a focus on tunnel heading stability and to a lesser degree, tunnel construction methods. The ability to use Optum G2 to solve tunnel heading stability problems and apply the powerful new finite element limit analysis software to a broader spectrum of problems was another desired learning objective. It was also expected that a greater understanding of tunnel heading stability problems with a negative pressure ratio, having a failure mechanism similar to ‘uplift’ or ‘blowout’, will be obtained and transmitted through this paper, as it appears that this topic has not been thoroughly researched thus far. The research and modelling was expected to culminate in a new factor of safety approach, similar to slope stability, which can be applied to tunnel heading stability. The final output of this approach was a number of useful stability design charts for use by practicing engineers in the preliminary stages of tunnel design. An overview of the research objectives included; fully understand tunnel heading stability and its practical application, learn and utilise Optum G2, gain a higher level understanding of the blowout effect with regards to tunnel heading stability, develop a new theoretical factor of safety approach to tunnel heading stability and produce new design stability charts.

### 1.4 Organisation of Thesis

**Chapter 2: General Review** – This chapter introduces the concept and function of tunnels. A brief guide to tunnelling specific terminology is provided along with a summarised history of tunnelling, highlighting the most important breakthroughs throughout time. Modern tunnel construction techniques are discussed and the design criteria specific to tunnelling projects are outlined. A literature review of tunnel stability is conducted to assist in developing the factor of safety approach for tunnel stability.

**Chapter 3: Numerical Modeling Review** – This chapter will explain the numerical modelling techniques used in this project. Optum G2 is introduced and an outline of finite element limit analysis (FELA) software is presented. The gravity multiplier and strength reduction methods used in this project are explained and Optum G2 is explained in more detail. A slope stability and tunnel heading stability example will be performed in Optum G2 to show all the steps involved in a finite element limit analysis.

**Chapter 4: 2D Shallow Tunnel Heading Analysis: Collapse** – This chapter introduces and defines the problem to be investigated, specifically, a shallow tunnel heading in undrained clay where the predominant failure mechanism can be related to collapse. The Optum G2 numerical modelling process is presented and the upper and lower bound factor of safety values are analysed and compared. The results obtained using the gravity multiplier and strength reduction methods are compared internally and then externally to previously published results. The relationship between the factor of safety and the defining dimensionless parameters, the pressure ratio, strength ratio and depth ratio will be investigated. The failure modes experienced are described by displaying the displacement vector fields. A final conclusion relating to shallow tunnel heading stability in undrained clay exhibiting a collapse failure mechanism is presented.

**Chapter 5: 2D Shallow Tunnel Heading Analysis: Blowout** – Similarly to chapter four, this chapter introduces and defines the problem to be investigated, specifically, a shallow tunnel heading in undrained clay where the predominant failure mechanism can be related to blowout. The significance of the blowout failure mechanism is highlighted and a historical example is provided. The Optum G2 numerical modelling process is presented and the upper and lower bound factor of safety values are analysed and compared. The results obtained using the gravity multiplier and strength reduction methods are compared internally to determine the most suitable method. The relationship between the factor of safety and the defining dimensionless parameters, the pressure ratio, strength ratio and depth ratio will be investigated. The failure modes experienced are described by displaying the displacement vector fields. A final conclusion relating to shallow tunnel heading stability in undrained clay exhibiting a blowout failure mechanism is presented.

**Chapter 6: 2D Shallow Tunnel Heading Analysis: Stability Design Charts** – Similarly to chapters four and five, this chapter introduces the problem to be investigated, specifically, a shallow tunnel heading in undrained clay. The Optum G2 numerical modelling process is presented and the collapse and blowout failure mechanism are directly compared so that the entire relationship can be investigated. The relationship between the factor of safety and the defining dimensionless parameters, the pressure ratio, strength ratio and depth ratio will be investigated. The failure modes experienced are described by displaying the displacement vector fields. Ultimately a variety of tunnel heading stability design charts, for use by practicing engineers in the preliminary tunnel design stages, are formulated by applying the factor of safety approach. Selected examples are provided to highlight the usefulness of the design charts. A final conclusion relating to shallow tunnel

heading stability in undrained clay and the development of stability design charts is presented.

**Chapter 7: Conclusion** – This chapter concludes the dissertation by summarising the work and highlighting the major findings. Recommendations are also made regarding future research related to the topic of tunnel stability based on the findings of this dissertation.

# **CHAPTER 2:**

## **GENERAL REVIEW**

### **2.1 Introduction**

In the world of civil engineering, tunnels are complex underground structures involving a number of challenging factors and unknowns not typically experienced when designing aboveground structures. No two tunnel construction projects will ever be identical, this is largely due to the complex and constantly varying nature of the soil medium. The soil medium is the body of soil through which the tunnel void passes. In tunnel construction the ground acts as both a loading and supporting mechanism, unlike other conventional structures which assume the soil provides a uniform foundation while timber, concrete and/or steel are provided as structural supports. Engineering judgement is especially important when designing and constructing tunnels as it is not possible to calculate discrete values for all surcharge loadings and soil properties and features that will be encountered while tunnelling. These factors are determined by soil testing and load calculations to a point, but are largely based on estimation and assumptions (Chapman, Metje & Stärk 2010). To develop the level of engineering judgement needed for tunnel design and construction an engineer must have a sound knowledge of construction processes, concrete engineering, structural analysis, mechanical engineering, hydraulic engineering and most importantly geology and geomechanics. An understanding of soil conditions, especially the strength and stability, and how they will affect the tunnelling process are of paramount importance.

### **2.2 Significance of Tunnels**

Tunnels are constructed for a number of reasons including providing alternative travel routes for traffic and pedestrians, rail transport, waste disposal, storage of goods, housing of services and military purposes. A transport tunnel is generally considered when it is necessary to circumnavigate an object on the Earth's surface, be that a mountain, river, structure or existing transport infrastructure. Tunnels have long been a fascinating and important civil structure, but heading into the future their importance continues to grow as cities become increasingly congested and overpopulated. As tunnelling technology advances, society is becoming increasingly reliant on tunnels as a solution to complex transport problems (Zhao, Shirlaw & Krishnan 2000).

## 2.3 Tunnelling Terminology

The method by which a tunnel is constructed depends on the purpose of the tunnel, site location, ground conditions, size, cost, and construction methods available. It is necessary to fully understand the different construction methods and the unique terminology relevant to each when designing a tunnel. However, to comprehend this research a basic understanding of key terminology is all that is required and any additional tunnel specific terms will be explained as they appear. Key tunnelling terminology is outlined below in Figure 2.1.

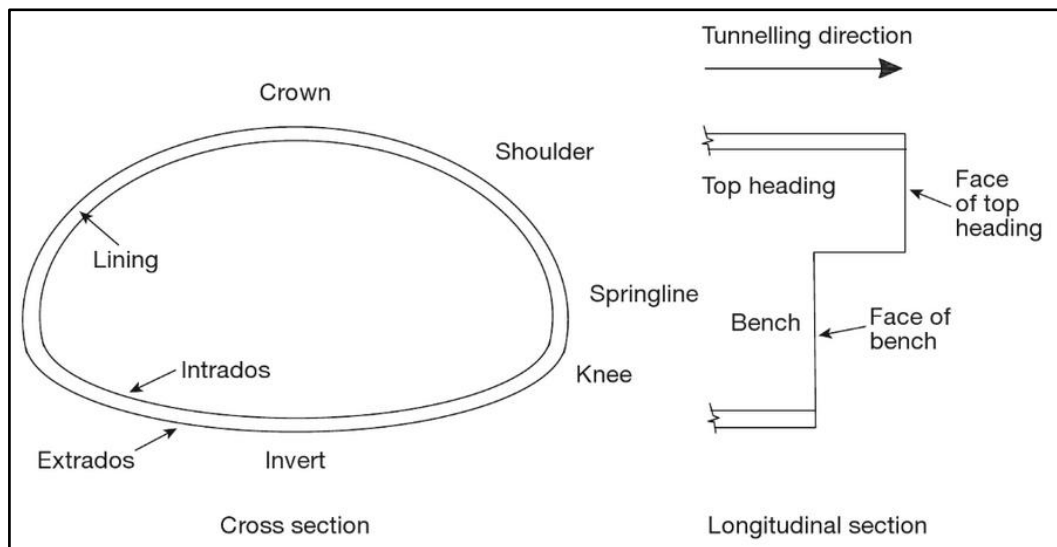


Figure 2.1: Terminology relevant to tunnel cross section and longitudinal section (Chapman, Metje & Stärk 2010).

## 2.4 History of Tunnels

Megaw and Bartlett (1981) performed extensive research on the construction of tunnels throughout history. The origin of tunnelling can be dated back thousands of years to ancient mining operations and water supply. These early tunnels were dug by hand with primitive tools made from bone, wood and stone. Between 2500 B.C. and 1200 B.C. hand tools made from bronze grew in popularity and eventually developed into iron tools by approximately 1000 B.C. Notable early examples of tunnels include; a 1000 metre long lined water supply tunnel constructed through a ridge on the island of Samos in 687 B.C., over 350km of gravity flow aqueducts built in Rome between 312 B.C. and 52 A.D., and the 1750 metre long Pausilippo tunnel which was built in 36 B.C. and acted as a road between Naples and Pozzouli.

Gunpowder was first used in tunnel construction in 1679 to build the tunnel that would become the pioneer of the Canal Age. The Canal du Midi was built between 1666 and 1681 and connected the Atlantic Ocean to the Mediterranean Sea. The 157 metre long tunnel section of the canal was necessary to pass under a ridge, and was the first tunnel on record that was constructed using gunpowder blasting as opposed to earlier fire setting techniques. The tunnel, which had a square cross section, was built between 1679 and 1681, and was originally unlined. In 1691 a structural lining was added to the tunnel.

It is well documented that Brunel's great Thames Tunnel, a proposed dual carriageway under the Thames River in London, commencing in 1825, was the first shield driven tunnel and the first tunnel to pass under a tidal river. Sir Marc Isambard Brunel was the great mind behind Brunel's Shield, the machine that revolutionised tunnelling and formed the primitive design basis of modern day tunnel boring machines. Brunel's shield, shown in Figure 2.2, was designed to provide; a skin covering the ground on all sides, access for excavation while offering full face support and a means to move the shield forward into the excavated void while a brick lining was constructed behind it. The shield itself consisted of a cast iron framework, with twelve internal three tier frames. The earth in front of the shield was excavated with hand tools allowing the shield to be propelled forward by a number of screw jacks, which jacked off the completed brick lining. The tunnel was by far the most ambitious of its time and was eventually opened in 1842 as a pedestrian tunnel, after five inundations from the river above, many deaths and a great deal of over expenditure.

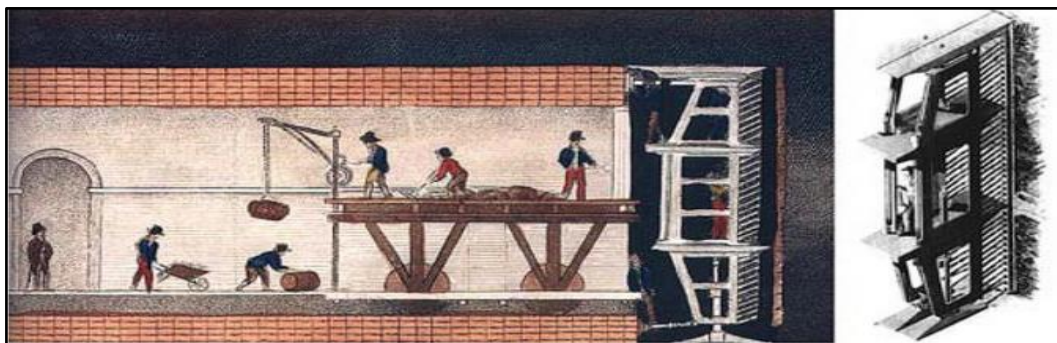


*Figure 2.2: Brunel's shield, a diagram showing a longitudinal section and one of the twelve frames (Guglielmetti et al. 2007).*

The railway age saw a great number of tunnels constructed to provide efficient transport routes. Over fifty tunnels were constructed between 1830 and 1890 in Great Britain alone. During this phase of the nineteenth century a number of alpine tunnels were constructed. Tunnels of this nature posed a whole new set of challenges to engineers. Ventilation

problems were a big issue and this forced new developments in blasting and drilling techniques, such as compressed air rock drills. The first of these great Alpine tunnels to be constructed was the col de Frejus, a 12.23 kilometre long tunnel 1340 metres above sea level, carrying the railway from France to Turin. Mountain streams were used to provide ventilation and to compress air for the drills. Construction began in 1857 and was completed in 1871 by a workforce of approximately 4000 men.

1869 marked an important year for tunnelling development as it was the year that the subaqueous Tower subway in London was completed. The tunnel was constructed using a shield and cast iron lining and was used for a cable-hauled car, but now houses water mains. The 402 metre long tunnel was driven through clay nineteen metres below the water line and seven metres below the river bed. The shield mechanism used became known as Greathead's shield and is known as the forefather of all modern day shields. It was during this project that grouting as a form of tunnel ground support was developed as well. The cast iron lining did not entirely fill the void so cement grout had to be injected to fill the gap between the lining and the soil. The Hudson River Tunnel, shown in Figure 2.3, was another important project of the time which also utilised Greathead's shield and for the first time on a large scale tunnel, compressed air as a face stabilisation method. The soil/air pressure balance proved to be very unstable and after a serious accident, in which 20 lives were lost, the funding ran out and the tunnel was sealed off and left incomplete.

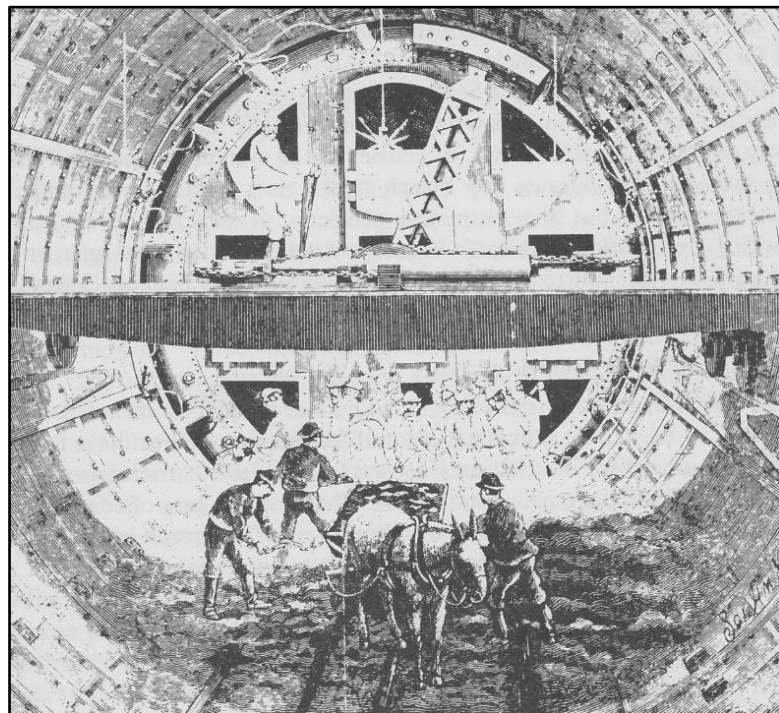


*Figure 2.3: Hudson River Tunnel. Excavation utilising Greathead's shield, cast iron lining and compressed air (Megaw & Bartlett 1981).*

Maidl, Maidl and Thewes (2013) claimed that the first tunnel boring machine (TBM), where the entire machine face excavated the tunnel simultaneously using disc cutters, was constructed in 1851 and patented in 1856 by Charles Wilson. Wilson's machine was trialled on the East portal of the Hoosac tunnel in Massachusetts. It soon became evident that the machine was not capable of tunnelling through the hard igneous rocks of New York. In 1875 Fredrick Beaumont obtained a patent to develop a new cutterhead design. Colonel English eventually took over this patent and by 1880 had developed a cutterhead which allowed for chisel heads to be exchanged without withdrawing the TBM. In the following years Beaumont successfully built two of England's tunnel boring machines, shown below in Figure 2.4, and was involved in the partial construction of the Channel Tunnel. Over 1500 metres had been excavated either end of the tunnel before political reasons brought the project to a halt. The project was finally completed in 1994.

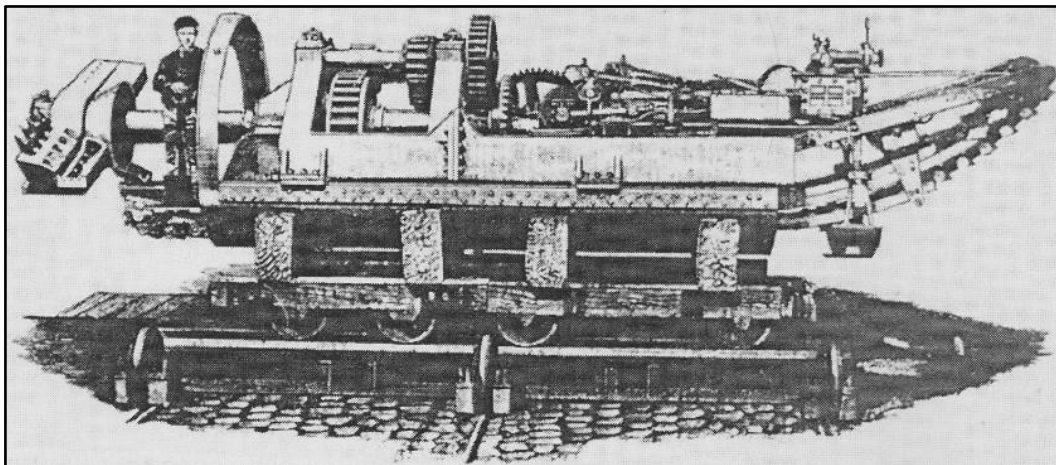


*Figure 2.4: Illustration of English and Beaumont's tunnel boring machine (Maidl, Maidl & Thewes 2013).*

By the beginning of the 20<sup>th</sup> century many of the basic techniques involved in the construction of bored tunnels had been devised and proved through past success and failure. At this point in time tunnelling was considered a viable option so long as the developer was able to afford the process. This acceptance of tunnelling resulted in many new tunnel projects serving varied purposes throughout the world, including railways, metro systems, highway tunnels, water supply, sewer and waste removal, storage of goods and the housing of services such as pipes and cables. Tunnel boring machines underwent continual development and refinement throughout the 20<sup>th</sup> century. Throughout this time many advancements were also made in regards to lining systems and ground improvement techniques. Some of these advancements included; grouting, ground freezing, face dowelling, ground reinforcing, sprayed concrete linings, cast in-situ concrete linings and precast segmental concrete linings. Tunnel construction techniques continued to advance

across the world, improving the safety and efficiency of tunnel designs, Maidl, Maidl and Thewes (2013) further detail these modern advancements in tunnelling.

## **2.5 Tunnel Construction Methods**

There are a number of different tunnel construction methods available to suit a range of different project conditions. Maidl, Maidl and Thewes (2013) have extensively researched and presented modern tunnel construction techniques. Presented in this section, will be a number of the most widely adopted methods used today.

The nature of the tunnel project will always be of paramount importance when determining the construction methods and techniques to be implemented. The function of the tunnel, location, soil conditions, nature of the obstacle being circumnavigated, tunnel dimensions, location of water table, tunnel depth, and quality of tests and available information all form part of the decision making process. Other factors affecting the project will include the timeline, finances, safety, noise, labour, available machinery and the environmental impact. There is no 'one size fits all' method available for tunnel construction and engineering judgement must be implemented to assess each project separately of all others.

Drill and blast tunnelling has been around in some form since the 17<sup>th</sup> century and has continually evolved over this time. The drill and blast method is generally used in hard ground conditions, ranging from low strength rock to the very strongest rock. This method, while quite affordable, is best suited to short tunnels in hard ground as the process can be quite slow when compared to TBM tunnelling. Each advancement forward in the tunnel can be specifically tailored to changing ground conditions, however this will severely slow down the process. The technique involves the drilling of boreholes into the tunnel face so that explosives, usually dynamite, can be placed in these holes and detonated in a controlled manner to loosen the rock face and advance the tunnel. The drilling is generally carried out by drilling rigs with pneumatic tyres, as shown in Figure 2.5. The exact depth and position of the boreholes along with the amount of explosives used is crucial to ensure safe and precise tunnelling. Once the explosives have been detonated and the site is declared safe, mucking can begin. Mucking is the process of removing the spoil from the tunnel. This is usually achieved by using conveyer belts, conventional machinery such as tracked loaders, excavators, locomotives and dump trucks, or variants of conventional machinery modified for the space constraints of tunnelling. Once the tunnel advancement is clear, the supporting material is installed and the process is repeated. The supporting material can

be in the form of timber, steel, grouting, anchors, dowelling or concrete. Artificial ventilation in the form of a ducting system is necessary when drilling and blasting to ensure that workers receive enough oxygen and the dust and fumes created from the blasting can be appropriately diluted.



*Figure 2.5: Typical face drilling rig used in drill and blast tunnelling (Atlas Copco 2014).*

Tunnel boring machines, or TBMs as they are more commonly referred to, are growing in popularity, especially in the development of transport tunnels in major cities around the world. TBMs are available in a wide variety of configurations dependant on the particular requirements of each tunnelling project. Machines can excavate either part-face or full-face and can be either with shield or without shield. Full face tunnel boring machines are capable of excavating both hard and soft ground and are the most common form of TBM used in large tunnelling projects. Gripper and shield tunnel boring machines are suitable for use in hard rock conditions. Shield machines, as shown in Figure 2.6, have a cylindrical steel construction (shield) between the cutterhead and support erection system to resist the pressure exerted by the soil and prevent collapse in unstable ground. In the case of a shield TBM, thrust is provided to the cutterhead by hydraulically jacking off of the installed tunnel lining. Gripper machines are hydraulically braced to the walls of the excavation, allowing for thrust force to be applied to the cutterhead. When tunnelling in soft ground, especially

when dealing with ground water pressure, it is common practice to use an earth pressure balance (EPB) machine or slurry shield machine. EPB machines were designed for use in cohesive soils and use the excavated soil to support the tunnel face. The excavated material is passed through a plenum where it is plasticised by mixing the soil with foams/slurry and other chemical additives before it is removed by a pressure controlled screw conveyor. The thrust force on the cutterhead, and the rate at which the material is removed through the screw conveyor, controls the pressure on the plenum. Slurry shield TBMs work on a similar principal to EPB machines but face support is provided by pressurising boring fluid (slurry) inside the cutterhead chamber. This boring fluid is generally a bentonite based slurry and is pumped to the cutterhead from a purpose built slurry plant. The slurry also acts as a means of removing the excavated soil as it is transferred back to the slurry plant where it is filtered and pumped back to the cutterhead for reuse through a system of pipes. Compressed air is sometimes used in conjunction with a slurry shield machine to help stabilise the face.

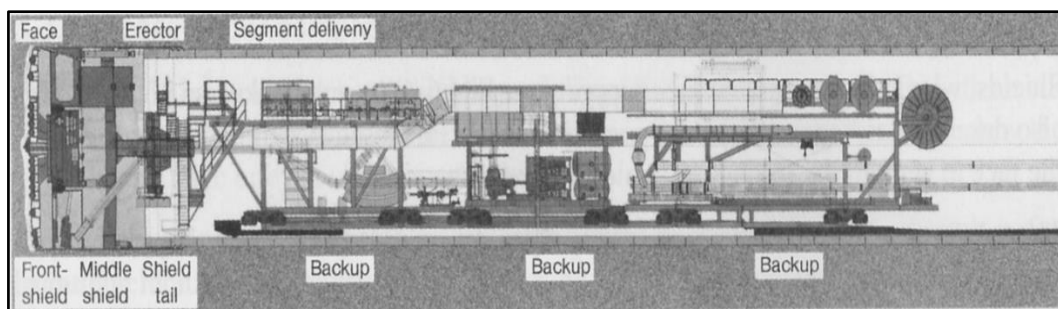


*Figure 2.6: Diagram of typical tunnel boring machine with shield (Maidl, Maidl & Thewes 2013).*

Bickel, King and Kuesel (1996) explained the cut and cover method of tunnelling. The cut and cover method is a simple construction method used to build shallow tunnels that do not pass under surface water or existing permanent structures. The tunnel section is excavated and a support system is constructed overhead before the tunnel is again covered over. There is two different forms of cut and cover tunnelling; the top-down method and the bottom-up method. The top-down method involves constructing the tunnel support walls, generally in the form of slurry walls or secant piling, before making a shallow excavation to allow for the construction of the tunnel roof, which is generally in the form of precast beams or cast in-situ concrete. Once the roof is built the ground surface is then restored above and the excavation takes place below the permanent tunnel roof, where a base slab will be constructed. The top-down method is favoured when immediate reinstatement of roadways or other surface features is necessary. The bottom-down method involves supplying all necessary ground support then excavating the entire tunnel section. The tunnel is

constructed within the trench, generally of cast in-situ concrete, precast concrete, corrugated steel arches or precast concrete arches. Once the tunnel is constructed, the trench is backfilled above the roof of the tunnel to restore the surface. Cut and cover tunnelling is limited to shallow constructions and a number of issues related to the construction's short term and long term ability to resist water and lateral earth pressures can be encountered, especially when using ground anchors, diaphragm walls and sheet piling.



*Figure 2.7: Example of bottom-up cut and cover tunnelling (Wallis 2002).*

There are a number of construction methods available around the world, and choosing the correct one will largely depend on the ground conditions, along with the location, depth and size of the tunnel. Every tunnel designed will have its own unique requirements and not all construction methods will be suitable for all tunnelling projects. Sometimes, although as unfavourable as it is, more than one major construction method may need to be implemented on a single tunnelling project. It is the responsibility of the practicing engineers involved in the design of the tunnel to decide on the correct construction technique. A general design criteria applies to tunnels and is used to guide the decision making process of engineers involved in the design and construction of tunnels.

## 2.6 Design Criteria

Designing and building tunnels poses a great challenge to geotechnical engineers. The complexity and uncertainty of ground conditions along with the sensitive nature of the surface above are two of the biggest challenges incorporated in tunnelling. Guglielmetti, et al. (2007) outlined the primary design criteria to be considered when designing a tunnel as:

- The study of the settlement and consequent damage that the excavation could cause to the ground surface and existing structures above and around the tunnel, over both the short term and long term. This should include the consideration of any additional ground treatment or reinforcement that needs to be provided for existing structures.
- The design of the face support pressure for the excavation to ensure the required stability requirements are maintained throughout construction.
- The design of the tunnel's final structural lining to ensure it can resist all earth and water pressure and current and future surcharge loading.
- The design of the tail void grouting to fill the space between the structural lining and the excavated earth void.

Face stability of the tunnel heading is a particularly important aspect of the design process, especially when using a TBM in soft ground conditions. The pressure balance needs to be maintained to avoid collapse or blowout of the face. There are a number of examples throughout history which demonstrate the consequences of a pressure imbalance caused by an unexpected change in soil conditions. The short term and long term settlement caused by the structure is also another very important design aspect, especially in urbanised cities where a great deal of infrastructure is built on the surface above the tunnel. The surface settlement is influenced by a number of factors including; the classification and uniformity of the soil medium, the behavior of the soil medium while tunnelling, the presence of underground water, the surcharge loading, the control of the tunnel face pressure and the stability and strength provided by the temporary and permanent tunnel lining. Most urban tunnelling is performed at shallow depths to avoid excess costs. Tunnelling at shallow depths increases the risks of settlement and even under the most strictly controlled tunnelling environments it will be impossible to avoid all settlement. Ideally engineers will aim to adopt large factor of safety values for tunnel designs, however this will not always be possible. This study will investigate the heading stability of shallow tunnels in undrained clay.

## 2.7 Tunnel Stability Review

As tunnelling technology developed and the transport needs of cities grew it became necessary, and possible, to build tunnels in increasingly challenging soil conditions. Many urban tunnels are constructed in saturated cohesive soils at shallow depths. A stability analysis must be performed as part of the initial tunnel design process to determine the feasibility of the project. The stability of tunnels has been researched through both two-dimensional and three-dimensional analysis. Two-dimensional tunnelling analyses have been extensively conducted for tunnel headings and tunnels with a circular or square cross section. Much of the research has focused on tunnels in an undrained cohesive soil medium. Undrained cohesive soil is a material where the internal angle of friction is equal to zero, this means that the undrained shear strength of the soil is simply equal to the cohesive strength of the soil. The stability of constructions in such soils can be quantified by a dimensionless stability number ( $N$ ). The stability number was first proposed by Broms and Bennermark (1967) who performed extensive study on the plastic flow of clays at vertical faces. The stability number is defined in Equation 2.1.

$$\text{Stability Number } (N) = \frac{\sigma_s - \sigma_t + \gamma(C + \frac{D}{2})}{S_u} \quad (2.1)$$

where  $\sigma_s = \text{uniform surcharge applied at the surface [N/m}^2\text{]};$   
 $\sigma_t = \text{internal tunnel pressure [N/m}^2\text{]};$   
 $\gamma = \text{unit weight of the soil [N/m}^3\text{]};$   
 $C = \text{tunnel cover [m]};$   
 $D = \text{tunnel diameter [m]}; \text{ and}$   
 $S_u = \text{undrained shear strength of the soil [N/m}^2\text{]}.$

Asadi and Sloan (1991) explain the theory of active and passive tunnel failure mechanisms. An active tunnel failure mechanism, or collapse, is created by the weight of the soil and surcharge pressure at the surface and is resisted by the internal tunnel pressure. A passive tunnel failure mechanism, or blowout, is created by the pressure in the tunnel and resisted by the weight of the soil and the surcharge pressure at the surface. A lot of previous work has been performed to develop and better understand the stability number and its application to slopes and tunnelling. Broms and Bennermark (1967) were the first to introduce the stability number as it is known today, and their work ventured into both the theoretical and practical application of the stability number and its application to a circular

void. Peck (1969) studied the theoretical stability number and further developed the design criteria for a circular section. Numerous experiments were conducted at the University of Cambridge during the 1970's by Cairncross (1973), Seneviratine (1973) and Mair (1979) on the stability of circular tunnels in cohesive soil. The experiments involved modelling a tunnel and using a centrifuge to increase the gravity until a state of collapse was reached. This experimental method was again employed by Idinger, et al. (2011) who further investigated the stability of tunnel headings. Atkinson and Potts (1977) applied the upper and lower bound limit theorem to non-cohesive soils which was followed up by Davis, et al. (1980) who applied the upper and lower bound theorem to undrained cohesive soil. The upper and lower bound solutions provide a range for the factor of safety rather than an exact value, allowing the user to make a more informed decision on the factor of safety to be adopted. The pressure ratio of a homogeneous soil medium was established as a function of two independent parameters. Equation 2.2 shows the revised pressure ratio.

$$\text{Pressure Ratio (PR)} = \frac{\sigma_s - \sigma_t}{S_u} = f\left(\frac{C}{D}, \frac{\gamma D}{S_u}\right) \quad (2.2)$$

where  $\frac{C}{D}$  = the depth ratio; and  
 $\frac{\gamma D}{S_u}$  = the strength ratio.

Finite element limit analysis techniques are constantly improving, with researchers like Sloan (1988, 1989) and Lyamin and Sloan (2002a, 2002b) at the forefront of development. This constant advancement has meant that the method followed by Davis, et al. (1980) has been adopted to develop numerous tunnel stability research papers. These research projects modelled a range of geometrical tunnel profiles, including circular, square, rectangular, twin circular and tunnel heading, in a number of different soil mediums with varying material properties and complex loading conditions. The accuracy of results obtained from the lower and upper bound theorem were continually improving as the finite element limit analysis method was further researched. Sloan (2013) summarised the advancements of the finite element limit analysis method and describes how the upper and lower bound values are obtained by combining the finite element method with the limit theorems of classical plasticity.

Wilson, et al. (2011, 2013) investigated the stability of circular and square tunnel geometries through a two-dimensional plane strain analysis. It was assumed that the shear strength of the soil increased linearly with depth, meaning that another dimensionless

parameter was included in the stability problem. Equation 2.3 defines the stability number adopted for the square tunnel stability research.

$$N = \frac{\sigma_s - \sigma_t}{c_{u0}} = f\left(\frac{H}{B}, \frac{\gamma B}{c_{u0}}, \frac{\rho B}{c_{u0}}\right) \quad (2.3)$$

where  $c_{u0}$  = undrained shear strength of soil at surface  $\left[\frac{N}{m^2}\right]$ ;  
 $\rho$  = soil strength factor;  
 $H$  = depth of tunnel [m];  
 $B$  = the tunnel side length [m];  
 $\frac{\gamma D}{c_{u0}}$  = strength ratio normalised to soil strength at surface ; and  
 $\frac{\rho D}{c_{u0}}$  = strength increase normalised to surface soil strength.

The strength factor ( $\rho$ ) denotes the rate of strength increase with depth. The tunnel pressure, soil strength and soil strength factor must be normalised to the undrained shear strength of the soil at the surface ( $c_{u0}$ ) to account for the increase of soil strength with depth. For both studies conducted by Wilson, et al. (2011, 2013) the strength increase ratio was varied from zero to one. It is important to note that when the strength increase ratio is equal to zero the soil medium is classified as homogeneous. The upper and lower bound results obtained through the finite element limit analysis were compared to results obtained by a more conventional semi-analytical rigid block analysis. It was found that the upper and lower bound results from the finite element limit analysis were in very good agreeance with the rigid block results. Figure 2.8 shows an example of the stability chart developed for an undrained square tunnel with H/B equal to two.

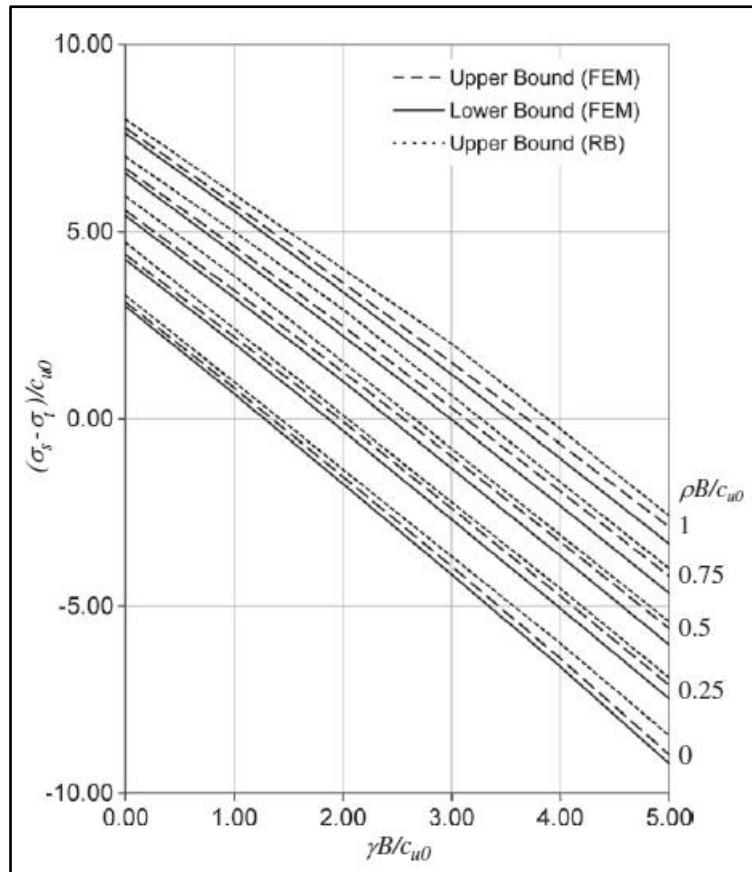


Figure 2.8: Design stability chart for square tunnel,  $H/B=2$  (Wilson et al. 2013).

Augarde, Lyamin and Sloan. (2003) performed a two-dimensional plane strain analysis on the stability of a tunnel heading. The model was in the form of the longitudinal cross section of a tunnel and the face of the heading was modelled as an infinitely long flat wall which was free to move. The roof and floor of the tunnel were fixed to simulate the installation of a supportive lining. In this type of two-dimensional tunnel heading analysis it is important to note that the transverse shape of the tunnel is not considered. This study presented a number of design stability charts similar to those produced by Wilson, et al. (2011, 2013). The limit analysis theory was again applied to a tunnel heading problem by Mollon, Dias and Soubra (2010), who investigated a three-dimensional multi-block failure mechanism for cohesive and frictional soil.

## 2.8 Factor of Safety Approach

Tschuchnigg, Schweiger and Sloan (2015) note that in the realm of geotechnical engineering there is no unique definition for the factor of safety. Bearing capacity problems usually define the factor of safety with respect to load capacity whereas slope stability problems usually define the factor of safety in relation to the soil strength. This research is based off the latter definition. The stability number can be further simplified by assuming an unsupported tunnel under Greenfield conditions and neglecting the surcharge pressure ( $\sigma_s$ ) and the internal tunnel pressure ( $\sigma_i$ ). In this scenario the pressure ratio is equal to zero. Letting the pressure ratio equal zero reduces the problem to a familiar format seen when analysing the stability of a simple slope. Das (2010) describes the factor of safety in a homogeneous clay soil as the ratio of the soil's undrained shear strength to the average shear stress developed along the potential failure plane. The factor of safety against sliding, shown in Equation 2.4, is developed by taking the moment of resistance.

$$FoS = \frac{S_u}{C_d} \quad (2.4)$$

where  $FoS =$  the factor of safety; and  
 $C_d =$  the cohesion developed to induce failure [ $N/m^2$ ].

The minimum factor of safety value could relate to failure in the form of either a toe, midpoint or slope circle. Figure 2.9(a) shows a detailed diagram of a midpoint circle. The critical stability number for a slope circle is given in Equation 2.5.

$$m = \frac{C_d}{\gamma H} = f\left(\beta, \frac{D}{H}\right) \quad (2.5)$$

where  $m =$  slope stability number;  
 $\beta =$  slope angle [ $^\circ$ ];  
 $D =$  depth factor [ $m$ ]; and  
 $H =$  height of slope [ $m$ ].

The depth function using this method is defined as the ratio of the total depth, from the top of the slope to the solid base layer, to the height of the slope. The critical height which limits a slope to a minimum factor of safety can be found from Figure 2.9(b).

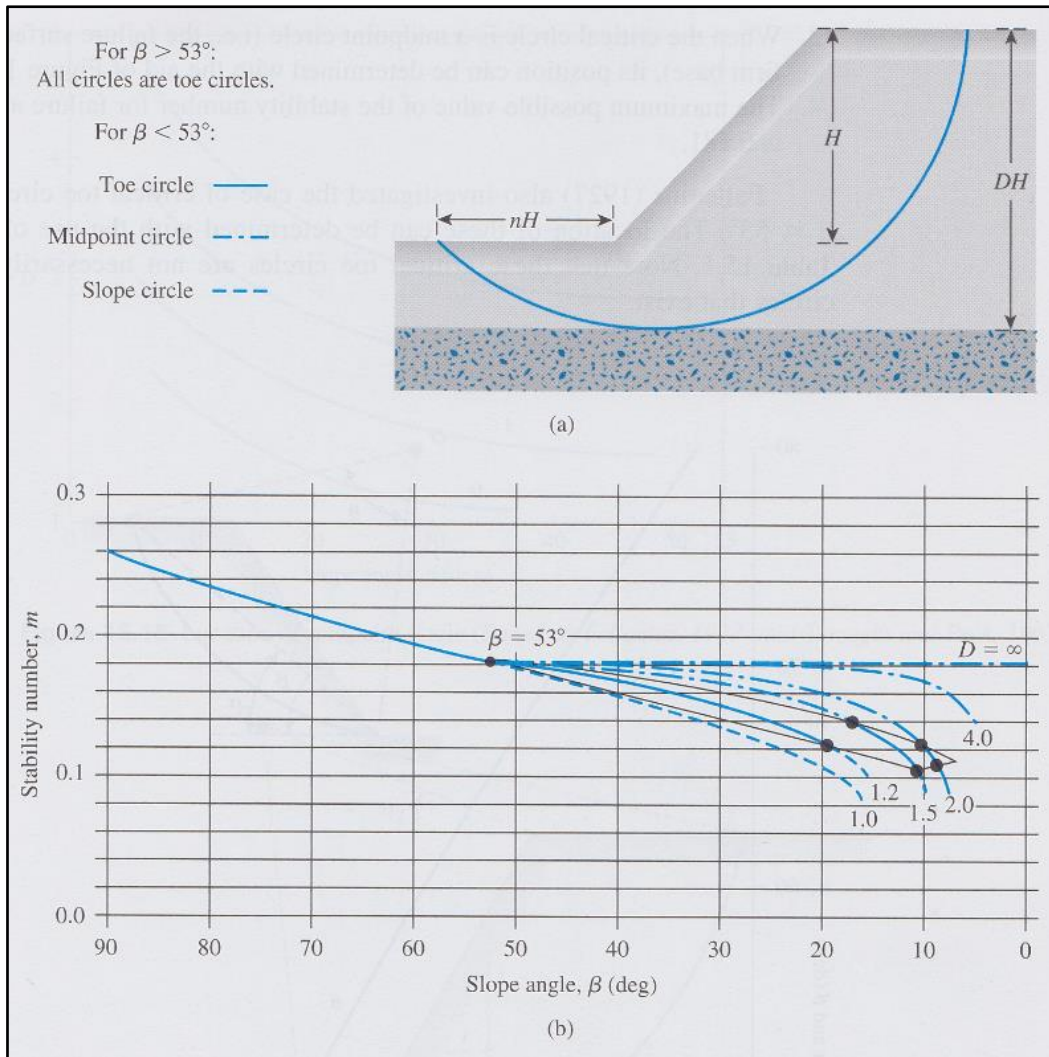


Figure 2.9: (a) Midpoint circle diagram outlining parameters; (b) Stability number plotted against slope angle (Das 2010).

Taylor (1937) developed a stability coefficient ( $N_s$ ), defined in Equation 2.6 which relates to a critical failure surface where the factor of safety is a minimum.

$$N_s = \frac{S_u}{(FoS)\gamma H} = f(\beta, D) \quad (2.6)$$

where  $S_u =$  undrained shear strength of soil [ $N/m^2$ ];  
 $FoS =$  factor of safety; and  
 $D =$  depth factor.

For a critical situation the factor of safety ( $FoS$ ) is equal to one. This allows for the limiting dimensions of slopes to be calculated. The factor of safety for a slope problem can be rearranged, as in Equation 2.7, and shown as a function of the depth function, slope angle and strength ratio.

$$FoS = f\left(\frac{D}{H}, \beta, \frac{S_u}{\gamma H}, \right) \quad (2.7)$$

A similar approach to that employed by Taylor can be applied to the stability of tunnels. The purpose of this study is to apply the factor of safety approach to tunnel heading stability problems with a non-zero pressure ratio. This study uses the finite element limit analysis technique to determine factor of safety values for a broad range of undrained tunnel heading stability problems. The factor of safety to be defined in this study is also a function of a number of dimensionless parameters similar to the factor of safety defined in Equation 2.7. The dimensionless parameters are varied within a practical range to ensure that results are applicable to a broad spectrum of real life scenarios. The factor of safety results will then be used to develop a number of stability design charts, similar to Taylor's slope stability charts, but applicable to the preliminary stages of tunnel design.

# **CHAPTER 3:**

## **NUMERICAL MODELLING REVIEW**

### **3.1 Optum G2 Introduction**

Optum G2 is a finite element limit analysis (FELA) software package designed for analysing the stability and deformation of a wide variety of geotechnical scenarios. Optum G2 is a relatively new program, it utilises a graphical user interface and shares many common features with other popular geotechnical analysis software. However, this software differs from conventional stability analysis software in the way that it is able to rigorously calculate upper and lower bound values for the factor of safety. This upper and lower bound theorem allows the user to calculate an average value for the factor of safety while also being aware of the worst case failure scenario. Another unique feature incorporated in the software is the ability to use automatic adaptive mesh refinement to maximize the accuracy of results. These features, coupled with the program's user-friendly interface and powerful processing abilities make it suitable for analysing a broad range of two-dimensional plane strain geotechnical problems (Optum CE 2013).

Some may argue that since a tunnel is a three-dimensional structure it must be analysed in 3D. However, a 2D analysis has a number of benefits over a 3D analysis including; fast model setup and analysis times, low cost, a more user friendly and accessible process and a more conservative factor of safety than 3D modelling. In projects where the absolute highest accuracy is necessary and 2D modelling cannot supply a factor of safety that meets the design requirements then it is necessary to resort to 3D modelling.

### **3.2 Finite Element Limit Analysis**

Finite element limit analysis software is similar to conventional finite element analysis software but instead of calculating a discrete value for the factor of safety it is able to calculate a set of limits, known as upper and lower bound values. The failure mode does not have to be assumed prior to beginning the analysis, meaning that the software is capable of automatically calculating the factor of safety for the worst and best case failure scenarios. The only necessary inputs are the geometrical model, defined boundaries and basic soil strength parameters. Optum G2 is also capable of dealing with complex inputs including;

layered soil profiles, pore water pressures, anisotropic strength characteristics, staged construction and complex loadings in up to three dimensions.

Lysmer (1970) investigated the lower bound finite element limit analysis theorem and focused on optimizing the method's application to plane strain soil mechanics problems. Pastor and Turgeman (1976) and Bottero, et al. (1980) investigated the upper bound limit analysis theorem and its application to two-dimensional plane strain problems involving Tresca and Mohr-Coulomb material. These early research projects focused on slope stability and the pulling out of foundations. Lyamin and Sloan (2002b) further explored the upper bound limit analysis theorem with the only unknowns being the plastic multiplier, nodal velocities and elemental stresses. Further research and significant optimization of the lower bound limit analysis theorem was performed by Lyamin and Sloan (2002a). Sloan (2013) analysed extensive literature related to the advancement of the finite element limit analysis theorem and its application to geotechnical stability analysis. A number of practical examples were presented covering; slopes, excavations, anchors, foundations and tunnels.

### 3.3 Gravity Multiplier Method

The gravity multiplier method (GMM) is an inbuilt method of analysis within the FE limit analysis software. Like its name suggests, it operates by increasing the gravity constant ( $g$ ) gradually until a state of failure is reached. All other parameters remain the same and the factor by which the gravity is multiplied to cause failure is equivalent to the factor of safety. When using the gravity multiplier method the factor of safety can be defined as shown in Equation 3.1.

$$\text{Factor of Safety (FoS)} = \frac{g_{cr}}{g} \quad (3.1)$$

where  $g_{cr}$  = the gravitational acceleration at failure [ $m/s^2$ ]; and  
 $g$  = the actual gravitational acceleration =  $9.81[m/s^2]$ .

The gravity multiplier method is not overly labour intensive on the computer's processor, allowing for a fast and generally rather accurate solution when the pressure ratio equals zero. This method was used alongside, and compared to, the strength reduction method

when computing the factor of safety bounds for tunnel heading problems with varying pressure ratios.

### 3.4 Strength Reduction Method

The strength reduction method (SRM) is not dissimilar to the gravity multiplier method. When using the strength reduction method the strength properties of the soil are incrementally decreased until a limit of failure is reached. All other model and loading parameters remain the same and the factor by which the soil's strength is reduced is equivalent to the factor of safety. When using the strength reduction method the factor of safety can be defined as shown in Equation 3.2.

$$\text{Factor of Safety (FoS)} = \frac{S_u}{S_{u.cr}} \quad (3.2)$$

where  $S_u = \text{original undrained shear strength of the soil [N/m}^2\text{]}; \text{ and}$   
 $S_{u.cr} = \text{undrained shear strength of the soil at failure [N/m}^2\text{]}.$

Many other finite element programs such as Plaxis and FLAC also utilise the strength reduction method. Tschuchnigg, Schweiger and Sloan (2015) described the strength reduction technique as a displacement-based finite element method and noted that a reasonable agreement is usually made between strength reduction methods and FELA methods for slope stability problems. When using Mohr-Coulomb soil properties the strength properties that are reduced are the cohesive strength and the internal angle of friction. If Tresca material properties are assumed, as they are in this study, the strength reduction process is simplified and only the cohesive strength of the soil is decreased, as the internal angle of friction is already equal to zero when dealing with undrained clay. The strength reduction method has seen extensive use in slope stability analysis and is growing in popularity and acceptance for tunnel stability analysis. Cai, Ugai and Hagiwara (2002) compared the finite element strength reduction method to the limit equilibrium method for circular excavations in soft clay and found the two to have a good degree of agreement. Huang, et al. (2012) again used the strength reduction method to investigate the stability of shallow tunnels in a saturated soil medium and validated their initial results by comparing to other published results. The strength reduction method will be used extensively in this study to investigate the factor of safety for shallow tunnel headings where the pressure ratio is less than, equal to and greater than zero.

### 3.5 Optum G2 Modelling

Optum G2 is a finite element limit analysis software program designed to solve geotechnical problems. The program contains a myriad of features for solving simple problems right through to complex multi-staged projects. Upon opening the program the user will be greeted with a screen similar to the one shown in Figure 3.1. The pop-up in the foreground contains the option to start a new project, load an existing one, access the user manual, watch a number of instructional videos or run a variety of preprogrammed examples. The design grid is in the background with the stage, properties, project and customisation manager to the right, with the taskbar containing the four functional tabs; geometry, materials, features and results, above.

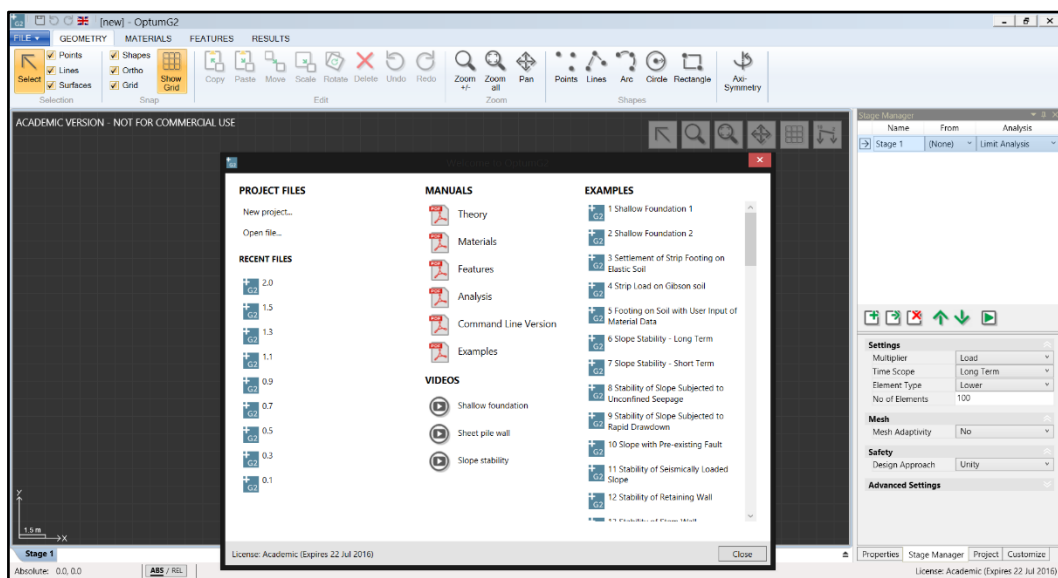


Figure 3.1: Optum G2 opening screen (Optum Computational Engineering 2016).

The first step is to model the geometry of the problem. The geometry tab contains a number of options such as; point, line, arc, circle and rectangle to create the 2D model. All points are assigned their own number and co-ordinates and can be manually inputted or snapped to pre-existing nodes. Familiar tools; copy, paste, move, scale, rotate, delete, undo and redo are used to finish the model geometry and make any necessary changes. Buttons on the design grid give the user the ability to select, zoom in and out, zoom to selection, pan and turn the gridlines on and off. Figure 3.2 demonstrates the input of geometry using different tools.

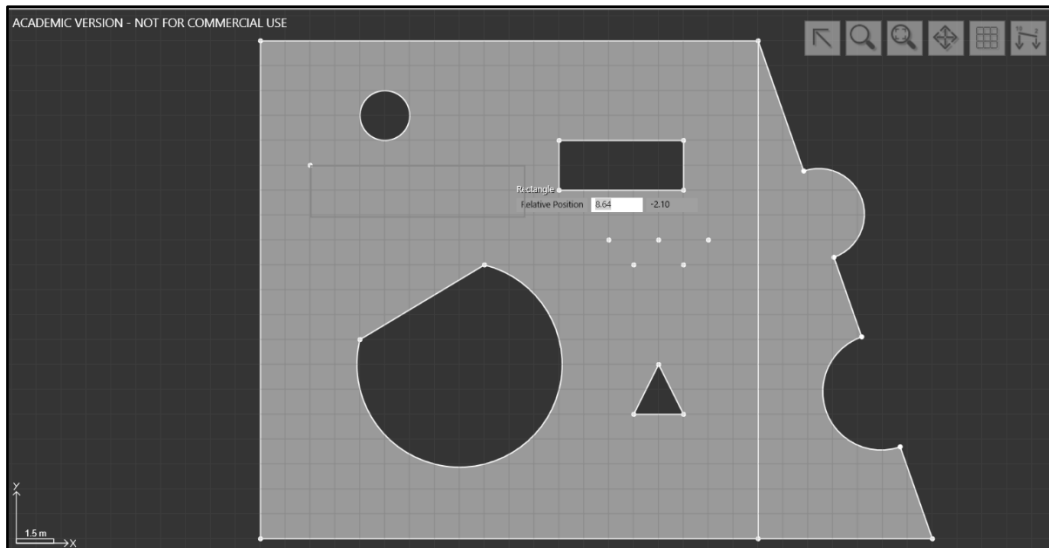


Figure 3.2: Geometrical model demonstrating the different tools available (Optum Computational Engineering 2016).

Once the model geometry has been established, the materials can be chosen. The program comes with a broad range of pre-programmed materials but it is also possible to input a new material. There are eight different categories of materials available; solids, fluids, plates, connectors, geogrids, hinges, pile rows and nail rows. The solid category is used to represent materials such as soil, concrete and rock. A number of soil modelling options are available including Mohr-Coulomb (MC) and Tresca. MC materials assume linear elasticity and exhibit a yield function dependant on the cohesive strength ( $c$ ) and angle of friction of the soil ( $\phi$ ). There is a wide variety of predefined Mohr Coulomb materials including; soft clay, firm clay, stiff clay, loose sand, medium sand and dense sand. Tresca materials are dependent only on undrained shear strength ( $S_u$ ). Once the desired material type has been chosen, a number of properties related to that material can be manually varied in the 'Properties' bar that appears on the right hand side of the screen. For a Mohr-Coulomb material these variable properties include; drainage, stiffness, strength, flow rule, tension cut-off, compression cap, fissures, unit weight, initial conditions and hydraulic model. For a Tresca material these variable properties are limited to; stiffness, strength, tension cut-off, unit weight, initial conditions and hydraulic conductivity. A simple model with multiple soil layers is shown in Figure 3.3.

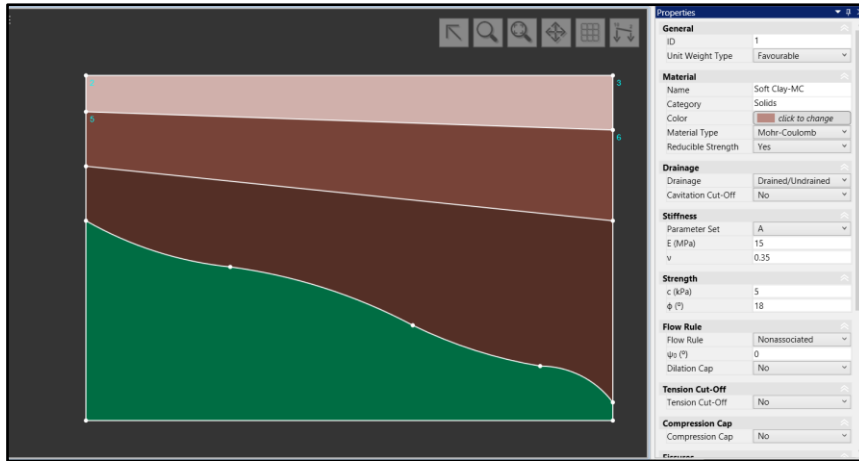


Figure 3.3: Model showing a number of different material layers (Optum Computational Engineering 2016).

The features tab allows the user to set; flow BC, consolidation BC, boundaries, fixed loads, multiplier loads, anchors and connectors, soil support, mesh size and the focus section. It is necessary to set boundary conditions to prevent the model from moving in the ‘x’ or ‘y’ directions. A ‘full’ support prevents the model from moving in all directions, while a ‘normal’ support only prevents movement in the parallel direction and a ‘tangential’ support only prevents movement in the perpendicular direction. A fixed load is applied to represent constant loads such as surcharge on the soil or permanent internal tunnel support. A multiplier load is applied with a unit load to allow the solver to amplify the load until a state of failure is reached, this feature can be used to find the limiting load on a soil structure. A water table or fixed pressure can be easily added at this stage along with any soil supports such as anchors, geogrids, piles and soil nails. Figure 3.4 shows the mesh of a model with boundary conditions and a distributed surcharge pressure applied.

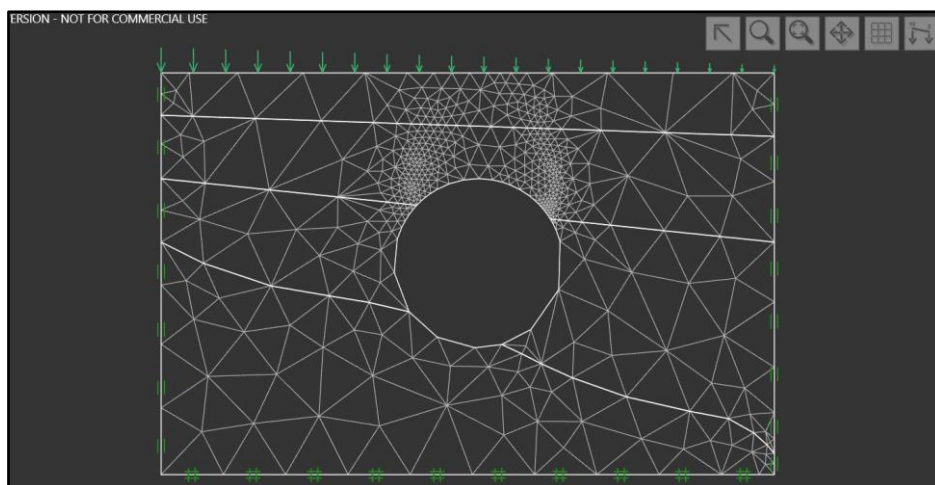


Figure 3.4: Mesh view of a model with boundary conditions and a fixed distributed pressure (Optum Computational Engineering 2016).

The stage manager can be selected from the tabs towards the bottom right of the screen. It is here that the analysis is set up and a multi-staged project can be created. The drop-down box titled ‘analysis’ is used to select the type of analysis to be performed, options include; limit analysis, strength reduction, mesh, seepage, initial stress, elastic, elastoplastic, multiplier elastoplastic and consolidation. This research focuses on using only the limit analysis and strength reduction options. Selecting limit analysis allows the user to choose either a gravity or load multiplier, while selecting strength reduction allows the user to choose whether the strength of the solids or structures will be reduced. Both methods require that a time scope be chosen, either short or long term, to indicate whether the changes to the model will happen immediately or over a longer period of time. When analysing a problem in undrained clay it is necessary to use a long term analysis, but for sand, gravel or other coarse materials a short and long term analysis should be assigned to fully evaluate the problem. The element type can be set to upper, lower, six or fifteen element Gauss or a custom user specified element type. This study will focus on using only the lower and upper element types to ascertain the upper and lower bound factor of safety values. The number of elements in the initial mesh can be defined to influence the accuracy of the solution. Mesh adaptivity is a feature unique to Optum G2 and is used to perform adaptive mesh iterations to refine the failure mechanism and further increase the accuracy of results. For the gravity reduction and strength reduction methods it is recommended that at least three iterations be adopted along with shear dissipation as the adaptivity control (Optum CE 2013). The design approach can be set to provide a key factor of safety based on design codes but will be ignored and left as the default unity setting for this research. Figure 3.5 shows the stage manager.

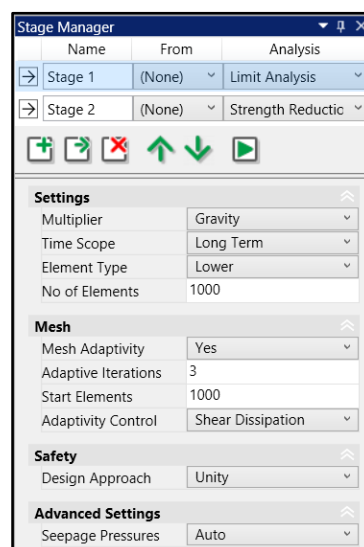
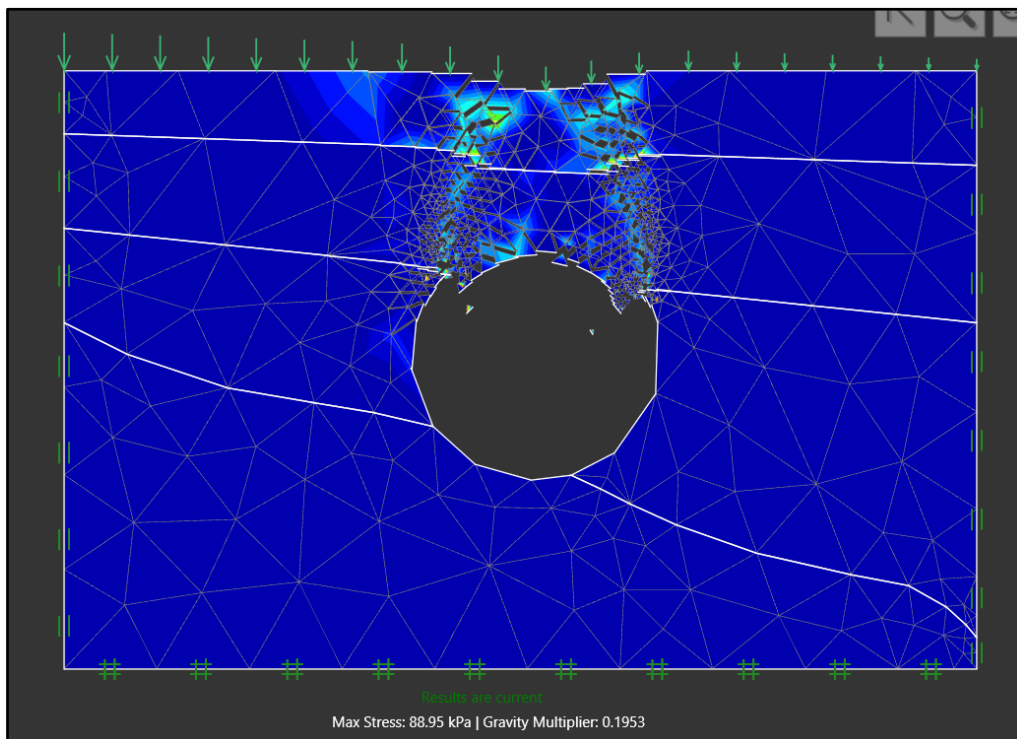


Figure 3.5: Stage manager window displaying the options for a limit analysis (Optum Computational Engineering 2016).

Once the analysis has been performed through the stage manager window the outcome will be displayed in a pop-up screen and can be examined further through the results tab. A number of options are available to plot different features such as; displacement, strain, stress, material parameters, plastic multiplier, yield function and shear dissipation. An animation can be run to demonstrate the failure mechanism of the model. Results can be graphed, exported, generated in a report or viewed through a log. Figure 3.6 shows the results for a model that has been analysed using the lower bound gravity multiplier method, found under the limit analysis category. The animation of the model is shown at approximately eighty percent deformation scale with the mesh and plastic multiplier overlaid.



*Figure 3.6: Solved model with deformation scale at eighty percent & plastic multiplier shown (Optum Computational Engineering 2016).*

### **3.6 Optum G2 Slope Example**

A basic slope stability example will be presented and detailed using the Optum G2 software to show the power and simplicity of the software. The procedure employed involves; create the geometric slope model and define any material layers, define supports/restraints, select materials, apply loading, run analysis and investigate results. A one is to one slope with

varying material layers will be analysed in this example to highlight the potential and simplicity of the software.

1. Create the geometrical model, defining any desired material layering.

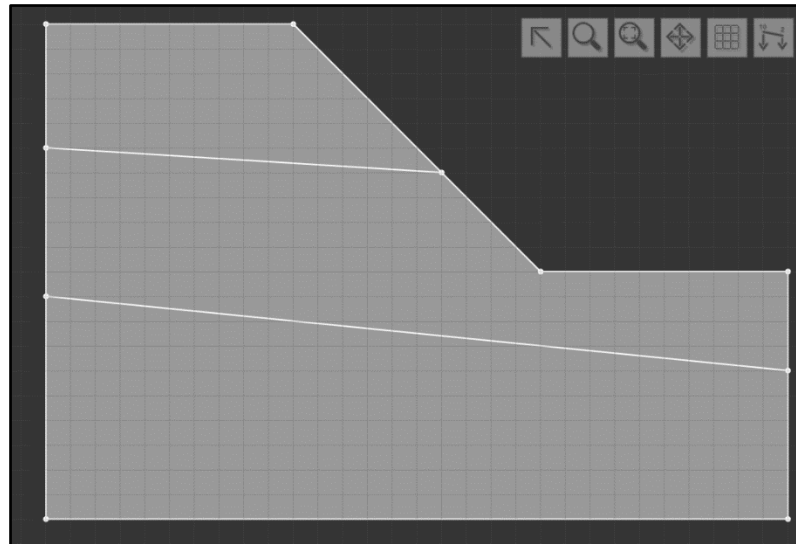


Figure 3.7: Geometrical model of slope stability problem (Optum Computational Engineering 2016).

2. Define the restraints for the geometrical model so that the model as a whole is not able to move in the horizontal and vertical plane. Full restraints have been assigned to the base and sides of the model to prevent movement.

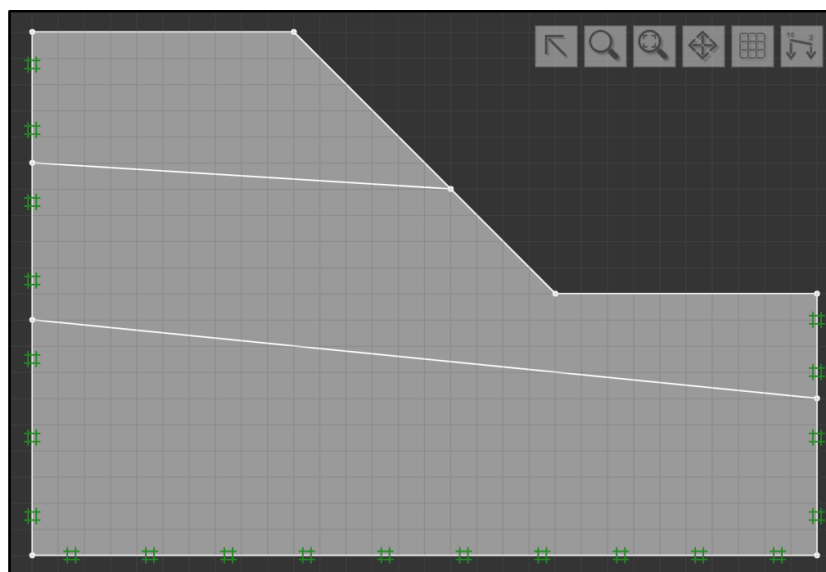


Figure 3.8: Full restraints applied to the geometrical model (Optum Computational Engineering 2016).

3. Select the materials required for each layer. In this case Soft Clay-MC, Firm Clay-MC and Stiff Clay-MC were chosen in the order of top to base layer.

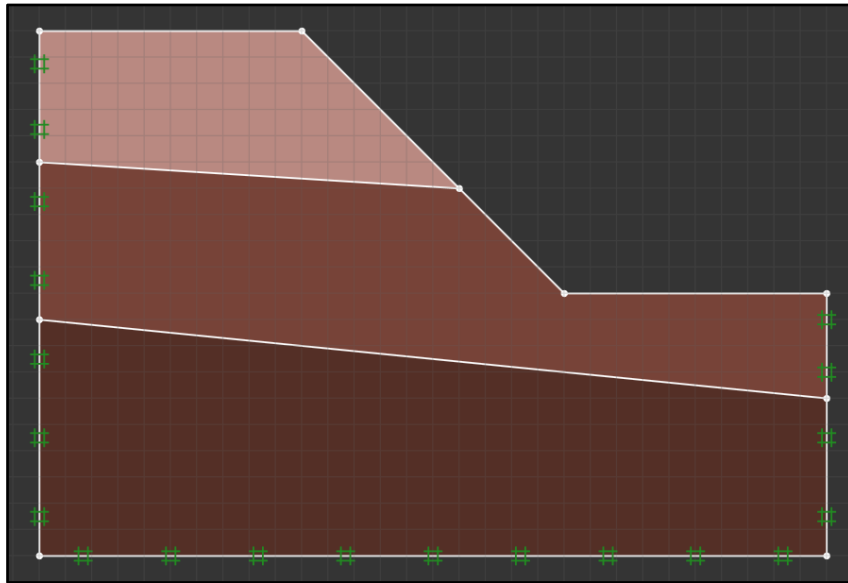


Figure 3.9: Material types assigned to layers (Optum Computational Engineering 2016).

4. Apply loading conditions to the model. In this case a uniform surcharge of 10kPa will be applied.

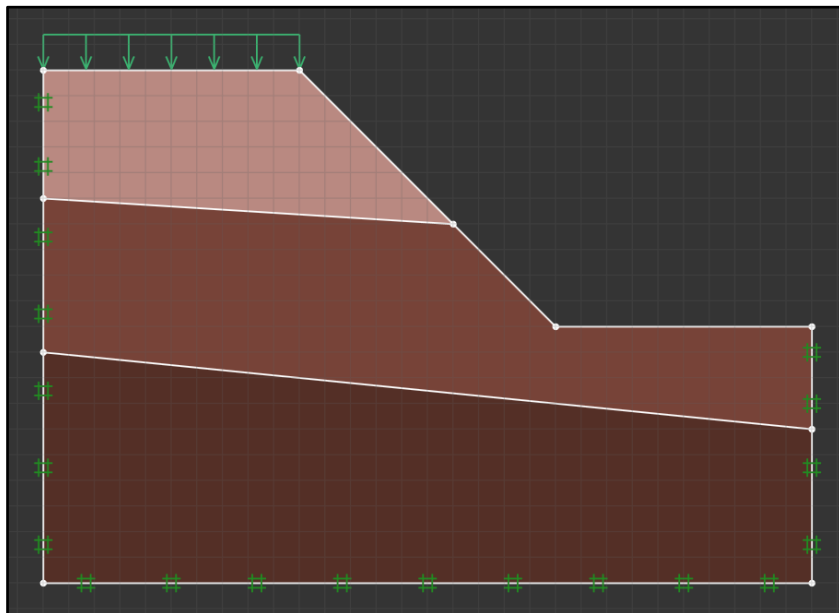


Figure 3.10: 10kPa surcharge pressure applied to model (Optum Computational Engineering 2016).

- Determine the type of analysis to be conducted and set up the stage manager accordingly. A lower and upper bound analysis using the strength reduction method (SRM) has been chosen in this example.

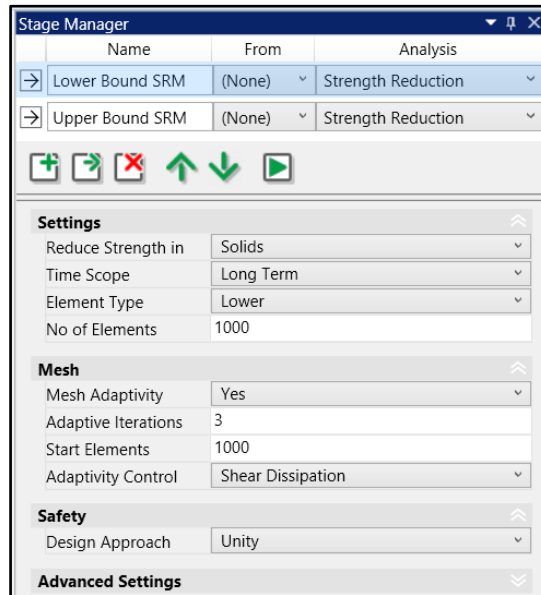


Figure 3.11: Stage Manager for upper and lower bound SRM (Optum Computational Engineering 2016).

- Run analysis and view results log.

ADAPT STEP	ITR	REDUCTION FACTOR	STABILITY
1	1	1.000E+00	Unstable
1	2	5.000E-01	Stable
1	3	7.500E-01	Stable
1	4	8.750E-01	Unstable
1	5	8.125E-01	Stable
1	6	8.438E-01	Unstable
1	7	8.281E-01	Stable
1	8	8.359E-01	Unstable
1	9	8.320E-01	Unstable
1	10	8.301E-01	Unstable
1	11	8.291E-01	Stable
2	1	8.291E-01	Unstable
2	2	7.603E-01	Stable
2	3	7.947E-01	Unstable
2	4	7.775E-01	Stable
2	5	7.861E-01	Unstable
2	6	7.818E-01	Unstable
2	7	7.796E-01	Stable
3	1	7.796E-01	Unstable
3	2	7.599E-01	Stable
3	3	7.698E-01	Stable
3	4	7.747E-01	Unstable
3	5	7.722E-01	Stable

No OF TRIANGLES = 904  
 No OF EDGES = 1444  
 No OF NODES = 479  
 BEST STRENGTH REDUCTION FACTOR = 0.775

Figure 3.12: Results log displaying upper bound FoS calculation (Optum Computational Engineering 2016).

7. Analyse the results to determine a range of important information including; method of failure, max stresses, max shear and displacement.



Figure 3.13: Results of slope stability analysis showing fifty percent deformation and the plastic multiplier (Optum Computational Engineering 2016).

This basic example has illustrated how to perform a slope stability analysis on a simple slope with varying soil layers and a surcharge pressure in Optum G2. The process for analysing a tunnel problem is very similar and will be demonstrated in the following example.

### 3.7 Optum G2 Tunnel Heading Example

Analysing a tunnel heading problem in Optum G2 is achieved in a similar fashion to a slope stability problem. The basic procedure consists of; create the geometric tunnel heading model and define any material layers, define supports/restraints, select materials, apply loading, run analysis and investigate results. A two-dimensional tunnel heading problem with an equivalent surcharge and internal pressure, hence a pressure ratio equal to zero, will be analysed in this example to display all features of the modelling process utilised throughout this project.

1. Create the geometrical model, defining any desired material layering. For this example a depth ratio of two has been chosen, meaning the tunnel diameter is six metres and the cover above the tunnel is twelve metres. The model must be designed large enough so that boundary conditions do not adversely influence results.

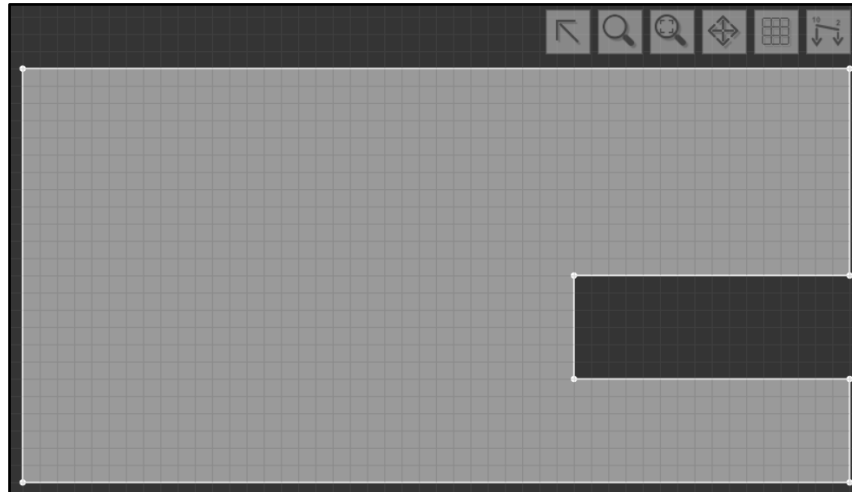


Figure 3.14: Geometrical model for tunnel heading problem with depth ratio equals two (Optum Computational Engineering 2016).

2. Define the restraints for the geometrical model so that the model as a whole is not able to move in the horizontal and vertical plane. Full restraints have been assigned to the base and sides of the model while normal restraints are assigned to the roof and base of the tunnel excavation. The heading face has no restraints.

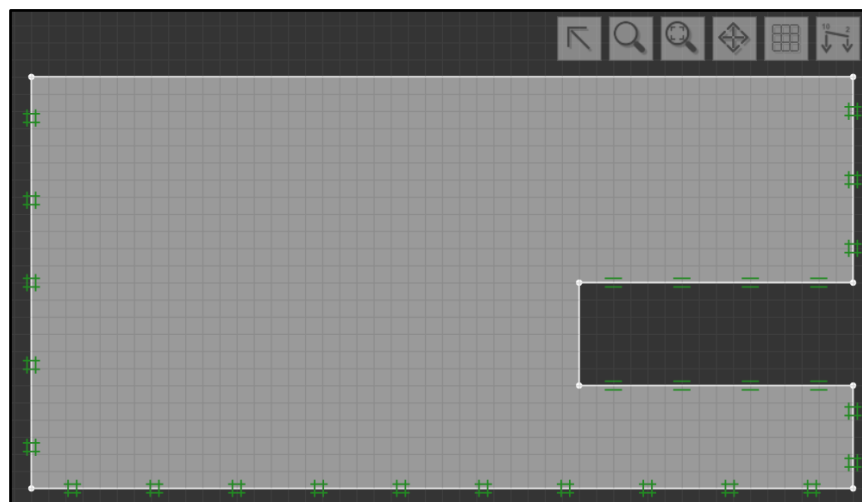


Figure 3.15: Tunnel heading stability model restraints (Optum Computational Engineering 2016).

3. Assign materials to all layers of the model. This example assumes that the entire soil medium is homogeneous so will use only one material type. The chosen material is a Tresca Basic material with a specific weight of  $18\text{kN/m}^2$  and an undrained shear strength of  $97.2\text{kPa}$ , resulting in a strength ratio of 0.9 when normalised to diameter.

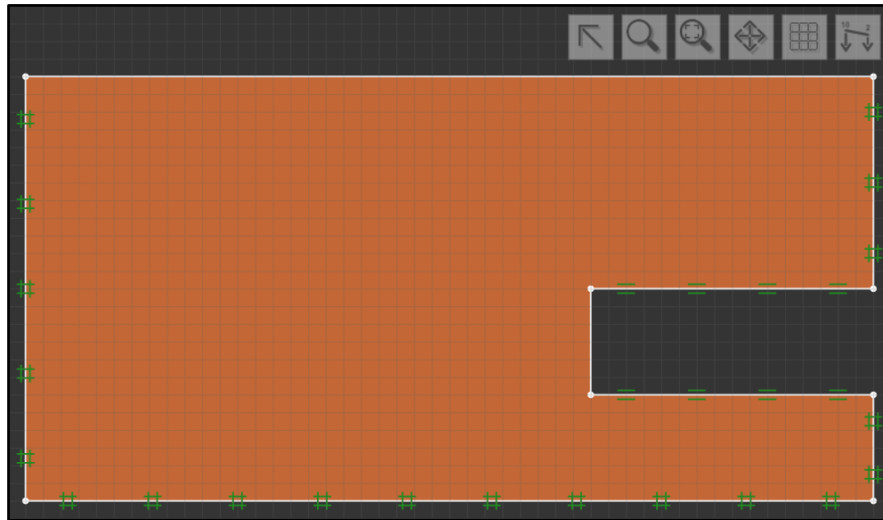


Figure 3.16: Material type assigned to tunnel heading example (Optum Computational Engineering 2016).

4. Apply loading conditions to the model. In this case a surcharge pressure of  $50\text{kPa}$  and an internal tunnel pressure of  $50\text{kPa}$  will be applied, resulting in a pressure ratio equal to zero.

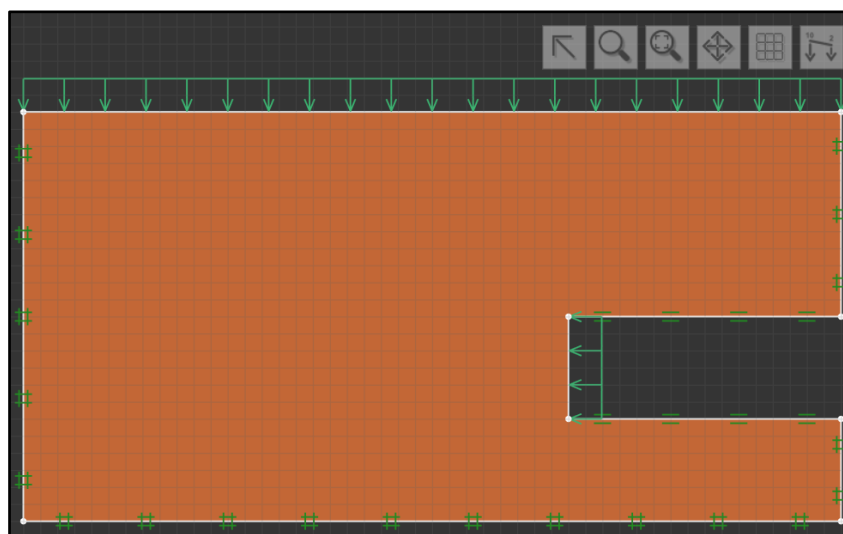


Figure 3.17:  $50\text{kPa}$  surcharge and internal tunnel pressure applied to tunnel heading model example (Optum Computational Engineering 2016).

- Determine the type of analysis to be conducted and set up the stage manager accordingly. A lower and upper bound analysis using the strength reduction method (SRM), followed by an upper and lower bound analysis using the gravity multiplier method has been established in this example.

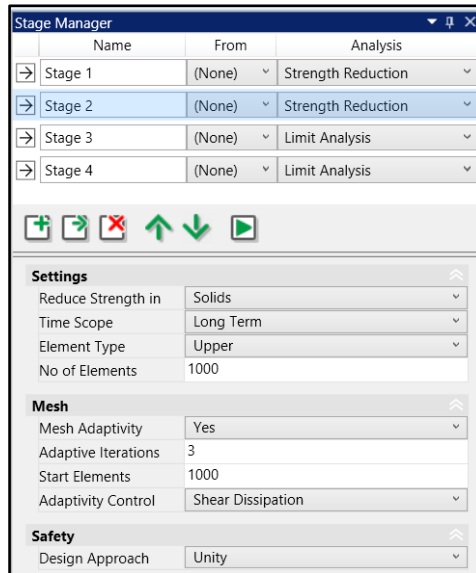


Figure 3.18: Stage manager for upper and lower bound SRM and GMM (Optum Computational Engineering 2016).

- Run analysis and view results log.

```

=====
STAGE:                               Stage 3
ANALYSIS TYPE:                       Limit Analysis
ELEMENT TYPE:                         Lower
TIME SCOPE:                           Long Term
=====
ADAPT  ITR          COLLAPSE      SOLVER STATUS
STEP   STEP          MULTIPLIER
-----
1      1            1.781E+00   Converged
2      1            1.824E+00   Converged
3      1            1.839E+00   Converged
=====
No OF TRIANGLES = 958
No OF EDGES    = 1466
No OF NODES    = 509
COLLAPSE MULTIPLIER = 1.839
=====
STAGE:                               Stage 4
ANALYSIS TYPE:                       Limit Analysis
ELEMENT TYPE:                         Upper
TIME SCOPE:                           Long Term
=====
ADAPT  ITR          COLLAPSE      SOLVER STATUS
STEP   STEP          MULTIPLIER
-----
1      1            2.109E+00   Converged
2      1            2.006E+00   Converged
3      1            1.979E+00   Converged
=====
No OF TRIANGLES = 1039
No OF EDGES    = 1590
No OF NODES    = 552
COLLAPSE MULTIPLIER = 1.979
=====

```

Figure 3.19: Results log showing upper and lower bound GMM results (Optum Computational Engineering 2016).

7. Analyse the results to determine a range of important information including; method of failure, displacement, max stresses and max strain.

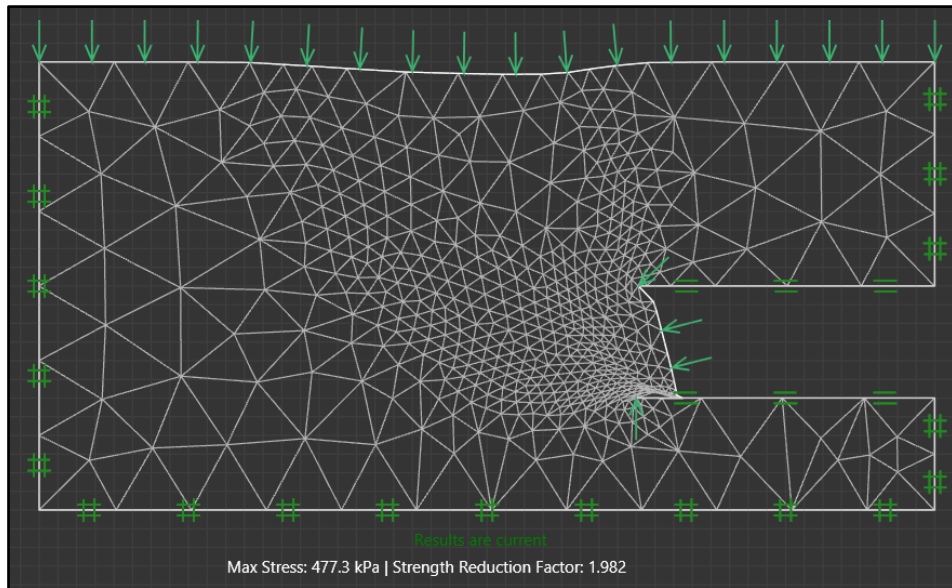


Figure 3.20: Upper bound SRM results of tunnel heading example showing fifty percent deformation with mesh overlay (Optum Computational Engineering 2016).

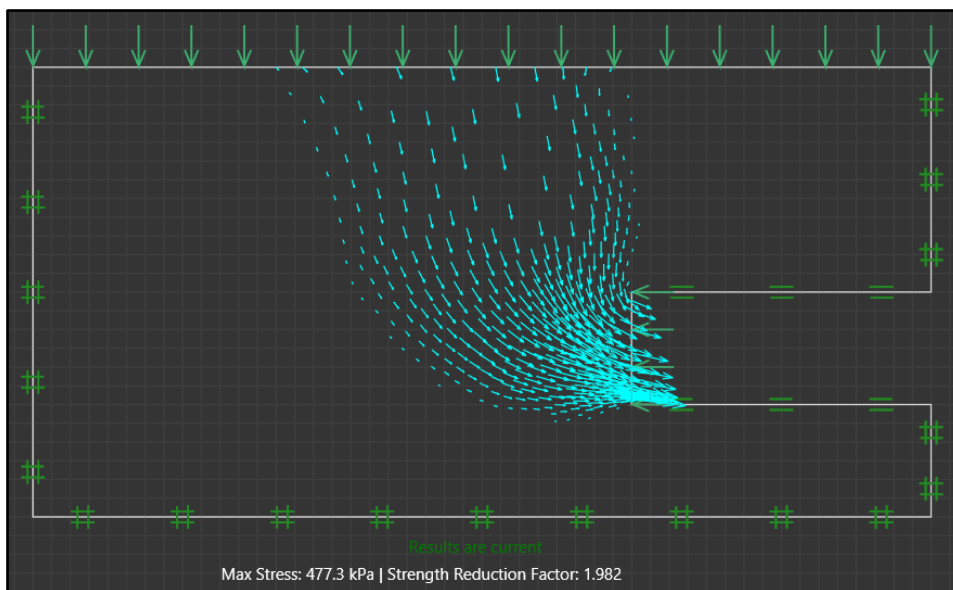


Figure 3.21: Upper bound SRM results of tunnel heading example showing displacement vectors (Optum Computational Engineering 2016).

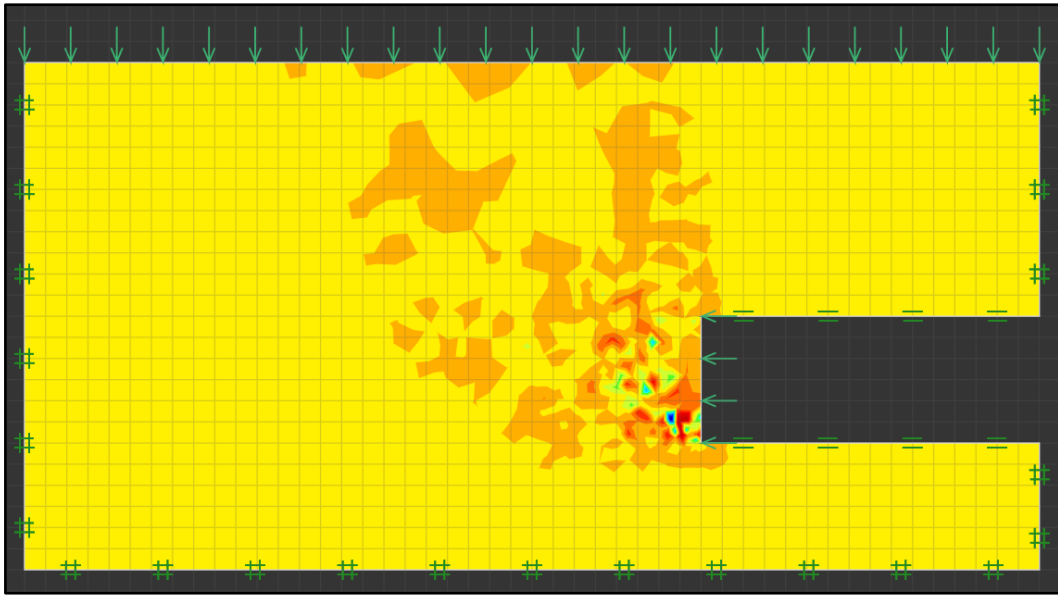


Figure 3.22: Upper bound SRM results of tunnel heading example showing shear strain (Optum Computational Engineering 2016).

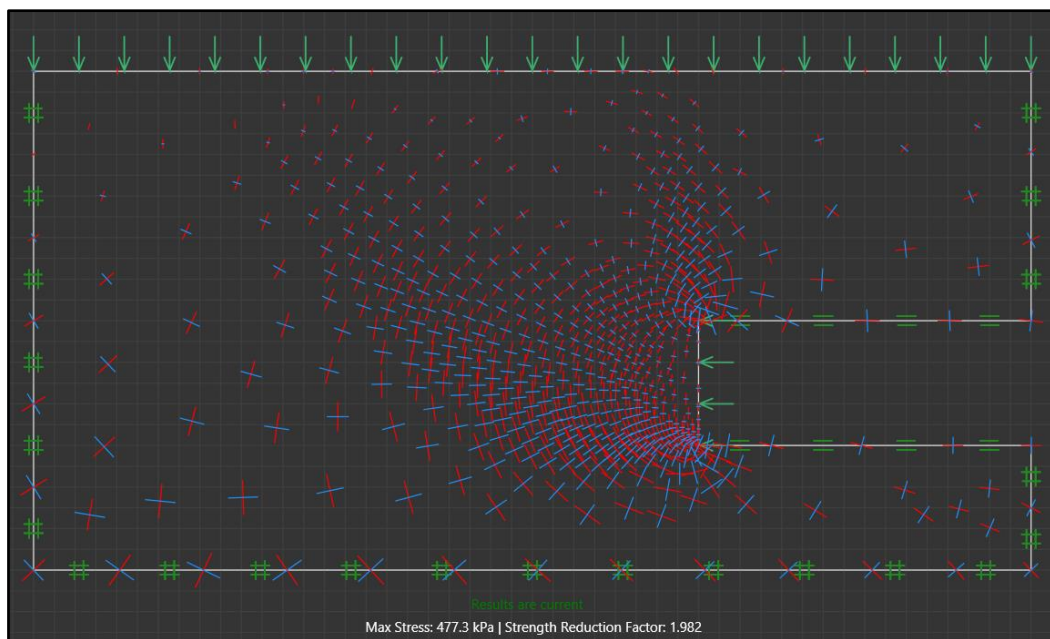


Figure 3.23: Upper bound SRM results of tunnel heading example showing  $\sigma_1$ ,  $\sigma_2$  vectors (Optum Computational Engineering 2016).

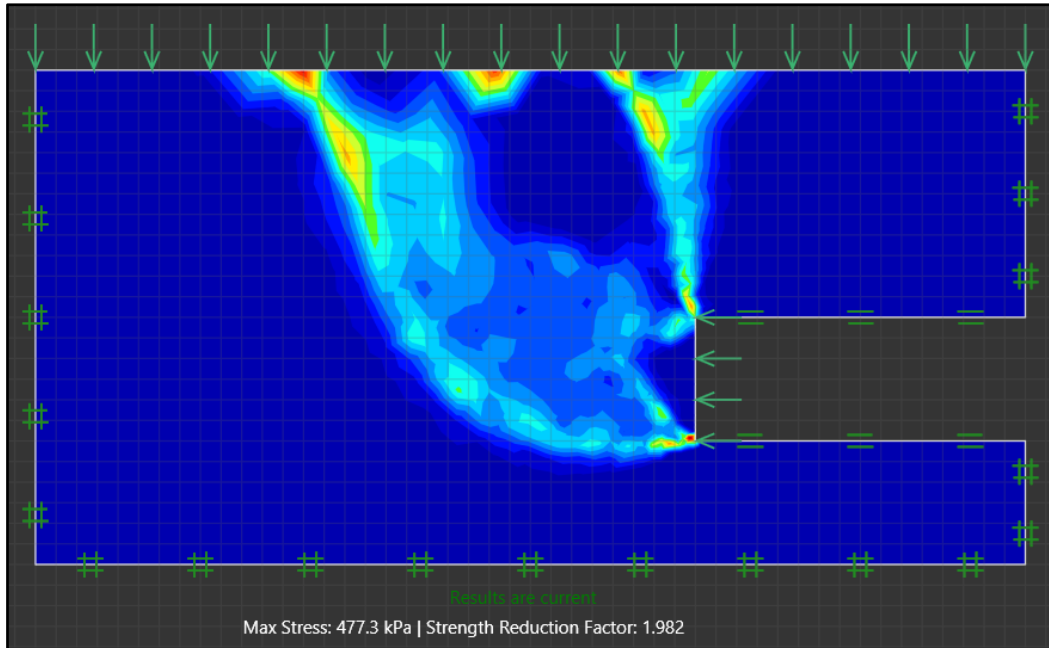


Figure 3.24: Upper bound SRM results of tunnel heading example showing plastic multiplier (Optum Computational Engineering 2016).

This basic example has illustrated how to perform a multi-stage stability analysis on a simple tunnel heading problem with a surcharge and internal tunnel pressure in Optum G2. A similar process was followed to develop all models in this project, with this example displaying all of the functions utilised throughout. To provide a greater understanding of two-dimensional tunnel heading problems the full problem statements are detailed in Chapters 4, 5 and 6. The results achieved from this type of analysis can be used to further investigate the nature of the failure and to ultimately develop stability design charts.

# CHAPTER 4:

## TUNNEL HEADING ANALYSIS:

### COLLAPSE

#### 4.1 Introduction

As the world's population grows and available space on the Earth's surface decreases it is becoming increasingly necessary to construct subterranean infrastructure. As the need for tunnels increases so too does the required complexity of tunnelling projects. Tunnels present a unique challenge for engineers, who must assess the stability of prospective tunnels and the settlement of the Earth's surface that could be caused by the tunnelling process. The safe design of tunnels is critical, especially in urban areas where a shallow void must pass under existing infrastructure sensitive to ground movement. Downward movement or collapse is the most common and easily understood tunnel failure mechanism. This chapter will address the tunnel heading stability problem for collapse by using Optum G2 to compute the upper and lower bound factor of safety values for a number of different scenarios. The relationship between the factor of safety and the three dimensionless parameters; depth ratio, strength ratio and pressure ratio, will be discussed with a focus on the collapse failure mechanism.

#### 4.2 Problem Statement

In reality, tunnels are complex three-dimensional underground structures, however for the purpose of stability analysis they can be simplified to a basic two-dimensional model. The longitudinal section of the tunnel heading will be modelled under two-dimensional plane strain conditions. The undrained clay soil medium will be represented by a homogeneous Tresca material, which has an undrained shear strength ( $S_u$ ) and unit weight ( $\gamma$ ). The cover above the tunnel ( $C$ ) and the height of the tunnel ( $D$ ) are the important dimensional parameters needed to create the model. The surcharge pressure ( $\sigma_s$ ) and internal tunnel pressure ( $\sigma_i$ ) are varied to test the stability of the model under a number of different pressure ratios capable of inducing failure by collapse. Figure 4.1 defines the tunnel heading stability problem.

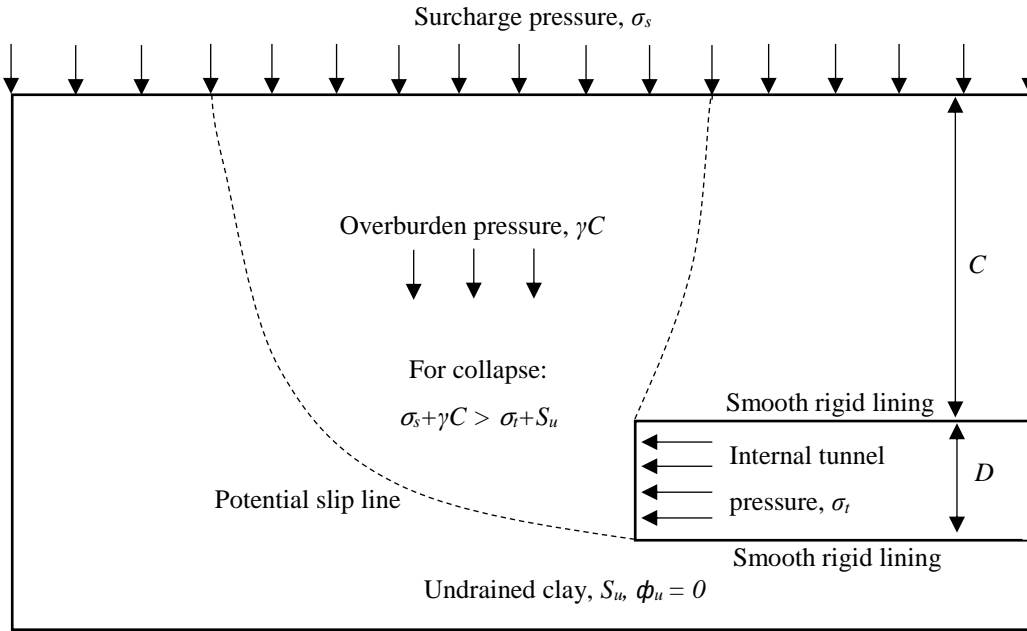


Figure 4.1: Tunnel heading stability problem statement.

Figure 4.1 presents a conceptual model of the tunnel heading problem making it possible to comprehend the three important dimensionless variable parameters. The depth ratio ( $DR$ ), shown in Equation 4.1, relates the geometrical properties of the model, tunnel height and tunnel cover. To represent shallow tunnelling conditions the depth ratio was varied between 1 and 3 in increments of one. Tunnel height remained constant at 6m while cover was varied.

$$\text{Depth Ratio } (DR) = \frac{C}{D} \quad (4.1)$$

where  $C = \text{cover above tunnel [m]}$ ; and  
 $D = \text{height of tunnel excavation [m]}$ .

The strength ratio ( $SR$ ) can be represented in two different ways for this problem. The soil strength can be normalised to either the cover ( $C$ ), as shown in Equation 4.2, or the tunnel height ( $D$ ), as shown in Equation 4.3. Both formulations of the strength ratio were tested for this project and it was found that normalising the strength ratio to the tunnel height ( $D$ ), as shown in Equation 4.3, produced the clearest and most effective results. To cover a broad range of practical scenarios the strength ratio ( $S_u/\gamma D$ ) is varied between 0.10 and 2.00 in increments of 0.20 up to 1.50 and then a final increment of 0.50. Unit weight and tunnel height were kept constant at  $18\text{kN/m}^3$  and 6m respectively while undrained shear strength was varied.

$$\text{Strength Ratio (SR)} = \frac{S_u}{\gamma C} \quad (4.2)$$

$$\text{Strength Ratio (SR)} = \frac{S_u}{\gamma D} \quad (4.3)$$

where  $S_u = \text{undrained shear strength of soil [N/m}^2\text{]}; \text{ and}$   
 $\gamma = \text{unit weight of soil [N/m}^3\text{]}.$

The third dimensionless variable to be considered is the pressure ratio (*PR*). Classically this parameter has been defined as the load parameter but has been redefined as the pressure ratio in this project for simplicity and uniformity. The pressure ratio, shown in Equation 4.4, can be defined as the resultant applied pressure, be that a surcharge or internal tunnel pressure, compared to the undrained shear strength of the soil. To produce an acceptable range of data for modelling purposes the pressure ratio was varied between -16 and +10 with a focus on points ranging between -1.5 and +10 when analysing the collapse failure mechanism.

$$\text{Pressure Ratio (PR)} = \frac{\sigma_s - \sigma_t}{S_u} \quad (4.4)$$

where  $\sigma_s = \text{the applied surcharge pressure [N/m}^2\text{]}; \text{ and}$   
 $\sigma_t = \text{the applied internal tunnel pressure [N/m}^2\text{]}.$

The upper and lower bound factor of safety values are a function of these three dimensionless parameters and can therefore be expressed as shown in Equation 4.5.

$$\text{Factor of Safety (FoS)} = f\left(\frac{C}{D}, \frac{S_u}{\gamma D}, \frac{\sigma_s - \sigma_t}{S_u}\right) \quad (4.5)$$

To gain a basic understanding of tunnel stability it is beneficial to first focus on a case where the pressure ratio is equal to zero. A pressure ratio of zero represents Greenfield conditions and means that the factor of safety is simplified to a function of only the depth ratio and strength ratio as shown in Equation 4.6.

$$\text{Factor of Safety (FoS)} = f\left(\frac{C}{D}, \frac{S_u}{\gamma D}\right) \quad (4.6)$$

In previous tunnel heading stability literature the results and design charts are not expressed in a factor of safety format. They are generally represented as a stability number, which is a function of a particular depth ratio and strength ratio with a corresponding factor of safety of one. This stability number can generally cover a broader range of collapse failure scenarios when applied to a single design chart than a factor of safety approach, but is often confusing and somewhat impractical for practicing engineers interested in the factor of safety that a particular scenario can provide. As this stability number relates to a factor of safety of one it is defined as the critical pressure ratio ( $PR_c$ ) in this thesis. The approach used to calculate the critical pressure ratio is shown in Equation 4.7. The corresponding strength ratio, shown in Equation 4.8, is the inverse of the strength ratio adopted in this thesis, and is defined as the critical strength ratio ( $SR_c$ ) as it also only relates to a factor of safety of one. To find the critical pressure ratio and critical strength ratio, both the pressure ratio and strength ratio adopted in this thesis must be normalised by multiplying by the corresponding factor of safety.

$$PR_c = \frac{\sigma_s - \sigma_t}{S_u} * FOS \quad (4.7)$$

$$SR_c = \left( \frac{S_u}{\gamma D} \right)^{-1} * FOS \quad (4.8)$$

Other Tresca material properties that had a marginal effect on factor of safety results included; Poisson's ratio ( $\nu$ ) = 0.49 and Young's modulus ( $E$ ) = 30MPa. A graphical example of the collapse failure mechanism produced by Optum G2 is shown in Figure 4.2. The model represents a scenario with depth ratio of two, strength ratio of 1.10 and pressure ratio of positive ten and shows the plastic multiplier overlay with a deformation scale of sixty percent.

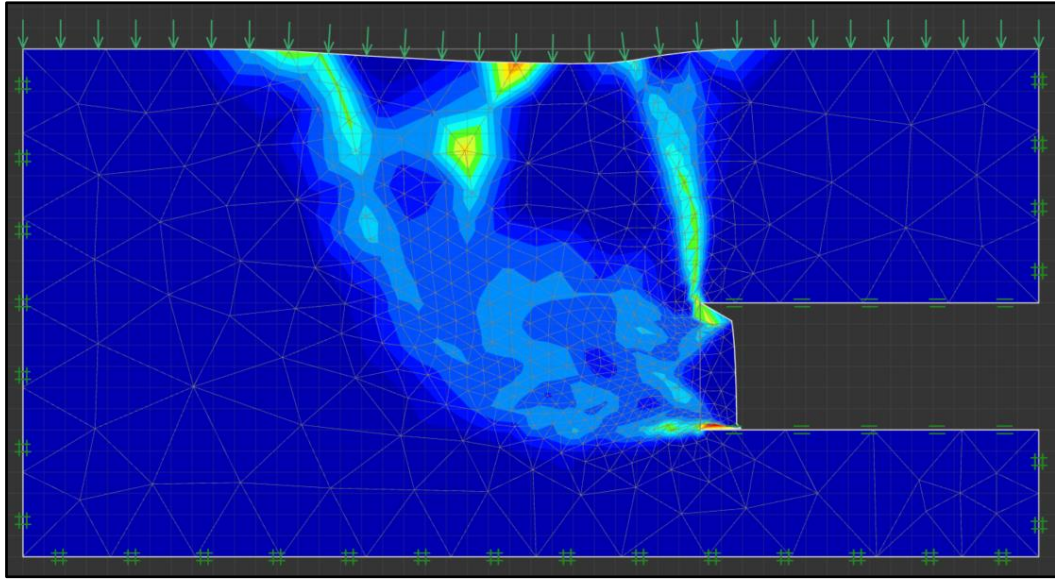


Figure 4.2: Example of collapse failure mechanism produced in Optum G2 showing plastic multiplier and 60% deformation scale.  $DR = 2$ ,  $SR = 1.10$ ,  $PR = +10$ .

### 4.3 2D Tunnel Heading Numerical Modelling

Due to the complex and uncertain behavior of soil, geotechnical investigations are a difficult undertaking. Numerical modelling techniques are continually improving and can now offer an accurate solution to such problems. Finite element limit analysis is an example of one such technique that has been used successfully in the past for modelling tunnels. This project employs the FELA technique through the relatively new program, Optum G2. The numerical procedures used in Optum G2 are based on the standard finite element method and the limit theorems of classical plasticity.

When creating the geometrical model it is important to consider the size of the domain. A model that is too small will not act as an infinite excavation and results will be affected by the boundary restraints, while a model that is too large will have excessive central processing unit (CPU) run time and produce less accurate results due to mesh dilution. The boundary conditions of the model are also very important to ensure that the model is restrained within space and that the only two surfaces that can displace are the ground surface and the face of the tunnel heading. The base and sides of the model were fully restrained in the 'x' and 'y' directions while the smooth rigid lining was restrained only in the normal direction to simulate a concrete lining. The size of the model was chosen so that these restraints had very little effect on the results. Figure 4.3 shows a typical two-dimensional finite element model of the tunnel heading problem.

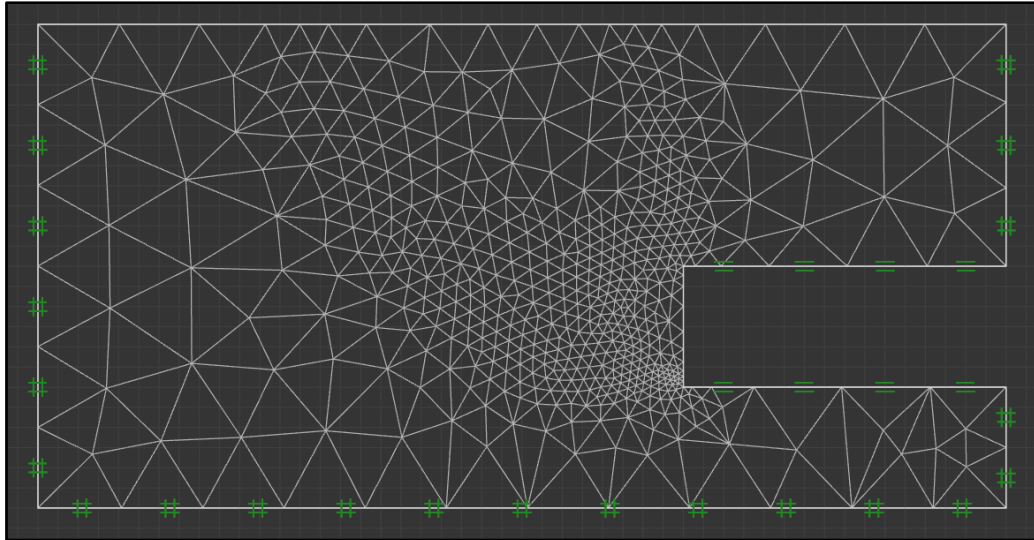


Figure 4.3: Tunnel heading finite element mesh with mesh adaptivity.

The number of finite elements was set at 1000 for all scenarios. Mesh adaptivity was enabled, allowing for three iterations with 1000 starting elements. Figure 4.3 displays this same scenario for a depth ratio of two. It can be seen that little mesh distortion occurs around the model boundaries meaning the boundaries have no noticeable impact on results.

Tunnel height ( $D$ ) of 6m and unit weight of the soil ( $\gamma$ ) of 18kN/m<sup>2</sup> were adopted as constant values for all scenarios. The depth ratio ( $C/D$ ) was varied from 1 to 3 by adjusting the cover ( $C$ ) by 6m each time. The undrained shear strength of the clay ( $S_u$ ) was varied incrementally from 10.8kPa to 216kPa to obtain strength ratios ( $S_u/\gamma D$ ) varying from 0.10 to 2.00. The strength ratio increased in increments of 0.20 up until the strength ratio of 1.50 is reached and then in one final increment of 0.50. The pressure ratio ( $(\sigma_s - \sigma_t)/S_u$ ) was varied from -16 to +10. While it is still possible for collapse to occur at all pressure ratios tested, the majority of points were focused in the range of negative two to positive ten for the collapse failure mechanism.

#### 4.4 Factor of Safety Bounds

Upper and lower bound factor of safety values were computed for the various scenarios by using the gravity multiplier method (GMM) and the strength reduction method (SRM). To perform an analysis using the gravity multiplier method the software incrementally increases the gravity by a multiplying factor until a state of failure is reached. The factor by which the gravity is multiplied can be taken as the factor of safety. For example, if the

gravity must be multiplied by three to cause failure then the factor of safety in this scenario is three. Equation 4.9 shows the formulation of the factor of safety from the gravity multiplier method.

$$\text{Factor of Safety (FoS)} = \frac{g_{cr}}{g} \quad (4.9)$$

where  $g_{cr}$  = the gravitational acceleration at failure [ $m/s^2$ ]; and  
 $g$  = the actual gravitational acceleration =  $9.81[m/s^2]$ .

To perform an analysis using the strength reduction method the software performs a number of iterations and incrementally varies the strength of the soil until an optimum state of failure is reached. Unlike the gravity multiplier method, the strength reduction method decreases the shear strength of the soil until failure is reached and then performs a number of iterations to work on optimizing this value until the exact failure multiplier is found. Similarly to the gravity multiplier method, the amount by which the strength of the soil is reduced to induce an optimum state of failure can be taken as the factor of safety. For example if the strength of the soil must be decreased by two times then the corresponding factor of safety value is two. Equation 4.10 shows the formulation of the factor of safety from the strength reduction method.

$$\text{Factor of Safety (FoS)} = \frac{S_u}{S_{u.cr}} \quad (4.10)$$

where  $S_u$  = original undrained shear strength of the soil [ $N/m^2$ ]; and  
 $S_{u.cr}$  = undrained shear strength of the soil at failure [ $N/m^2$ ].

Both the gravity multiplier method and strength reduction method were used to calculate the upper and lower bound factor of safety values for the majority of scenarios but to decide which method was capable of producing the most accurate results the two methods had to be compared. An internal comparison was performed to determine the accuracy of upper and lower bound results and to compare the factor of safety values produced by the gravity multiplier method and strength reduction method.

## 4.5 Internal Comparison of Collapse Results

To better understand the tunnel heading stability problem it is logical to initially set the pressure ratio equal to zero and investigate the problem under Greenfield conditions. Table 4.1 presents the results for a scenario where the pressure ratio is equal to zero. The percentage difference (*PD*) between the upper and lower bound results found by both the strength reduction method and gravity multiplier method have been calculated as per Equation 4.11. All lower and upper bound results calculated by the strength reduction method and gravity multiplier method are available in Appendix B – ‘Initial Results and Plots’.

$$\text{Percentage Difference (PD)} = ABS \left( \frac{UB \text{ FoS} - LB \text{ FoS}}{\text{Average FoS}} \right) * 100 \quad (4.11)$$

Table 4.1: SRM and GMM results obtained for PR = 0 with comparison of upper bound and lower bound.

Lower & Upper Bound FoS Comparison, PR = 0							
DR	SR	SRM LB	SRM UB	PD (%)	GMM LB	GMM UB	PD (%)
1	0.10	0.265	0.284	6.92	0.265	0.283	6.57
	0.30	0.793	0.851	7.06	0.795	0.850	6.69
	0.50	1.326	1.421	6.92	1.325	1.417	6.71
	0.70	1.857	1.984	6.61	1.855	1.984	6.72
	0.90	2.386	2.554	6.80	2.385	2.551	6.73
	1.10	2.909	3.127	7.22	2.915	3.118	6.73
	1.30	3.449	3.690	6.75	3.445	3.685	6.73
	1.50	3.974	4.252	6.76	3.975	4.252	6.73
	2.00	5.305	5.683	6.88	5.300	5.670	6.75
2	0.10	0.204	0.220	7.55	0.204	0.220	7.55
	0.30	0.610	0.660	7.87	0.613	0.660	7.38
	0.50	1.020	1.100	7.55	1.022	1.100	7.35
	0.70	1.427	1.541	7.68	1.430	1.540	7.41
	0.90	1.840	1.982	7.43	1.839	1.979	7.33
	1.10	2.242	2.422	7.72	2.248	2.419	7.33
	1.30	2.649	2.862	7.73	2.657	2.859	7.32
	1.50	3.056	3.303	7.77	3.065	3.299	7.35
	2.00	4.080	4.402	7.59	4.087	4.399	7.35
3	0.10	0.166	0.180	8.09	0.165	0.180	8.70
	0.30	0.499	0.541	8.08	0.496	0.541	8.68
	0.50	0.832	0.902	8.07	0.826	0.901	8.69
	0.70	1.166	1.263	7.99	1.157	1.262	8.68
	0.90	1.490	1.624	8.61	1.488	1.622	8.62
	1.10	1.825	1.984	8.35	1.818	1.982	8.63
	1.30	2.157	2.345	8.35	2.149	2.343	8.64
	1.50	2.498	2.708	8.07	2.479	2.703	8.65
	2.00	3.328	3.608	8.07	3.306	3.605	8.65

Table 4.1 shows that the upper and lower bound results obtained by both methods of analysis have a good level of agreement for all scenarios and show a constant percentage difference over the whole range of strength ratios for each depth ratio. It can be seen that the percentage difference between upper and lower bound results increases as the depth ratio increases. Figure 4.4 provides a graphical representation of the upper and lower bound results obtained through the strength reduction method while Figure 4.5 provides a graphical representation of the upper and lower bound results obtained through the gravity multiplier method. It can be seen that the factor of safety increases linearly with the strength ratio when the pressure ratio equals zero.

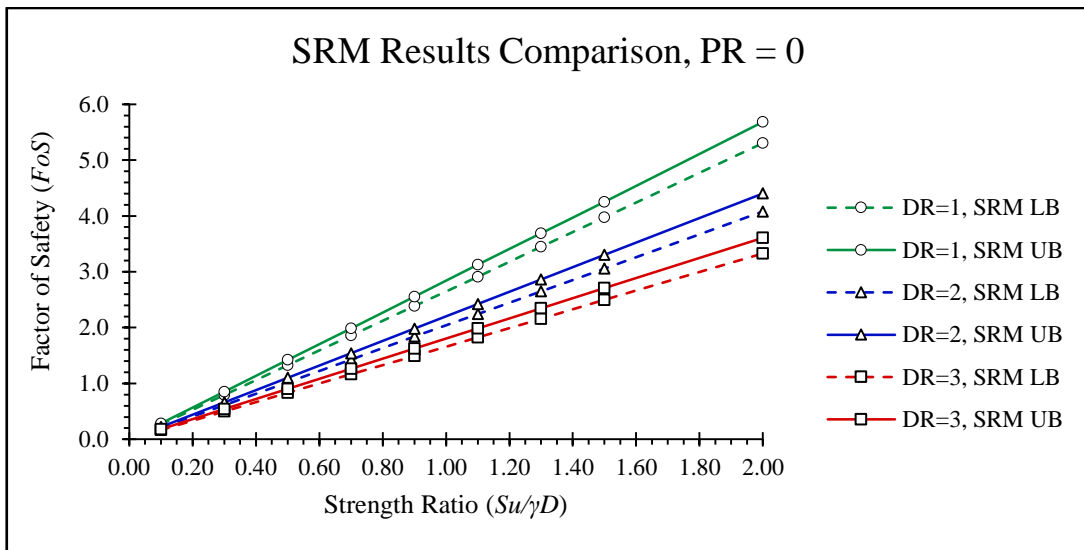


Figure 4.4: Graphical comparison of upper and lower bound results obtained through SRM for  $PR = 0$ .

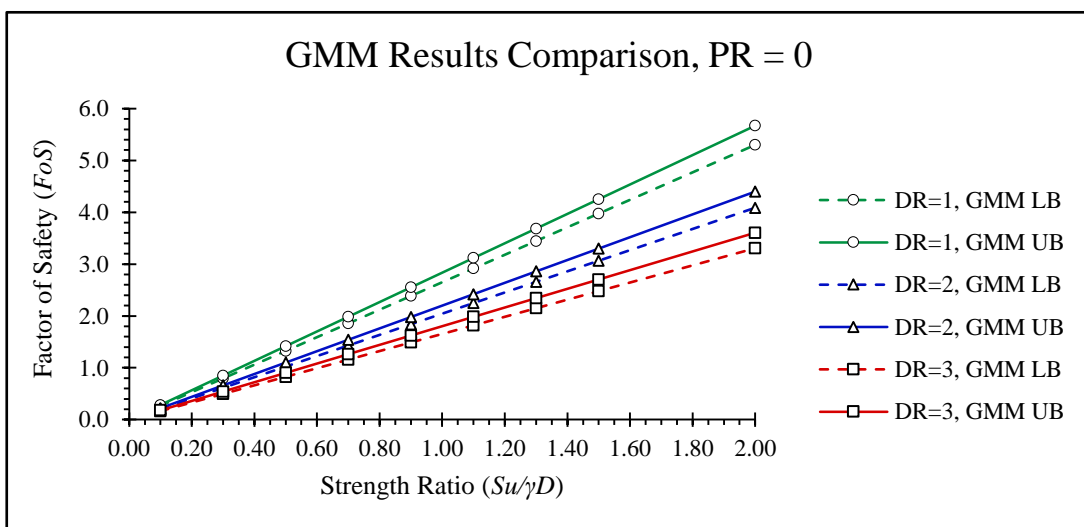


Figure 4.5: Graphical comparison of upper and lower bound results obtained through GMM for  $PR = 0$ .

To accurately compare the results obtained from the strength reduction method and the gravity multiplier method to one another it was necessary to calculate the average factor of safety values for each and the corresponding percentage difference. Table 4.2 compares the average factor of safety results obtained from the strength reduction method with the average factor of safety results obtained from the gravity multiplier method for a pressure ratio equal to zero. The percentage difference (*PD*) was calculated according to Equation 4.12.

$$\text{Percentage Difference (PD)} = ABS \left( \frac{\text{Av. GMM FoS} - \text{Av. SRM FoS}}{\text{Av. FoS}} \right) * 100 \quad (4.12)$$

Table 4.2: Comparison of SRM and GMM results for PR = 0.

GMM & SRM FoS Results Comparison, PR = 0									
	DR = 1			DR = 2			DR = 3		
SR	SRM AV	GMM AV	PD (%)	SRM AV	GMM AV	PD (%)	SRM AV	GMM AV	PD (%)
0.10	0.275	0.274	0.18	0.212	0.212	0.00	0.173	0.173	0.29
0.30	0.822	0.823	0.06	0.635	0.637	0.24	0.520	0.519	0.29
0.50	1.374	1.371	0.18	1.060	1.061	0.09	0.867	0.864	0.40
0.70	1.921	1.920	0.05	1.484	1.485	0.07	1.215	1.210	0.41
0.90	2.470	2.468	0.08	1.911	1.909	0.10	1.557	1.555	0.13
1.10	3.018	3.017	0.05	2.332	2.334	0.06	1.905	1.900	0.24
1.30	3.570	3.565	0.13	2.756	2.758	0.09	2.251	2.246	0.22
1.50	4.113	4.114	0.01	3.180	3.182	0.08	2.603	2.591	0.46
2.00	5.494	5.485	0.16	4.241	4.243	0.05	3.468	3.456	0.36

It can be concluded from Table 4.2 that the factor of safety results obtained from the strength reduction method and the gravity multiplier are very similar (less than 1% different for all scenarios) and have a high level of agreement when the pressure ratio is equal to zero. To further assess the usefulness of both methods it was necessary to compare the CPU run time taken to calculate the factor of safety. Table 4.3 compares the CPU run time of the strength reduction method and gravity multiplier method over various scenarios representing a collapse failure mechanism.

Table 4.3: CPU run time comparison for various collapse scenarios.

CPU Run Time Comparison (Collapse)					
Depth Ratio (C/D)	Pressure Ratio $((\sigma_s - \sigma_t)/S_u)$	Strength Ratio $(S_w/\gamma D)$	SRM UB Time (s)	GMM UB Time (s)	Run Time Difference (s)
1	0	1.10	34	6	28
	+3	2.00	35	6	29
	+10	0.10	31	6	25
2	-3	0.50	33	6	27
	0	0.90	48	7	41
	5	0.30	35	6	29
3	-1	1.10	44	6	38
	1	1.30	32	7	25
	10	0.70	29	6	23
Average			35.7	6.2	29.4

The sample data used for the CPU run time comparison was selectively chosen to represent a broad range of scenarios resulting in failure due to collapse, with differing depth ratios, strength ratios and pressure ratios. The upper bound factor of safety values were used for the purpose of run time analysis to keep the test conditions constant. It can be seen from Table 4.3 that the strength reduction method can take anywhere between 23 to 41 seconds longer than the gravity multiplier method when calculating the upper bound factor of safety for the same scenario. From the sample data it is calculated that the strength reduction method takes an average time of 35.7 seconds to calculate the upper bound factor of safety while the gravity multiplier method takes an average time of just 6.2 seconds. This large difference in run time is likely due to the iterative nature of the strength reduction method. Instead of just returning the first multiplier found to cause failure like the gravity multiplier method, the strength reduction method will optimise the final result by closing in on an optimum factor of safety and then increasing and decreasing the material strength in small increments until the most accurate solution is found. The fast processing time of the gravity multiplier method is a very attractive quality when performing large scale analysis of multiple models but to comprehensively compare both of the methods the factor of safety results from a scenario with a non-zero pressure ratio must be compared.

Table 4.4 presents the upper and lower bound factor of safety results for a scenario where the pressure ratios is equal to positive five. The percentage difference (*PD*) between the upper and lower bound results found by both the strength reduction method and gravity multiplier method have been calculated as per Equation 4.11.

Table 4.4: SRM and GMM results obtained for PR = +5 with comparison of upper bound and lower bound.

Lower & Upper Bound FoS Comparison, PR = +5							
DR	SR	SRM LB	SRM UB	PD (%)	GMM LB	GMM UB	PD (%)
1	0.10	0.201	0.216	7.19	-0.059	-0.042	33.66
	0.30	0.407	0.436	6.88	-0.177	-0.125	34.44
	0.50	0.510	0.546	6.82	-0.294	-0.208	34.26
	0.70	0.573	0.613	6.75	-0.412	-0.291	34.42
	0.90	0.615	0.657	6.60	-0.530	-0.374	34.51
	1.10	0.644	0.688	6.61	-0.648	-0.458	34.36
	1.30	0.668	0.713	6.52	-0.766	-0.541	34.43
	1.50	0.686	0.731	6.35	-0.883	-0.624	34.37
	2.00	0.716	0.760	5.96	-1.178	-0.832	34.43
	2	0.10	0.171	0.184	7.32	0.006	0.023
0.30		0.386	0.415	7.24	0.017	0.068	120.0
0.50		0.514	0.556	7.85	0.028	0.114	121.1
0.70		0.601	0.650	7.83	0.039	0.160	121.6
0.90		0.664	0.715	7.40	0.050	0.205	121.5
1.10		0.706	0.766	8.15	0.061	0.251	121.7
1.30		0.748	0.807	7.59	0.073	0.296	120.8
1.50		0.773	0.836	7.83	0.084	0.342	121.1
2.00		0.831	0.893	7.19	0.112	0.456	121.1
3		0.10	0.146	0.158	7.89	0.023	0.039
	0.30	0.351	0.380	7.93	0.069	0.116	50.81
	0.50	0.485	0.528	8.49	0.115	0.193	50.65
	0.70	0.585	0.634	8.04	0.161	0.270	50.58
	0.90	0.654	0.714	8.77	0.208	0.347	50.09
	1.10	0.714	0.775	8.19	0.254	0.424	50.15
	1.30	0.761	0.826	8.19	0.300	0.502	50.37
	1.50	0.796	0.867	8.54	0.346	0.579	50.38
	2.00	0.861	0.940	8.77	0.461	0.772	50.45

Table 4.4 shows that the upper and lower bound results obtained from the strength reduction method show a similar level of agreement to those found when the pressure ratio was equal to zero. The trend showing the percentage difference increase between upper and lower bound values as the depth ratio increases is seen here too. Table 4.4 also shows that the gravity multiplier method is not capable of calculating an appropriate factor of safety once the pressure ratio is greater than zero. Upper and lower bound values calculated by the gravity multiplier method have a large percentage difference and all factor of safety results returned from the gravity multiplier method for a depth ratio of one are negative. Table 4.5 further compares the results obtained from the strength reduction method and gravity multiplier method for a pressure ratio of positive five. The percentage difference (*PD*) was calculated according to Equation 4.12.

Table 4.5: Comparison of SRM and GMM results for PR = +5.

GMM & SRM FoS Results Comparison, PR = +5									
SR	DR = 1			DR = 2			DR = 3		
	SRM AV	GMM AV	PD (%)	SRM AV	GMM AV	PD (%)	SRM AV	GMM AV	PD (%)
0.10	0.209	-0.051	327.8	0.178	0.015	169.7	0.152	0.031	132.2
0.30	0.422	-0.151	423.2	0.401	0.043	161.6	0.366	0.093	119.2
0.50	0.528	-0.251	562.4	0.535	0.071	153.1	0.507	0.154	106.7
0.70	0.593	-0.352	782.1	0.626	0.100	145.1	0.610	0.216	95.52
0.90	0.636	-0.452	1182	0.690	0.128	137.5	0.684	0.278	84.56
1.10	0.666	-0.553	2157	0.736	0.156	130.0	0.745	0.339	74.85
1.30	0.691	-0.654	7264	0.778	0.185	123.2	0.794	0.401	65.72
1.50	0.709	-0.754	6497	0.805	0.213	116.2	0.832	0.463	57.03
2.00	0.738	-1.005	1305	0.862	0.284	100.8	0.901	0.617	37.44

Table 4.5 further reinforces the unsuitability of the gravity multiplier method for analysing shallow tunnel heading stability problems with a non-zero positive pressure ratio. Large percentage differences in results indicate that the gravity multiplier method is incapable of analysing scenarios with a pressure ratio greater than zero. This could be because the gravity multiplier is in fact increasing the applied surcharge pressure as well as the gravity so the failure load is unsuitably amplified. Finding the exact explanation as to why the gravity multiplier method is unable to accurately analyse stability problems with a pressure ratio greater than zero will require further future research. Interestingly the accuracy of the gravity multiplier method results seem to increase as the depth ratio increases, this is an area that could also require further investigation. Figure 4.6 plots the upper and lower bound factors of safety found from the strength reduction method to further demonstrate the acceptability of the strength reduction method and its application to analysing tunnel heading stability problems with a pressure ratio greater than zero.

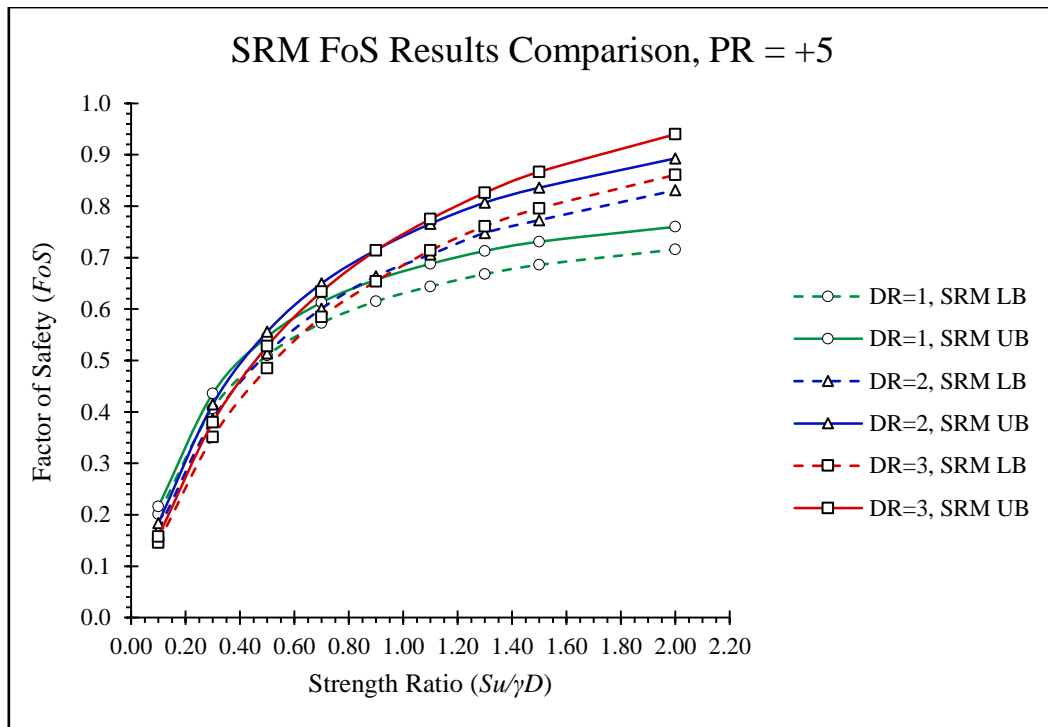


Figure 4.6: Graphical comparison of upper and lower bound results obtained through SRM for  $PR = +5$ .

Figure 4.6 reinforces the trend shown in Table 4.4, that is the upper and lower bound solutions have a good level of agreement but become increasingly different as the depth ratio increases. Figure 4.6 also shows that when the pressure ratio is greater than zero the factor of safety no longer increases linearly with the strength ratio like it does when the pressure ratio equals zero. This new concept is further explained in Section 4.7 ‘Optimum G2 Tunnel Heading Collapse Results and Discussion’.

Performing an internal comparison of results made it apparent that the gravity multiplier method would not be suitable for analysing tunnel heading stability problems with a pressure ratio greater than zero so the strength reduction method was adopted for this portion of research. To verify the results obtained from the strength reduction method they had to be compared to published results from an external source.

## 4.6 External Comparison of Collapse Results

To validate the factor of safety bounds obtained from Optum G2 it was important to compare a sample of results with verified results published by another source. This comparison was necessary to ensure that results from this project and the conclusions drawn from it are accurate and relevant to previous work. Augarde, Lyamin and Sloan (2003) investigated the stability of an undrained plane strain heading and presented a number of results which were used to validate the results obtained in this project. The upper and lower bound results obtained in these earlier studies were presented as a critical pressure ratio rather than as a factor of safety so a dimensional analysis along with linear interpolation/extrapolation had to be performed to transform the results from this study into the same format as the published results. The critical pressure ratio ( $PR_c$ ) assumes a factor of safety of one meaning that the corresponding strength ratio ( $SR_c$ ) also only applies to a factor of safety equal to one, to overcome this and compare results, both dimensionless ratios from this project must be normalised by multiplying by the corresponding factor of safety. The average value from the lower and upper bound factor of safety solutions was adopted for this comparison exercise. Equation 4.13 was used to transform the strength ratio that has been adopted in this research into the critical strength ratio used by Augarde, Lyamin and Sloan (2003). Equation 4.14 was used to transform the pressure ratio used in this research into the critical pressure ratio used by Augarde, Lyamin and Sloan (2003). Table 4.6 contains a comparison of sample scenarios relating to a collapse failure mechanism and Figure 4.7 provides a graphical comparison of this data.

$$SR_c = \left( \frac{S_u}{\gamma D} \right)^{-1} * FOS \quad (4.13)$$

$$PR_c = \frac{\sigma_s - \sigma_t}{S_u} * FOS \quad (4.14)$$

Table 4.6: Comparison of collapse results to external publication.

Comparison of Collapse Results to Augarde, Lyamin and Sloan (2003)						
		Augarde, Lyamin & Sloan (2003)	This Thesis (SRM)			Augarde, Lyamin & Sloan (2003)
SR <sub>c</sub>	DR	LB PR <sub>c</sub>	LB PR <sub>c</sub>	Average PR <sub>c</sub>	UB PR <sub>c</sub>	UB PR <sub>c</sub>
1.00	1	2.460	2.602	2.736	2.870	2.890
	2	2.400	2.639	2.852	3.064	3.180
	3	2.200	2.329	2.584	2.838	3.000
2.00	1	0.850	1.033	1.178	1.322	1.390
	2	-0.200	0.098	0.309	0.520	0.680
	3	-1.400	-1.221	-0.960	-0.699	-0.500
3.00	1	-0.740	-0.668	-0.491	-0.313	-0.110
	2	-2.840	-2.488	-2.275	-2.062	-1.820
	3	-5.030	-4.863	-4.575	-4.287	-4.000

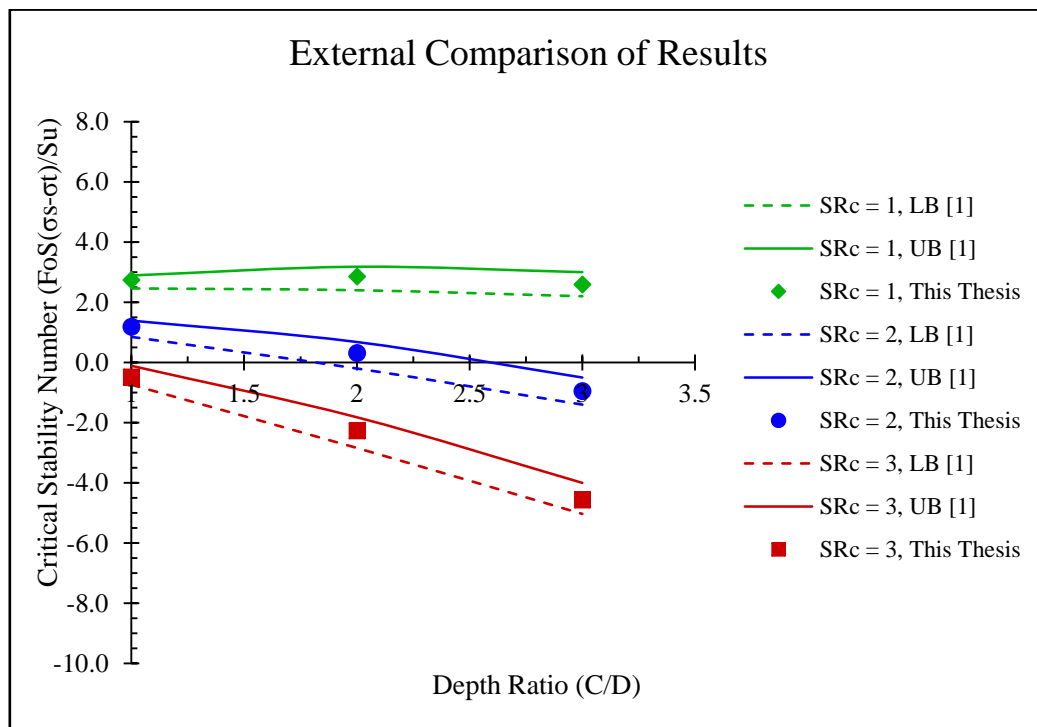


Figure 4.7: Comparison of collapse results to external publication. [1] Denotes data obtained from Augarde, Lyamin and Sloan (2003).

The raw data forming the comparison sample was selected to include factor of safety values which represented a broad range of scenarios resulting in failure by collapse, with differing strength ratios, pressure ratios and depth ratios. The raw data along with the calculations involved in the transformation can be viewed in Appendix C – ‘External Comparison’.

Once the results from this study were transformed and linearly interpolated or extrapolated, so they could be directly compared to the results presented by Augarde, Lyamin and Sloan (2003), it was apparent that they were very similar and have a good level of agreement. Figure 4.7 shows that the average critical pressure ratio for all scenarios chosen as part of the sample fell within the upper and lower bound solutions from the published results. Closer inspection of Table 5.5 shows that all lower and upper bound values chosen as part of the sample actually fell between the upper and lower bound solutions from the published results. This outcome indicates that the strength reduction method, when applied to all developed models, produces accurate upper and lower bound factor of safety values and can be used for estimating tunnel heading stability.

#### **4.7 Optum G2 Tunnel Heading Collapse Results and Discussion**

The stability of a tunnel heading relating to the collapse failure mechanism is a complex topic. Pressure ratios  $((\sigma_s - \sigma_t)/S_u)$  equal to zero, greater than zero and less than zero can all induce tunnel heading failure by the collapse mechanism, with the depth ratio  $(C/D)$  and strength ratio  $(Su/\gamma D)$  being the other critical dimensionless parameters. Optum G2 was used to model and analyse a range of tunnel heading scenarios where the major failure mechanism was collapse. Two stages of testing were conducted. The first stage of testing adopted the strength reduction method to rigorously compute both the upper and lower bound factor of safety values for a broad range of practical pressure ratios. The second stage also adopted the strength reduction method but only calculated the upper bound factor of safety values that were required to fill in critical gaps in the data for modelling purposes. For this reason, the upper bound factor of safety values found from the strength reduction method will be adopted as the factor of safety values used in all modelling and data analysis. All upper bound factor of safety results calculated through the strength reduction method are available in Appendix D – ‘Final Results and Plots’.

To determine the method of failure corresponding to each factor of safety value it was necessary to view the displacement vector field overlay for each model in Optum G2. An example of a collapse displacement vector field for a pressure ratio of zero, depth ratio of two and strength ratio of 1.50 is shown in Figure 4.8.

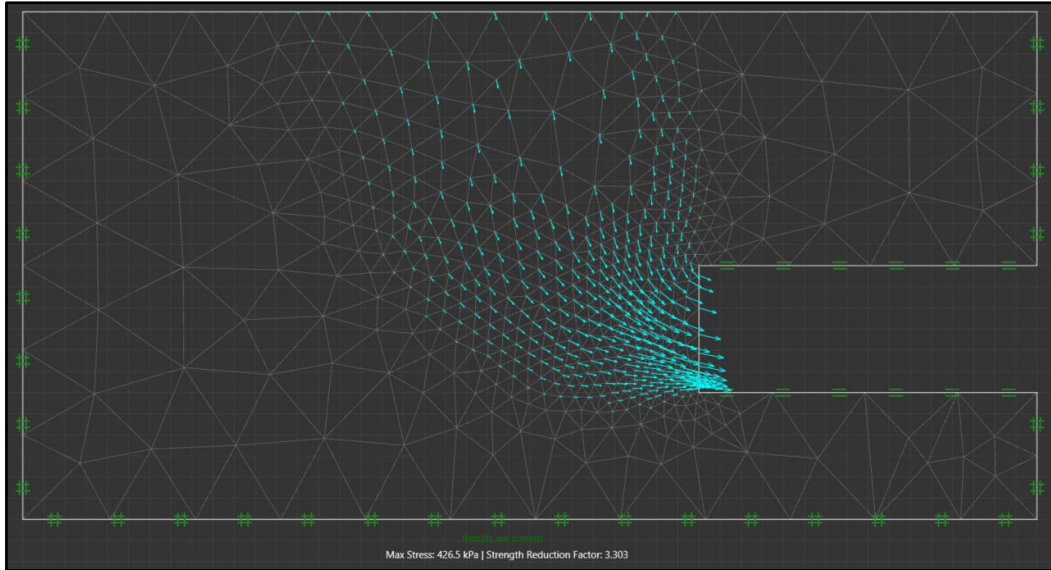


Figure 4.8: Tunnel heading failure by collapse showing displacement vector field and mesh overlay.  $PR=0$ ,  $DR=2$  &  $SR=1.50$ .

The direction of the displacement vector arrows in Figure 4.8 indicate a downward displacement at failure, or failure by collapse. The length of the displacement vector arrows indicate that the maximum displacement will be occurring at the tunnel face with the ground surface displacing less. The field created by the displacement vector arrows shows the failure zone with the outside edges being potential slip lines as described in Figure 4.1. The corresponding data for the model shown in Figure 4.8, that is, a depth ratio equal to two and a strength ratio equal to 1.50, inclusive of all pressure ratios related to failure by collapse is presented in Table 4.7. The corresponding plot of factor of safety verse pressure ratio for the same case is shown in Figure 4.9.

Table 4.7: Factor of safety results for collapse failure related to model with  $DR = 2$  and  $SR = 1.50$ .

Factor of Safety Results for Collapse when $DR = 2$		
SR ( $S_u/\gamma D$ )	PR ( $(\sigma_s - \sigma_t)/S_u$ )	FoS (UB SRM)
1.50	-1.5	13.026
	-1	7.746
	0	3.303
	+1	2.080
	+3	1.193
	+5	0.836
	+10	0.477

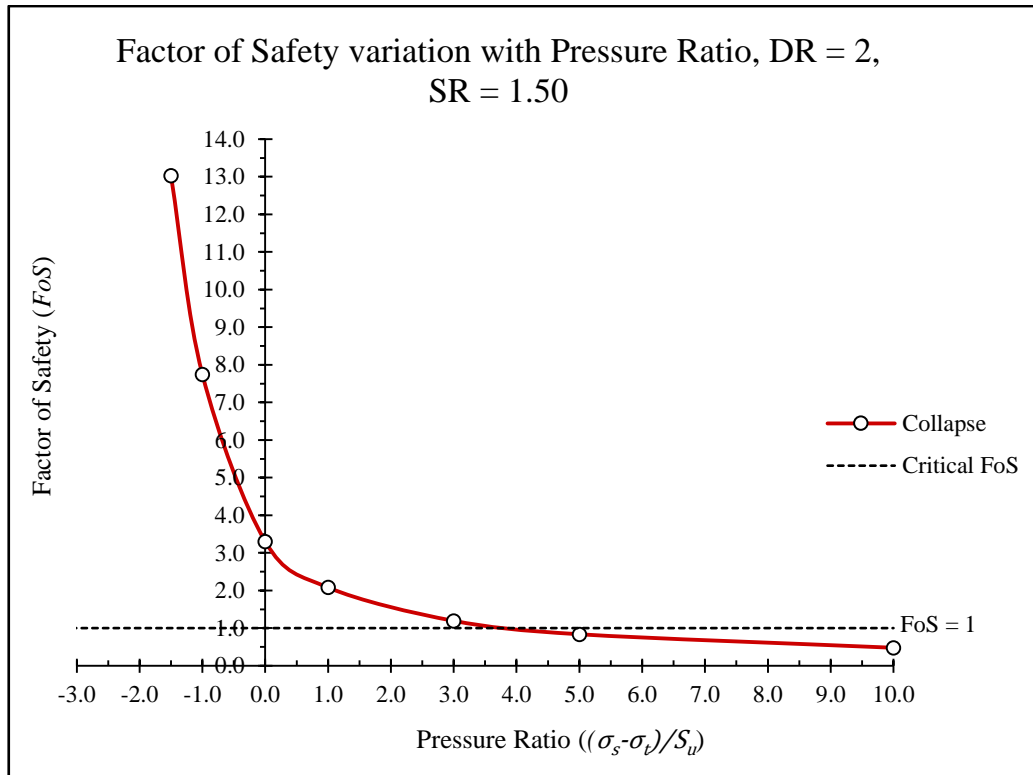


Figure 4.9: Plot of factor of safety verse pressure ratio for tunnel heading problem, DR = 2 and SR = 1.50.

Figure 4.9 shows the full range of scenarios relating to the collapse failure mechanism for a tunnel heading model with a depth ratio of two and a strength ratio of 1.50. It can be seen from the curve that the factor of safety decreases as the pressure ratio increases infinitely while the factor of safety increases infinitely as the pressure ratio decreases. It is thought that the curve is hyperbolic in nature and that a pair of asymptotes exist. It is hypothesised that a ‘weightless scenario’ exists about the asymptote where the factor of safety is at a maximum. This theory will be discussed in more detail after the displacement vector fields are examined. This plot shows that a critical factor of safety of one is unachievable for this scenario once the pressure ratio reaches approximately positive 3.5. Interestingly the optimum factor of safety is achieved at a slightly negative pressure ratio. In this particular case a pressure ratio of negative 1.5 produces the highest factor of safety of approximately thirteen. This result is in line with what is expected in practice as a negative pressure ratio is formed by applying an internal tunnel pressure which acts to resist the overburden pressure of the soil. A positive pressure ratio is the opposite and is applied by increasing the surcharge pressure which assists the overburden pressure in causing tunnel heading failure by collapse. To create a pressure ratio of negative 1.5 a uniform internal tunnel pressure 1.5 times the undrained shear strength of the soil must be applied to the tunnel face. All corresponding displacement vector fields relating to the scenario in Figure 4.8 and 4.9 are displayed in Figures 4.10 through to 4.16 in descending order of pressure ratio.

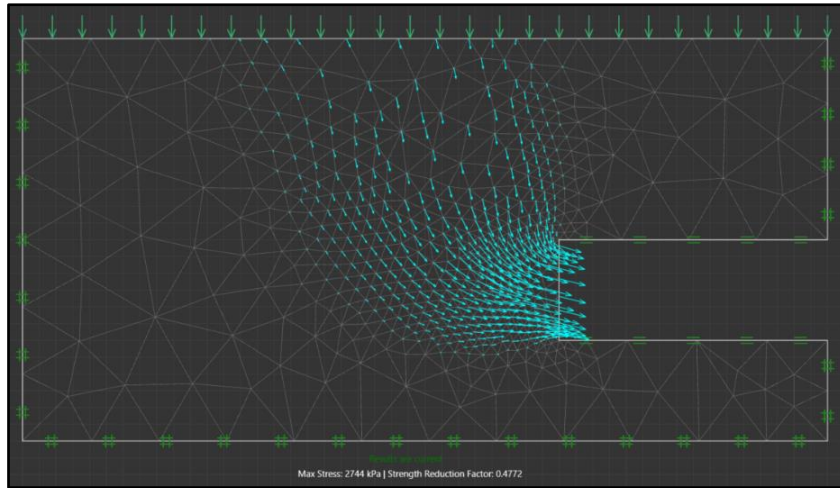


Figure 4.10: Displacement vector field.  $PR = +10$ ,  $DR = 2$ ,  $SR = 1.50$ .

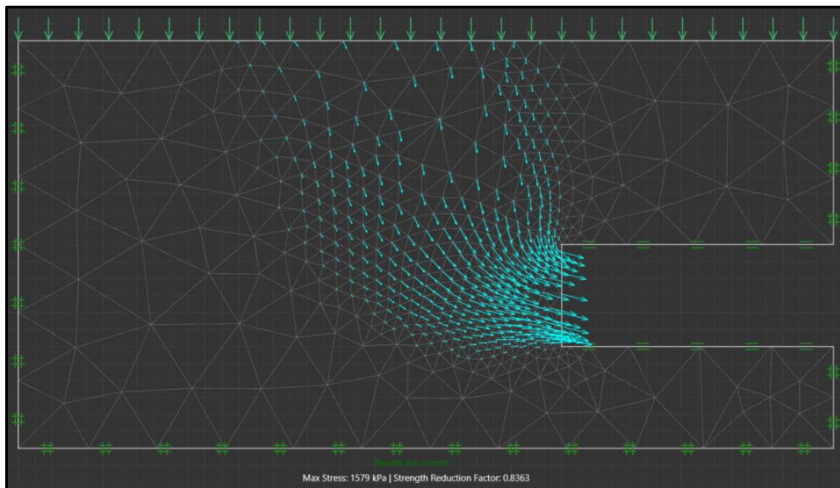


Figure 4.11: Displacement vector field.  $PR = +5$ ,  $DR = 2$ ,  $SR = 1.50$ .

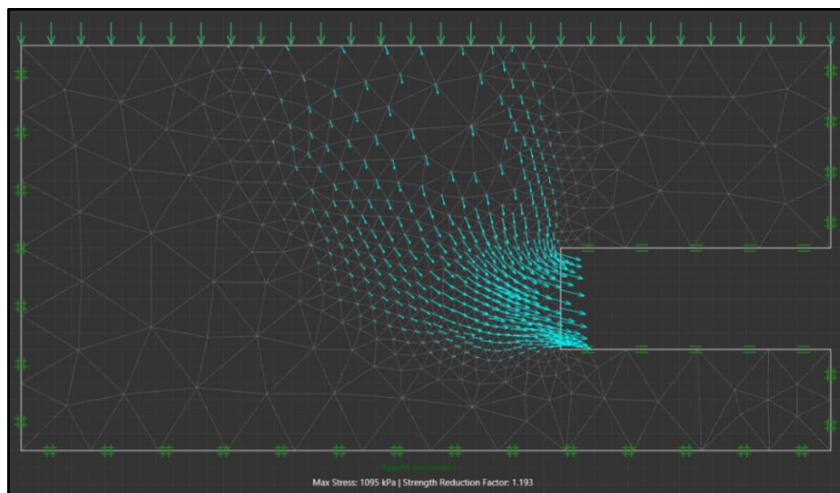


Figure 4.12: Displacement vector field.  $PR = +3$ ,  $DR = 2$ ,  $SR = 1.50$ .

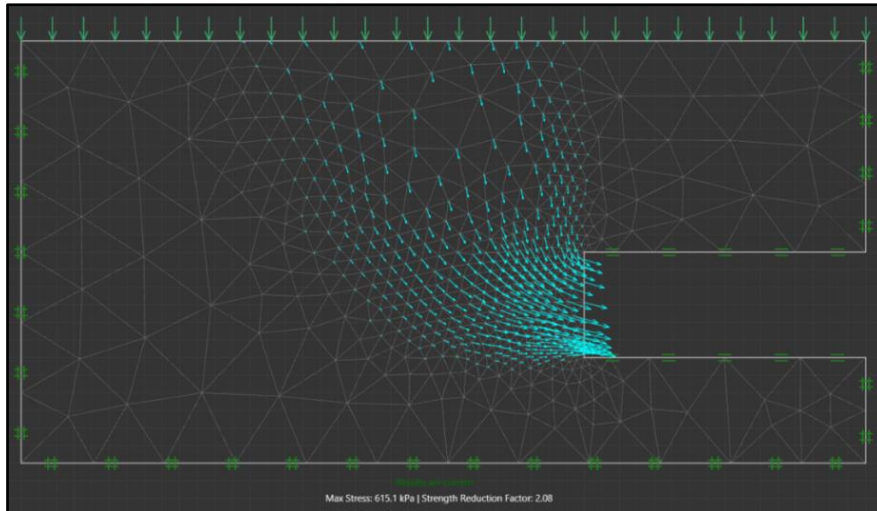


Figure 4.13: Displacement vector field.  $PR = +1$ ,  $DR = 2$ ,  $SR = 1.50$ .

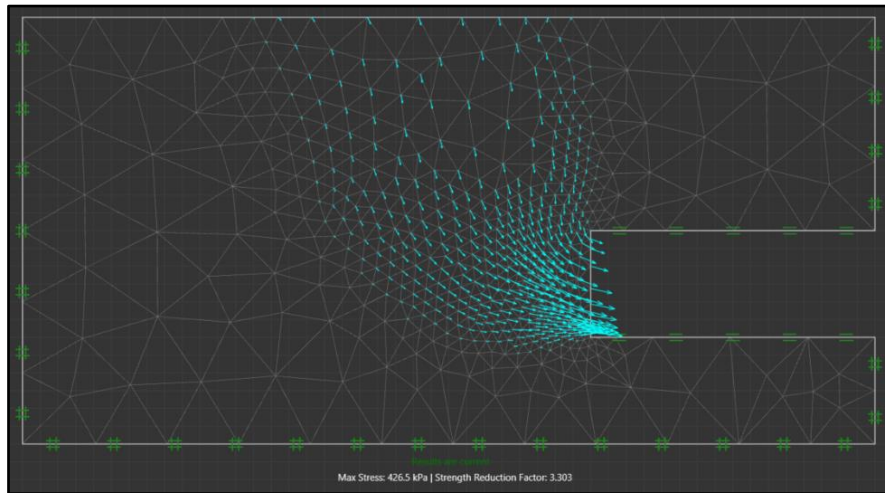


Figure 4.14: Displacement vector field.  $PR = 0$ ,  $DR = 2$ ,  $SR = 1.50$ .

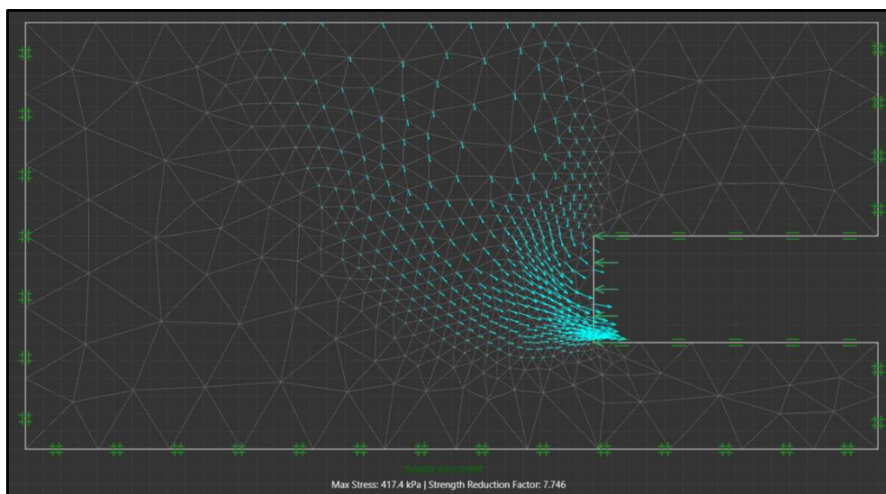


Figure 4.15: Displacement vector field.  $PR = -1$ ,  $DR = 2$ ,  $SR = 1.50$ .

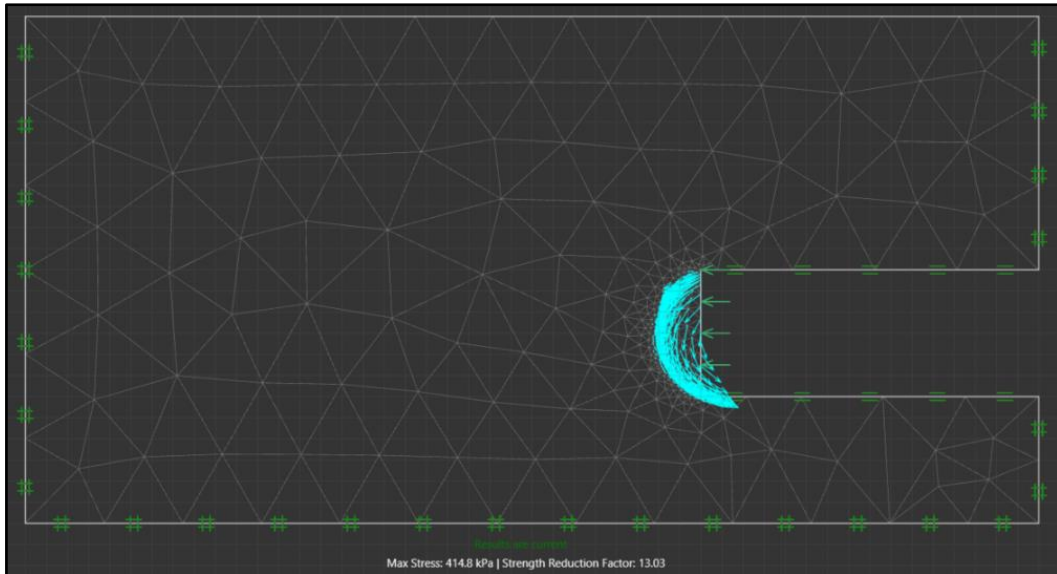


Figure 4.16: Displacement vector field.  $PR = -1.5$ ,  $DR = 2$ ,  $SR = 1.50$ .

Figures 4.10 through to 4.16 confirm that the failure mechanism corresponding to the results presented in Table 4.7 and Figure 4.9 is indeed collapse. It can also be seen that as the pressure ratio decreases so too does the magnitude of the displacement vectors. These results are as to be expected, however Figure 4.16 presents an interesting vector field, with the arrows swirling around the tunnel face in a counter clockwise direction. It is thought that at this point the tunnel heading problem is approaching a weightless situation, as is confirmed by the plot in Figure 4.8. In practice it is possible that this weightless situation could exist when the internal tunnel pressure plus the resistance contributed by the shear strength of the soil is exactly equal to the downward pressure caused by the surcharge and overburden pressures.

It has long been known that the factor of safety increases linearly with the strength ratio for a case where the pressure ratio is equal to zero. It was noted in Section 4.5 ‘Internal Comparison of Collapse Results’ that the relationship between the factor of safety and the strength ratio was not linear for a case with a non-zero pressure ratio. Figures 4.17, 4.18 and 4.19 explore this relationship further by plotting the upper bound factor of safety against the strength ratio for all positive pressure ratios tested for a depth ratio of one, two and three respectively. The upper bound factor of safety for all positive pressure ratios is presented in Table 4.8.

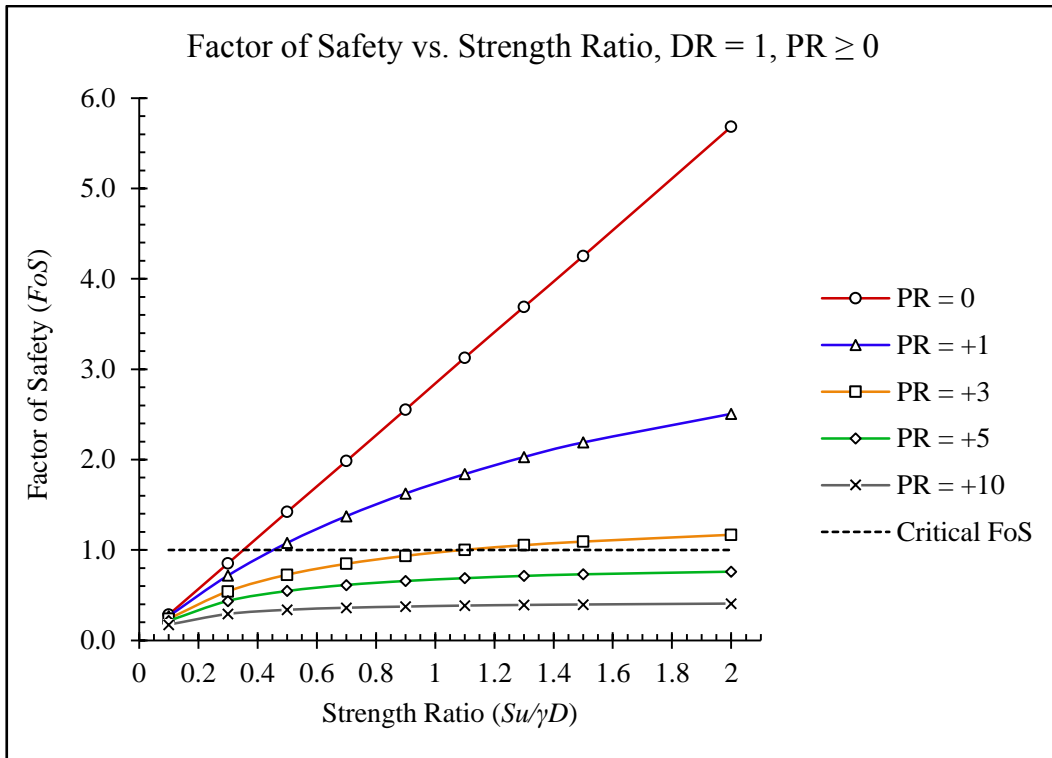


Figure 4.17: Factor of safety vs. strength ratio for all positive pressure ratios. DR = 1.

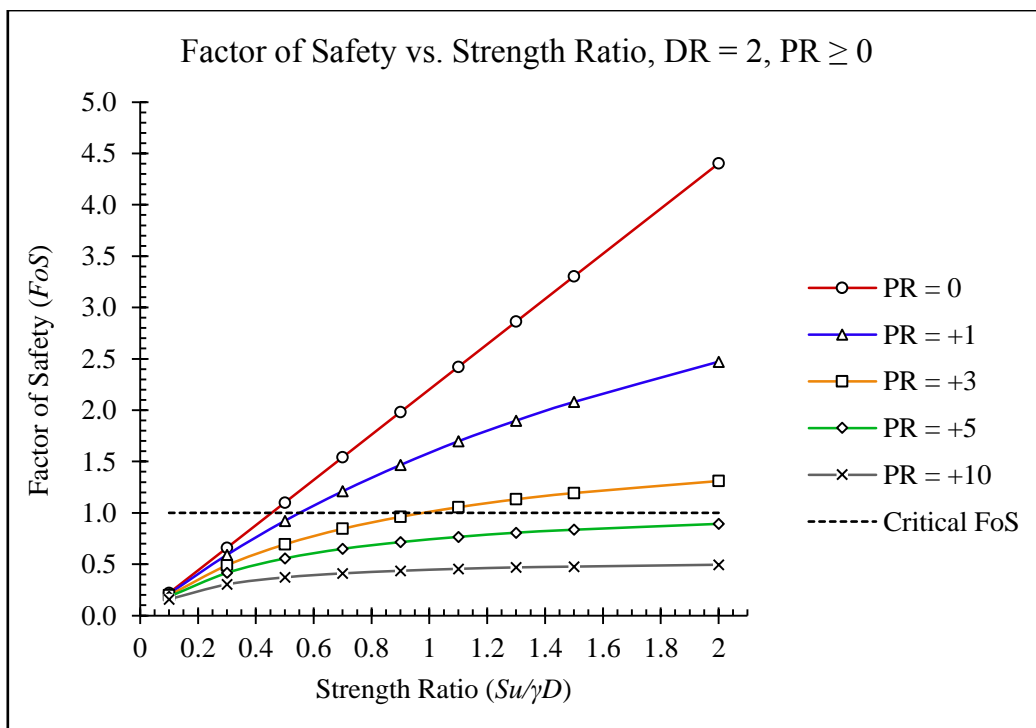


Figure 4.18: Factor of safety vs. strength ratio for all positive pressure ratios. DR = 2.

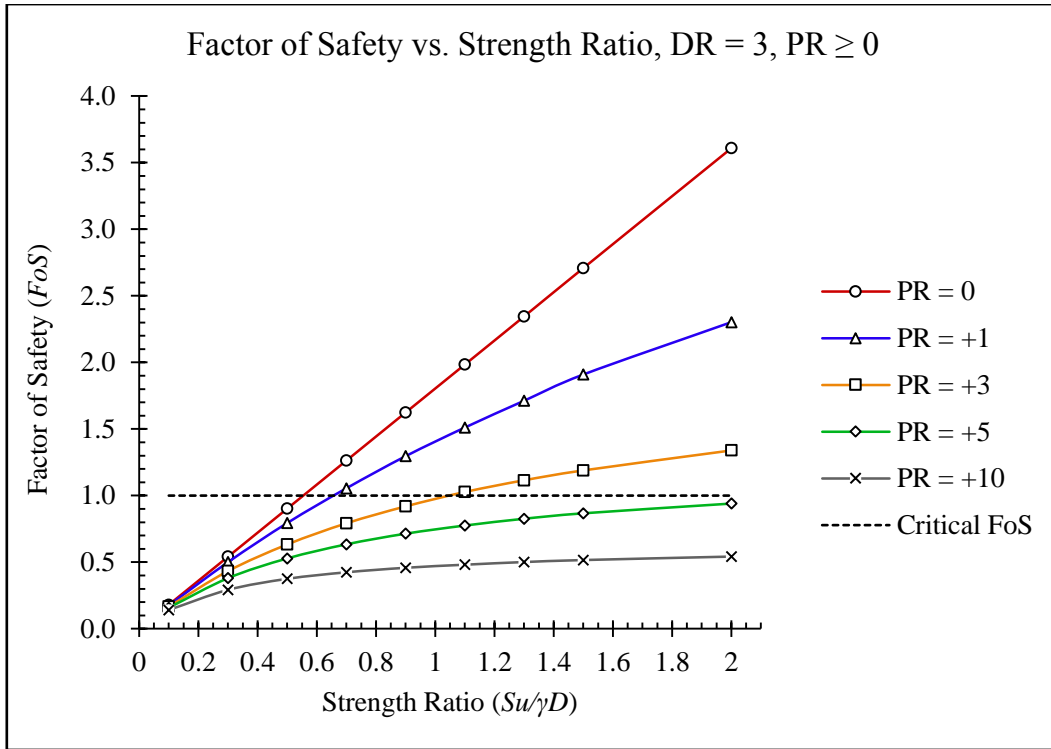


Figure 4.19: Factor of safety vs. strength ratio for all positive pressure ratios. DR = 3.

Table 4.8: Upper bound factor of safety results for all positive pressure ratios.

Factor of Safety Results for all Positive Pressure Ratios						
DR	SR	Pressure Ratio				
		0	+1	+3	+5	+10
1	0.10	0.284	0.267	0.239	0.216	0.174
	0.30	0.851	0.717	0.542	0.436	0.292
	0.50	1.421	1.078	0.726	0.546	0.338
	0.70	1.984	1.374	0.847	0.613	0.361
	0.90	2.554	1.625	0.935	0.657	0.374
	1.10	3.127	1.839	1.002	0.688	0.385
	1.30	3.690	2.028	1.053	0.713	0.392
	1.50	4.252	2.190	1.093	0.731	0.397
	2.00	5.683	2.506	1.168	0.760	0.407
	2	0.10	0.220	0.212	0.197	0.184
0.30		0.660	0.591	0.489	0.415	0.303
0.50		1.100	0.922	0.693	0.556	0.372
0.70		1.541	1.210	0.845	0.650	0.411
0.90		1.982	1.466	0.961	0.715	0.436
1.10		2.422	1.697	1.055	0.766	0.455
1.30		2.862	1.898	1.132	0.807	0.469
1.50		3.303	2.080	1.193	0.836	0.477
2.00		4.402	2.472	1.310	0.893	0.495
3		0.10	0.180	0.175	0.166	0.158
	0.30	0.541	0.500	0.433	0.380	0.292
	0.50	0.902	0.794	0.633	0.528	0.375
	0.70	1.263	1.055	0.792	0.634	0.424
	0.90	1.624	1.296	0.919	0.714	0.458
	1.10	1.984	1.511	1.027	0.775	0.481
	1.30	2.345	1.712	1.115	0.826	0.501
	1.50	2.708	1.909	1.189	0.867	0.516
	2.00	3.608	2.302	1.339	0.940	0.542

Figures 4.17 through to 4.19 show that the factor of safety increases linearly with the strength ratio for a pressure ratio of zero but this linear relationship does not exist when the pressure ratio is greater than zero. This is likely due to the fact that the surcharge pressure is a function of the undrained shear strength of the soil and is amplified as the soil strength increases. It can be seen that the factor of safety decreases for any given strength ratio as the pressure ratio increases, this is to be expected as a larger positive pressure ratio is directly linked to a larger surcharge pressure. Examining the trend of Figures 4.17 and 4.18 it appears that for a depth ratio of one and two, a pressure ratio greater than five will never be able to achieve a factor of safety greater than or equal to one. Figure 4.19 tells a similar story, if a reasonable strength ratio is adopted, a depth ratio of three is also incapable of achieving a factor of safety of one or greater for a pressure ratio greater than five. This

would indicate that when dealing with undrained shallow tunnel heading stability problems in practice, a pressure ratio of five or greater should always be avoided if the depth ratio is less than or equal to three.

## **4.8 Conclusion**

The stability, of two-dimensional undrained plane strain tunnel headings exhibiting a collapse failure mechanism, was investigated using a factor of safety approach. Factor of safety values were computed in Optum G2 using finite element limit analysis. The upper and lower bound factor of safety values were rigorously computed for the majority of scenarios, with a very good level of agreement found between the lower and upper bounds and a percentage difference of less than nine percent for all scenarios tested. The gravity multiplier method and strength reduction method were compared, with the results exhibiting a very good level of agreement for scenarios where the pressure ratio was equal to zero. When the pressure ratio was equal to zero the gravity multiplier method and strength reduction method showed a maximum factor of safety percentage difference of less than one percent for all scenarios tested. The CPU run time of the gravity multiplier method was, on average, nearly six times faster than the strength reduction method. Upon comparing both methods, for scenarios with a pressure ratio greater than zero, it became apparent that the gravity multiplier method was producing unreasonable factor of safety values and was unable to perform the analysis accurately, so the strength reduction method was adopted.

A sample of lower bound and upper bound factor of safety results computed in Optum G2 were compared to results published by Augarde, Lyamin and Sloan (2003). The factor of safety results obtained from the Optum G2 strength reduction method had to be converted into critical pressure ratios, with corresponding critical strength ratios, by performing a dimensional analysis and linear interpolation/extrapolation, so they could be directly compared to the published results. It was found that all average critical pressure ratios calculated via the strength reduction method fell well in between the published lower and upper bound critical pressure ratio values. Furthermore, all lower bound and upper bound critical pressure ratio values found via the strength reduction method actually fell between the published lower and upper bound critical pressure ratio values. The similarity between results indicates that the Optum G2 strength reduction method, using a factor of safety approach, is capable of producing accurate tunnel heading stability results suitable for use by a practicing engineer.

Analysing the relationship between the factor of safety and the pressure ratio for a collapse failure mechanism indicates that an individual hyperbolic curve exists for each depth ratio and strength ratio combination. As the pressure ratio increases infinitely, the factor of safety decreases toward an asymptotic solution. As the pressure ratio reduces to an asymptotic solution, the factor of safety increases infinitely. The point where the factor of safety increases infinitely is thought to represent a weightless situation, where the opposing pressures of a tunnel heading stability problem are in balance. Analysing the relationship between the factor of safety and the pressure ratio suggests that the optimum factor of safety value for most practical cases will occur at a slightly negative pressure ratio rather than at a pressure ratio of zero. Investigating the displacement vector fields reinforced the factor of safety results found, and indicated that a weightless situation may exist once the displacement vector field starts swirling about the tunnel face.

For a pressure ratio of zero, the factor of safety increases linearly as the strength ratio increases. This research showed that the same relationship does not exist for a pressure ratio greater than zero. For a non-zero positive pressure ratio, the factor of safety still increases as the strength ratio increases, but each pressure ratio and depth ratio combination produces its own unique curve. Analysing the curves produced, it is expected that an asymptotic factor of safety solution, or a limiting factor of safety value, exists for each curve. It was also found when analysing the stability of an undrained shallow tunnel heading with a depth ratio less than or equal to three, that a pressure ratio greater than or equal to positive five should be avoided for all practical strength ratios, as a critical factor of safety of one is unobtainable. The understanding of tunnel heading stability relating to a collapse failure mechanism is revisited in Chapter 6 and ultimately culminates in the development of undrained shallow tunnel heading stability design charts for use by practicing engineers in the preliminary stages of tunnel design.

# **CHAPTER 5:**

## **TUNNEL HEADING ANALYSIS:**

### **BLOWOUT**

#### **5.1 Introduction**

As the world's population grows and available space on the Earth's surface decreases it is becoming increasingly necessary to construct subterranean infrastructure. As the need for tunnels increases so too does the required complexity of tunnelling projects. Tunnels present a unique challenge for engineers, who must assess the stability of prospective tunnels and the settlement of the Earth's surface that could be caused by the tunnelling process. The safe design of tunnels is critical, especially in urban areas where a shallow void must pass under existing infrastructure sensitive to ground movement. Typically the stability of tunnels is analysed with a collapse failure mechanism in mind but it is also important to assess the stability of a tunnel for failure due to a blowout. This requirement is particularly necessary when considering tunnel construction by an earth pressure balance TBM, where the pressure on the cutterhead must be constantly varied to prevent failure due to collapse or blowout. This chapter will address the tunnel heading stability problem for blowout by using Optum G2 to compute the upper and lower bound factor of safety values for a number of different scenarios. The relationship between the factor of safety and the three dimensionless parameters; depth ratio, strength ratio and pressure ratio, will be discussed with a focus on the blowout failure mechanism.

#### **5.2 Problem Statement**

In reality, tunnels are complex three-dimensional underground structures, however for the purpose of stability analysis they can be simplified to a basic two-dimensional model. The longitudinal section of the tunnel heading will be modelled under two-dimensional plane strain conditions. The undrained clay soil medium will be represented by a homogeneous Tresca material, which has an undrained shear strength ( $S_u$ ) and unit weight ( $\gamma$ ). The cover above the tunnel ( $C$ ) and the height of the tunnel ( $D$ ) are the important dimensional parameters needed to create the model. The surcharge pressure ( $\sigma_s$ ) and internal tunnel pressure ( $\sigma_t$ ) are varied to test the stability of the model under a number of different pressure

ratios capable of inducing failure by blowout. Figure 5.1 defines the tunnel heading stability problem.

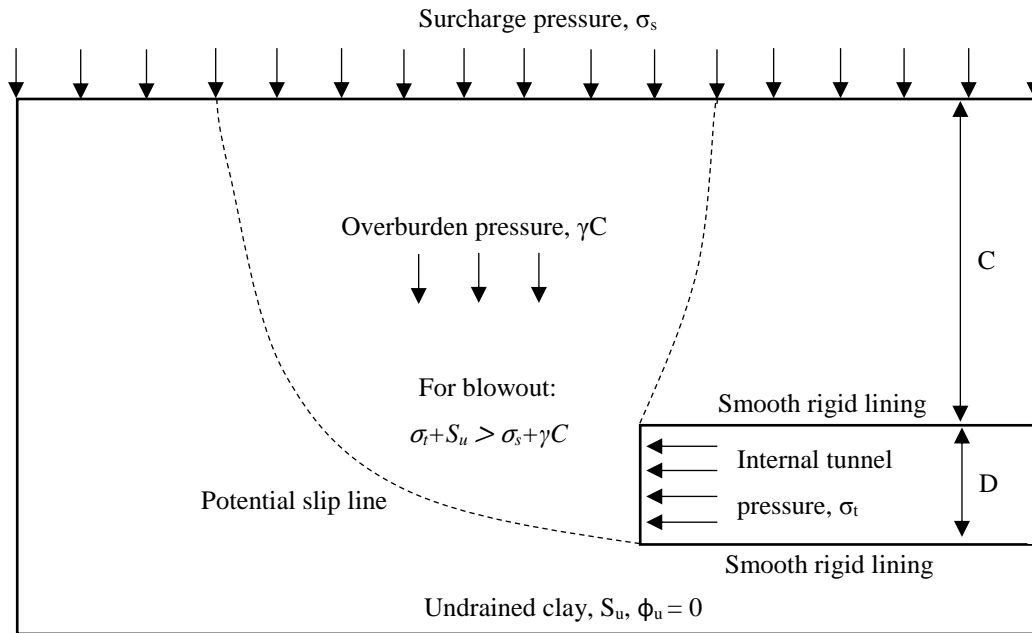


Figure 5.1: Tunnel heading stability problem statement.

Figure 5.1 presents a conceptual model of the tunnel heading problem making it possible to comprehend the three important dimensionless variable parameters. The depth ratio ( $DR$ ), shown in Equation 5.1, relates the geometrical properties of the model, tunnel height and tunnel cover. To represent shallow tunnelling conditions the depth ratio was varied between 1 and 3 in increments of one. Tunnel height remained constant at 6m while cover was varied.

$$\text{Depth Ratio } (DR) = \frac{C}{D} \quad (5.1)$$

where  $C = \text{cover above tunnel [m]}$ ; and  
 $D = \text{height of tunnel excavation [m]}$ .

The strength ratio ( $SR$ ) can be represented in two different ways for this problem. The soil strength can be normalised to either the cover ( $C$ ), as shown in Equation 5.2, or the tunnel height ( $D$ ), as shown in Equation 5.3. Both formulations of the strength ratio were tested for this project and it was found that normalising the strength ratio to the tunnel height ( $D$ ), as shown in Equation 5.3, produced the clearest and most effective results. To cover a broad range of practical scenarios the strength ratio ( $S_u/\gamma D$ ) is varied between 0.10 and 2.00

in increments of 0.20 up to 1.50 and then a final increment of 0.50. Unit weight and tunnel height were kept constant at 18kN/m<sup>3</sup> and 6m respectively while undrained shear strength was varied.

$$\text{Strength Ratio (SR)} = \frac{S_u}{\gamma C} \quad (5.2)$$

$$\text{Strength Ratio (SR)} = \frac{S_u}{\gamma D} \quad (5.3)$$

where  $S_u = \text{undrained shear strength of soil [N/m}^2\text{]}; \text{ and}$   
 $\gamma = \text{unit weight of soil [N/m}^3\text{]}.$

The third dimensionless variable to be considered is the pressure ratio (*PR*). Classically this parameter has been defined as the load parameter but has been redefined as the pressure ratio in this project for simplicity and uniformity. The pressure ratio, shown in Equation 5.4, can be defined as the resultant applied pressure, be that a surcharge or internal tunnel pressure, compared to the undrained shear strength of the soil. To produce an acceptable range of data for modelling purposes the pressure ratio was varied between -16 and +10 with a focus on points ranging between -1 and -16 when analysing the collapse failure mechanism.

$$\text{Pressure Ratio (PR)} = \frac{\sigma_s - \sigma_t}{S_u} \quad (5.4)$$

where  $\sigma_s = \text{the applied surcharge pressure [N/m}^2\text{]}; \text{ and}$   
 $\sigma_t = \text{the applied internal tunnel pressure [N/m}^2\text{]}.$

The upper and lower bound factor of safety values are a function of these three dimensionless parameters and can therefore be expressed as shown in Equation 5.5.

$$\text{Factor of Safety (FoS)} = f\left(\frac{C}{D}, \frac{S_u}{\gamma D}, \frac{\sigma_s - \sigma_t}{S_u}\right) \quad (5.5)$$

In previous tunnel heading stability literature the results and design charts are not expressed in a factor of safety format. They are generally represented as a stability number, which is

a function of a particular depth ratio and strength ratio with a corresponding factor of safety of one. This stability number can generally cover a broader range of collapse failure scenarios when applied to a single design chart than a factor of safety approach, but is often confusing and somewhat impractical for practicing engineers interested in the factor of safety that a particular scenario can provide. As this stability number relates to a factor of safety of one it is defined as the critical pressure ratio ( $PR_c$ ) in this thesis. The approach used to calculate the critical pressure ratio is shown in Equation 5.6. The corresponding strength ratio, shown in Equation 5.7, is the inverse of the strength ratio adopted in this thesis, and is defined as the critical strength ratio ( $SR_c$ ) as it also only relates to a factor of safety of one. To find the critical pressure ratio and critical strength ratio, both the pressure ratio and strength ratio adopted in this thesis must be normalised by multiplying by the corresponding factor of safety.

$$PR_c = \frac{\sigma_s - \sigma_t}{S_u} * FOS \quad (5.6)$$

$$SR_c = \left( \frac{S_u}{\gamma D} \right)^{-1} * FOS \quad (5.7)$$

Other Tresca material properties that had a marginal effect on factor of safety results included; Poisson's ratio ( $\nu$ ) = 0.49 and Young's modulus ( $E$ ) = 30MPa. A graphical example of the blowout failure mechanism produced by Optum G2 is shown in Figure 5.2. The model represents a scenario with depth ratio of two, strength ratio of 1.10 and pressure ratio of negative sixteen and shows the plastic multiplier overlay with a deformation scale of sixty percent.

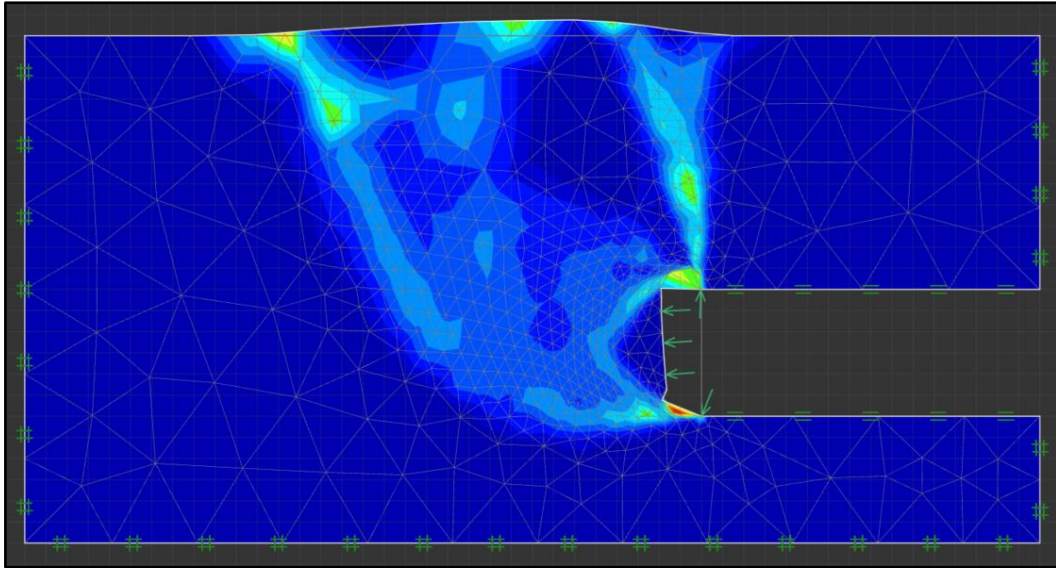


Figure 5.2: Example of blowout failure mechanism produced in Optum G2 showing plastic multiplier and 60% deformation scale.  $DR = 2$ ,  $SR = 1.10$ ,  $PR = -16$ .

### 5.3 Significance of the Blowout Failure Mechanism

Most previous tunnel stability research has been predominantly focused on the collapse failure mechanism, and historically, the majority of tunnel failures have occurred in this fashion. However, the ever increasing use of tunnel boring machines, especially earth pressure balance and slurry shield machines, which are capable of applying a great deal of pressure at the excavation face, could lead to an increase in tunnel failures caused by blowout during the construction phase.

The Civil Engineering and Development Department (2012) described one such example of a blowout failure during tunnel construction which occurred in 1998 on the Docklands Light Rail tunnel project in the United Kingdom. The tunnel was of a circular cross-section, 5.2 metres in diameter, and was to be excavated by an earth pressure balance TBM. To prevent water from seeping into the tunnel it was pressurised with compressed air, as shown in Figure 5.3. The combination of high internal tunnel pressure and insignificant overburden cover lead to catastrophic blowout failure. A shower of mud and rock from the explosive blowout broke windows up to 100 metres away and a seven metre deep by twenty-two metre wide sinkhole formed on the surface in the grounds of the George Green School, as shown in Figure 5.4. It was found that the contractor had not considered the factor of safety against the blowout failure mechanism and was consequently fined one million Great British Pounds, the third highest ever fine for a construction accident as of January 2004 (Institution of Civil Engineers 2004).

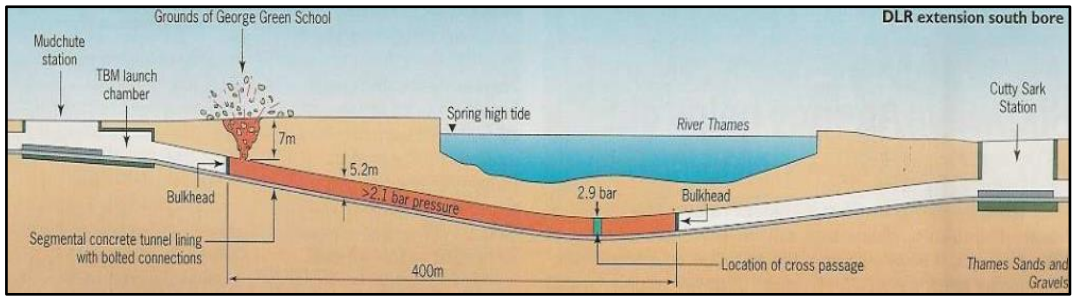


Figure 5.3: Docklands blowout failure diagram (Institution of Civil Engineers 1998).



Figure 5.4: Sinkhole caused by blowout (Institution of Civil Engineers 1998).

## 5.4 2D Tunnel heading Numerical Modelling

Due to the complex and uncertain behavior of soil, geotechnical investigations are a difficult undertaking. Numerical modelling techniques are continually improving and can now offer an accurate solution to such problems. Finite element limit analysis is an example of one such technique that has been used successfully in the past for modelling tunnels. This project employs the FELA technique through the relatively new program, Optum G2. The numerical procedures used in Optum G2 are based on the standard finite element method and the limit theorems of classical plasticity.

When creating the geometrical model it is important to consider the size of the domain. A model that is too small will not act as an infinite excavation and results will be affected by the boundary restraints, while a model that is too large will have excessive central processing unit (CPU) run time and produce less accurate results due to mesh dilution. The boundary conditions of the model are also very important to ensure that the model is restrained within space and that the only two surfaces that can displace are the ground surface and the face of the tunnel heading. The base and sides of the model were full restrained in the 'x' and 'y' directions, while the smooth rigid lining was restrained only in the normal direction to simulate a concrete lining. The size of the model was chosen so that these restraints had very little effect on the results. Figure 5.5 shows a typical two-dimensional finite element model of the tunnel heading problem.

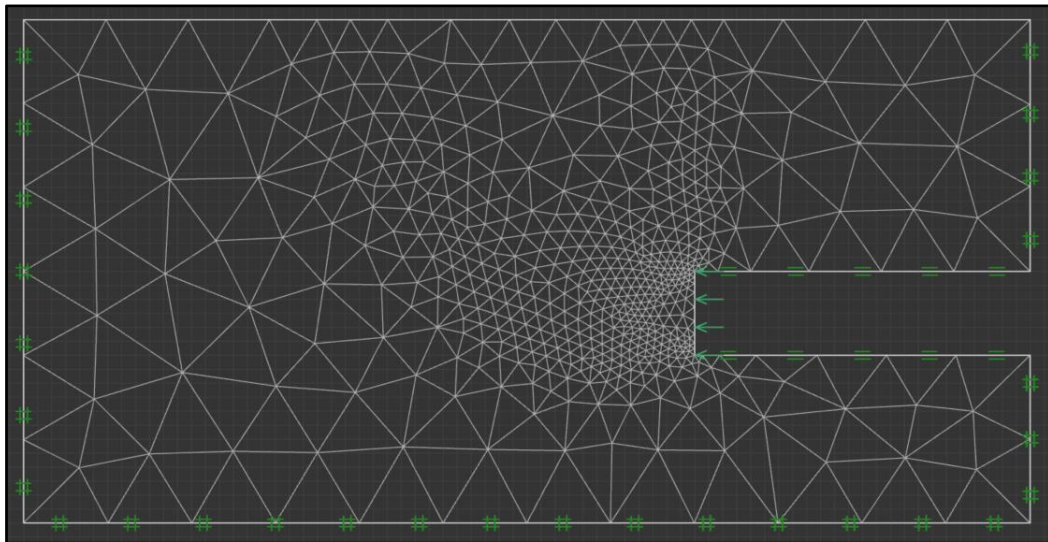


Figure 5.5: Tunnel heading finite element mesh with mesh adaptivity.

The number of finite elements was set at 1000 for all scenarios. Mesh adaptivity was enabled, allowing for three iterations with 1000 starting elements. Figure 5.5 displays this same scenario for a depth ratio of two. It can be seen that little mesh distortion occurs around the model boundaries, meaning the boundaries have no noticeable impact on results.

Tunnel height ( $D$ ) of 6m and unit weight of the soil ( $\gamma$ ) of 18kN/m<sup>2</sup> were adopted as constant values for all scenarios. The depth ratio ( $C/D$ ) was varied from 1 to 3 by adjusting the cover ( $C$ ) by 6m each time. The undrained shear strength of the clay ( $S_u$ ) was varied incrementally from 10.8kPa to 216kPa to obtain strength ratios ( $S_u/\gamma D$ ) varying from 0.10 to 2.00. The strength ratio increased in increments of 0.20 up until the strength ratio of 1.50 is reached and then in one final increment of 0.50. The pressure ratio ( $(\sigma_s - \sigma_t)/S_u$ ) was

varied from -16 to +10 with the majority of points focused in the range of negative one to negative sixteen for a blowout failure mechanism.

## 5.5 Factor of Safety Bounds

Upper and lower bound factor of safety values were computed for the various scenarios by using the gravity multiplier method (GMM) and the strength reduction method (SRM). To perform an analysis using the gravity multiplier method the software incrementally increases the gravity by a multiplying factor until a state of failure is reached. The factor by which the gravity is multiplied can be taken as the factor of safety. For example, if the gravity must be multiplied by three to cause failure then the factor of safety in this scenario is three. Equation 5.8 shows the formulation of the factor of safety from the gravity multiplier method.

$$\text{Factor of Safety (FoS)} = \frac{g_{cr}}{g} \quad (5.8)$$

where  $g_{cr}$  = the gravitational acceleration at failure [ $m/s^2$ ]; and  
 $g$  = the actual gravitational acceleration =  $9.81[m/s^2]$ .

To perform an analysis using the strength reduction method the software performs a number of iterations and incrementally varies the strength of the soil until an optimum state of failure is reached. Unlike the gravity multiplier method, the strength reduction method decreases the shear strength of the soil until failure is reached and then performs a number of iterations to work on optimizing this value until the exact failure multiplier is found. Similarly to the gravity multiplier method, the amount by which the strength of the soil is reduced to induce an optimum state of failure can be taken as the factor of safety. For example if the strength of the soil must be decreased by two times then the corresponding factor of safety value would be two. Equation 5.9 shows the formulation of the factor of safety from the strength reduction method.

$$\text{Factor of Safety (FoS)} = \frac{S_u}{S_{u.cr}} \quad (5.9)$$

where  $S_u$  = original undrained shear strength of the soil [ $N/m^2$ ]; and  
 $S_{u.cr}$  = undrained shear strength of the soil at failure [ $N/m^2$ ].

Both the gravity multiplier method and strength reduction method were used to calculate the upper and lower bound factor of safety values for the majority of scenarios but to decide which method was capable of producing the most accurate results the two methods had to be compared. An internal comparison was performed to determine the accuracy of upper and lower bound results and to compare the factor of safety values produced by the gravity multiplier method and strength reduction method in Section 4.5 “Internal Comparison of Results”. It was found that the strength reduction method was the only method capable of calculating accurate factor of safety values for a scenario with a positive pressure ratio, nevertheless it was still necessary to compare the methods for a negative pressure ratio.

## 5.6 Internal Comparison of Blowout Results

Section 4.5 ‘Internal Comparison of Results’ contained a comparison of results obtained for scenarios with a pressure ratio equal to zero and then to positive five in order to determine the accuracy of results obtained for cases exhibiting a collapse failure mechanism. It was determined that for a pressure ratio of zero the upper and lower bound factor of safety results have a very good level of agreement, as do the results obtained from both the strength reduction method and gravity multiplier method. Upon performing a comparison of results achieved for a non-zero pressure ratio it became apparent that the gravity multiplier method was incapable of correctly performing the tunnel heading stability analysis for positive pressure ratios. The lower and upper bound factor of safety values obtained by the strength reduction method for a positive pressure ratio still showed a very good level of agreement, hence the strength reduction method was adopted. It was necessary to also compare the lower and upper bound factor of safety results and the gravity multiplier method and strength reduction method for a negative pressure ratio predominantly resulting in failure due to blowout. Table 5.1 shows the comparison of lower and upper bound factor of safety results from both the strength reduction method and gravity multiplier method for scenarios predominantly resulting in failure due to the blowout mechanism. The percentage difference has been calculated as per Equation 5.10. All lower and upper bound results calculated by the strength reduction method and gravity multiplier method are available in Appendix B – ‘Initial Results and Plots’.

$$\text{Percentage Difference (PD)} = \text{ABS} \left( \frac{\text{UB Fos} - \text{LB Fos}}{\text{Average Fos}} \right) * 100 \quad (5.10)$$

Table 5.1: Comparison of upper and lower bound factor of safety results for PR = -8.

Lower & Upper Bound FoS Comparison, PR = -8									
DR	SR	SRM LB	SRM UB	SRM AV	PD (%)	GMM LB	GMM UB	GMM AV	PD (%)
1	0.10	0.525	0.561	0.543	6.63	0.753	0.772	0.763	2.49
	0.30	1.269	1.354	1.312	6.48	2.258	2.315	2.287	2.49
	0.50	0.815	0.872	0.844	6.76	3.763	3.858	3.811	2.49
	0.70	0.700	0.747	0.724	6.50	5.269	5.402	5.336	2.49
	0.90	0.647	0.691	0.669	6.58	6.774	6.945	6.860	2.49
	1.10	0.619	0.661	0.640	6.56	8.279	8.488	8.384	2.49
	1.30	0.600	0.640	0.620	6.45	9.785	10.031	9.908	2.48
	1.50	0.583	0.626	0.605	7.11	11.290	11.575	11.433	2.49
	2.00	0.566	0.604	0.585	6.50	15.053	15.433	15.243	2.49
2	0.10	0.295	0.319	0.307	7.82	0.511	0.526	0.519	2.89
	0.30	2.476	2.610	2.543	5.27	1.533	1.578	1.556	2.89
	0.50	1.655	1.784	1.720	7.50	2.555	2.630	2.593	2.89
	0.70	1.148	1.248	1.198	8.35	3.577	3.682	3.630	2.89
	0.90	0.987	1.062	1.025	7.32	4.599	4.734	4.667	2.89
	1.10	0.899	0.971	0.935	7.70	5.621	5.786	5.704	2.89
	1.30	0.841	0.919	0.880	8.86	6.643	6.838	6.741	2.89
	1.50	0.807	0.881	0.844	8.77	7.665	7.890	7.778	2.89
	2.00	0.761	0.828	0.795	8.43	10.220	10.520	10.370	2.89
3	0.10	0.214	0.233	0.224	8.50	0.388	0.403	0.396	3.79
	0.30	1.474	1.612	1.543	8.94	1.164	1.208	1.186	3.71
	0.50	4.077	4.489	4.283	9.62	1.941	2.013	1.977	3.64
	0.70	1.901	2.076	1.989	8.80	2.717	2.819	2.768	3.68
	0.90	1.403	1.535	1.469	8.99	3.493	3.624	3.559	3.68
	1.10	1.210	1.316	1.263	8.39	4.269	4.429	4.349	3.68
	1.30	1.100	1.195	1.148	8.28	5.045	5.234	5.140	3.68
	1.50	1.023	1.122	1.073	9.23	5.821	6.040	5.931	3.69
	2.00	0.929	1.018	0.974	9.14	7.762	8.053	7.908	3.68

Table 5.1 shows that the lower and upper bound results obtained by the strength reduction method have a good level of agreement, with the percentage difference less than ten percent for all scenarios tested. It can also be seen that the general trend of the percentage difference increasing as the depth ratio increases, as discovered for both a zero and positive pressure ratio, is also applicable for a situation with a negative pressure ratio. The lower and upper bound factor of safety results obtained from the gravity multiplier method have a very good level of agreement, with the percentage difference less than four percent for all scenarios tested. When comparing the strength reduction method to the gravity

multiplier method it can be seen that the results do not appear to be similar, so both methods must be directly compared. The CPU run times of both methods, for scenarios resulting in failure due to the blowout mechanism, are compared in Table 5.2 and the factor of safety results obtained from both methods, for scenarios predominantly resulting in failure due to the blowout mechanism for a pressure ratio of negative eight, are compared in Table 5.3. The percentage difference between gravity multiplier method and strength reduction method results was calculated according to Equation 5.11.

$$\text{Percentage Difference (PD)} = ABS \left( \frac{\text{Av. GMM FoS} - \text{Av. SRM FoS}}{\text{Av. FoS}} \right) * 100 \quad (5.11)$$

Table 5.2: CPU run time comparison for various blowout scenarios.

CPU Run Time Comparison (Blowout)					
Depth Ratio (C/D)	Pressure Ratio (( $\sigma_s - \sigma_t$ )/ $S_u$ )	Strength Ratio ( $S_u/\gamma D$ )	SRM UB Time (s)	GMM UB Time (s)	Run Time Difference (s)
1	-16	0.30	48	7	41
	-5	1.10	35	6	29
	-2	1.50	33	6	27
2	-8	0.50	39	6	33
	-3	1.30	35	6	29
	-1.5	2.00	47	7	40
3	-16	0.70	37	6	31
	-8	0.90	30	6	24
	-2	2.00	51	7	44
Average			39.4	6.3	33.1

The sample data used for the CPU run time comparison was selectively chosen to represent a broad range of scenarios resulting in failure due to blowout with differing depth ratios, strength ratios and pressure ratios. The upper bound factor of safety values were used for the purpose of run time analysis to keep the test conditions constant. It can be seen from Table 5.2 that the strength reduction method can take anywhere between 24 to 44 seconds longer than the gravity multiplier method when calculating the upper bound factor of safety for the same scenario. From the sample data it is calculated that the strength reduction method takes an average time of 39.4 seconds to calculate the upper bound factor of safety while the gravity multiplier method takes an average time of just 6.3 seconds. This large difference in run time is likely due to the iterative nature of the strength reduction method. Instead of just returning the first multiplier found to cause failure like the gravity multiplier method, the strength reduction method will optimise the final result by closing in on an

optimum factor of safety and then increasing and decreasing the material strength in small increments until the most accurate solution is found. The fast processing time of the gravity multiplier method is a very attractive quality when performing large scale analysis of multiple models but to comprehensively compare both of the methods the factor of safety results from a scenario with a non-zero pressure ratio resulting in failure due to blowout must be compared.

Table 5.3: Comparison of GMM and SRM results for PR = -8.

GMM & SRM FoS Results Comparison, PR = -8									
SR	DR = 1			DR = 2			DR = 3		
	SRM AV	GMM AV	PD (%)	SRM AV	GMM AV	PD (%)	SRM AV	GMM AV	PD (%)
0.10	0.543	0.763	33.63	0.307	0.519	51.24	0.224	0.396	55.57
0.30	1.312	2.287	54.20	2.543	1.556	48.19	1.543	1.186	26.16
0.50	0.844	3.811	127.5	1.720	2.593	40.49	4.283	1.977	73.67
0.70	0.724	5.336	152.2	1.198	3.630	100.7	1.989	2.768	32.78
0.90	0.669	6.860	164.4	1.025	4.667	127.9	1.469	3.559	83.12
1.10	0.640	8.384	171.6	0.935	5.704	143.6	1.263	4.349	109.9
1.30	0.620	9.908	176.4	0.880	6.741	153.8	1.148	5.140	126.9
1.50	0.605	11.433	179.9	0.844	7.778	160.8	1.073	5.931	138.7
2.00	0.585	15.243	185.2	0.795	10.370	171.5	0.974	7.908	156.1

Table 5.3 shows that the results achieved from the strength reduction method and the gravity multiplier method have a very low level of agreement. The average factor of safety results obtained from both methods deviate further from one another as the strength ratio increases. Interestingly, the percentage difference between methods gets smaller as the depth ratio increases, this is an area that could be studied further. To determine which method is producing the most accurate set of results it is necessary to compare the failure mechanism relevant to both. Figures 5.6 and 5.7 show the displacement vector fields and define the failure mechanisms related to the strength reduction method and gravity multiplier method respectively. The scenario chosen was for a model with a strength ratio of two, depth ratio of one and pressure ratio of negative eight, to highlight the highest percentage difference calculated in Table 5.3.

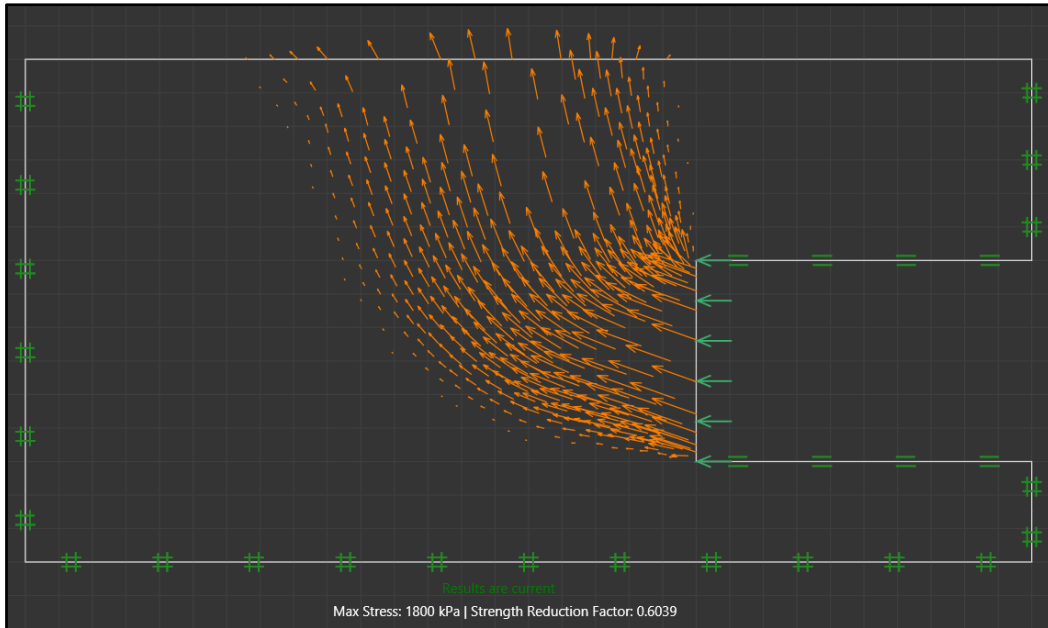


Figure 5.6: Displacement vector field showing failure mechanism for SRM upper bound.  $DR = 1$ ,  $SR = 2.00$ ,  $PR = -8$  and corresponding  $FoS = 0.604$ .

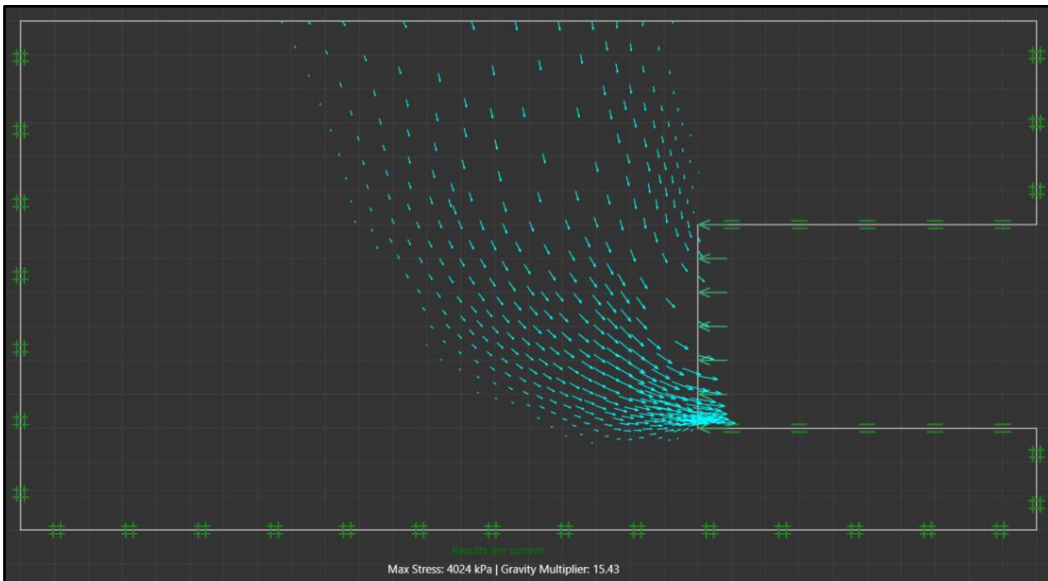


Figure 5.7: Displacement vector field showing failure mechanism for GMM upper bound.  $DR = 1$ ,  $SR = 2.00$ ,  $PR = -8$  and corresponding  $FoS = 15.43$ .

Figure 5.6 indicates that the factor of safety calculated from the strength reduction method relates to a blowout failure mechanism, while Figure 5.7 indicates that the factor of safety calculated from the gravity multiplier method relates to a collapse failure mechanism. This comparison, when paired with the unreasonably large factor of safety results obtained from the GMM, suggest that the gravity multiplier method is not capable of analysing tunnel

heading stability problems relating to a blowout failure mechanism. The reason for this difference in results is due to the definition of the gravity multiplier method. The GMM works by multiplying the gravity which always acts uniformly in the downward direction. When an internal tunnel pressure is applied to the tunnel face the gravity multiplier method increases the gravity until the downward load can overcome the supporting internal tunnel pressure, resulting in a large factor of safety against collapse. The GMM does not account for any failure mechanism other than collapse and is therefore not capable of determining that the minimum factor of safety for a scenario may relate to a blowout failure. For this reason, the strength reduction method was chosen to perform the analysis of all tunnel heading stability problems with a pressure ratio less than zero. Figure 5.8 plots the upper and lower bound factors of safety found from the strength reduction method to further demonstrate the acceptability of the strength reduction method and its application to analysing tunnel heading stability problems with a pressure ratio less than zero.

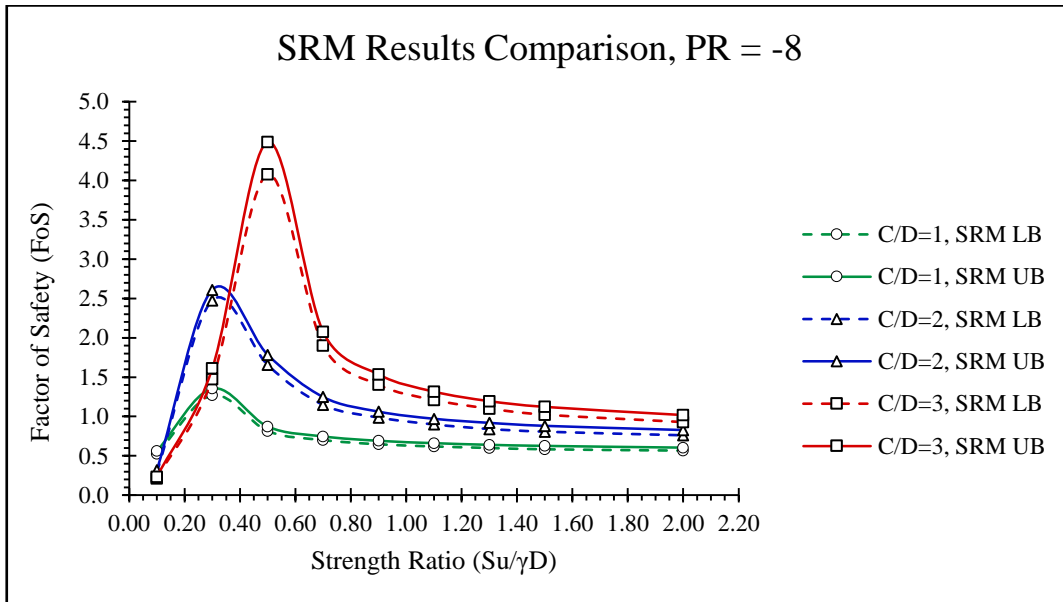


Figure 5.8: Graphical comparison of upper and lower bound results obtained through SRM for PR = -8.

Figure 5.8 reinforces the trend shown in Table 5.1, that is the upper and lower bound solutions have a good level of agreement but become increasingly different as the depth ratio increases. Figure 5.8 also shows that when the pressure ratio is less than zero, the factor of safety no longer increases linearly with the strength ratio like it does when the pressure ratio equals zero. This new concept is further explained in Section 5.7 “Optimum G2 Tunnel Heading Blowout Results and Discussion”.

Performing an internal comparison of results made it apparent that the gravity multiplier method would not be suitable for analysing tunnel heading stability problems with a pressure ratio less than zero, so the strength reduction method was adopted for this portion of research. It was not possible to compare blowout factor of safety results to previously published results. It became apparent that the blowout failure mechanism was not considered by Augarde, Lyamin and Sloan (2003) and that the approach adopted in Section 4.6 “External Comparison of Collapse Results” was not capable of transforming a factor of safety relating to a blowout failure into a critical pressure ratio as presented in the published results. Very little previous research has been focused on the blowout failure mechanism relating to shallow undrained tunnel heading stability, meaning it was not possible to directly compare results. Ultimately the factor of safety results obtained from the strength reduction method in Optum G2 have been verified in Section 4.6, and those relating to blowout failure are logical and reasonable. Due to lack of comparable previous work the results produced by the Optum G2 strength reduction method for a blowout scenario are considered to be acceptable.

## **5.7 Optum G2 Tunnel Heading Blowout Results and Discussion**

The stability of a tunnel heading relating to the blowout failure mechanism is a complex topic. Only pressure ratios  $((\sigma_s - \sigma_t)/S_u)$  less than zero can induce tunnel heading failure by the blowout mechanism, with the depth ratio  $(C/D)$  and strength ratio  $(S_u/\gamma D)$  being the other critical dimensionless parameters. Optum G2 was used to model and analyse a range of tunnel heading scenarios where the major failure mechanism was blowout. Two stages of testing were conducted. The first stage of testing adopted the strength reduction method to rigorously compute both the upper and lower bound factor of safety values for a broad range of practical pressure ratios. The second stage also adopted the strength reduction method but only calculated the upper bound factor of safety values that were required to fill in critical gaps in the data for modelling purposes. For this reason, the upper bound factor of safety values found from the strength reduction method will be adopted as the factor of safety value used in all modelling and data analysis. All upper bound factor of safety results calculated through the strength reduction method are available in Appendix D – ‘Final Results and Plots’.

To determine the method of failure corresponding to each factor of safety value it was necessary to view the displacement vector field overlay for each model in Optum G2. An

example of a blowout displacement vector field for a pressure ratio of negative five, depth ratio of two and strength ratio of 1.50 is shown in Figure 5.9.

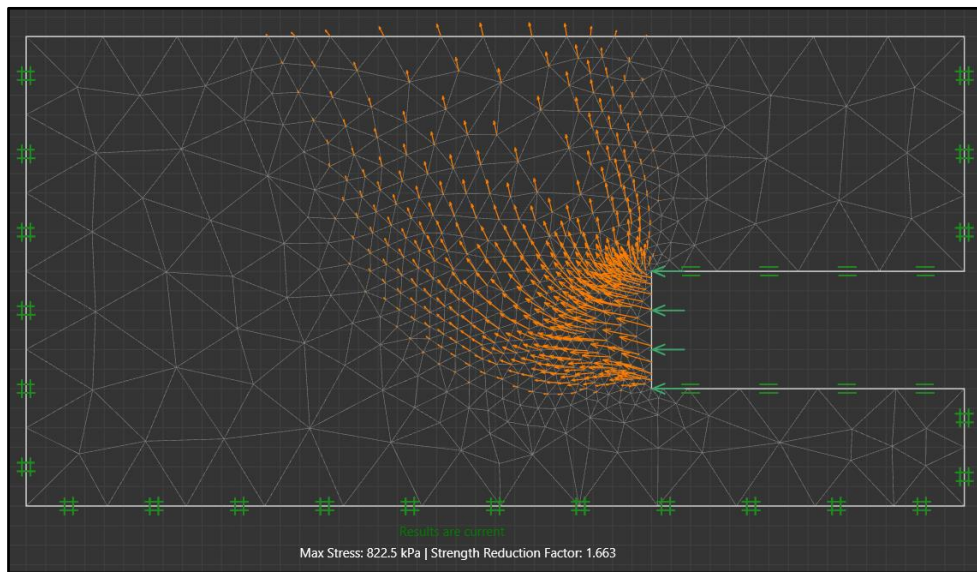


Figure 5.9: Tunnel heading failure by blowout showing displacement vector field. PR = -5, DR = 2 & SR = 1.50.

The direction of the displacement vector arrows in Figure 5.9 indicates an upward displacement at failure, or failure by blowout. The length of the displacement vector arrows indicates that the maximum displacement will be occurring at the tunnel face with the ground surface displacing less. The field created by the displacement vector arrows shows the failure zone with the outside edges being potential slip lines as described in Figure 5.1. The corresponding data for the model shown in Figure 5.9, that is, a depth ratio equal to two and a strength ratio equal to 1.50, inclusive of all pressure ratios related to failure by blowout, is presented in Table 5.4. The corresponding plot of factor of safety verse pressure ratio for the same case is shown in Figure 5.10.

Table 5.4: Factor of safety results for collapse failure related to model with DR = 2 and SR = 1.50.

Factor of Safety Results for Blowout when DR = 2		
SR ( $S_u/\gamma D$ )	PR ( $(\sigma_s - \sigma_t)/S_u$ )	FoS (UB SRM)
1.50	-16	0.389
	-8	0.881
	-5	1.663
	-3	4.088
	-2	13.034

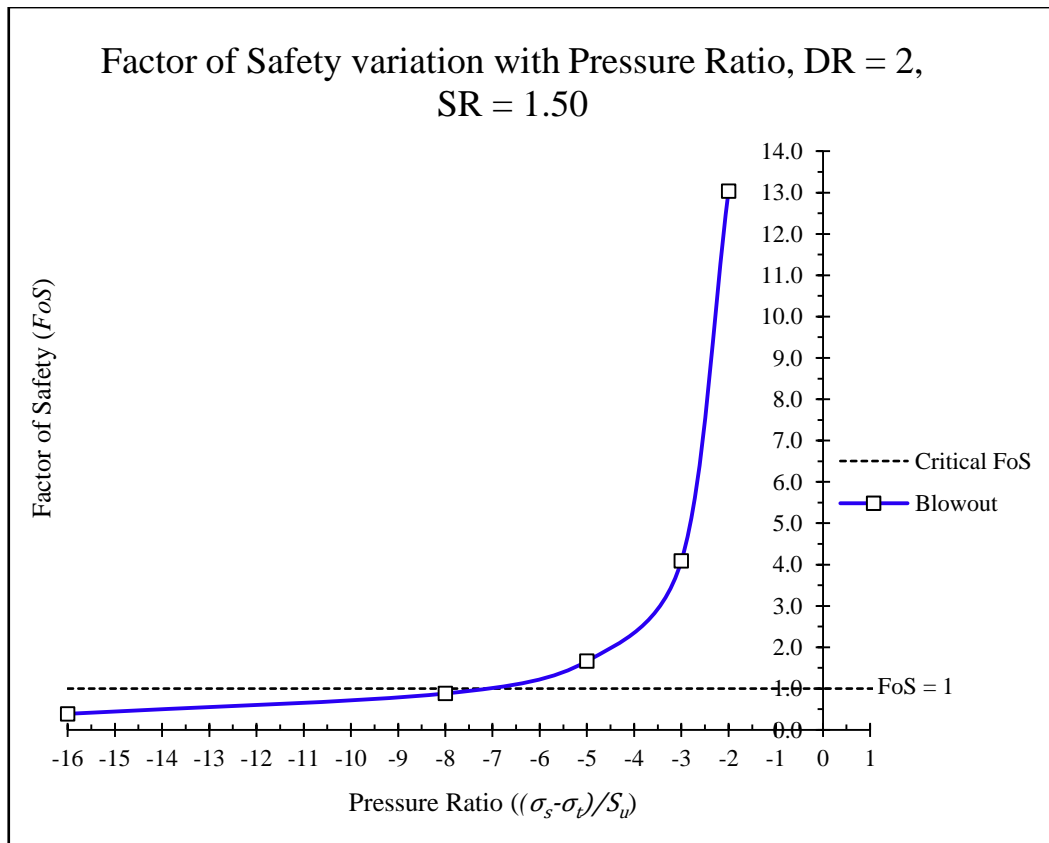


Figure 5.10: Plot of factor of safety verse pressure ratio for tunnel heading problem, DR = 2 and SR = 1.50.

Figure 5.10 shows the full range of scenarios relating to the blowout failure mechanism for a tunnel heading model with a depth ratio of two and a strength ratio of 1.50. It can be seen from the curve that the factor of safety decreases as the pressure ratio decreases infinitely while the factor of safety increases infinitely as the pressure ratio increases. It is thought that the curve is hyperbolic in nature and that a pair of asymptotes exist. It is hypothesised that a ‘weightless scenario’ exists about the asymptote where the factor of safety is at a maximum. This theory will be discussed in more detail after the displacement vector fields are examined. This plot shows that a critical factor of safety of one is unachievable for this scenario once the pressure ratio reaches approximately negative seven. The optimum factor of safety is achieved at a slightly negative pressure ratio, and in this particular case a pressure ratio of negative two produces the highest factor of safety of approximately thirteen. This result is in line with what is expected in practice as a negative pressure ratio is formed by applying an internal tunnel pressure which acts to resist the overburden pressure of the soil. As the pressure ratio decreases further, the factor of safety against blowout failure is decreased, similar to a tunnel boring machine exerting excessive pressure on a tunnel face excavation. To create a pressure ratio of negative two a uniform internal tunnel pressure two times the undrained shear strength of the soil must be applied to the

tunnel face. All corresponding displacement vector fields relating to the scenario in Figure 5.9 and 5.10 are displayed in Figures 5.11 through to 5.15 in ascending order of pressure ratio.

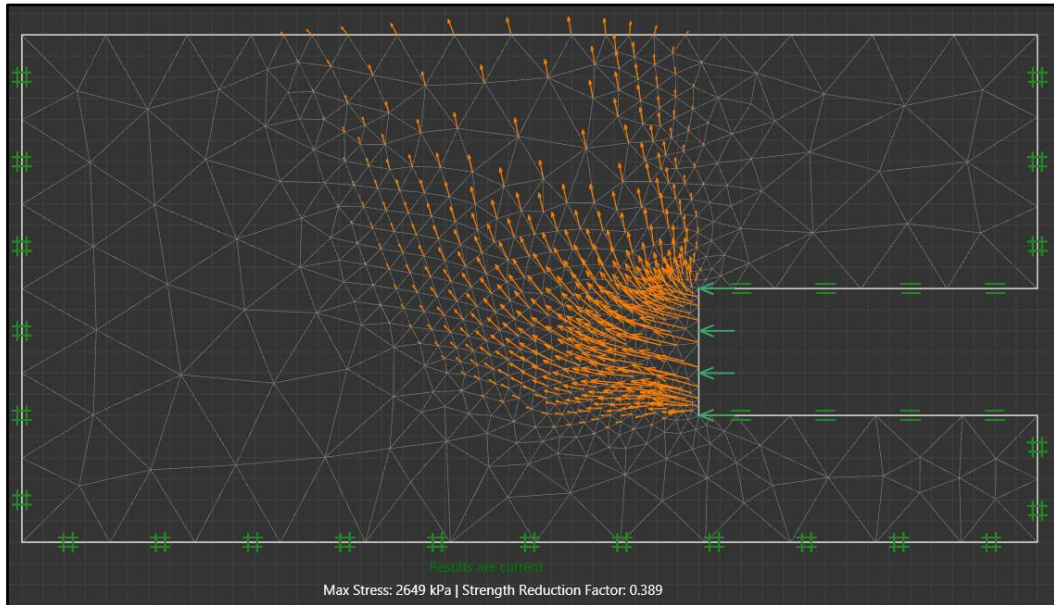


Figure 5.11: Displacement vector field.  $PR = -16$ ,  $DR = 2$ ,  $SR = 1.50$ .

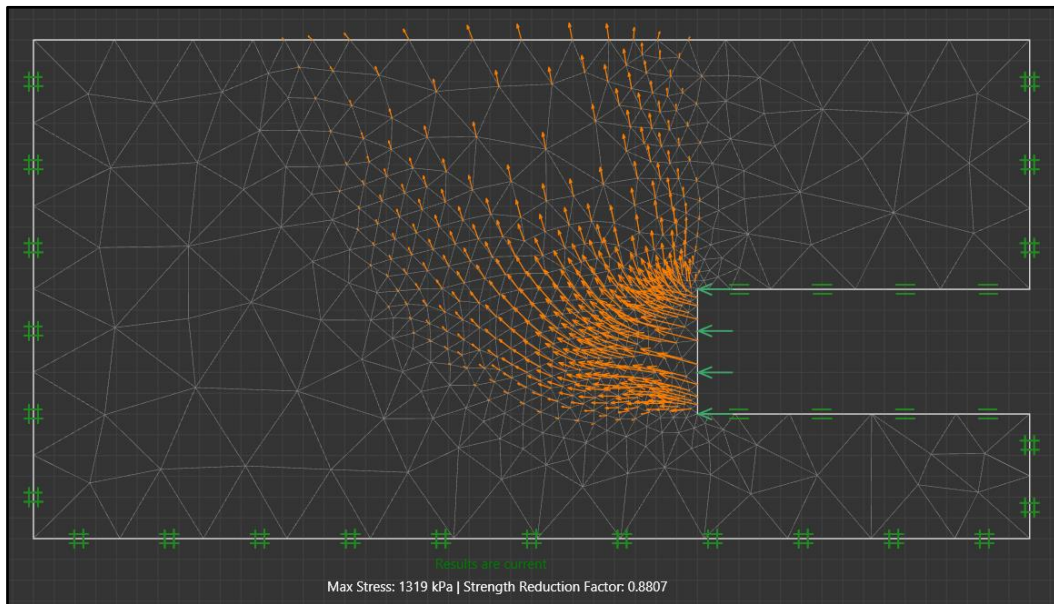


Figure 5.12: Displacement vector field.  $PR = -8$ ,  $DR = 2$ ,  $SR = 1.50$ .

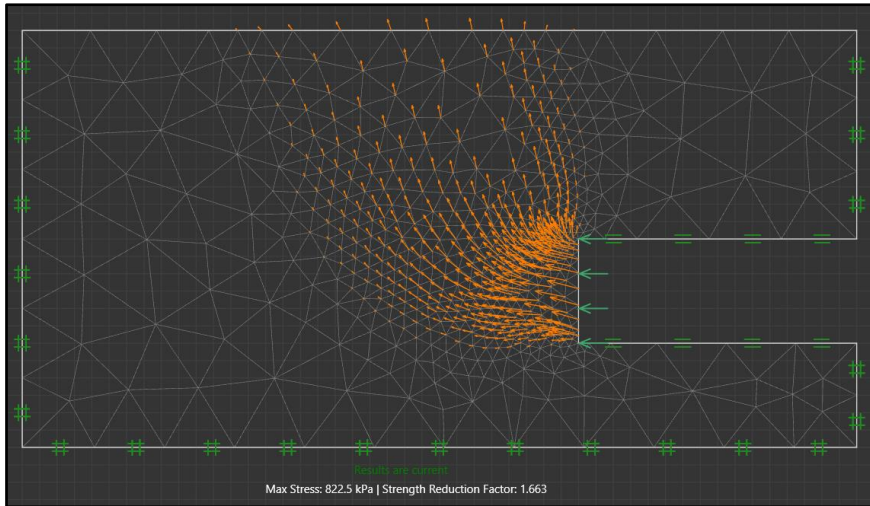


Figure 5.13: Displacement vector field.  $PR = -5$ ,  $DR = 2$ ,  $SR = 1.50$ .

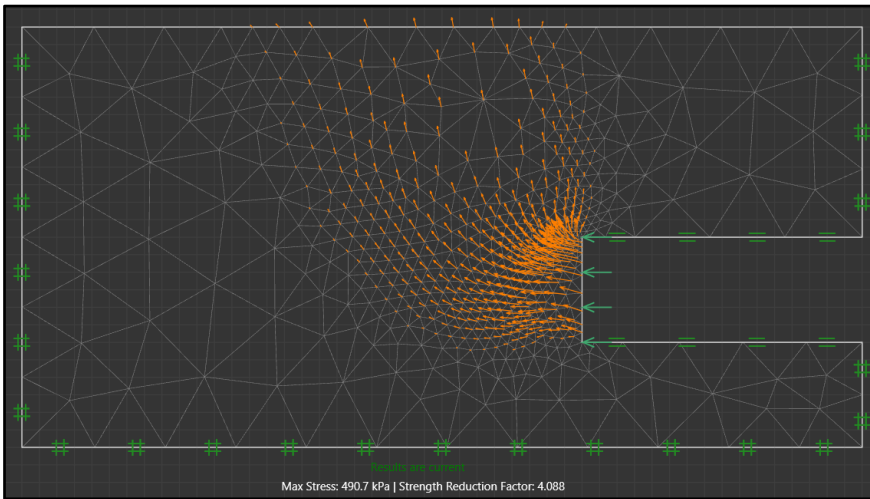


Figure 5.14: Displacement vector field.  $PR = -3$ ,  $DR = 2$ ,  $SR = 1.50$ .

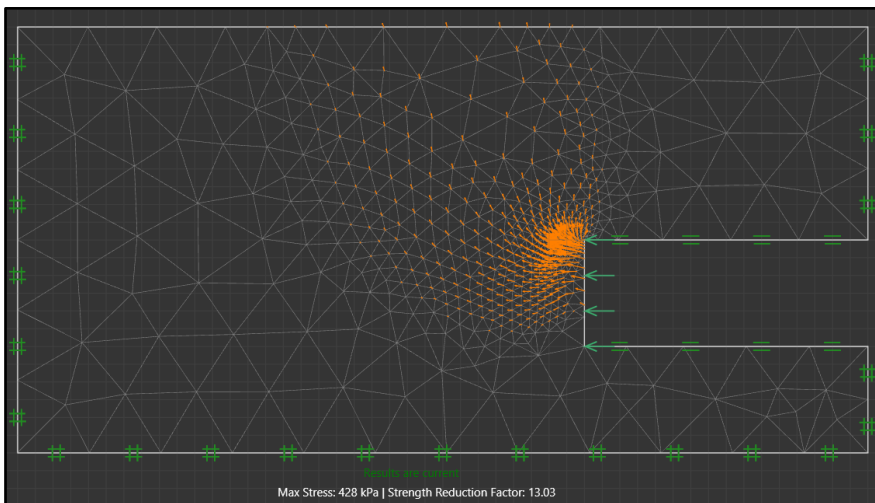


Figure 5.15: Displacement vector field.  $PR = -2$ ,  $DR = 2$ ,  $SR = 1.50$

Figures 5.11 through to 5.15 confirm that the failure mechanism corresponding to the results presented in Table 5.4 and Figure 5.10 is indeed blowout. It can be seen that as the pressure ratio decreases, the displacement vector field becomes denser and the arrows become longer. These results are as to be expected and represent the decrease in factor of safety as the pressure ratio decreases as seen in Figure 5.10. Figure 5.15, displaying a pressure ratio of negative two, presents a situation where the problem is approaching the weightless condition. If a slightly higher pressure ratio was to be applied then the arrows would swirl in a counter-clockwise direction about the tunnel face, similarly to the situation shown in Figure 4.16, which presents a pressure ratio of negative 1.5 for this same model. In practice, it is possible that this weightless situation could exist when the internal tunnel pressure plus the resistance contributed by the shear strength of the soil is exactly equal to the downward pressure caused by the surcharge and overburden pressures.

It has long been known that the factor of safety increases linearly with the strength ratio for a case where the pressure ratio is equal to zero. It was noted in Section 5.6 “Internal Comparison of Blowout Results” that the relationship between the factor of safety and the strength ratio was not linear for a case with a negative pressure ratio. Figures 5.16, 5.17 and 5.18 explore this relationship further by plotting the upper bound factor of safety against the strength ratio for all negative pressure ratios tested for a depth ratio of one, two and three respectively. The upper bound factor of safety for all negative pressure ratios is presented in table 5.5.

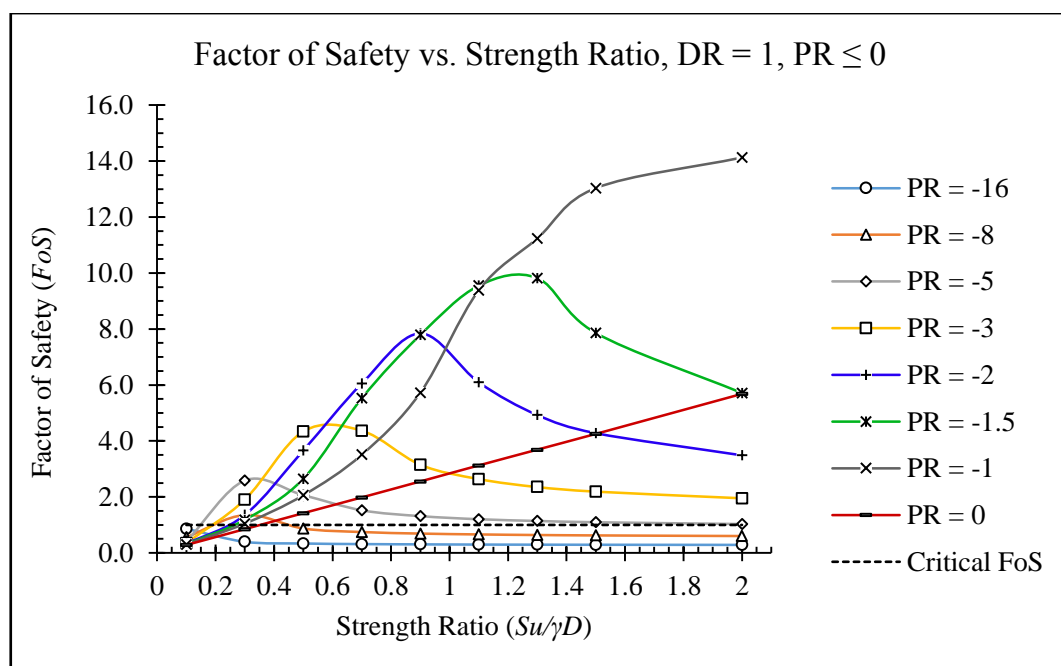


Figure 5.16: Factor of safety vs. strength ratio for all negative pressure ratios.  $DR = 1$ .

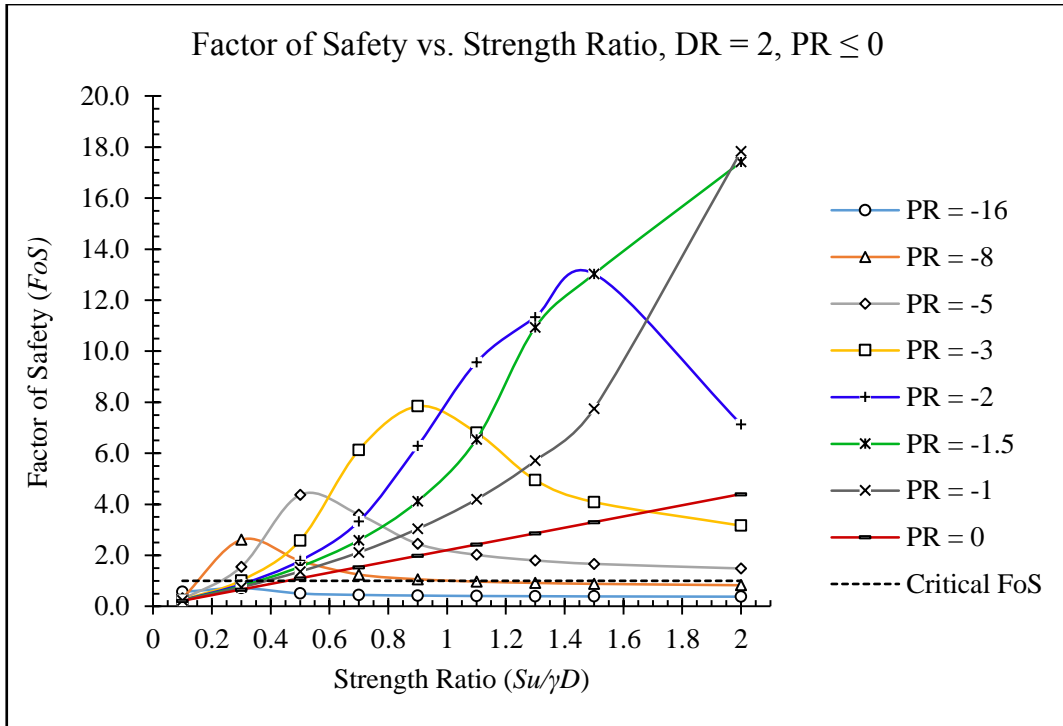


Figure 5.17: Factor of safety vs. strength ratio for all negative pressure ratios. DR = 2.

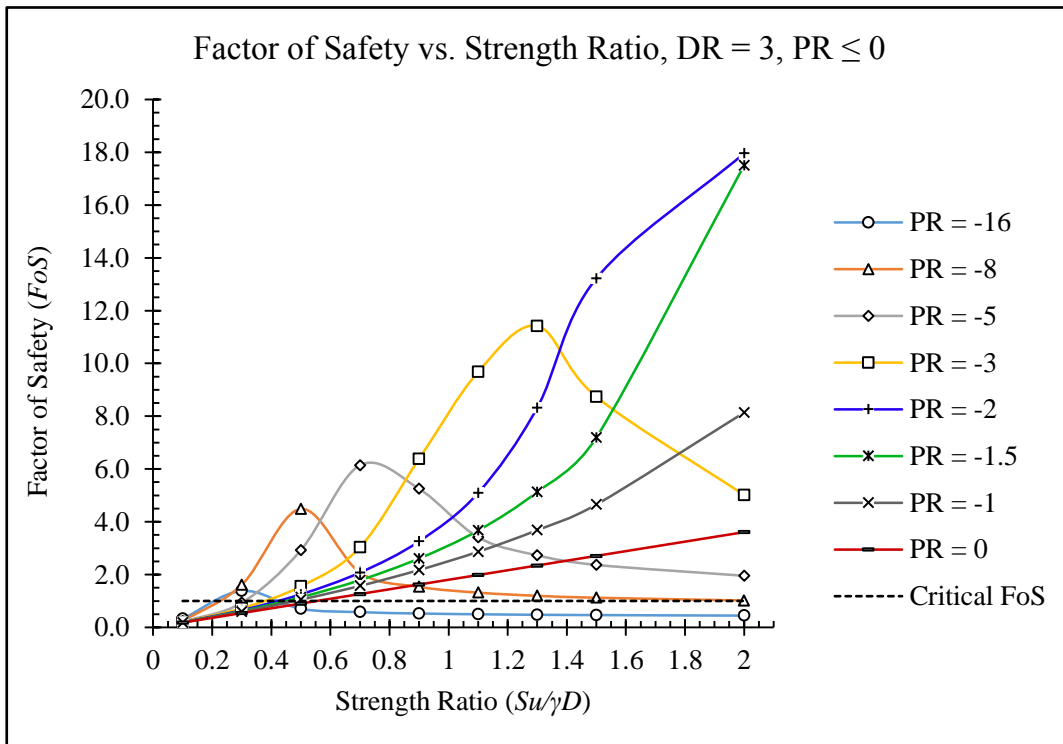


Figure 5.18: Factor of safety vs. strength ratio for all negative pressure ratios. DR = 3.

Table 5.5: Upper bound factor of safety results for all negative pressure ratios.

Factor of Safety Results for all Negative Pressure Ratios								
DR	SR	Pressure Ratio						
		-16	-8	-5	-3	-2	-1.5	-1
1	0.10	0.864	0.561	0.413	0.350	0.325	0.314	0.303
	0.30	0.398	1.354	2.587	1.906	1.357	1.184	1.048
	0.50	0.337	0.872	2.064	4.341	3.663	2.649	2.061
	0.70	0.316	0.747	1.523	4.365	6.053	5.528	3.510
	0.90	0.306	0.691	1.315	3.150	7.840	7.787	5.720
	1.10	0.299	0.661	1.204	2.638	6.093	9.548	9.384
	1.30	0.295	0.640	1.142	2.353	4.926	9.817	11.237
	1.50	0.292	0.626	1.096	2.190	4.278	7.859	13.033
	2.00	0.287	0.604	1.032	1.952	3.487	5.713	14.127
2	0.10	0.566	0.319	0.273	0.249	0.238	0.234	0.229
	0.30	0.714	2.610	1.550	1.014	0.864	0.799	0.748
	0.50	0.504	1.784	4.369	2.583	1.789	1.554	1.366
	0.70	0.448	1.248	3.599	6.127	3.330	2.591	2.115
	0.90	0.423	1.062	2.451	7.841	6.288	4.119	3.039
	1.10	0.406	0.971	2.021	6.811	9.564	6.547	4.196
	1.30	0.398	0.919	1.800	4.953	11.341	10.934	5.712
	1.50	0.389	0.881	1.663	4.088	13.034	13.026	7.746
	2.00	0.379	0.828	1.486	3.164	7.137	17.415	17.831
3	0.10	0.325	0.233	0.210	0.197	0.191	0.188	0.185
	0.30	1.382	1.612	0.932	0.724	0.650	0.618	0.591
	0.50	0.704	4.489	2.925	1.553	1.252	1.142	1.050
	0.70	0.577	2.076	6.140	3.036	2.076	1.788	1.571
	0.90	0.525	1.535	5.250	6.381	3.258	2.609	2.173
	1.10	0.496	1.316	3.412	9.679	5.095	3.670	2.865
	1.30	0.477	1.195	2.729	11.415	8.322	5.136	3.685
	1.50	0.465	1.122	2.367	8.736	13.221	7.194	4.653
	2.00	0.445	1.018	1.954	5.014	17.957	17.506	8.138

Figures 5.16 through to 5.18 show that the factor of safety increases linearly with the strength ratio for a pressure ratio of zero, but this linear relationship does not exist when the pressure ratio is less than zero. This is likely due to the fact that the internal tunnel pressure is a function of the undrained shear strength of the soil and is amplified as the soil strength increases. The curve for a depth ratio of two and a pressure ratio of negative three from Figure 5.17 is taken as an example and reproduced in Figure 5.19.

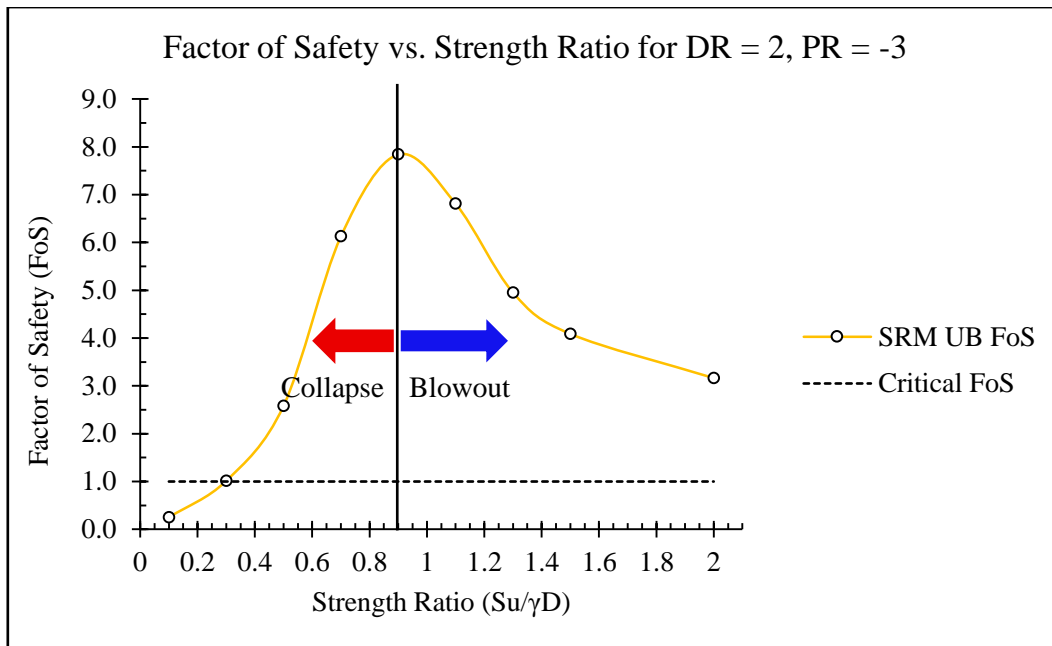


Figure 5.19: Factor of safety vs. strength ratio for DR = 2, PR = -3.

Figure 5.19 shows that it is possible to break the curve down into two distinctive segments. The rising limb of the curve, to the left of the divider, corresponds to the collapse failure mechanism while the falling limb of the curve, to the right of the divider, corresponds to the blowout failure mechanism. It can be seen that while the collapse failure mechanism governs, the factor of safety increases rapidly as the strength ratio increases. After the optimum factor of safety value is reached and the blowout failure mechanism governs, the factor of safety immediately decreases rapidly. As the strength ratio is further increased the rate at which the factor of safety decreases becomes smaller, converging toward an asymptotic solution.

From figures 5.16 through to 5.19 it can be seen that for each pressure ratio, the factor of safety reaches an optimum point at a specific strength ratio, showing that an optimum strength ratio/pressure ratio combination exists and that a higher strength ratio does not always result in a higher factor of safety when dealing with negative pressure ratios. This is due to the pressure ratio being a function of the undrained shear strength, meaning that the internal tunnel pressure is amplified at a greater rate than the soil strength. These charts reinforce the need to constantly check tunnel design as soil and loading conditions change by showing the large impact that one parameter can have on the other.

## 5.8 Conclusion

The stability, of two-dimensional undrained plane strain tunnel headings exhibiting a blowout failure mechanism, was investigated using a factor of safety approach. Factor of safety values were computed in Optum G2 using finite element limit analysis. The upper and lower bound factor of safety values were rigorously computed for the majority of scenarios, with a very good level of agreement found between the lower and upper bounds and a percentage difference of less than ten percent for all scenarios tested. The gravity multiplier method and strength reduction method were compared to determine the most useful method to be applied to a scenario with a negative pressure ratio. The CPU run time of the gravity multiplier method was, on average, over six times faster than the strength reduction method. Upon comparing both methods for scenarios with a pressure ratio less than zero it became apparent that the gravity multiplier method was producing unreasonable factor of safety values and was unable to perform the analysis accurately, so the strength reduction method was adopted. Very little research has previously been carried out on tunnel failure due to blowout and it became clear that Augarde, Lyamin and Sloan (2003) did not consider blowout failure, meaning the results from this thesis could not be directly compared to those published in previous studies. It was concluded that the factor of safety results obtained from the strength reduction method in Optum G2 relating to blowout failure are logical and reasonable, and due to lack of comparable previous work are considered to be accurate for the purpose of estimating undrained tunnel heading stability.

Analysing the relationship between the factor of safety and the pressure ratio for a blowout failure mechanism indicates that an individual hyperbolic curve exists for each depth ratio and strength ratio combination. As the pressure ratio decreases infinitely, the factor of safety decreases toward an asymptotic solution. As the pressure ratio increases toward an asymptotic solution, the factor of safety increases infinitely. The point where the factor of safety is infinite is thought to represent a weightless situation, where the opposing pressures of a tunnel heading stability problem are in balance. Analysing the relationship between the factor of safety and the pressure ratio suggests that the optimum factor of safety value for most practical cases will occur at a slightly negative pressure ratio. Investigating the displacement vector fields reinforced the factor of safety results found, and indicated that a weightless situation may exist once the displacement vector field starts swirling about the tunnel face.

For a pressure ratio of zero, the factor of safety increases linearly as the strength ratio increases. This research showed that the same relationship does not exist for a pressure ratio less than zero. For a negative pressure ratio, the factor of safety increases until an optimum point is reached and then begins to fall. Analysing the curves produced, it could be seen that the rising limb of the curve relates to failure due to collapse, while the falling limb of the curve relates to failure due to blowout. The understanding of tunnel heading stability relating to a blowout failure mechanism is revisited in Chapter 6, and ultimately culminates in the development of undrained shallow tunnel heading stability design charts for use by practicing engineers in the preliminary stages of tunnel design.

# CHAPTER 6:

## TUNNEL HEADING ANALYSIS:

### STABILITY DESIGN CHARTS

#### 6.1 Introduction

As the world's population grows and available space on the Earth's surface decreases, it is becoming increasingly necessary to construct subterranean infrastructure. As the need for tunnels increases so too does the required complexity of tunnelling projects. Tunnels present a unique challenge for engineers, who must assess the stability of prospective tunnels and the settlement of the Earth's surface that could be caused by the tunnelling process. The safe design of tunnels is critical, especially in urban areas where a shallow void must pass under existing infrastructure sensitive to ground movement. It is necessary to analyse the stability of a tunnel heading over a range of scenarios, covering failure due to both the collapse and blowout mechanisms. Often practicing engineers will refer to a number of simple stability design charts to assess a range of scenarios while in the preliminary stages of tunnel design. This chapter will address the entire tunnel heading stability problem by using Optum G2 to compute the upper and lower bound factor of safety values for a number of different scenarios. The factor of safety approach is then adopted to develop a number of tunnel heading stability design charts for use by practicing engineers in the preliminary stages of tunnel design.

#### 6.2 Problem Statement

In reality, tunnels are complex three-dimensional underground structures, however for the purpose of stability analysis they can be simplified to a basic two-dimensional model. The longitudinal section of the tunnel heading will be modelled under two-dimensional plane strain conditions. The undrained clay soil medium will be represented by a homogeneous Tresca material, which has an undrained shear strength ( $S_u$ ) and unit weight ( $\gamma$ ). The cover above the tunnel ( $C$ ) and the height of the tunnel ( $D$ ) are the important dimensional parameters needed to create the model. The surcharge pressure ( $\sigma_s$ ) and internal tunnel pressure ( $\sigma_t$ ) are varied to test the stability of the model under a number of different pressure

ratios capable of inducing failure by collapse. Figure 6.1 defines the tunnel heading stability problem.

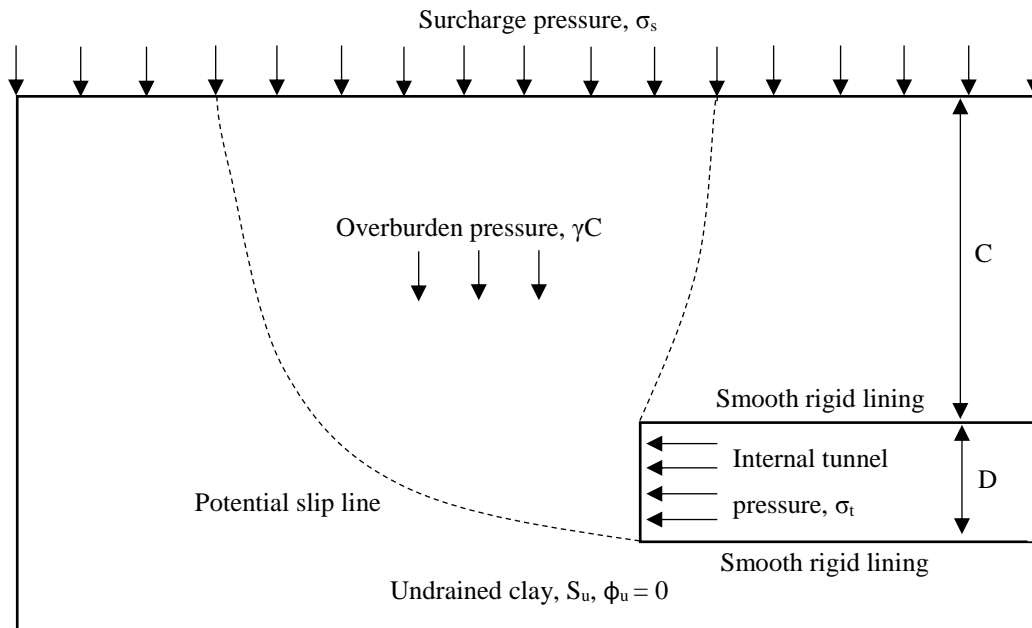


Figure 6.1: Tunnel heading stability problem statement.

Figure 6.1 presents a conceptual model of the tunnel heading problem making it possible to comprehend the three important dimensionless variable parameters. The depth ratio ( $DR$ ), shown in Equation 6.1, relates the geometrical properties of the model, tunnel height and tunnel cover. To represent shallow tunnelling conditions the depth ratio was varied between 1 and 3 in increments of one. Tunnel height remained constant at 6m while cover was varied.

$$\text{Depth Ratio } (DR) = \frac{C}{D} \quad (6.1)$$

where  $C = \text{cover above tunnel [m]}$ ; and  
 $D = \text{height of tunnel excavation [m]}$ .

The strength ratio ( $SR$ ) can be represented in two different ways for this problem. The soil strength ratio can be normalised to either the cover ( $C$ ), as shown in Equation 6.2, or the tunnel height ( $D$ ), as shown in Equation 6.3. Both formulations of the strength ratio were tested for this project and it was found that normalising the strength ratio to the tunnel height ( $D$ ), as shown in Equation 6.3, produced the clearest and most effective results. To cover a broad range of practical scenarios the strength ratio ( $S_u/\gamma D$ ) is varied between 0.10

and 2.00 in increments of 0.20 up to 1.50 and then a final increment of 0.50. Unit weight and tunnel height were kept constant at 18kN/m<sup>3</sup> and 6m respectively, while undrained shear strength was varied.

$$\text{Strength Ratio (SR)} = \frac{S_u}{\gamma C} \quad (6.2)$$

$$\text{Strength Ratio (SR)} = \frac{S_u}{\gamma D} \quad (6.3)$$

where  $S_u$  = undrained shear strength of soil [N/m<sup>2</sup>]; and  
 $\gamma$  = unit weight of soil [N/m<sup>3</sup>].

The third dimensionless variable to be considered is the pressure ratio (*PR*). Classically this parameter has been defined as the load parameter, but has been redefined as the pressure ratio in this project for simplicity and uniformity. The pressure ratio, shown in Equation 6.4, can be defined as the resultant applied pressure, be that a surcharge or internal tunnel pressure, compared to the undrained shear strength of the soil. To produce an acceptable range of data for modelling purposes the pressure ratio was varied between -16 and +10.

$$\text{Pressure Ratio (PR)} = \frac{\sigma_s - \sigma_t}{S_u} \quad (6.4)$$

where  $\sigma_s$  = the applied surcharge pressure [N/m<sup>2</sup>]; and  
 $\sigma_t$  = the applied internal tunnel pressure [N/m<sup>2</sup>].

The upper and lower bound factor of safety values are a function of these three dimensionless parameters and can therefore be expressed as shown in Equation 6.5.

$$\text{Factor of Safety (FoS)} = f\left(\frac{C}{D}, \frac{S_u}{\gamma D}, \frac{\sigma_s - \sigma_t}{S_u}\right) \quad (6.5)$$

In previous tunnel heading stability literature the results and design charts are not expressed in a factor of safety format. They are generally represented as a stability number, which is a function of a particular depth ratio and strength ratio with a corresponding factor of safety

of one. This stability number can generally cover a broader range of collapse failure scenarios when applied to a single design chart than a factor of safety approach, but is often confusing and somewhat impractical for practicing engineers interested in the factor of safety that a particular scenario can provide. As this stability number relates to a factor of safety of one it is defined as the critical pressure ratio ( $PR_c$ ) in this thesis. The approach used to calculate the critical pressure ratio is shown in Equation 6.6. The corresponding strength ratio, shown in Equation 6.7, is the inverse of the strength ratio adopted in this thesis, and is defined as the critical strength ratio ( $SR_c$ ) as it also only relates to a factor of safety of one. To find the critical pressure ratio and critical strength ratio, both the pressure ratio and strength ratio adopted in this thesis must be normalised by multiplying by the corresponding factor of safety.

$$PR_c = \frac{\sigma_s - \sigma_t}{S_u} * FOS \quad (6.6)$$

$$SR_c = \left( \frac{S_u}{\gamma D} \right)^{-1} * FOS \quad (6.7)$$

Other Tresca material properties that had a marginal effect on factor of safety results included; Poisson's ratio ( $\nu$ ) = 0.49 and Young's modulus ( $E$ ) = 30MPa.

### 6.3 2D Tunnel Heading Numerical Modelling

Due to the complex and uncertain behavior of soil, geotechnical investigations are a difficult undertaking. Numerical modelling techniques are continually improving and can now offer an accurate solution to such problems. Finite element limit analysis is an example of one such technique that has been used successfully in the past for modelling tunnels. This project employs the FELA technique through the relatively new program, Optum G2. The numerical procedures used in Optum G2 are based on the standard finite element method and the limit theorems of classical plasticity.

When creating the geometrical model it is important to consider the size of the domain. A model that is too small will not act as an infinite excavation and results will be affected by the boundary restraints, while a model that is too large will have excessive central processing unit (CPU) run time and produce less accurate results due to mesh dilution. The

boundary conditions of the model are also very important to ensure that the model is restrained within space and that the only two surfaces that can displace are the ground surface and the face of the tunnel heading. The base and sides of the model were fully restrained in the 'x' and 'y' directions, while the smooth rigid lining was restrained only in the normal direction to simulate a concrete lining. The size of the model was chosen so that these restraints had very little effect on the results. Figure 6.2 shows a typical two-dimensional finite element model of the tunnel heading problem.

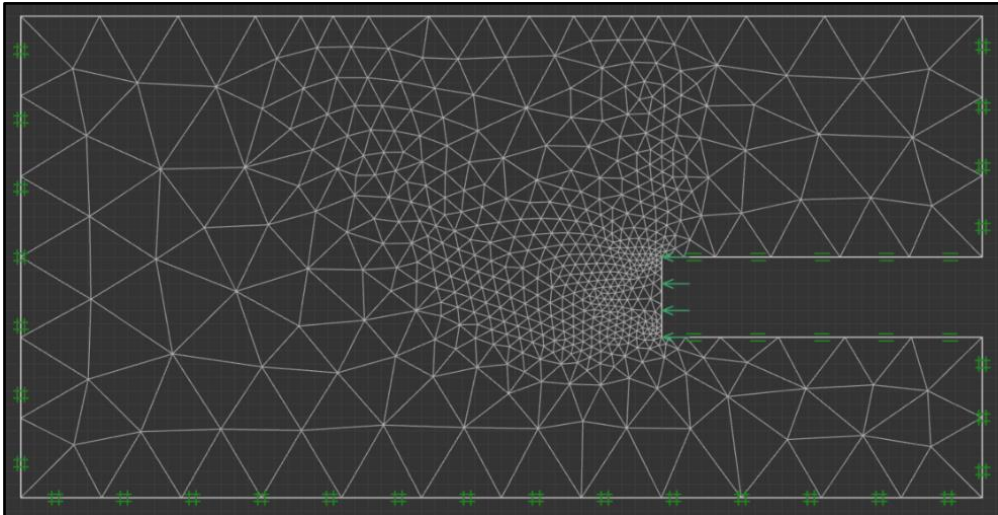


*Figure 6.2: Tunnel heading finite element mesh with mesh adaptivity.*

The number of finite elements was set at 1000 for all scenarios. Mesh adaptivity was enabled, allowing for three iterations with 1000 starting elements. Figure 6.2 displays this same scenario for a depth ratio of two. It can be seen that little mesh distortion occurs around the model boundaries, meaning the boundaries have no noticeable impact on results.

Tunnel height ( $D$ ) of 6m and unit weight of the soil ( $\gamma$ ) of 18kN/m<sup>2</sup> were adopted as constant values for all scenarios. The depth ratio ( $C/D$ ) was varied from 1 to 3 by adjusting the cover ( $C$ ) by 6m each time. The undrained shear strength of the clay ( $S_u$ ) was varied incrementally from 10.8kPa to 216kPa to obtain strength ratios ( $S_u/\gamma D$ ) varying from 0.10 to 2.00. The strength ratio increased in increments of 0.20 up until the strength ratio of 1.50 is reached and then in one final increment of 0.50. The pressure ratio ( $(\sigma_s - \sigma_t)/S_u$ ) was varied from -16 to +10.

## 6.4 Factor of Safety Bounds

Upper and lower bound factor of safety values were computed for the various scenarios by using the gravity multiplier method (GMM) and the strength reduction method (SRM). To perform an analysis using the gravity multiplier method the software incrementally increases the gravity by a multiplying factor until a state of failure is reached. The factor by which the gravity is multiplied can be taken as the factor of safety. For example, if the gravity must be multiplied by three to cause failure then the factor of safety in this scenario is three. Equation 6.8 shows the formulation of the factor of safety from the gravity multiplier method.

$$\text{Factor of Safety (FoS)} = \frac{g_{cr}}{g} \quad (6.8)$$

where  $g_{cr}$  = the gravitational acceleration at failure [ $m/s^2$ ]; and  
 $g$  = the actual gravitational acceleration =  $9.81[m/s^2]$ .

To perform an analysis using the strength reduction method the software performs a number of iterations and incrementally varies the strength of the soil until an optimum state of failure is reached. Unlike the gravity multiplier method, the strength reduction method decreases the shear strength of the soil until failure is reached and then performs a number of iterations to work on optimizing this value until the exact failure multiplier is found. Similarly to the gravity multiplier method, the amount by which the strength of the soil is reduced to induce an optimum state of failure can be taken as the factor of safety. For example if the strength of the soil must be decreased by two times then the corresponding factor of safety value would be two. Equation 6.9 shows the formulation of the factor of safety from the strength reduction method.

$$\text{Factor of Safety (FoS)} = \frac{S_u}{S_{u.cr}} \quad (6.9)$$

where  $S_u$  = original undrained shear strength of the soil [ $N/m^2$ ]; and  
 $S_{u.cr}$  = undrained shear strength of the soil at failure [ $N/m^2$ ].

Both the gravity multiplier method and strength reduction method were used to calculate the upper and lower bound factor of safety values for the majority of scenarios, but through the internal and external comparisons performed in Chapter 4 and 5 it was apparent that the

strength reduction method was the most suited to analysing stability problems with a range of different pressure ratios. The strength reduction method was adopted for all tunnel heading factor of safety results and corresponding design stability charts presented in this chapter.

## **6.5 Optum G2 Tunnel Heading Results and Discussion**

The stability of a tunnel heading is a complex topic. Optum G2 was used to model and analyse a range of tunnel heading scenarios considering both the collapse and blowout failure mechanisms. Varying the dimensionless parameters; pressure ratio  $((\sigma_s - \sigma_t)/S_u)$ , depth ratio  $(C/D)$  and strength ratio  $(S_u/\gamma D)$ , can dictate the failure mechanism of the heading. Two stages of testing were conducted. The first stage of testing adopted the strength reduction method to rigorously compute both the upper and lower bound factor of safety values for a broad range of practical pressure ratios. The second stage also adopted the strength reduction method but only calculated the upper bound factor of safety values that were required to fill in critical gaps in the data for modelling purposes. For this reason, the upper bound factor of safety values found from the strength reduction method will be adopted as the factor of safety values used in all modelling and data analysis. All upper bound factor of safety results calculated through the strength reduction method are available in Appendix D – ‘Final Results and Plots’.

The collapse and blowout failure mechanisms relating to a model with a depth ratio of two and strength ratio of 1.50 have been individually presented and discussed in Chapters 4 and 5 respectively. Table 6.1 contains the upper bound factor of safety values for all pressure ratios related to this model, while Figure 6.3 shows the full plot of factor of safety against pressure ratio.

Table 6.1: Factor of safety results for model with  $C/D = 2$  and  $SR = 1.50$ .

Factor of Safety Results, DR = 2		
SR ( $S_u/\gamma D$ )	PR ( $(\sigma_s - \sigma_t)/S_u$ )	FoS (UB SRM)
1.5	-16	0.389
	-8	0.881
	-5	1.663
	-3	4.088
	-2	13.034
	-1.5	13.026
	-1	7.746
	0	3.303
	1	2.08
	3	1.193
	5	0.836
	10	0.477

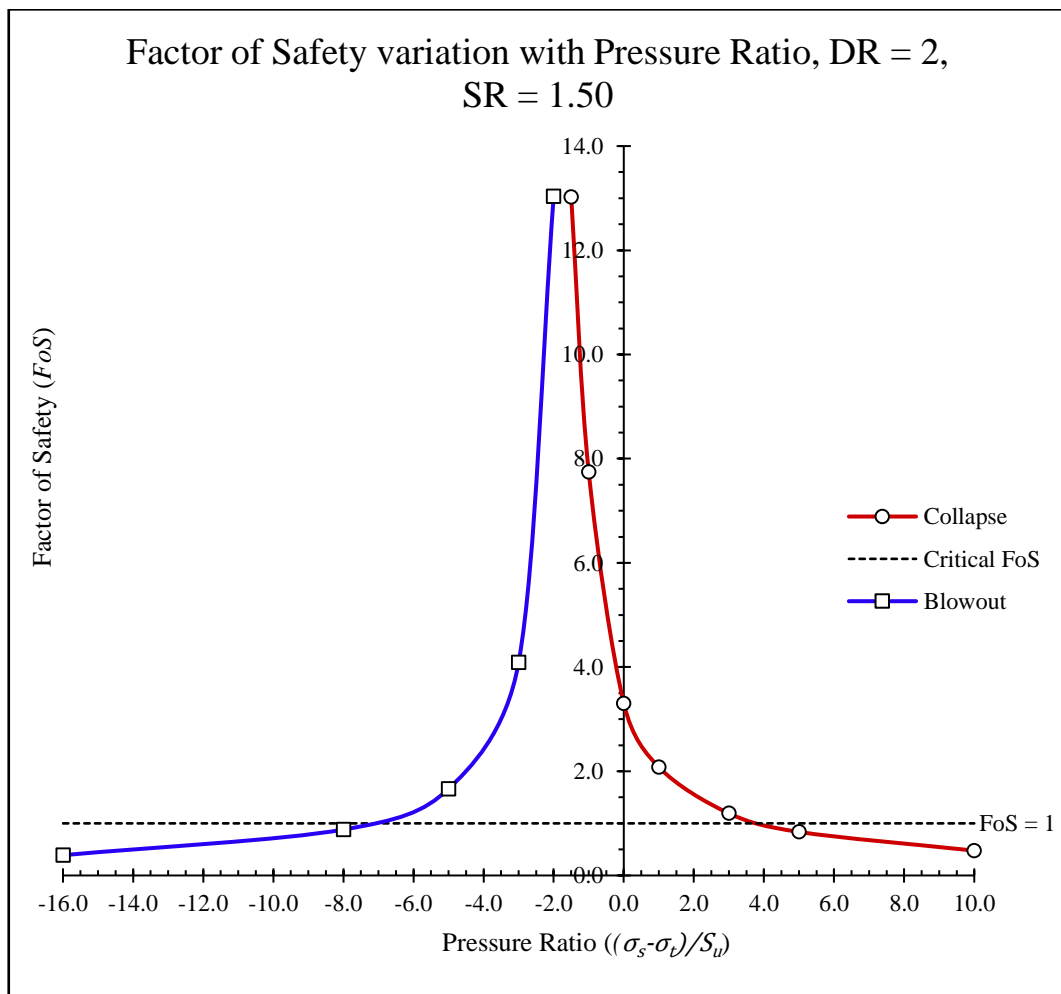


Figure 6.3: Factor of safety variation with pressure ratio for model with  $DR = 2$  and  $SR = 1.50$ .

Figure 6.3 shows the full range of scenarios relating to both the collapse and blowout failure mechanisms for a tunnel heading model with a depth ratio of two and a strength ratio of 1.50. It can be seen that the collapse and blowout curves are almost mirror images of one another. The similarity of the curves would only increase further as more pressure ratio scenarios are analysed and plotted. These mirror curves indicate that the relationship between the pressure ratio and the factor of the safety is the same as the pressure ratio is increased or decreased past the maximum collapse or blowout factor of safety respectively. The curves appear to be hyperbolic in nature, meaning that a pair of asymptotes exists for each. As the pressure ratio increases and decreases infinitely the factor of safety reaches a limiting value. As the factor of safety increases infinitely the curves converge toward a limiting pressure ratio asymptote. It is thought that a weightless condition is represented at the stage where the factor of safety approaches infinity. This theory makes sense when thinking practically, as a point where failure could not occur would exist when the supporting internal tunnel pressure paired with the resistance supplied by the soil strength is exactly equal to the downward pressure caused by the overburden and surcharge pressures. When attempting to analyse scenarios which fall in this gap between curves, Optum G2 consistently returns a limiting factor of safety value approximately equal to the maximum factor of safety value found for the collapse and blowout failure mechanisms. Figure 6.4 shows the displacement vector field for the same model of depth ratio two and strength ratio 1.5 for an intermediate pressure ratio of -1.75.

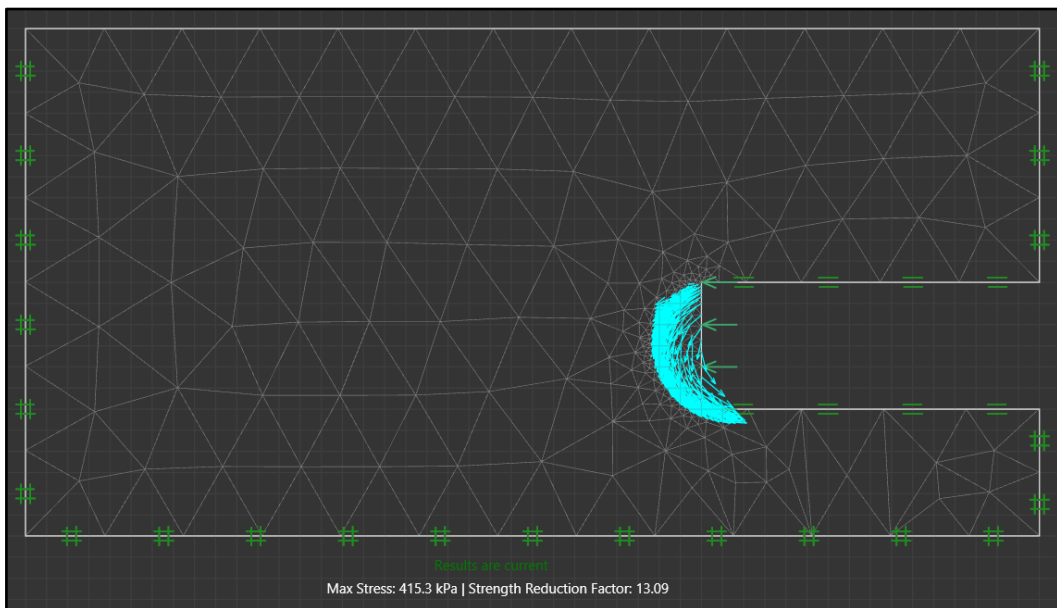


Figure 6.4: Displacement vector field for intermediate weightless scenario,  $DR = 2$ ,  $SR = 1.50$ ,  $PR = -1.75$ , corresponding  $FoS = 13.09$ .

The displacement vector field for the intermediate weightless scenario analysis, shown in Figure 6.4, swirls about the tunnel face, indicating that failure is not actually caused by a collapse or blowout at this point. It can also be seen that the calculated upper bound factor of safety at this point is 13.09 which is approximately equal to the maximum collapse and blowout factor of safety values. This behaviour is thought to be a limitation of the program and that the actual factor of safety at this point increases infinitely.

Figure 6.5 shows the relationship between the factor of safety and the pressure ratio for all strength ratios tested for a depth ratio of two.

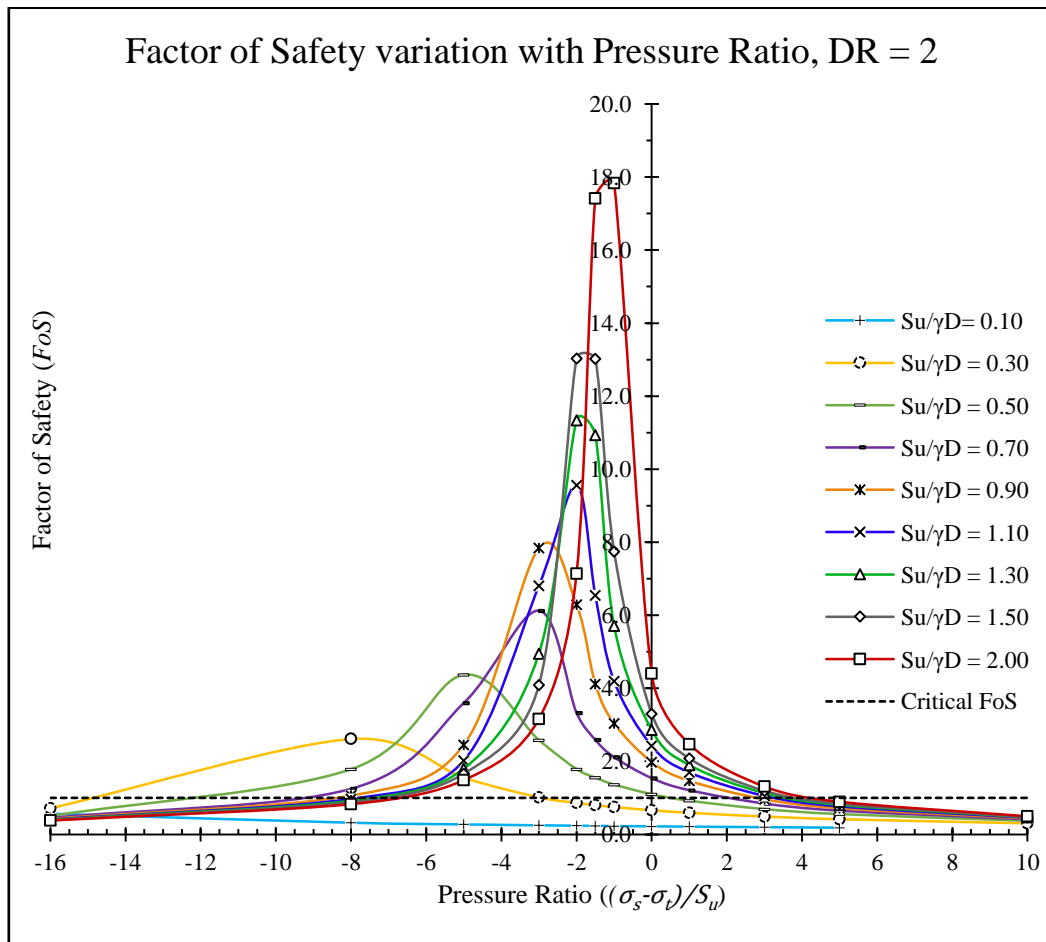


Figure 6.5: Factor of safety variation with pressure ratio for all strength ratios. DR = 2.

The actual behavior of the curves shown in Figure 6.5 is the same to that shown in Figure 6.3 but for ease of graphing and viewing they have not been split into separate collapse and blowout curves, but instead are represented as continuous curves. The accuracy of the curves decreases as the strength ratio decreases due to the spacing of the pressure ratios analysed within this range. Figure 6.5 shows that the maximum factor of safety for all scenarios is achieved when the pressure ratio is negative, the higher the strength ratio, the

higher (closer to zero) the negative pressure ratio must be to achieve the maximum factor of safety. Figure 6.5 also confirms the widely accepted truth that the maximum factor of safety increases as the strength ratio increases. Figures 6.3 and 6.5 assist in understanding the behavior of the factor of safety in relation to the dimensionless parameters as they are presented in the stability design charts.

## 6.6 Tunnel Heading Stability Design Charts

All modelling and research performed in this project culminated in the development of stability design charts for use by practicing engineers in the preliminary design stages of shallow tunnel headings in undrained clay. The stability design charts have been developed to encompass a broad range of undrained shallow tunnel heading scenarios and have been presented in terms of a factor of safety for practicality and ease of interpretation. The design charts developed are in the form of contour plots, which have been produced in Surfer 8, a powerful graphing software package from Golden Software. The first batch of design stability charts, presented in Figures 6.6 through to 6.8, have been developed for optimum effectiveness for cases where the depth ratio of the proposed tunnel remains constant and the strength ratio and pressure ratio vary along the length of the tunnel.

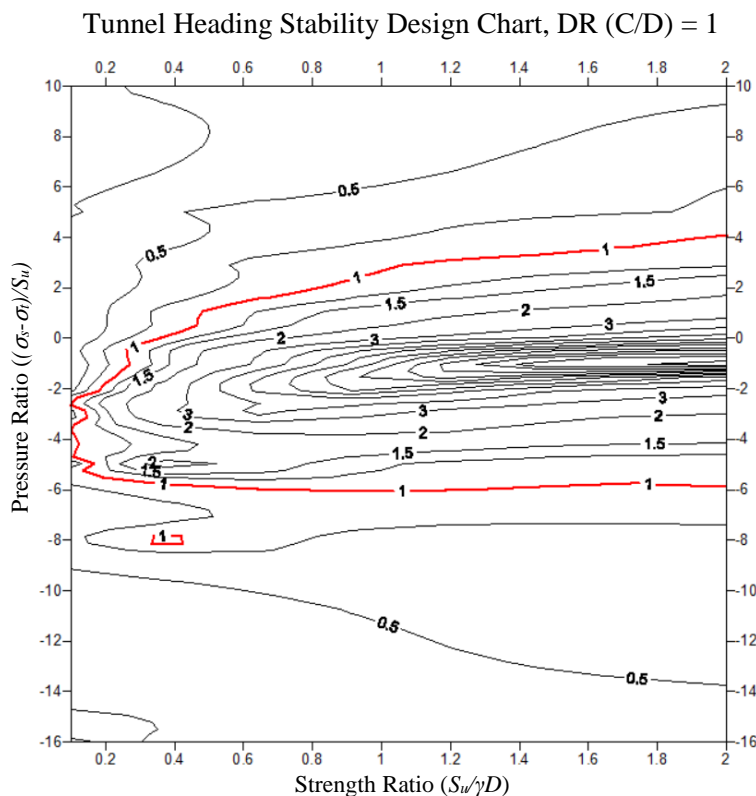


Figure 6.6: Tunnel heading stability design chart for DR = 1.

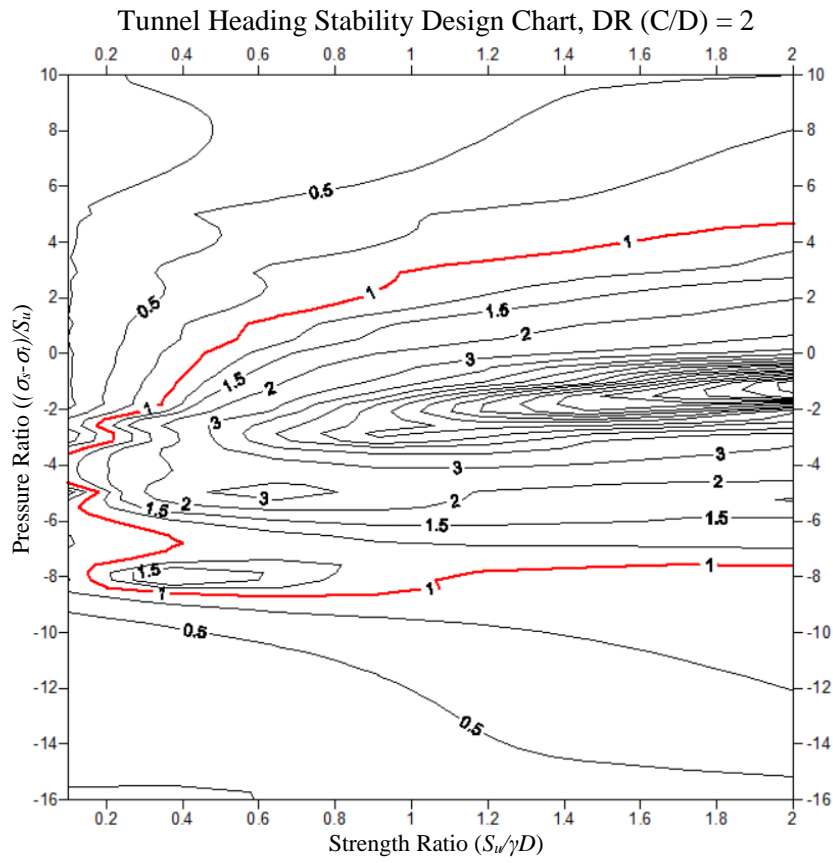


Figure 6.7: Tunnel heading stability design chart for DR = 2.

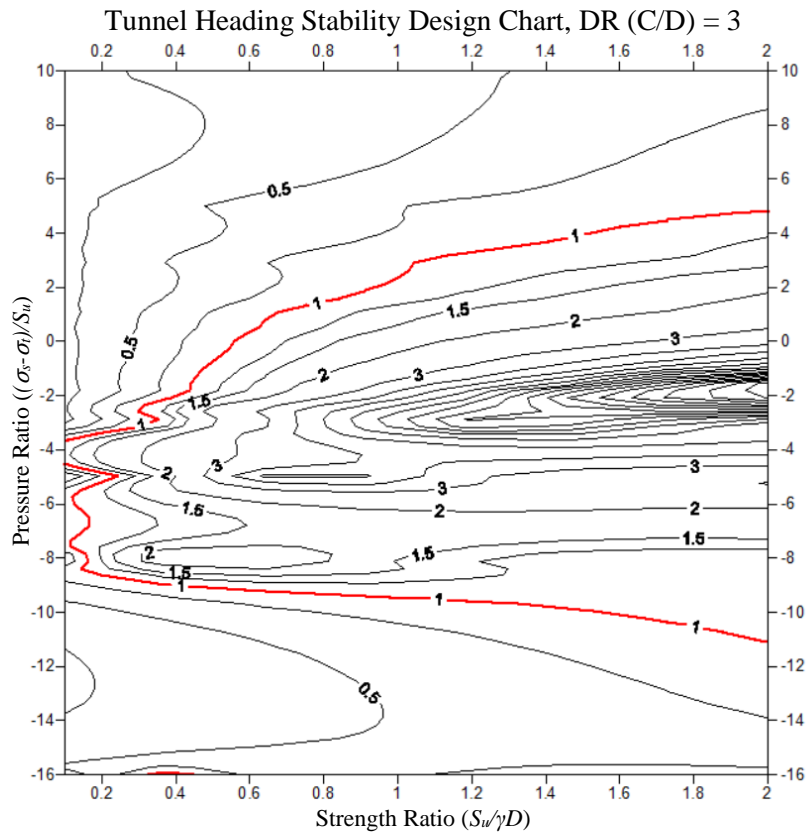


Figure 6.8: Tunnel heading stability design chart for DR = 3.

Figures 6.6, 6.7 and 6.8 show the tunnel heading stability design charts for scenarios of varying strength ratios and pressure ratios with a constant depth ratio of one, two and three respectively. These charts are most useful in their application to tunnel heading stability problems with a relatively constant depth ratio and varying strength and pressure ratios. The red contour indicates the critical factor of safety, one, which forms the failure envelope for each particular depth ratio. All scenarios which fall inside the failure envelope have a factor of safety greater than one and are deemed safe, while all scenarios that fall outside of the failure envelope have a factor of safety less than one and are deemed unsafe. All other contours are provided to give a more detailed factor of safety estimate for any given scenario. From these charts it can be seen that the optimum factor of safety is consistently achieved at a slightly negative pressure ratio. Comparing all three charts it can be seen that the safe zone encompassed by the failure envelope grows larger as the depth ratio is increased, indicating that a larger depth ratio results in a greater number of safe scenarios, with a factor of safety greater than one. The second batch of design stability charts, presented in Figures 6.9 through to 6.17, have been developed for optimum effectiveness for cases where the strength ratio of the proposed tunnel remains constant and the depth ratio and pressure ratio vary along the length of the tunnel.

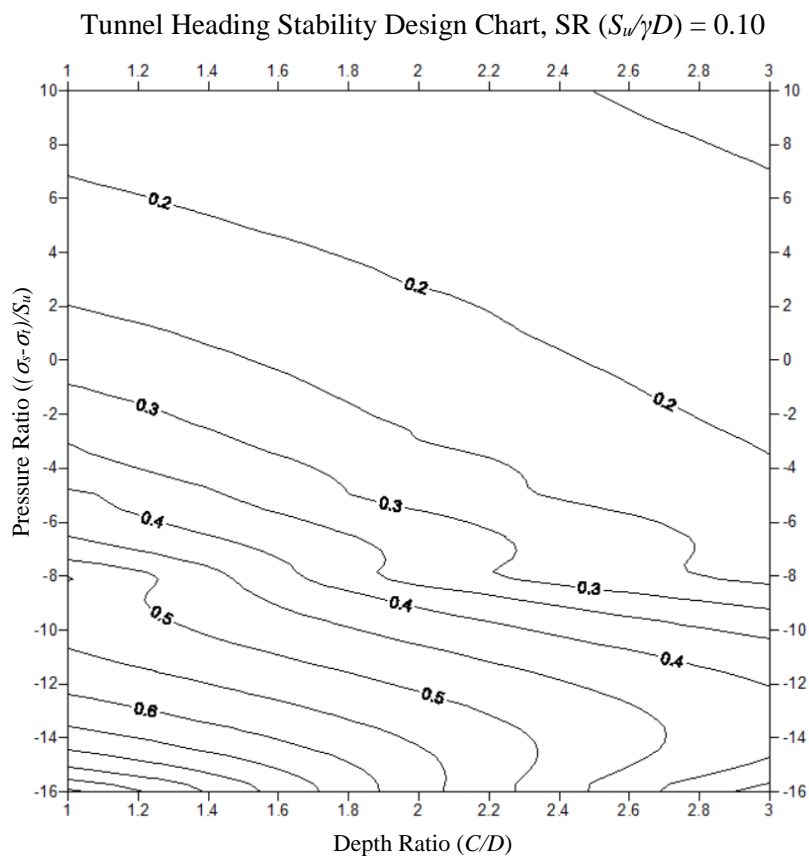


Figure 6.9: Tunnel heading stability design chart for  $SR = 0.10$ .

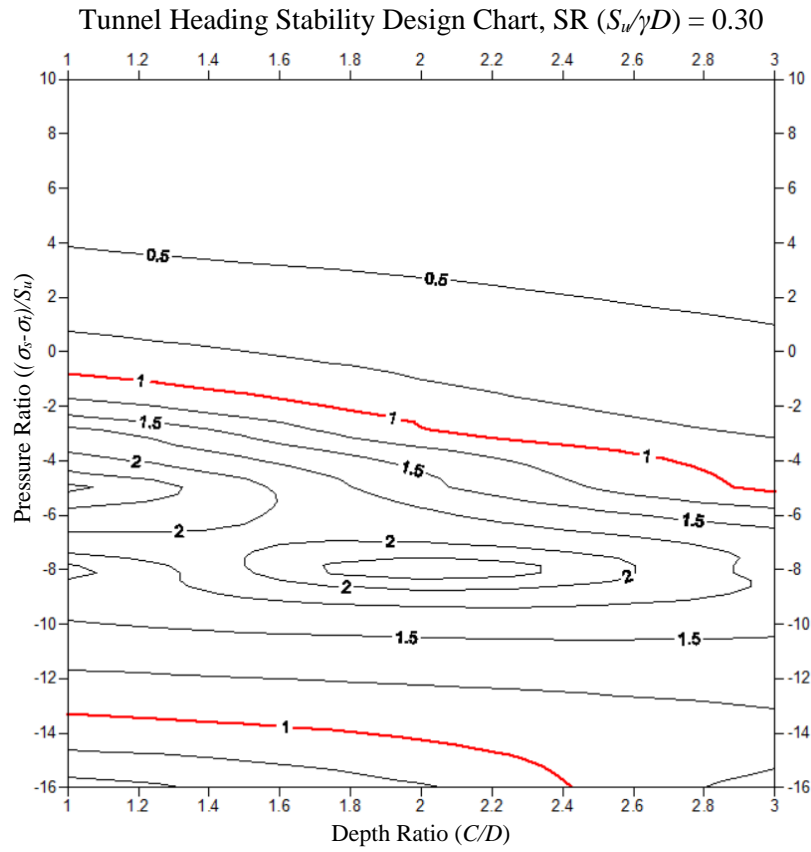


Figure 6.10: Tunnel heading stability design chart for  $SR = 0.30$ .

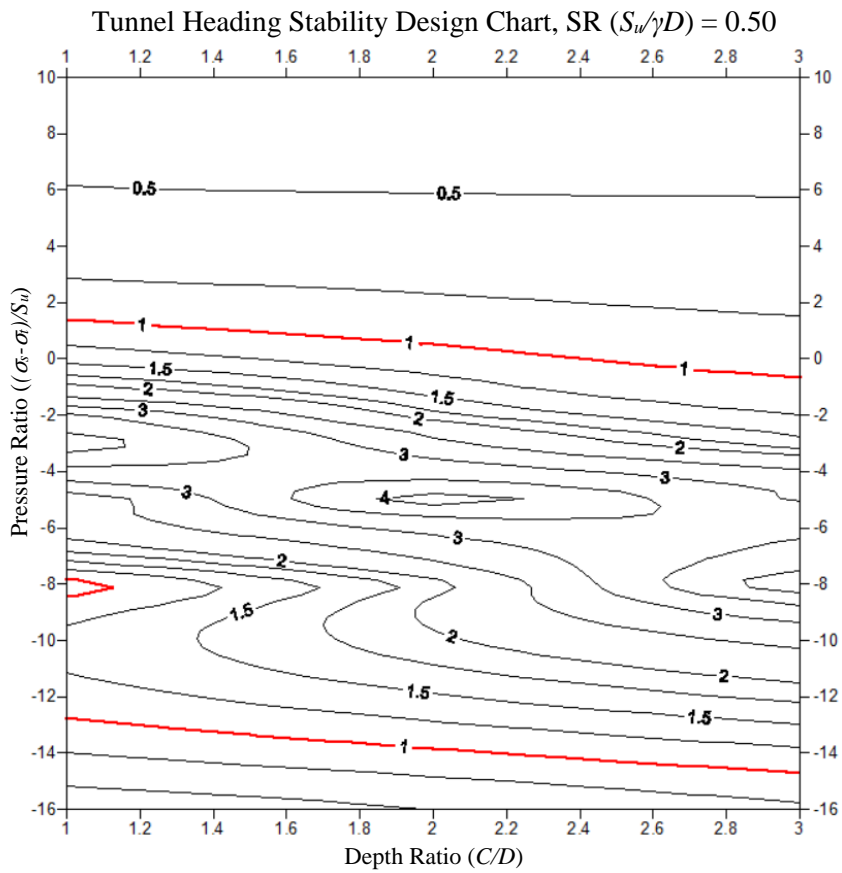


Figure 6.11: Tunnel heading stability design chart for  $SR = 0.50$ .

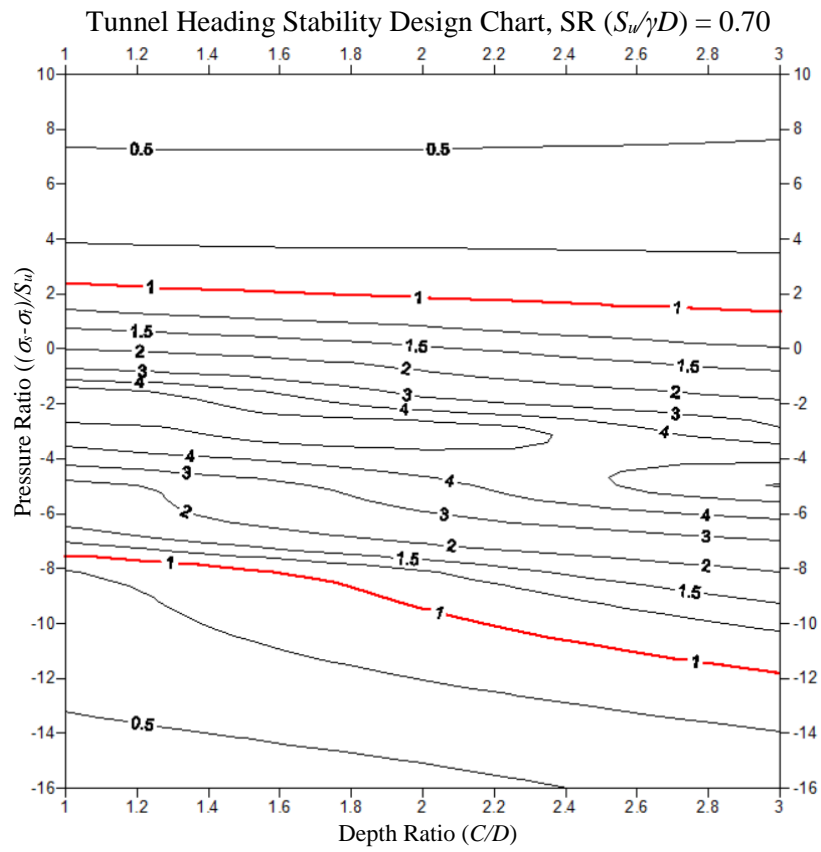


Figure 6.12: Tunnel heading stability design chart for  $SR = 0.70$ .

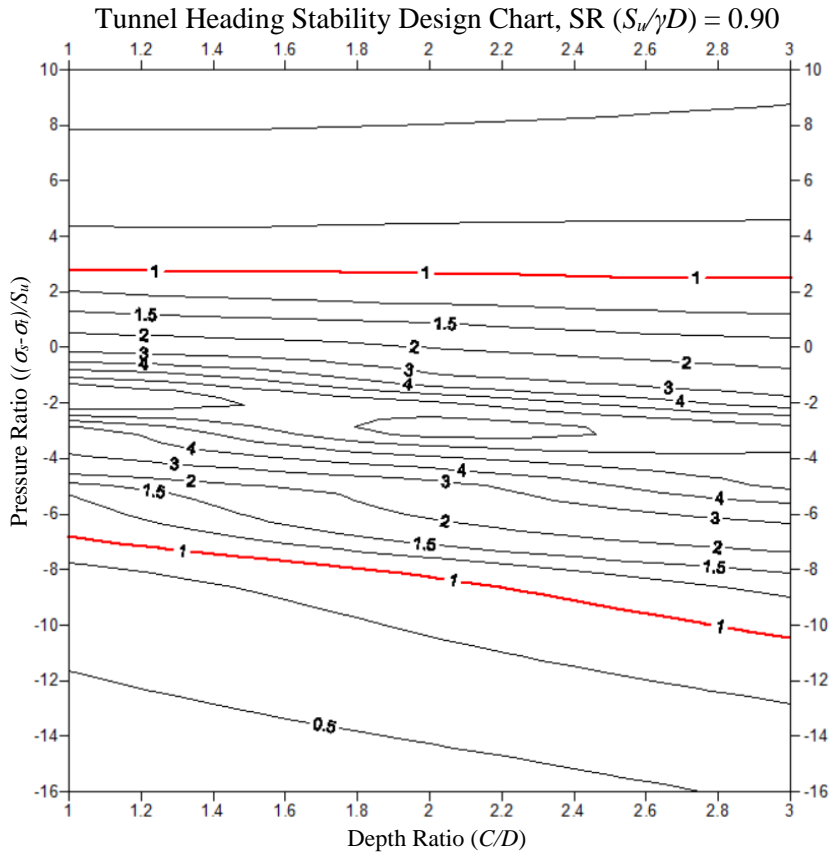


Figure 6.13: Tunnel heading stability design chart for  $SR = 0.90$ .

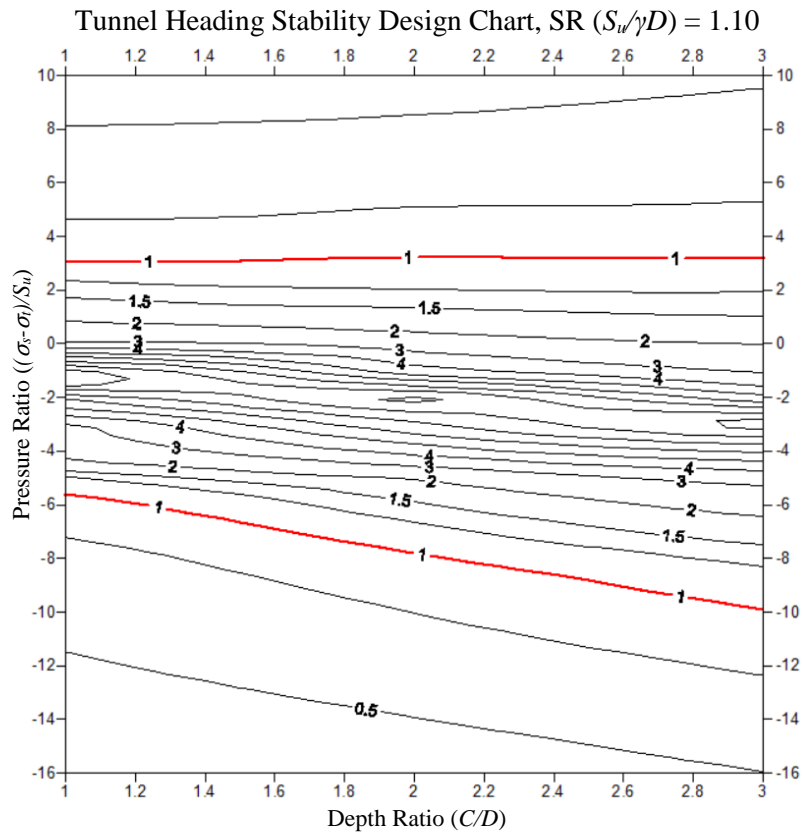


Figure 6.14: Tunnel Heading Stability Design Chart for  $SR = 1.10$ .

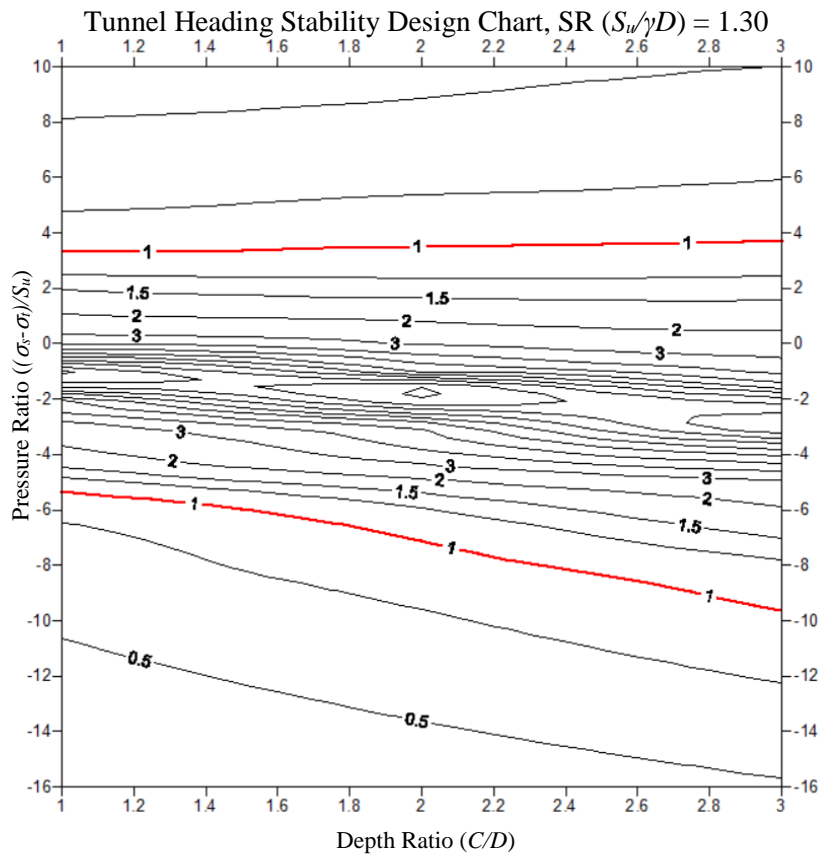


Figure 6.15: Tunnel heading stability design chart for  $SR = 1.30$ .

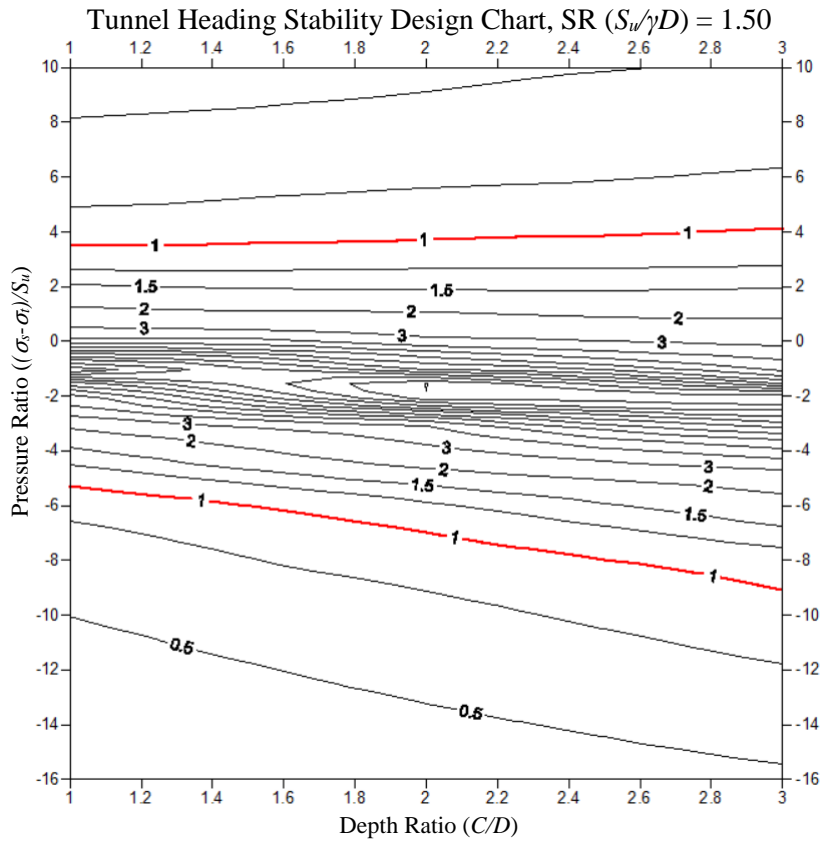


Figure 6.16: Tunnel heading stability design chart for  $SR = 1.50$ .

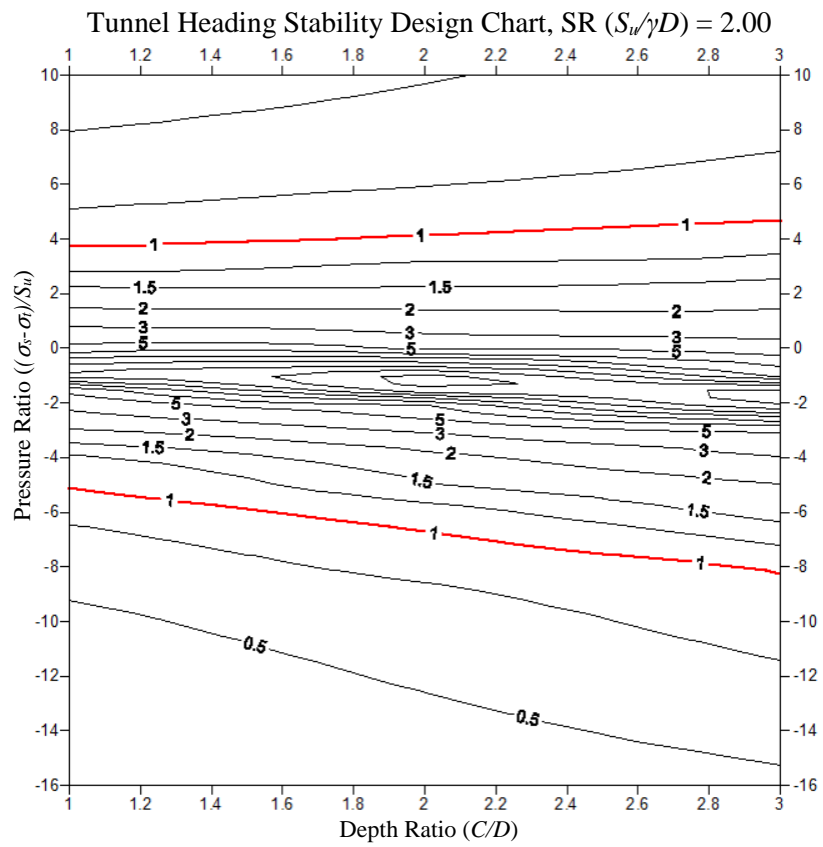


Figure 6.17: Tunnel heading stability design chart for  $SR = 2.00$ .

Figures 6.9 through to 6.17 show the tunnel heading stability design charts for scenarios of varying depth ratios and pressure ratios with a constant strength ratio, ranging between 0.10 and 2.00. These charts are most useful in their application to tunnel heading stability problems with a relatively constant strength ratio and varying depth and pressure ratios. The red contour indicates the critical factor of safety, one, which forms the failure envelope for each particular depth ratio. All scenarios which fall inside the failure envelope have a factor of safety greater than one and are deemed safe, while all scenarios that fall outside of the failure envelope have a factor of safety less than one and are deemed unsafe. All other contours are provided to give a more detailed factor of safety estimate for any given scenario. From these charts it can be seen that the optimum factor of safety is consistently achieved at a slightly negative pressure ratio. It can be concluded that the higher the strength ratio, the higher (closer to zero but still negative) the pressure ratio must be to achieve the maximum factor of safety. Comparing all charts it can be seen that the safe zone encompassed by the failure envelope grows smaller as the strength ratio is increased but, at the same time, shifts to accommodate a more practical range of pressure ratios. Figure 6.9 shows that a critical factor of safety of one is not achievable for a scenario with a strength ratio of 0.10, irrespective of depth ratio or pressure ratio. The key to applying these tunnel heading design stability charts to real life examples is understanding how to use them properly.

## 6.7 Tunnel Heading Stability Design Examples

A number of examples have been provided to assist practicing engineers in the application of the tunnel heading stability design charts.

### **Example 1: Analysis of an existing unsupported tunnel heading.**

Determine the factor of safety for an existing unsupported tunnel heading with no surcharge pressure ( $\sigma_s$ ) and no supporting internal tunnel pressure ( $\sigma_t$ ). The soil medium is undrained clay with a shear strength ( $S_u$ ) of 60kPa and a unit weight ( $\gamma$ ) of 15kN/m<sup>3</sup>. The cover above the tunnel ( $C$ ) is 10m and the height of the tunnel ( $D$ ) is 5m.

$$\frac{C}{D} = \frac{10}{5} = 2, \quad \frac{S_u}{\gamma D} = \frac{60}{15 * 5} = 0.80, \quad \frac{\sigma_s - \sigma_t}{S_u} = \frac{0 - 0}{60} = 0$$

*Referring to Figure 6.7, FoS  $\approx$  1.75, Interpolating from results, FoS = 1.76*

### Example 2: Design of a tunnel to be excavated by TBM.

It is proposed to use a TBM to excavate a shallow tunnel below a residential suburb in undrained clay. The designer must determine the maximum cover above the tunnel ( $C$ ) so that the TBM can operate safely. It is estimated that the existing infrastructure exerts a surcharge pressure ( $\sigma_s$ ) of 176kPa while the TBM exerts a face support pressure ( $\sigma_t$ ) of 88kPa. The TBM cutter-head diameter ( $D$ ) is 5m, the shear strength of the soil ( $S_u$ ) is 88kPa, the unit weight of the soil ( $\gamma$ ) is 16kN/m<sup>3</sup> and the required factor of safety ( $FoS$ ) is 1.50.

$$\frac{S_u}{\gamma D} = \frac{88}{16 * 5} = 1.10, \quad \frac{\sigma_s - \sigma_t}{S_u} = \frac{176 - 88}{88} = 1.0$$

$$\text{From figure 6.14, } \frac{C}{D} \approx 3, \quad \therefore C = 3 * D = 3 * 5 = 15\text{m}$$

*Any deeper and the overburden pressure will be too great.*

### Example 3: Determining face support for TBM excavation.

It is proposed to use a TBM to excavate a shallow tunnel below the CBD of a large city through undrained clay. The designer must determine the safe operating range for tunnel face support pressure ( $\sigma_t$ ) provided by the TBM. It is estimated that existing surface infrastructure exerts a surcharge pressure ( $\sigma_s$ ) of 250kPa. The tunnel diameter ( $D$ ) is 6m while the cover above the tunnel ( $C$ ) is 12m. The shear strength of the soil ( $S_u$ ) is 84kPa, the unit weight of the soil ( $\gamma$ ) is 20kN/m<sup>3</sup> and the required minimum factor of safety ( $FoS$ ) is 2.0.

$$\frac{C}{D} = \frac{12}{6} = 2, \quad \frac{S_u}{\gamma D} = \frac{84}{20 * 6} = 0.70$$

$$\text{From Figure 6.7, } \frac{\sigma_s - \sigma_t}{S_u} = -1.25 \quad \& \quad -5.75$$

$$\therefore \sigma_t = -(-1.25 * S_u) + \sigma_s = (1.25 * 84) + 250 = 355\text{kPa}$$

$$\& \sigma_t = -(-5.75 * S_u) + \sigma_s = (5.75 * 84) + 250 = 733\text{kPa}$$

$$\therefore 355\text{kPa (collapse limit)} \leq \sigma_t \leq 733\text{kPa (blowout limit)}$$

Example three is particularly useful in a practical sense, as it allows for the determination of a safe operating range for the pressure to be applied at the tunnel excavation face by a tunnel boring machine. The range can be increased by decreasing the minimum target factor of safety or decreased by increasing the minimum target factor of safety.

## 6.8 Conclusion

The stability, of two-dimensional plane strain tunnel headings in undrained clay, was investigated using a factor of safety approach. Factor of safety values were computed in Optum G2 using finite element limit analysis. The upper and lower bound factor of safety values were rigorously computed for the majority of scenarios by using the strength reduction method in Optum G2. The upper bound factor of safety values were adopted and the full relationship between the factor of safety and pressure ratio for a set depth ratio and strength ratio was discussed. It was determined that when the factor of safety is plotted against the pressure ratio, a set of similar hyperbolic curves are created, mirrored about the vertical axis. As the pressure ratio increases or decreases infinitely, the factor of safety approaches an asymptotic minimum value. As the pressure ratio approaches an asymptotic optimum value, the factor of safety appears to increase infinitely, this point is thought to represent a weightless situation. It appears that a limitation in the software may exist as the model approached this weightless point, as the displacement vector field started swirling about the tunnel face and the factor of safety flat-lined between the maximum factor of safety for collapse and the maximum factor of safety for blowout. In reality it is plausible that the factor of safety actually increases infinitely at this point.

When comparing the relationship between the factor of safety and the pressure ratio for various strength ratios it can be seen that, for all scenarios, the optimum factor of safety is always achieved at a negative pressure ratio rather than at a pressure ratio of zero. For lower strength ratios the maximum factor of safety is achieved at lower pressure ratios and vice versa for higher strength ratios. The widely accepted truth that the maximum factor of safety increases as the strength ratio increases was also confirmed.

A number of tunnel heading stability design charts, covering a broad range of shallow undrained tunnel heading scenarios, were presented. Two different types of charts were created. The first, a factor of safety contour chart plotting the pressure ratio against the strength ratio for a constant depth ratio, and the second, a factor of safety contour chart plotting the pressure ratio against the depth ratio for a constant strength ratio. The first type of chart is most applicable to a tunnel design with a consistent vertical alignment, while the second type is most applicable to a tunnel design where the soil medium varies constantly along the length of the excavation. It is expected that these charts will be of use to engineers in the preliminary stages of tunnel design. A few basic examples were provided to highlight the variety of practical scenarios these charts could be applied to.

It was discovered that one particularly useful practical application of the design charts is the ability to determine a safe operating range for the pressure that can be applied to the tunnel excavation face by a tunnel boring machine during construction.

# CHAPTER 7:

## CONCLUSION

### 7.1 Summary

The stability of two-dimensional plane strain tunnel heading in an undrained material has been investigated in this dissertation. The analysis focused on scenarios with varying pressure ratios in order to consider failure caused by both the collapse and blowout failure mechanisms. Factor of safety values were calculated in Optum G2 using finite element limit analysis through the strength reduction method and the gravity multiplier method. Each case was set up with 1000 finite elements and three iterations of mesh adaptivity to allow for the rigorous computation of lower and upper bound factor of safety values. The strength reduction method incrementally reduced the undrained shear strength of the soil until a state of failure was reached and the gravity multiplier method amplified the gravity until a state of failure was reached. Previously, the stability of such a problem was derived by increasing the surcharge pressure until a limiting pressure ratio for an active collapse mechanism was reached (Davis et al. 1980).

Comparing the strength reduction method and gravity multiplier method it was found that the two methods had a good level of agreement for a scenario with a pressure ratio equal to zero. The CPU run time of the strength reduction method was nearly six times slower than the gravity multiplier method due to the highly iterative process needed to reduce the strength until an optimum state of failure was reached. Upon further comparison it was found that the gravity multiplier method was not suitable for analysing scenarios with a non-zero pressure ratio, so the strength reduction method was adopted for all final analysis results.

A sample of factor of safety values and corresponding strength ratios, relating to scenarios exhibiting failure by collapse, were converted into critical stability numbers and critical strength ratios, respectively. The conversion of these results allowed for them to be directly compared to results previously published by Augarde, Lyamin and Sloan (2003). The comparison showed a very good level of agreement, indicating that the Optum G2 strength reduction method was capable of accurately analysing tunnel heading stability related to the collapse failure mechanism. It appeared that Augarde, Lyamin and Sloan (2003) did

not consider failure by blowout, so no published results could be found to directly check the validity of the blowout results found in this dissertation.

Analysing the relationship between the factor of safety and the pressure ratio, for any given strength ratio and depth ratio combination, it was discovered that a pair of identical hyperbolic curves exist. The curves are mirrored about the vertical axis, with one curve relating to failure due to the collapse mechanism and the other relating to failure due to the blowout mechanism. The factor of safety approaches an asymptotic solution as the pressure ratio increases or decreases infinitely, while the pressure ratio approaches an asymptotic solution as the factor of safety increases infinitely. It is thought that the point where the factor of safety increases infinitely, or the gap between the hyperbolic curves, represents a weightless scenario, where the combination of overburden and surcharge pressure is approximately equal to the combination of internal tunnel pressure and undrained soil strength. It was found that the optimum factor of safety occurs at a negative pressure ratio, rather than at a pressure ratio of zero, for all scenarios analysed. The displacement vector fields for all models were analysed to confirm the suspected failure mechanism and to gain a greater understanding of the model's behaviour at failure.

Analysing the relationship between the factor of safety and the strength ratio it was confirmed that, as discovered previously, the factor of safety increases linearly with the strength ratio for a pressure ratio of zero. However, upon investigating a non-zero pressure ratio, it was found that this linear relationship no longer applies. The positive pressure ratios produced a set of curves which showed that the factor of safety increases slower as the strength ratio increases, and that an asymptotic factor of safety solution is likely to exist for each scenario. The negative pressure ratios produced a set of curves which show that an optimum factor of safety exists, at the peak of each curve, for any given strength and pressure ratio combination. The findings from this dissertation also conform to the logical and widely accepted truth that the factor of safety increases with the undrained shear strength of the soil.

The research ultimately culminated in the development of a number of tunnel heading stability design charts for use by practicing engineers in the preliminary stages of tunnel design. The charts were developed by applying the factor of safety method, which ensures that they provide direct information and understanding of the tunnel heading stability. It is made clear by this research that tunnels must be designed for collapse and checked for blowout, so the charts were designed specifically to apply to scenarios related to both the collapse and blowout failure mechanism to allow for the easy facilitation of this design

process. A number of practical examples were provided, detailing some of the potential uses for the design charts. It was discovered that one particularly useful practical application of the design charts is the ability to determine a safe operating range for the pressure that can be applied to the tunnel excavation face by a tunnel boring machine during construction.

## **7.2 Future Research**

Based on the research outcomes from this dissertation, a number of future research directions are proposed. The first and foremost recommendation, is to continue on from this project and carry out additional modelling to increase the density of results, and in turn further develop the stability design charts and increase the understanding of tunnel stability related to the blowout failure mechanism. The factor of safety approach provides results in a practical and direct format but to reduce the number of design charts needed to provide complete coverage, it could be possible to develop a new stability number applicable to scenarios related to both collapse and blowout failure mechanisms.

Secondly, a similar process can be applied under different circumstances, this could include investigating; a drained soil medium, deep tunnels, and different cross-sectional profiles such as circular, square, rectangular or twin tunnels. Optum G2 proved to be very capable and user-friendly but it would be beneficial to undertake a similar process with the use of other two-dimensional analysis software such as FLAC, or even three-dimensional analysis software such as Plaxis.

## REFERENCES

Asadi, A & Sloan, S 1991, 'Undrained Stability of Shallow Square Tunnel', *Journal of Geotechnical Engineering*, vol 117, pp. 1152-1173.

Atkinson, J & Potts, D 1977, 'Stability of shallow circular tunnel in cohesionless soil', *Géotechnique*, vol 27, no. 2, pp. 203-215.

Atlas Copco 2014, *Boomer XE3 C: Face drilling rig*, viewed 22 May 2016, <<http://www.atlascopco.com/geus/products/drill-rigs-and-rock-drills/1401284/1520766/>>.

Augarde, C, Lyamin, A & Sloan, S 2003, 'Stability of an undrained plane strain heading revisited', *Comput Geotech*, vol 30, pp. 419-430.

Bickel, J, Kuesel, T & King, E 1996, *Tunnel Engineering Handbook*, 2nd edn, Chapman & Hall, New York.

Bottero, A, Negre, R, Pastor, J & Turgeman, S 1980, 'Finite element method and limit analysis theory for soil mechanics problems', *Computation Methods Applied Mechanics, Engineering*, vol 22, no. 1, pp. 131-140.

Broms, B & Bennermark, H 1967, 'Stability of Clay at Vertical Openings', *Journal of the Soil Mechanic and Foundations Division, Proceedings of the American Society of Civil Engineers*, vol 93, pp. 71-93.

Cairncross, A 1973, 'Deformation around model tunnels in stiff clay', University of Cambridge, Cambridge.

Cai, F, Ugai, K & Hagiwara, T 2002, 'Base Stability of Circular Excavations in Soft Clay', *Journal of Geotechnical and Geoenvironmental Engineering*, vol 128, no. 8, pp. 702-706.

Chapman, D, Metje, N & Stärk, A 2010, *Introduction to Tunnel Construction*, Spon Press, London.

Civil Engineering and Development Department 2012, *Catalogue of Notable Tunnel Failure Case Histories*, viewed 15 September 2016, <[http://www.cedd.gov.hk/tc/publications/geo/doc/notable\\_tunnel\\_cat.pdf](http://www.cedd.gov.hk/tc/publications/geo/doc/notable_tunnel_cat.pdf)>.

Das, B 2010, *Principles of Geotechnical Engineering*, 7th edn, Cengage Learning, Stamford.

Davis, E, Gunn, M, Mair, R & Seneviratne, H 1980, 'The stability of shallow tunnels and underground openings in cohesive material', *Géotechnique*, vol 30, no. 4, pp. 397-416.

Guglielmetti, V, Grasso, P, Mahtab, A & Xu, S 2007, *Mechanized Tunnelling in Urban Areas: Design methodology and construction control*, Taylor & Francis, Turin.

Huang, F, Zhang, D, Sun, Z & Jin, Q 2012, 'Upper bound solutions of stability factor of shallow tunnels in saturated soil based on strength reduction technique', Central South University Press and Springer-Verlag, Changsha.

Idinger, G, Aklik, P, Wu, W & Borja, R 2011, 'Centrifuge model test on the face stability of shallow tunnel', *Acta Geotechnica*, vol 6, pp. 105-117.

Institution of Civil Engineers 1998, 'Bulkhead location blamed for DLR blast.', *New Civil Engineer*, February 1998, pp. 3-4.

Institution of Civil Engineers 2004, 'Docklands tunnel blowout down to "elementary error", says judge.', *New Civil Engineer*, 22 January 2004, pp. 8-9.

Lyamin, A & Sloan, S 2002a, 'Lower bound limit analysis using non-linear programming', *International Journal for Numerical Methods in Engineering*, vol 55, no. 5, pp. 573-611.

Lyamin, A & Sloan, S 2002b, 'Upper bound limit analysis using linear finite elements and non-linear programming', *International Journal for Numerical and Analytical Methods in Geomechanics*, vol 26, no. 2, pp. 181-216.

Lysmer, J 1970, 'Limit analysis of plane problems in soil mechanics', *ASCE Journal of the Soil Mechanics and Foundations Division*, vol 96, pp. 1311-1334.

Maidl, B, Maidl, U & Thewes, M 2013, *Handbook of Tunnel Engineering 1; Structures and Methods*, 1st edn, Wilhelm Ernst & Sohn, Berlin.

Mair, R 1979, 'Centrifugal modelling of tunnel construction in soft clay', University of Cambridge, Cambridge.

Megaw, T & Bartlett, J 1981, *Tunnels; Planning, Design, Construction*, 1st edn, Ellis Horwood Limited, Chichester.

Mollon, G, Dias, D & Soubra, A 2010, 'Face stability analysis of circular tunnels driven by a pressurised shield', *Journal of Geotechnical and Geoenvironmental Engineering*, vol 136, pp. 215-229.

Optum CE 2013, *Optum G2*, viewed 23 May 2016, <<http://optumce.com/>>.

Optum Computational Engineering 2016, *Optum G2 Version 2016.04.04 [Computer software]*, Newcastle, Australia.

Pastor, J & Turgeman, S 1976, 'Mise en oeuvre numérique des méthodes de l'analyse limite pour les matériaux de von Mises et de Coulomb standards en déformation plane', *Mech Res Commun*, vol 3, pp. 469-474.

Peck, R 1969, 'Deep excavations and tunnelling in soft ground', in *Proceedings of 7th International Conference on Soil Mechanics and Foundation Engineering*, Mexico City.

Seneviratne, H 1979, 'Deformations and pore-pressures around model tunnels in soft clay', University of Cambridge, Cambridge.

Shiau, J, Sams, M & Chen, J 2016, 'Stability charts for a tall tunnel in undrained clay.', *Electronic Journal of Geotechnical Engineering, International Journal of Geomate*, vol 10, no. 2, Japan, pp. 1764-1769. SNIP = 0.825

Shiau, J, Sams, M and Chen, J 2016, 'Stability design charts for unsupported wide rectangular tunnels.' *Electronic Journal of Geotechnical Engineering*, vol 2, no. 1, pp. 139-150. SNIP = 0.604

Shiau, J., Sams, M, Zhang, J, & Kemp, R 2014, 'Settlement Analyses of Underground Circular Tunneling in Soft Clay.' *Geotechnical Aspects of Underground Construction in Soft Ground*, Seoul, pp. 347-352.

Shiau, J, Sams, M, & Kemp, R 2014, 'Physical Modelling and PIV Analyses of an Underground Tunnel Heading.' *Geotechnical Aspects of Underground Construction in Soft Ground*, Seoul, pp. 61-66.

Shiau, J & Kemp R 2013 'Developing a Numerical Model for the Stability Design of Tunnel Heading.' *Third International Conference on Geotechnique, Construction Materials and Environment*, Nagoya, Japan, pp. 13-15.

Shiau, J & Kemp R 2013, 'Settlement and Stability Analyses of Tunnels in Undrained Clays.', *Geotechnics for Sustainable Development - Geotec Hanoi 2013*, Phung (edt). Construction Publisher.

Sloan, S 1988, 'Lower bound limit analysis using finite elements and linear programming', *International Journal for Numerical and Analytical Methods in Geomechanics*, vol 12, pp. 61-67.

Sloan, S 1989, 'Upper bound limit analysis using finite elements and linear programming', *International Journal for Numerical and Analytical Methods in Geomechanics*, vol 13, pp. 263-282.

Sloan, S 2013, 'Geotechnical stability analysis', *Geotechnique*, vol 63, pp. 531-572.

Sloan, S & Assadi, A 1994, 'Undrained stability of a plane strain heading', *Can. Geotech. J.*, vol 31, pp. 443-450.

Taylor, D 1937, 'Stability of earth slopes', *Journal of the Boston Society of Civil Engineers*, vol 24, no. 3, pp. 197-246.

Tschuchnigg, F, Schweiger, H & Sloan, S 2015, 'Slope stability analysis by means of finite element limit analysis and finite element strength reduction techniques. Part 2: Back analyses of a case history', *Computers and Geotechnics*, vol 70, pp. 178-189.

Wallis, S 2002, *Dublin coping with complicated conditions*, viewed 22 May 2016, <<http://www.tunneltalk.com/Ireland-Dublin-Sept02-Port-Tunnel-site-visit.php>>.

Wilson, D, Abbo, A, Sloan, S & Lyamin, A 2011, 'Undrained stability of a circular tunnel where the shear strength increase linearly with depth', *Canadian Geotechnical Journal*, vol 48, pp. 1328-1342.

Wilson, D, Abbo, A, Sloan, S & Lyamin, A 2013, 'Undrained stability of a square tunnel where the shear strength increases linearly with depth', *Computers and Geotechnics*, vol 49, pp. 314-325.

Zhao, J, Shirlaw, J & Krishnan, R 2000, 'Tunnels and Underground Structures, Proceedings of the International Conference on Tunnels and Underground Structures', A.A. Balkema Publishers, Singapore.

# APPENDIX A – PROJECT SPECIFICATION

ENG4111/4112 Research Project

## Project Specification

For: Alexander Bell  
Title: Stability Design Charts for Tunnel Heading  
Major: Civil Engineering  
Supervisors: Dr. Jim Shiau  
Enrolment: ENG4111 – ONC S1, 2016  
ENG4112 – ONC S2, 2016  
Project Aim: To investigate the tunnelling procedure and common issues, perform a software modelling analysis on tunnel heading collapse and blowout problems, and develop stability design charts applicable to shallow tunnel heading in an undrained clay medium.

**Programme: Issue B, 25<sup>th</sup> September 2016**

1. Research background information relating to tunnelling in general and tunnel heading stability analysis. This will include investigating slope stability and the factor of safety approach.
2. Create a two-dimensional plane strain model of the simplified Greenfield (Pressure Ratio = 0) tunnel heading problem using the factor of safety approach in Optum G2. The strength reduction method and gravity multiplier method will be used to calculate the lower and upper bound factor of safety values. The results obtained in Optum G2 will be internally compared to determine the most accurate method which will then hopefully be validated by comparing to previously published results.
3. Develop additional Optum G2 models representing collapse and blowout scenarios. Where possible, these results will also be compared to previously published results.
4. Analyse and discuss the results obtained in Parts 2 and 3 then use the results to develop a set of tunnel heading stability design charts which will relate the factor of safety to important dimensional and soil parameters. These stability design charts are intended to be used in the preliminary stages of tunnel design.
5. Identify any gaps in the results and run a number of additional tests, using the most suitable method in Optum G2, to ensure full coverage.
6. Compile all research and results, discuss the stability design charts and provide examples detailing their use. The suitability of Optum G2 for modelling simple two-dimensional tunnelling problems exhibiting both collapse and blowout failure mechanisms will be determined.

## APPENDIX B – INITIAL RESULTS AND PLOTS

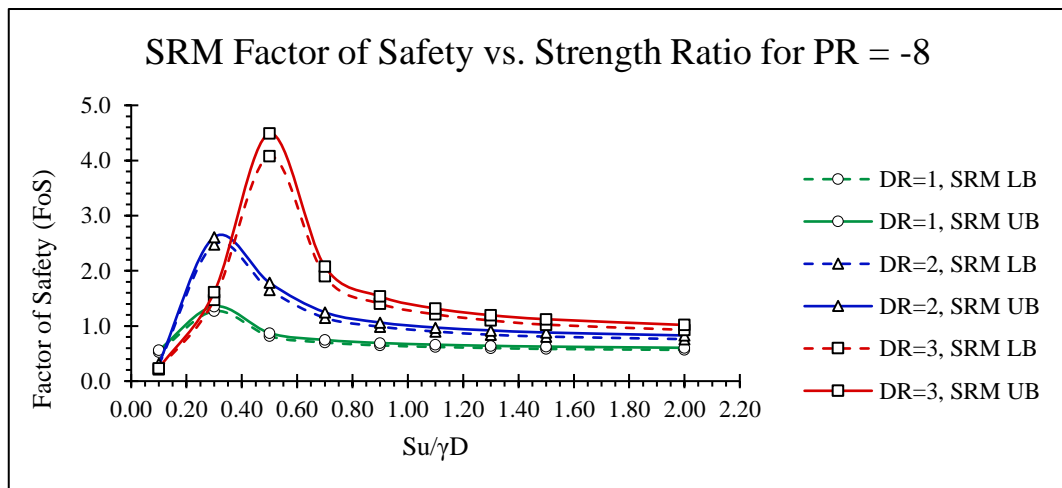
DR = 1    So C =        6    m                    Pressure Ratio = -8								
Trial #	Su/γD	Su (kPa)	Surcharge (kPa)	Internal (kPa)	SRM LB	SRM UB	GMM LB	GMM UB
1	0.10	10.8	0.0	86.4	0.525	0.561	0.753	0.772
2	0.30	32.4	0.0	259.2	1.269	1.354	2.258	2.315
3	0.50	54.0	0.0	432.0	0.815	0.872	3.763	3.858
4	0.70	75.6	0.0	604.8	0.700	0.747	5.269	5.402
5	0.90	97.2	0.0	777.6	0.647	0.691	6.774	6.945
6	1.10	118.8	0.0	950.4	0.619	0.661	8.279	8.488
7	1.30	140.4	0.0	1123.2	0.600	0.640	9.785	10.031
8	1.50	162.0	0.0	1296.0	0.583	0.626	11.290	11.575
9	2.00	216.0	0.0	1728.0	0.566	0.604	15.053	15.433

DR = 2    So C =        12    m                    Pressure Ratio = -8								
Trial #	Su/γD	Su (kPa)	Surcharge (kPa)	Internal (kPa)	SRM LB	SRM UB	GMM LB	GMM UB
1	0.10	10.8	0.0	86.4	0.295	0.319	0.511	0.526
2	0.30	32.4	0.0	259.2	2.476	2.610	1.533	1.578
3	0.50	54.0	0.0	432.0	1.655	1.784	2.555	2.630
4	0.70	75.6	0.0	604.8	1.148	1.248	3.577	3.682
5	0.90	97.2	0.0	777.6	0.987	1.062	4.599	4.734
6	1.10	118.8	0.0	950.4	0.899	0.971	5.621	5.786
7	1.30	140.4	0.0	1123.2	0.841	0.919	6.643	6.838
8	1.50	162.0	0.0	1296.0	0.807	0.881	7.665	7.890
9	2.00	216.0	0.0	1728.0	0.761	0.828	10.220	10.520

DR = 3    So C =        18    m                    Pressure Ratio = -8								
Trial #	Su/γD	Su (kPa)	Surcharge (kPa)	Internal (kPa)	SRM LB	SRM UB	GMM LB	GMM UB
1	0.10	10.8	0.0	86.4	0.214	0.233	0.388	0.403
2	0.30	32.4	0.0	259.2	1.474	1.612	1.164	1.208
3	0.50	54.0	0.0	432.0	4.077	4.489	1.941	2.013
4	0.70	75.6	0.0	604.8	1.901	2.076	2.717	2.819
5	0.90	97.2	0.0	777.6	1.403	1.535	3.493	3.624
6	1.10	118.8	0.0	950.4	1.210	1.316	4.269	4.429
7	1.30	140.4	0.0	1123.2	1.100	1.195	5.045	5.234
8	1.50	162.0	0.0	1296.0	1.023	1.122	5.821	6.040
9	2.00	216.0	0.0	1728.0	0.929	1.018	7.762	8.053



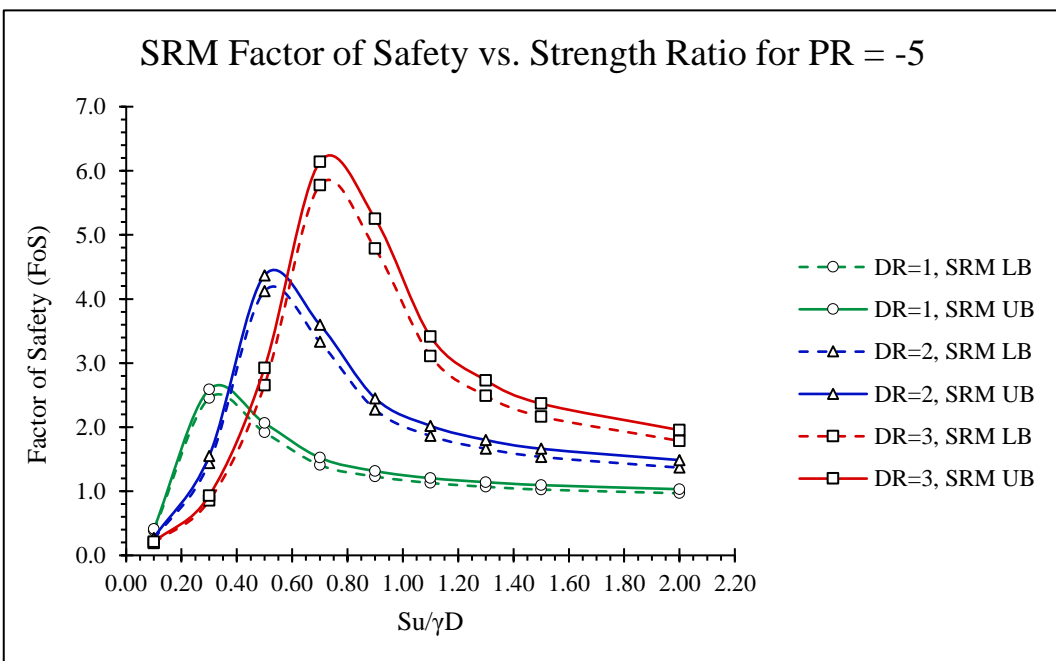
DR = 1      So C =      6   m      Pressure Ratio = -5								
Trial #	Su/γD	Su (kPa)	Surcharge (kPa)	Internal (kPa)	SRM LB	SRM UB	GMM LB	GMM UB
1	0.10	10.8	0.0	54.0	0.385	0.413	0.573	0.592
2	0.30	32.4	0.0	162.0	2.452	2.587	1.718	1.775
3	0.50	54.0	0.0	270.0	1.920	2.064	2.863	2.959
4	0.70	75.6	0.0	378.0	1.408	1.523	4.006	4.142
5	0.90	97.2	0.0	486.0	1.230	1.315	5.153	5.326
6	1.10	118.8	0.0	594.0	1.129	1.204	6.298	6.509
7	1.30	140.4	0.0	702.0	1.070	1.142	7.443	7.693
8	1.50	162.0	0.0	810.0	1.026	1.096	8.588	8.876
9	2.00	216.0	0.0	1080.0	0.969	1.032	11.444	11.835

DR = 2      So C =      12   m      Pressure Ratio = -5								
Trial #	Su/γD	Su (kPa)	Surcharge (kPa)	Internal (kPa)	SRM LB	SRM UB	GMM LB	GMM UB
1	0.10	10.8	0.0	54.0	0.252	0.273	0.396	0.412
2	0.30	32.4	0.0	162.0	1.442	1.550	1.189	1.236
3	0.50	54.0	0.0	270.0	4.123	4.369	1.982	2.059
4	0.70	75.6	0.0	378.0	3.331	3.599	2.775	2.883
5	0.90	97.2	0.0	486.0	2.273	2.451	3.567	3.707
6	1.10	118.8	0.0	594.0	1.863	2.021	4.359	4.531
7	1.30	140.4	0.0	702.0	1.664	1.800	5.153	5.354
8	1.50	162.0	0.0	810.0	1.536	1.663	5.945	6.178
9	2.00	216.0	0.0	1080.0	1.368	1.486	7.926	8.237

DR = 3      So C =      18   m      Pressure Ratio = -5								
Trial #	Su/γD	Su (kPa)	Surcharge (kPa)	Internal (kPa)	SRM LB	SRM UB	GMM LB	GMM UB
1	0.10	10.8	0.0	54.0	0.194	0.210	0.306	0.320
2	0.30	32.4	0.0	162.0	0.854	0.932	0.918	0.959
3	0.50	54.0	0.0	270.0	2.656	2.925	1.531	1.598
4	0.70	75.6	0.0	378.0	5.778	6.140	2.143	2.238
5	0.90	97.2	0.0	486.0	4.785	5.250	2.755	2.877
6	1.10	118.8	0.0	594.0	3.110	3.412	3.367	3.517
7	1.30	140.4	0.0	702.0	2.489	2.729	3.980	4.156
8	1.50	162.0	0.0	810.0	2.166	2.367	4.592	4.795
9	2.00	216.0	0.0	1080.0	1.786	1.954	6.123	6.394



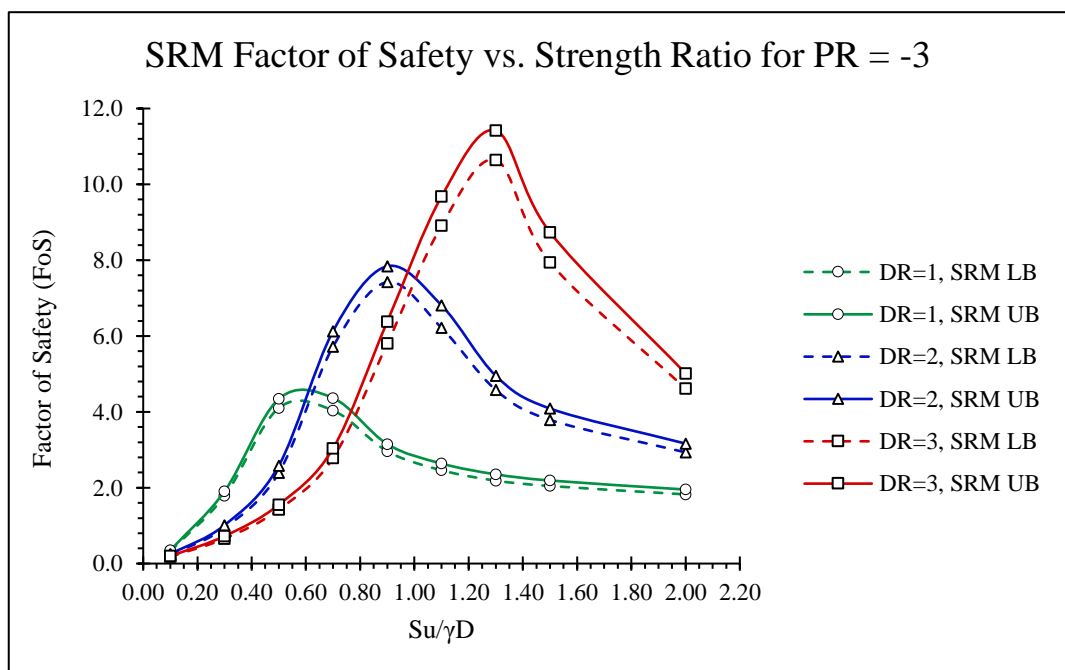
DR = 1      So C =      6   m      Pressure Ratio = -3								
Trial #	Su/ $\gamma$ D	Su (kPa)	Surcharge (kPa)	Internal (kPa)	SRM LB	SRM UB	GMM LB	GMM UB
1	0.10	10.8	0.0	32.4	0.325	0.350	0.452	0.470
2	0.30	32.4	0.0	97.2	1.785	1.906	1.356	1.410
3	0.50	54.0	0.0	162.0	4.103	4.341	2.260	2.350
4	0.70	75.6	0.0	226.8	4.036	4.365	3.165	3.290
5	0.90	97.2	0.0	291.6	2.961	3.150	4.069	4.230
6	1.10	118.8	0.0	356.4	2.461	2.638	4.973	5.169
7	1.30	140.4	0.0	421.2	2.187	2.353	5.877	6.109
8	1.50	162.0	0.0	486.0	2.045	2.190	6.781	7.049
9	2.00	216.0	0.0	648.0	1.824	1.952	9.042	9.399

DR = 2      So C =      12   m      Pressure Ratio = -3								
Trial #	Su/ $\gamma$ D	Su (kPa)	Surcharge (kPa)	Internal (kPa)	SRM LB	SRM UB	GMM LB	GMM UB
1	0.10	10.8	0.0	32.4	0.230	0.249	0.320	0.336
2	0.30	32.4	0.0	97.2	0.940	1.014	0.960	1.008
3	0.50	54.0	0.0	162.0	2.391	2.583	1.599	1.681
4	0.70	75.6	0.0	226.8	5.720	6.127	2.238	2.353
5	0.90	97.2	0.0	291.6	7.422	7.841	2.877	3.025
6	1.10	118.8	0.0	356.4	6.217	6.811	3.516	3.698
7	1.30	140.4	0.0	421.2	4.579	4.953	4.156	4.370
8	1.50	162.0	0.0	486.0	3.789	4.088	4.795	5.042
9	2.00	216.0	0.0	648.0	2.933	3.164	6.393	6.723

DR = 3      So C =      18   m      Pressure Ratio = -3								
Trial #	Su/ $\gamma$ D	Su (kPa)	Surcharge (kPa)	Internal (kPa)	SRM LB	SRM UB	GMM LB	GMM UB
1	0.10	10.8	0.0	32.4	0.181	0.197	0.250	0.264
2	0.30	32.4	0.0	97.2	0.658	0.724	0.749	0.792
3	0.50	54.0	0.0	162.0	1.423	1.553	1.249	1.319
4	0.70	75.6	0.0	226.8	2.782	3.036	1.748	1.847
5	0.90	97.2	0.0	291.6	5.801	6.381	2.247	2.375
6	1.10	118.8	0.0	356.4	8.909	9.679	2.747	2.903
7	1.30	140.4	0.0	421.2	10.640	11.415	3.246	3.430
8	1.50	162.0	0.0	486.0	7.941	8.736	3.746	3.958
9	2.00	216.0	0.0	648.0	4.611	5.014	4.994	5.278



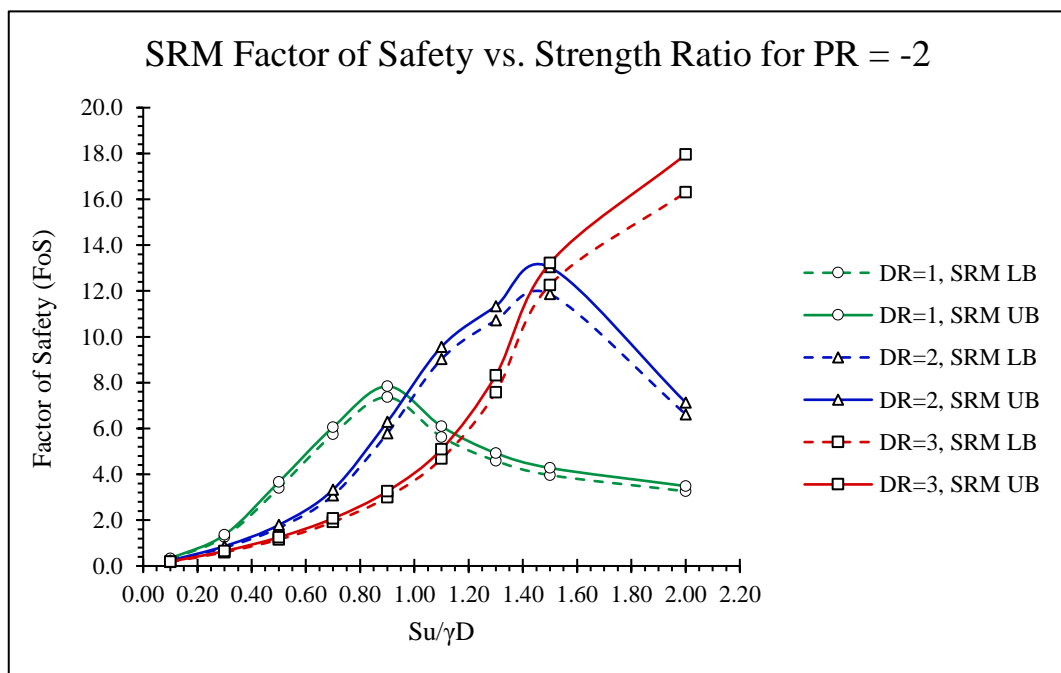
DR = 1    So C =    6   m    Pressure Ratio = -2								
Trial #	Su/ $\gamma$ D	Su (kPa)	Surcharge (kPa)	Internal (kPa)	SRM LB	SRM UB	GMM LB	GMM UB
1	0.10	10.8	0.0	21.6	0.302	0.325	0.391	0.408
2	0.30	32.4	0.0	64.8	1.269	1.357	1.172	1.225
3	0.50	54.0	0.0	108.0	3.395	3.663	1.953	2.042
4	0.70	75.6	0.0	151.2	5.747	6.053	2.734	2.859
5	0.90	97.2	0.0	194.4	7.364	7.840	3.515	3.675
6	1.10	118.8	0.0	237.6	5.629	6.093	4.296	4.492
7	1.30	140.4	0.0	280.8	4.588	4.926	5.077	5.309
8	1.50	162.0	0.0	324.0	3.964	4.278	5.858	6.126
9	2.00	216.0	0.0	432.0	3.260	3.487	7.811	8.168

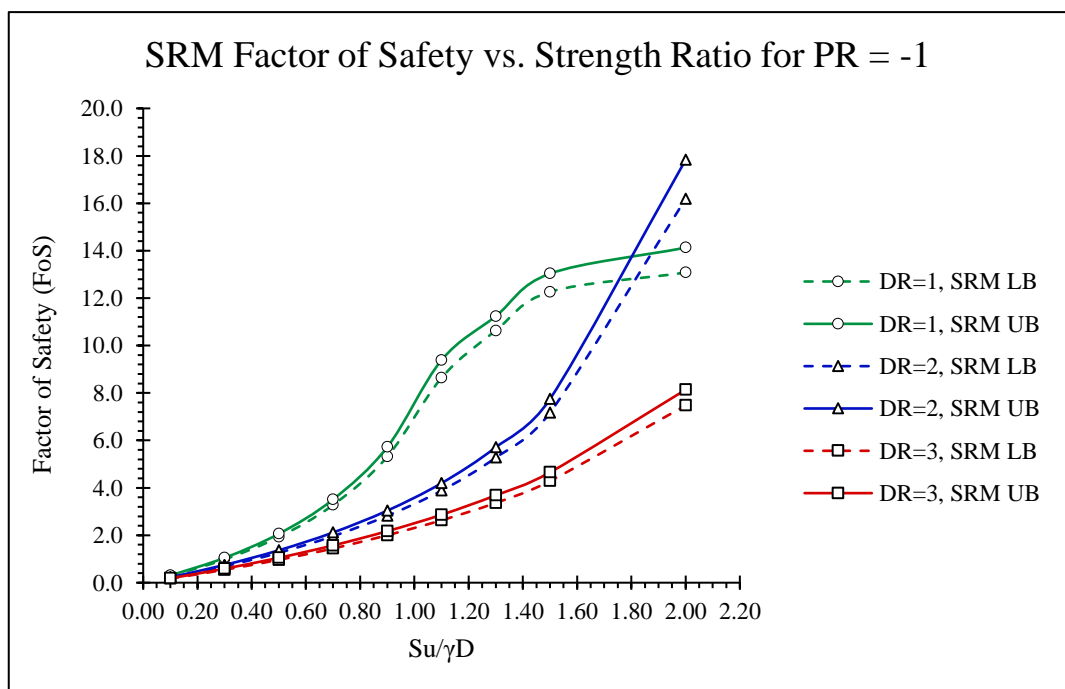
DR = 2    So C =    12   m    Pressure Ratio = -2								
Trial #	Su/ $\gamma$ D	Su (kPa)	Surcharge (kPa)	Internal (kPa)	SRM LB	SRM UB	GMM LB	GMM UB
1	0.10	10.8	0.0	21.6	0.222	0.238	0.280	0.298
2	0.30	32.4	0.0	64.8	0.802	0.864	0.840	0.893
3	0.50	54.0	0.0	108.0	1.660	1.789	1.400	1.489
4	0.70	75.6	0.0	151.2	3.082	3.330	1.961	2.085
5	0.90	97.2	0.0	194.4	5.785	6.288	2.521	2.680
6	1.10	118.8	0.0	237.6	9.026	9.564	3.081	3.276
7	1.30	140.4	0.0	280.8	10.716	11.341	3.641	3.872
8	1.50	162.0	0.0	324.0	11.863	13.034	4.201	4.467
9	2.00	216.0	0.0	432.0	6.621	7.137	5.602	5.956

DR = 3    So C =    18   m    Pressure Ratio = -2								
Trial #	Su/ $\gamma$ D	Su (kPa)	Surcharge (kPa)	Internal (kPa)	SRM LB	SRM UB	GMM LB	GMM UB
1	0.10	10.8	0.0	21.6	0.175	0.191	0.223	0.236
2	0.30	32.4	0.0	64.8	0.598	0.650	0.668	0.709
3	0.50	54.0	0.0	108.0	1.153	1.252	1.113	1.181
4	0.70	75.6	0.0	151.2	1.920	2.076	1.558	1.654
5	0.90	97.2	0.0	194.4	2.999	3.258	2.004	2.126
6	1.10	118.8	0.0	237.6	4.682	5.095	2.449	2.599
7	1.30	140.4	0.0	280.8	7.581	8.322	2.894	3.071
8	1.50	162.0	0.0	324.0	12.265	13.221	3.339	3.544
9	2.00	216.0	0.0	432.0	16.308	17.957	4.452	4.725



DR = 1      So C =      6   m      Pressure Ratio = -1								
Trial #	Su/γD	Su (kPa)	Surcharge (kPa)	Internal (kPa)	SRM LB	SRM UB	GMM LB	GMM UB
1	0.10	10.8	0.0	10.8	0.283	0.303	0.328	0.346
2	0.30	32.4	0.0	32.4	0.981	1.048	0.985	1.039
3	0.50	54.0	0.0	54.0	1.924	2.061	1.642	1.731
4	0.70	75.6	0.0	75.6	3.278	3.510	2.299	2.423
5	0.90	97.2	0.0	97.2	5.312	5.720	2.956	3.116
6	1.10	118.8	0.0	118.8	8.638	9.384	3.613	3.808
7	1.30	140.4	0.0	140.4	10.629	11.237	4.270	4.501
8	1.50	162.0	0.0	162.0	12.262	13.033	4.927	5.193
9	2.00	216.0	0.0	216.0	13.078	14.127	6.569	6.924
DR = 2      So C =      12   m      Pressure Ratio = -1								
Trial #	Su/γD	Su (kPa)	Surcharge (kPa)	Internal (kPa)	SRM LB	SRM UB	GMM LB	GMM UB
1	0.10	10.8	0.0	10.8	0.212	0.229	0.243	0.259
2	0.30	32.4	0.0	32.4	0.691	0.748	0.729	0.776
3	0.50	54.0	0.0	54.0	1.261	1.366	1.215	1.294
4	0.70	75.6	0.0	75.6	1.961	2.115	1.701	1.812
5	0.90	97.2	0.0	97.2	2.821	3.039	2.187	2.329
6	1.10	118.8	0.0	118.8	3.881	4.196	2.673	2.847
7	1.30	140.4	0.0	140.4	5.275	5.712	3.159	3.365
8	1.50	162.0	0.0	162.0	7.172	7.746	3.645	3.882
9	2.00	216.0	0.0	216.0	16.186	17.831	4.861	5.177
DR = 3      So C =      18   m      Pressure Ratio = -1								
Trial #	Su/γD	Su (kPa)	Surcharge (kPa)	Internal (kPa)	SRM LB	SRM UB	GMM LB	GMM UB
1	0.10	10.8	0.0	10.8	0.172	0.185	0.195	0.208
2	0.30	32.4	0.0	32.4	0.545	0.591	0.584	0.625
3	0.50	54.0	0.0	54.0	0.964	1.050	0.973	1.042
4	0.70	75.6	0.0	75.6	1.442	1.571	1.363	1.459
5	0.90	97.2	0.0	97.2	2.003	2.173	1.752	1.876
6	1.10	118.8	0.0	118.8	2.632	2.865	2.141	2.293
7	1.30	140.4	0.0	140.4	3.367	3.685	2.531	2.710
8	1.50	162.0	0.0	162.0	4.288	4.653	2.920	3.127
9	2.00	216.0	0.0	216.0	7.473	8.138	3.893	4.169



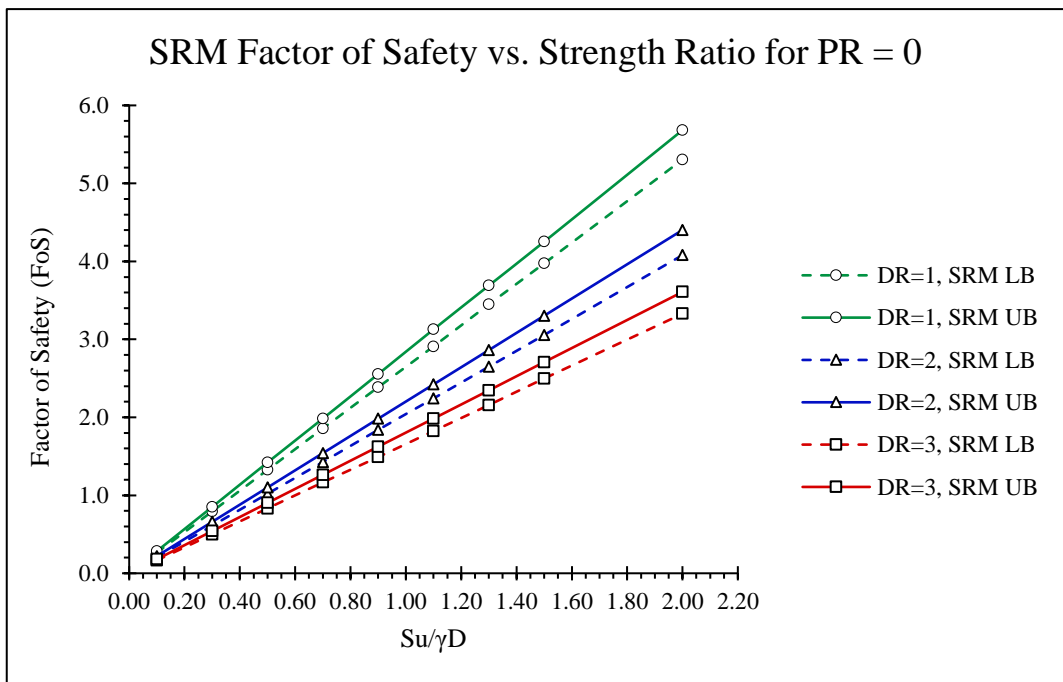
DR = 1		So C = 6 m			Pressure Ratio = 0			
Trial #	Su/γD	Su (kPa)	Surcharge (kPa)	Internal (kPa)	SRM LB	SRM UB	GMM LB	GMM UB
1	0.10	10.8	0.0	0.0	0.265	0.284	0.265	0.283
2	0.30	32.4	0.0	0.0	0.793	0.851	0.795	0.850
3	0.50	54.0	0.0	0.0	1.326	1.421	1.325	1.417
4	0.70	75.6	0.0	0.0	1.857	1.984	1.855	1.984
5	0.90	97.2	0.0	0.0	2.386	2.554	2.385	2.551
6	1.10	118.8	0.0	0.0	2.909	3.127	2.915	3.118
7	1.30	140.4	0.0	0.0	3.449	3.690	3.445	3.685
8	1.50	162.0	0.0	0.0	3.974	4.252	3.975	4.252
9	2.00	216.0	0.0	0.0	5.305	5.683	5.300	5.670

DR = 2		So C = 12 m			Pressure Ratio = 0			
Trial #	Su/γD	Su (kPa)	Surcharge (kPa)	Internal (kPa)	SRM LB	SRM UB	GMM LB	GMM UB
1	0.10	10.8	0.0	0.0	0.204	0.220	0.204	0.220
2	0.30	32.4	0.0	0.0	0.610	0.660	0.613	0.660
3	0.50	54.0	0.0	0.0	1.020	1.100	1.022	1.100
4	0.70	75.6	0.0	0.0	1.427	1.541	1.430	1.540
5	0.90	97.2	0.0	0.0	1.840	1.982	1.839	1.979
6	1.10	118.8	0.0	0.0	2.242	2.422	2.248	2.419
7	1.30	140.4	0.0	0.0	2.649	2.862	2.657	2.859
8	1.50	162.0	0.0	0.0	3.056	3.303	3.065	3.299
9	2.00	216.0	0.0	0.0	4.080	4.402	4.087	4.399

DR = 3		So C = 18 m			Pressure Ratio = 0			
Trial #	Su/γD	Su (kPa)	Surcharge (kPa)	Internal (kPa)	SRM LB	SRM UB	GMM LB	GMM UB
1	0.10	10.8	0.0	0.0	0.166	0.180	0.165	0.180
2	0.30	32.4	0.0	0.0	0.499	0.541	0.496	0.541
3	0.50	54.0	0.0	0.0	0.832	0.902	0.826	0.901
4	0.70	75.6	0.0	0.0	1.166	1.263	1.157	1.262
5	0.90	97.2	0.0	0.0	1.490	1.624	1.488	1.622
6	1.10	118.8	0.0	0.0	1.825	1.984	1.818	1.982
7	1.30	140.4	0.0	0.0	2.157	2.345	2.149	2.343
8	1.50	162.0	0.0	0.0	2.498	2.708	2.479	2.703
9	2.00	216.0	0.0	0.0	3.328	3.608	3.306	3.605



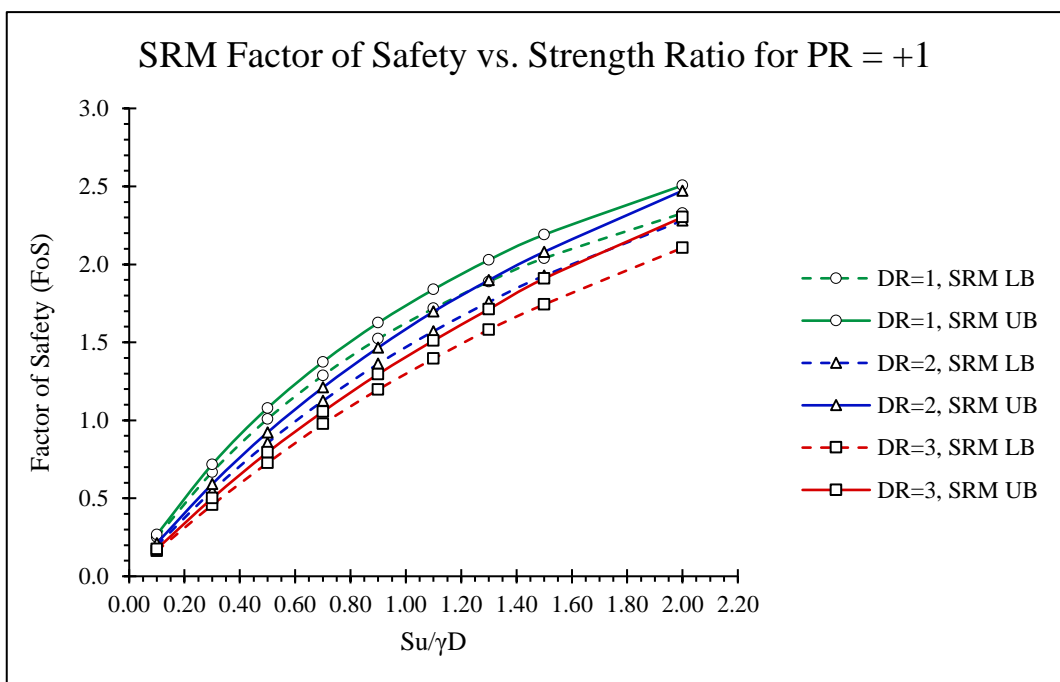
DR = 1      So C =      6   m      Pressure Ratio = 1								
Trial #	Su/γD	Su (kPa)	Surcharge (kPa)	Internal (kPa)	SRM LB	SRM UB	GMM LB	GMM UB
1	0.10	10.8	10.8	0.0	0.250	0.267	0.203	0.220
2	0.30	32.4	32.4	0.0	0.668	0.717	0.608	0.660
3	0.50	54.0	54.0	0.0	1.008	1.078	1.014	1.101
4	0.70	75.6	75.6	0.0	1.287	1.374	1.419	1.541
5	0.90	97.2	97.2	0.0	1.522	1.625	1.825	1.981
6	1.10	118.8	118.8	0.0	1.717	1.839	2.230	2.422
7	1.30	140.4	140.4	0.0	1.889	2.028	2.636	2.862
8	1.50	162.0	162.0	0.0	2.039	2.190	3.041	3.302
9	2.00	216.0	216.0	0.0	2.328	2.506	4.055	4.403

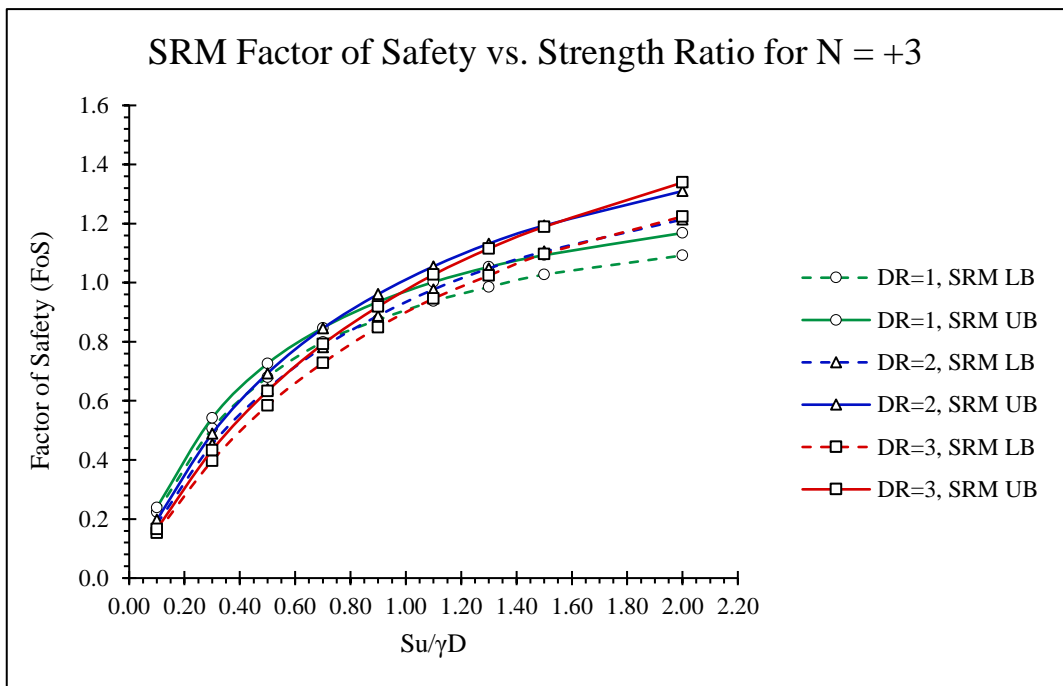
DR = 2      So C =      12   m      Pressure Ratio = 1								
Trial #	Su/γD	Su (kPa)	Surcharge (kPa)	Internal (kPa)	SRM LB	SRM UB	GMM LB	GMM UB
1	0.10	10.8	10.8	0.0	0.196	0.212	0.166	0.181
2	0.30	32.4	32.4	0.0	0.548	0.591	0.498	0.543
3	0.50	54.0	54.0	0.0	0.855	0.922	0.829	0.905
4	0.70	75.6	75.6	0.0	1.124	1.210	1.161	1.267
5	0.90	97.2	97.2	0.0	1.362	1.466	1.493	1.629
6	1.10	118.8	118.8	0.0	1.571	1.697	1.824	1.991
7	1.30	140.4	140.4	0.0	1.758	1.898	2.156	2.353
8	1.50	162.0	162.0	0.0	1.927	2.080	2.488	2.715
9	2.00	216.0	216.0	0.0	2.281	2.472	3.317	3.620

DR = 3      So C =      18   m      Pressure Ratio = 1								
Trial #	Su/γD	Su (kPa)	Surcharge (kPa)	Internal (kPa)	SRM LB	SRM UB	GMM LB	GMM UB
1	0.10	10.8	10.8	0.0	0.162	0.175	0.138	0.152
2	0.30	32.4	32.4	0.0	0.457	0.500	0.414	0.456
3	0.50	54.0	54.0	0.0	0.726	0.794	0.690	0.760
4	0.70	75.6	75.6	0.0	0.976	1.055	0.966	1.064
5	0.90	97.2	97.2	0.0	1.197	1.296	1.241	1.369
6	1.10	118.8	118.8	0.0	1.395	1.511	1.517	1.673
7	1.30	140.4	140.4	0.0	1.581	1.712	1.793	1.977
8	1.50	162.0	162.0	0.0	1.743	1.909	2.069	2.281
9	2.00	216.0	216.0	0.0	2.106	2.302	2.759	3.041



DR = 1      So C =      6   m      Pressure Ratio = 3								
Trial #	Su/γD	Su (kPa)	Surcharge (kPa)	Internal (kPa)	SRM LB	SRM UB	GMM LB	GMM UB
1	0.10	10.8	32.4	0.0	0.223	0.239	0.073	0.092
2	0.30	32.4	97.2	0.0	0.506	0.542	0.220	0.275
3	0.50	54.0	162.0	0.0	0.680	0.726	0.366	0.458
4	0.70	75.6	226.8	0.0	0.799	0.847	0.513	0.641
5	0.90	97.2	291.6	0.0	0.874	0.935	0.660	0.824
6	1.10	118.8	356.4	0.0	0.937	1.002	0.806	1.007
7	1.30	140.4	421.2	0.0	0.985	1.053	0.953	1.190
8	1.50	162.0	486.0	0.0	1.027	1.093	1.099	1.373
9	2.00	216.0	648.0	0.0	1.092	1.168	1.465	1.831
DR = 2      So C =      12   m      Pressure Ratio = 3								
Trial #	Su/γD	Su (kPa)	Surcharge (kPa)	Internal (kPa)	SRM LB	SRM UB	GMM LB	GMM UB
1	0.10	10.8	32.4	0.0	0.183	0.197	0.086	0.102
2	0.30	32.4	97.2	0.0	0.453	0.489	0.259	0.306
3	0.50	54.0	162.0	0.0	0.640	0.693	0.432	0.511
4	0.70	75.6	226.8	0.0	0.781	0.845	0.605	0.715
5	0.90	97.2	291.6	0.0	0.888	0.961	0.777	0.919
6	1.10	118.8	356.4	0.0	0.977	1.055	0.950	1.123
7	1.30	140.4	421.2	0.0	1.048	1.132	1.123	1.328
8	1.50	162.0	486.0	0.0	1.105	1.193	1.296	1.532
9	2.00	216.0	648.0	0.0	1.214	1.310	1.727	2.042
DR = 3      So C =      18   m      Pressure Ratio = 3								
Trial #	Su/γD	Su (kPa)	Surcharge (kPa)	Internal (kPa)	SRM LB	SRM UB	GMM LB	GMM UB
1	0.10	10.8	32.4	0.0	0.153	0.166	0.082	0.095
2	0.30	32.4	97.2	0.0	0.397	0.433	0.245	0.286
3	0.50	54.0	162.0	0.0	0.584	0.633	0.408	0.477
4	0.70	75.6	226.8	0.0	0.728	0.792	0.571	0.668
5	0.90	97.2	291.6	0.0	0.849	0.919	0.734	0.858
6	1.10	118.8	356.4	0.0	0.946	1.027	0.897	1.049
7	1.30	140.4	421.2	0.0	1.024	1.115	1.060	1.240
8	1.50	162.0	486.0	0.0	1.097	1.189	1.223	1.430
9	2.00	216.0	648.0	0.0	1.224	1.339	1.630	1.907



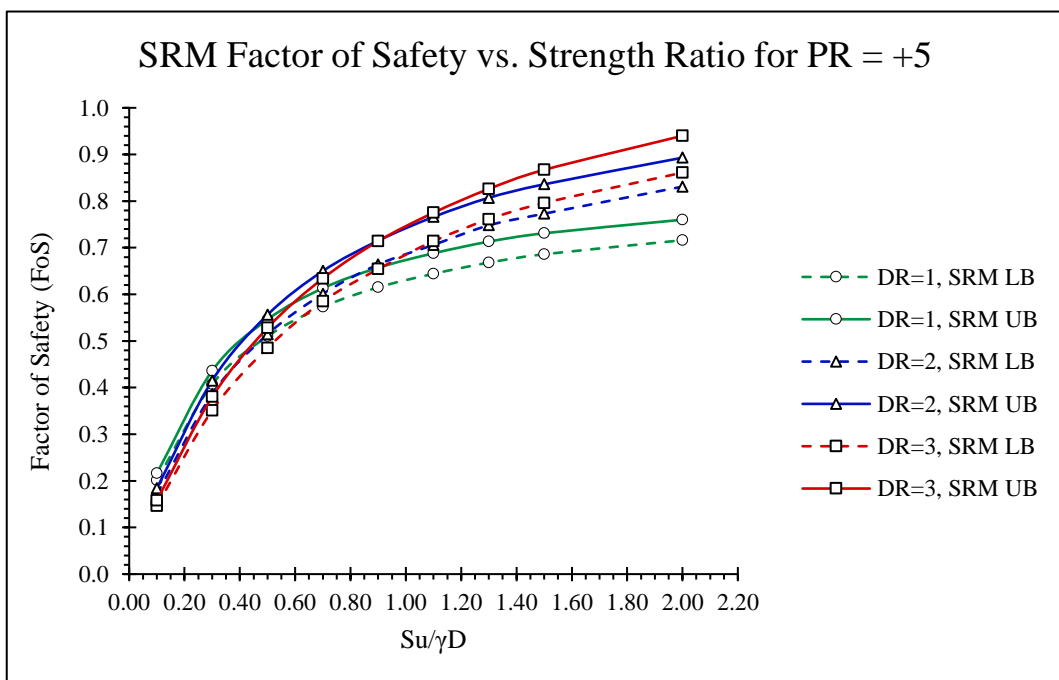
DR = 1    So C =    6    m    Pressure Ratio = 5								
Trial #	Su/ $\gamma$ D	Su (kPa)	Surcharge (kPa)	Internal (kPa)	SRM LB	SRM UB	GMM LB	GMM UB
1	0.10	10.8	54.0	0.0	0.201	0.216	-0.059	-0.042
2	0.30	32.4	162.0	0.0	0.407	0.436	-0.177	-0.125
3	0.50	54.0	270.0	0.0	0.510	0.546	-0.294	-0.208
4	0.70	75.6	378.0	0.0	0.573	0.613	-0.412	-0.291
5	0.90	97.2	486.0	0.0	0.615	0.657	-0.530	-0.374
6	1.10	118.8	594.0	0.0	0.644	0.688	-0.648	-0.458
7	1.30	140.4	702.0	0.0	0.668	0.713	-0.766	-0.541
8	1.50	162.0	810.0	0.0	0.686	0.731	-0.883	-0.624
9	2.00	216.0	1080.0	0.0	0.716	0.760	-1.178	-0.832

DR = 2    So C =    12    m    Pressure Ratio = 5								
Trial #	Su/ $\gamma$ D	Su (kPa)	Surcharge (kPa)	Internal (kPa)	SRM LB	SRM UB	GMM LB	GMM UB
1	0.10	10.8	54.0	0.0	0.171	0.184	0.006	0.023
2	0.30	32.4	162.0	0.0	0.386	0.415	0.017	0.068
3	0.50	54.0	270.0	0.0	0.514	0.556	0.028	0.114
4	0.70	75.6	378.0	0.0	0.601	0.650	0.039	0.160
5	0.90	97.2	486.0	0.0	0.664	0.715	0.050	0.205
6	1.10	118.8	594.0	0.0	0.706	0.766	0.061	0.251
7	1.30	140.4	702.0	0.0	0.748	0.807	0.073	0.296
8	1.50	162.0	810.0	0.0	0.773	0.836	0.084	0.342
9	2.00	216.0	1080.0	0.0	0.831	0.893	0.112	0.456

DR = 3    So C =    18    m    Pressure Ratio = 5								
Trial #	Su/ $\gamma$ D	Su (kPa)	Surcharge (kPa)	Internal (kPa)	SRM LB	SRM UB	GMM LB	GMM UB
1	0.10	10.8	54.0	0.0	0.146	0.158	0.023	0.039
2	0.30	32.4	162.0	0.0	0.351	0.380	0.069	0.116
3	0.50	54.0	270.0	0.0	0.485	0.528	0.115	0.193
4	0.70	75.6	378.0	0.0	0.585	0.634	0.161	0.270
5	0.90	97.2	486.0	0.0	0.654	0.714	0.208	0.347
6	1.10	118.8	594.0	0.0	0.714	0.775	0.254	0.424
7	1.30	140.4	702.0	0.0	0.761	0.826	0.300	0.502
8	1.50	162.0	810.0	0.0	0.796	0.867	0.346	0.579
9	2.00	216.0	1080.0	0.0	0.861	0.940	0.461	0.772



## APPENDIX C – EXTERNAL COMPARISON

Raw data used in lower bound strength reduction method comparison to Augarde, Lyamin and Sloan (2003)									
C/D	$S_u/\gamma D$	$\gamma D/S_u$	PR	FoS	$N_c$	$SR_c$	$SR_c$ Target	$N_c$ Interp.	$N_c$ (Published)
1	0.70	1.429	+3	0.799	2.397	1.141	1.00	2.602	2.460
	0.70	1.429	+5	0.573	2.865	0.819			
	0.50	2.000	+1	1.008	1.008	2.016	2.00	1.033	0.850
	0.50	2.000	+3	0.68	2.040	1.360			
	1.30	0.769	-1	10.629	-10.62	8.176	3.00	-0.668	-0.740
	1.30	0.769	0	3.449	0.000	2.653			
2	2.00	0.500	+1	2.281	2.281	1.141	1.00	2.639	2.400
	2.00	0.500	+3	1.214	3.642	0.607			
	1.10	0.909	0	2.242	0.000	2.038	2.00	0.098	-0.200
	1.10	0.909	+1	1.571	1.571	1.428			
	0.10	10.00	-8	0.295	-2.360	2.950	3.00	-2.488	-2.840
	0.10	10.00	-5	0.252	-1.260	2.520			
3	0.70	1.429	+3	0.728	2.184	1.040	1.00	2.329	2.200
	0.70	1.429	+5	0.585	2.925	0.836			
	0.30	3.333	-2	0.598	-1.196	1.993	2.00	-1.221	-1.400
	0.30	3.333	-1	0.545	-0.545	1.817			
	1.50	0.667	-1	4.288	-4.288	2.859	3.00	-4.863	-5.030
	1.50	0.667	0	2.708	0.000	1.805			

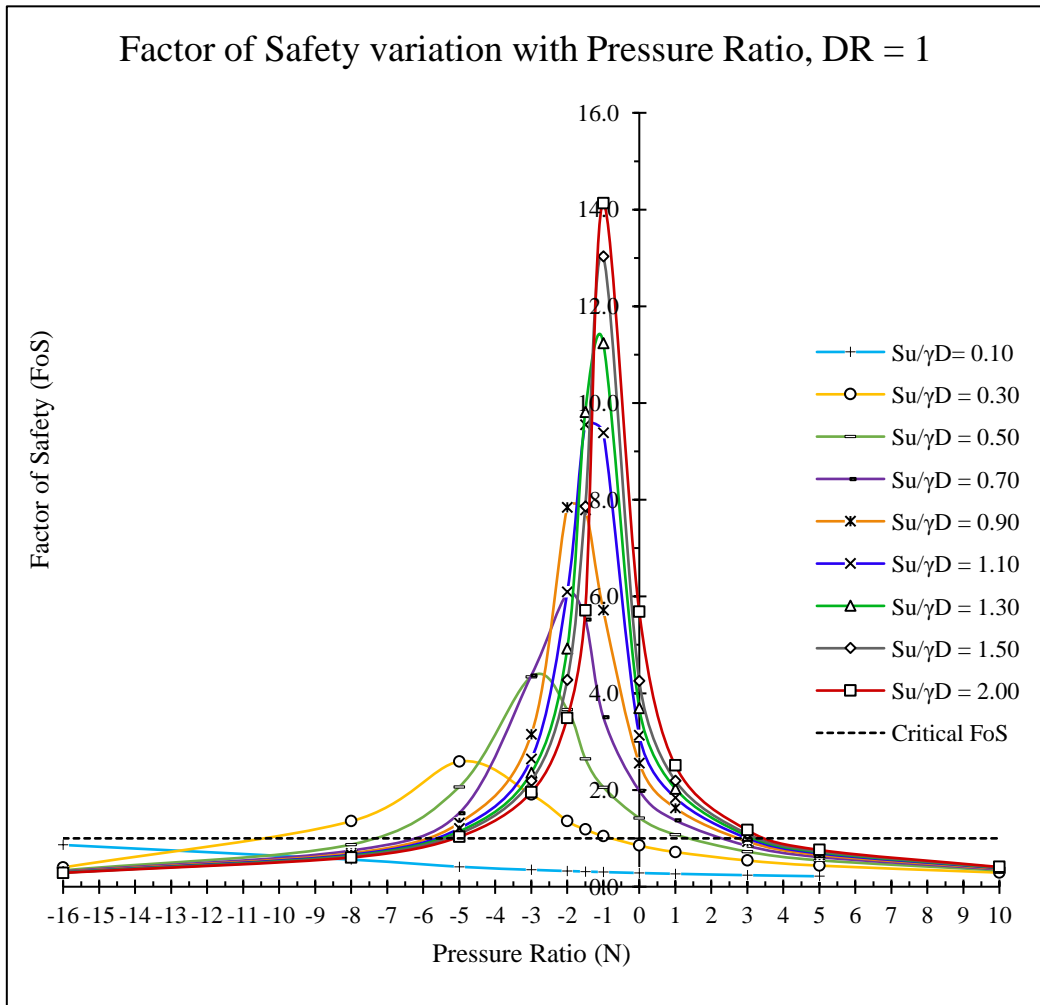
Raw data used in upper bound strength reduction method comparison to Augarde, Lyamin and Sloan (2003)									
C/D	$S_u/\gamma D$	$\gamma D/S_u$	PR	FoS	$N_c$	$SR_c$	$SR_c$ Target	$N_c$ Interp.	$N_c$ (Published)
1	0.70	1.429	3	0.847	2.541	1.210	1.00	2.870	2.890
	0.70	1.429	5	0.613	3.065	0.876			
	0.50	2.000	1	1.078	1.078	2.156	2.00	1.322	1.390
	0.50	2.000	3	0.726	2.178	1.452			
	1.30	0.769	-1	11.23	-11.23	8.644	3.00	-0.313	-0.110
	1.30	0.769	0	3.690	0.000	2.838			
2	2.00	0.500	1	2.472	2.472	1.236	1.00	3.064	3.180
	2.00	0.500	3	1.310	3.930	0.655			
	1.10	0.909	0	2.422	0.000	2.202	2.00	0.520	0.680
	1.10	0.909	1	1.697	1.697	1.543			
	0.10	10.00	-8	0.319	-2.552	3.190	3.00	-2.062	-1.820
	0.10	10.00	-5	0.273	-1.365	2.730			
3	0.70	1.429	3	0.792	2.376	1.131	1.00	2.838	3.000
	0.70	1.429	5	0.634	3.170	0.906			
	0.30	3.333	-2	0.650	-1.300	2.167	2.00	-0.699	-0.500
	0.30	3.333	-1	0.591	-0.591	1.970			
	1.50	0.667	-1	4.653	-4.653	3.102	3.00	-4.287	-4.000
	1.50	0.667	0	2.708	0.000	1.805			

## APPENDIX D – FINAL RESULTS AND PLOTS

FoS, Critical Strength Ratios and Critical Pressure Ratios for Upper Bound SRM Results, DR = 1								
Blue shading indicates blowout failure.								
Case	SR = ( $\gamma^*D$ )/ (Su) (1)	Su (kPa)	PR = ( $\sigma_s - \sigma_t$ )/ Su (2)	$\sigma_t$ (kPa) fix	$\sigma_s$ (kPa) fix	SRM UB FoS (3)	( $\gamma D$ )* (FoS)/ (Su) when FoS=1 (1)*(3)	PR <sub>c</sub> = ( $\sigma_s - \sigma_t$ )* (FoS)/(Su) when FoS=1 (2)*(3)
DR=1 SR=0.10	10.0	10.8	-16	172.8	0.0	0.864	8.640	-13.824
	10.0	10.8	-8	86.4	0.0	0.561	5.610	-4.488
	10.0	10.8	-5	54.0	0.0	0.413	4.130	-2.065
	10.0	10.8	-3	32.4	0.0	0.350	3.500	-1.050
	10.0	10.8	-2	21.6	0.0	0.325	3.250	-0.650
	10.0	10.8	-1.5	16.2	0.0	0.314	3.140	-0.471
	10.0	10.8	-1	10.8	0.0	0.303	3.030	-0.303
	10.0	10.8	0	0.0	0.0	0.284	2.840	0.000
	10.0	10.8	1	0.0	10.8	0.267	2.670	0.267
	10.0	10.8	3	0.0	32.4	0.239	2.390	0.717
	10.0	10.8	5	0.0	54.0	0.216	2.160	1.080
10.0	10.8	10	0.0	108.0	0.174	1.740	1.740	
DR=1 SR=0.30	3.33	32.4	-16	518.4	0.0	0.398	1.327	-6.368
	3.33	32.4	-8	259.2	0.0	1.354	4.513	-10.832
	3.33	32.4	-5	162.0	0.0	2.587	8.623	-12.935
	3.33	32.4	-3	97.2	0.0	1.906	6.353	-5.718
	3.33	32.4	-2	64.8	0.0	1.357	4.523	-2.714
	3.33	32.4	-1.5	48.6	0.0	1.184	3.947	-1.776
	3.33	32.4	-1	32.4	0.0	1.048	3.493	-1.048
	3.33	32.4	0	0.0	0.0	0.851	2.837	0.000
	3.33	32.4	1	0.0	32.4	0.717	2.390	0.717
	3.33	32.4	3	0.0	97.2	0.542	1.807	1.626
	3.33	32.4	5	0.0	162.0	0.436	1.453	2.180
3.33	32.4	10	0.0	324.0	0.292	0.973	2.920	
DR=1 SR=0.50	2.00	54.00	-16	864.0	0.0	0.337	0.674	-5.392
	2.00	54.00	-8	432.0	0.0	0.872	1.744	-6.976
	2.00	54.00	-5	270.0	0.0	2.064	4.128	-10.320
	2.00	54.00	-3	162.0	0.0	4.341	8.682	-13.023
	2.00	54.00	-2	108.0	0.0	3.663	7.326	-7.326
	2.00	54.00	-1.5	81.0	0.0	2.649	5.298	-3.974
	2.00	54.00	-1	54.0	0.0	2.061	4.122	-2.061
	2.00	54.00	0	0.0	0.0	1.421	2.842	0.000
	2.00	54.00	1	0.0	54.0	1.078	2.156	1.078
	2.00	54.00	3	0.0	162.0	0.726	1.452	2.178
	2.00	54.00	5	0.0	270.0	0.546	1.092	2.730
2.00	54.00	10	0.0	540.0	0.338	0.676	3.380	

DR=1 SR=0.70	1.43	75.60	-16	1209.6	0.0	0.316	0.451	-5.056
	1.43	75.60	-8	604.8	0.0	0.747	1.067	-5.976
	1.43	75.60	-5	378.0	0.0	1.523	2.176	-7.615
	1.43	75.60	-3	226.8	0.0	4.365	6.236	-13.095
	1.43	75.60	-2	151.2	0.0	6.053	8.647	-12.106
	1.43	75.60	-1.5	113.4	0.0	5.528	7.897	-8.292
	1.43	75.60	-1	75.6	0.0	3.510	5.014	-3.510
	1.43	75.60	0	0.0	0.0	1.984	2.834	0.000
	1.43	75.60	1	0.0	75.6	1.374	1.963	1.374
	1.43	75.60	3	0.0	226.8	0.847	1.210	2.541
	1.43	75.60	5	0.0	378.0	0.613	0.876	3.065
1.43	75.60	10	0.0	756.0	0.361	0.516	3.610	
DR=1 SR=0.90	1.11	97.20	-16	1555.2	0.0	0.306	0.340	-4.896
	1.11	97.20	-8	777.6	0.0	0.691	0.768	-5.528
	1.11	97.20	-5	486.0	0.0	1.315	1.461	-6.575
	1.11	97.20	-3	291.6	0.0	3.150	3.500	-9.450
	1.11	97.20	-2	194.4	0.0	7.840	8.711	-15.680
	1.11	97.20	-1.5	145.8	0.0	7.787	8.652	-11.681
	1.11	97.20	-1	97.2	0.0	5.720	6.356	-5.720
	1.11	97.20	0	0.0	0.0	2.554	2.838	0.000
	1.11	97.20	1	0.0	97.2	1.625	1.806	1.625
	1.11	97.20	3	0.0	291.6	0.935	1.039	2.805
	1.11	97.20	5	0.0	486.0	0.657	0.730	3.285
1.11	97.20	10	0.0	972.0	0.374	0.416	3.740	
DR=1 SR=1.10	0.91	118.80	-16	1900.8	0.0	0.299	0.272	-4.784
	0.91	118.80	-8	950.4	0.0	0.661	0.601	-5.288
	0.91	118.80	-5	594.0	0.0	1.204	1.095	-6.020
	0.91	118.80	-3	356.4	0.0	2.638	2.398	-7.914
	0.91	118.80	-2	237.6	0.0	6.093	5.539	-12.186
	0.91	118.80	-1.5	178.2	0.0	9.548	8.680	-14.322
	0.91	118.80	-1	118.8	0.0	9.384	8.531	-9.384
	0.91	118.80	0	0.0	0.0	3.127	2.843	0.000
	0.91	118.80	1	0.0	118.8	1.839	1.672	1.839
	0.91	118.80	3	0.0	356.4	1.002	0.911	3.006
	0.91	118.80	5	0.0	594.0	0.688	0.625	3.440
0.91	118.80	10	0.0	1188.0	0.385	0.350	3.850	
DR=1 SR=1.30	0.77	140.40	-16	2246.4	0.0	0.295	0.227	-4.720
	0.77	140.40	-8	1123.2	0.0	0.640	0.492	-5.120
	0.77	140.40	-5	702.0	0.0	1.142	0.878	-5.710
	0.77	140.40	-3	421.2	0.0	2.353	1.810	-7.059
	0.77	140.40	-2	280.8	0.0	4.926	3.789	-9.852
	0.77	140.40	-1.5	210.6	0.0	9.817	7.552	-14.726
	0.77	140.40	-1	140.4	0.0	11.23	8.644	-11.237
	0.77	140.40	0	0.0	0.0	3.690	2.838	0.000
	0.77	140.40	1	0.0	140.4	2.028	1.560	2.028
	0.77	140.40	3	0.0	421.2	1.053	0.810	3.159
	0.77	140.40	5	0.0	702.0	0.713	0.548	3.565
0.77	140.40	10	0.0	1404.0	0.392	0.302	3.920	

DR=1 SR=1.50	0.67	162.00	-16	2592.0	0.0	0.292	0.195	-4.672
	0.67	162.00	-8	1296.0	0.0	0.626	0.417	-5.008
	0.67	162.00	-5	810.0	0.0	1.096	0.731	-5.480
	0.67	162.00	-3	486.0	0.0	2.190	1.460	-6.570
	0.67	162.00	-2	324.0	0.0	4.278	2.852	-8.556
	0.67	162.00	-1.5	243.0	0.0	7.859	5.239	-11.789
	0.67	162.00	-1	162.0	0.0	13.03	8.689	-13.033
	0.67	162.00	0	0.0	0.0	4.252	2.835	0.000
	0.67	162.00	1	0.0	162.0	2.190	1.460	2.190
	0.67	162.00	3	0.0	486.0	1.093	0.729	3.279
	0.67	162.00	5	0.0	810.0	0.731	0.487	3.655
	0.67	162.00	10	0.0	1620.0	0.397	0.265	3.970
DR=1 SR=2.00	0.50	216.00	-16	3456.0	0.0	0.287	0.144	-4.592
	0.50	216.00	-8	1728.0	0.0	0.604	0.302	-4.832
	0.50	216.00	-5	1080.0	0.0	1.032	0.516	-5.160
	0.50	216.00	-3	648.0	0.0	1.952	0.976	-5.856
	0.50	216.00	-2	432.0	0.0	3.487	1.744	-6.974
	0.50	216.00	-1.5	324.0	0.0	5.713	2.857	-8.570
	0.50	216.00	-1	216.0	0.0	14.12	7.064	-14.127
	0.50	216.00	0	0.0	0.0	5.683	2.842	0.000
	0.50	216.00	1	0.0	216.0	2.506	1.253	2.506
	0.50	216.00	3	0.0	648.0	1.168	0.584	3.504
	0.50	216.00	5	0.0	1080.0	0.760	0.380	3.800
	0.50	216.00	10	0.0	2160.0	0.407	0.204	4.070

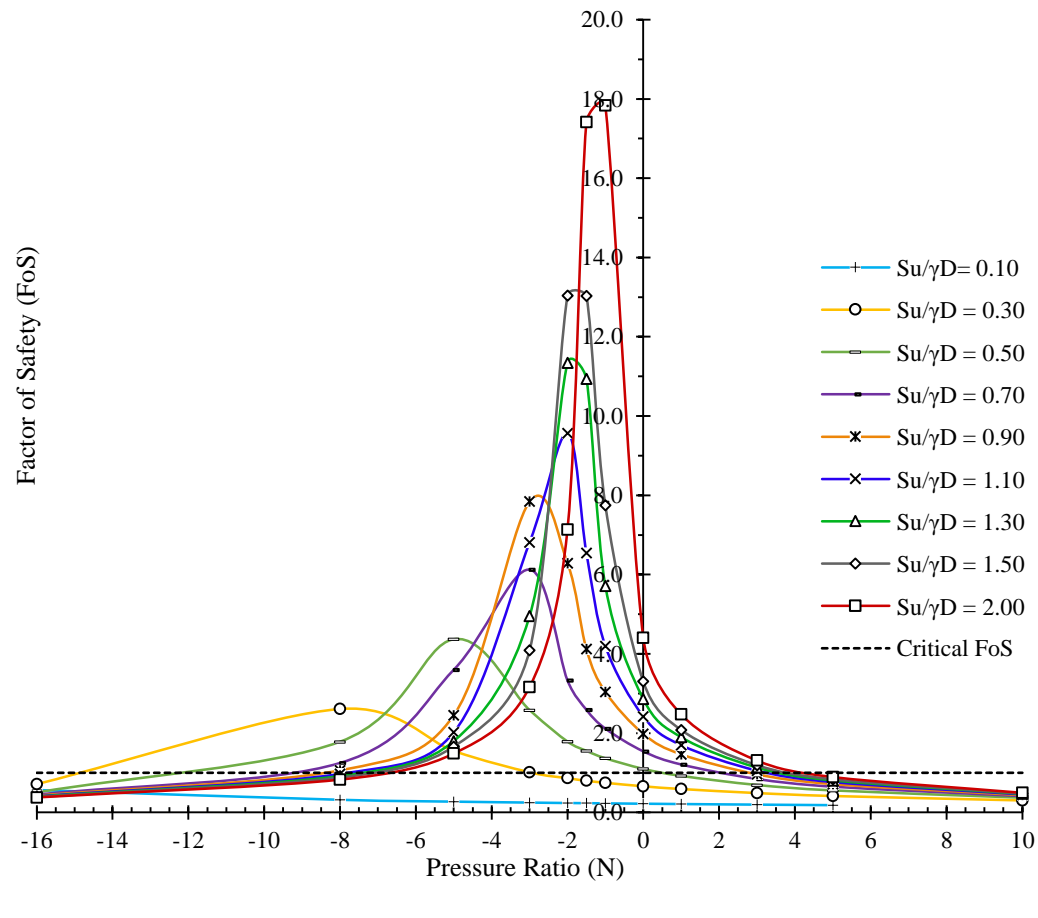


FoS, Critical Strength Ratios and Critical Pressure Ratios for Upper Bound SRM Results, DR = 2								
	Blue shading indicates blowout failure.							
Case	SR = ( $\gamma^*D$ )/ (Su) (1)	Su (kPa)	PR= ( $\sigma_s - \sigma_t$ )/ Su (2)	$\sigma_t$ (kPa) fix	$\sigma_s$ (kPa) fix	SRM UB FoS (3)	( $\gamma D$ )* (FoS)/ (Su) when FoS=1 (1)*(3)	PR <sub>c</sub> = ( $\sigma_s - \sigma_t$ )* (FoS)/(Su) when FoS=1 (2)*(3)
DR=2 SR=0.10	10.0	10.8	-16	172.8	0.0	0.566	5.660	-9.056
	10.0	10.8	-8	86.4	0.0	0.319	3.190	-2.552
	10.0	10.8	-5	54.0	0.0	0.273	2.730	-1.365
	10.0	10.8	-3	32.4	0.0	0.249	2.490	-0.747
	10.0	10.8	-2	21.6	0.0	0.238	2.380	-0.476
	10.0	10.8	-1.5	16.2	0.0	0.234	2.340	-0.351
	10.0	10.8	-1	10.8	0.0	0.229	2.290	-0.229
	10.0	10.8	0	0.0	0.0	0.220	2.200	0.000
	10.0	10.8	1	0.0	10.8	0.212	2.120	0.212
	10.0	10.8	3	0.0	32.4	0.197	1.970	0.591
DR=2 SR=0.30	3.33	32.4	-16	518.4	0.0	0.714	2.380	-11.424
	3.33	32.4	-8	259.2	0.0	2.610	8.700	-20.880
	3.33	32.4	-5	162.0	0.0	1.550	5.167	-7.750
	3.33	32.4	-3	97.2	0.0	1.014	3.380	-3.042
	3.33	32.4	-2	64.8	0.0	0.864	2.880	-1.728
	3.33	32.4	-1.5	48.6	0.0	0.799	2.663	-1.199
	3.33	32.4	-1	32.4	0.0	0.748	2.493	-0.748
	3.33	32.4	0	0.0	0.0	0.660	2.200	0.000
	3.33	32.4	1	0.0	32.4	0.591	1.970	0.591
	3.33	32.4	3	0.0	97.2	0.489	1.630	1.467
DR=2 SR=0.50	2.00	54.00	-16	864.0	0.0	0.504	1.008	-8.064
	2.00	54.00	-8	432.0	0.0	1.784	3.568	-14.272
	2.00	54.00	-5	270.0	0.0	4.369	8.738	-21.845
	2.00	54.00	-3	162.0	0.0	2.583	5.166	-7.749
	2.00	54.00	-2	108.0	0.0	1.789	3.578	-3.578
	2.00	54.00	-1.5	81.0	0.0	1.554	3.108	-2.331
	2.00	54.00	-1	54.0	0.0	1.366	2.732	-1.366
	2.00	54.00	0	0.0	0.0	1.100	2.200	0.000
	2.00	54.00	1	0.0	54.0	0.922	1.844	0.922
	2.00	54.00	3	0.0	162.0	0.693	1.386	2.079
2.00	54.00	5	0.0	270.0	0.556	1.112	2.780	
2.00	54.00	10	0.0	540.0	0.372	0.744	3.720	

DR=2 SR=0.70	1.43	75.60	-16	1209.6	0.0	0.448	0.640	-7.168
	1.43	75.60	-8	604.8	0.0	1.248	1.783	-9.984
	1.43	75.60	-5	378.0	0.0	3.599	5.141	-17.995
	1.43	75.60	-3	226.8	0.0	6.127	8.753	-18.381
	1.43	75.60	-2	151.2	0.0	3.330	4.757	-6.660
	1.43	75.60	-1.5	113.4	0.0	2.591	3.701	-3.887
	1.43	75.60	-1	75.6	0.0	2.115	3.021	-2.115
	1.43	75.60	0	0.0	0.0	1.541	2.201	0.000
	1.43	75.60	1	0.0	75.6	1.210	1.729	1.210
	1.43	75.60	3	0.0	226.8	0.845	1.207	2.535
1.43	75.60	5	0.0	378.0	0.650	0.929	3.250	
1.43	75.60	10	0.0	756.0	0.411	0.587	4.110	
DR=2 SR=0.90	1.11	97.20	-16	1555.2	0.0	0.423	0.470	-6.768
	1.11	97.20	-8	777.6	0.0	1.062	1.180	-8.496
	1.11	97.20	-5	486.0	0.0	2.451	2.723	-12.255
	1.11	97.20	-3	291.6	0.0	7.841	8.712	-23.523
	1.11	97.20	-2	194.4	0.0	6.288	6.987	-12.576
	1.11	97.20	-1.5	145.8	0.0	4.119	4.577	-6.179
	1.11	97.20	-1	97.2	0.0	3.039	3.377	-3.039
	1.11	97.20	0	0.0	0.0	1.982	2.202	0.000
	1.11	97.20	1	0.0	97.2	1.466	1.629	1.466
	1.11	97.20	3	0.0	291.6	0.961	1.068	2.883
1.11	97.20	5	0.0	486.0	0.715	0.794	3.575	
1.11	97.20	10	0.0	972.0	0.436	0.484	4.360	
DR=2 SR=1.10	0.91	118.80	-16	1900.8	0.0	0.406	0.369	-6.496
	0.91	118.80	-8	950.4	0.0	0.971	0.883	-7.768
	0.91	118.80	-5	594.0	0.0	2.021	1.837	-10.105
	0.91	118.80	-3	356.4	0.0	6.811	6.192	-20.433
	0.91	118.80	-2	237.6	0.0	9.564	8.695	-19.128
	0.91	118.80	-1.5	178.2	0.0	6.547	5.952	-9.821
	0.91	118.80	-1	118.8	0.0	4.196	3.815	-4.196
	0.91	118.80	0	0.0	0.0	2.422	2.202	0.000
	0.91	118.80	1	0.0	118.8	1.697	1.543	1.697
	0.91	118.80	3	0.0	356.4	1.055	0.959	3.165
0.91	118.80	5	0.0	594.0	0.766	0.696	3.830	
0.91	118.80	10	0.0	1188.0	0.455	0.414	4.550	
DR=2 SR=1.30	0.77	140.40	-16	2246.4	0.0	0.398	0.306	-6.368
	0.77	140.40	-8	1123.2	0.0	0.919	0.707	-7.352
	0.77	140.40	-5	702.0	0.0	1.800	1.385	-9.000
	0.77	140.40	-3	421.2	0.0	4.953	3.810	-14.859
	0.77	140.40	-2	280.8	0.0	11.341	8.724	-22.682
	0.77	140.40	-1.5	210.6	0.0	10.934	8.411	-16.401
	0.77	140.40	-1	140.4	0.0	5.712	4.394	-5.712
	0.77	140.40	0	0.0	0.0	2.862	2.202	0.000
	0.77	140.40	1	0.0	140.4	1.898	1.460	1.898
	0.77	140.40	3	0.0	421.2	1.132	0.871	3.396
0.77	140.40	5	0.0	702.0	0.807	0.621	4.035	
0.77	140.40	10	0.0	1404.0	0.469	0.361	4.690	

DR=2 SR=1.50	0.67	162.00	-16	2592.0	0.0	0.389	0.259	-6.224
	0.67	162.00	-8	1296.0	0.0	0.881	0.587	-7.048
	0.67	162.00	-5	810.0	0.0	1.663	1.109	-8.315
	0.67	162.00	-3	486.0	0.0	4.088	2.725	-12.264
	0.67	162.00	-2	324.0	0.0	13.034	8.689	-26.068
	0.67	162.00	-1.5	243.0	0.0	13.026	8.684	-19.539
	0.67	162.00	-1	162.0	0.0	7.746	5.164	-7.746
	0.67	162.00	0	0.0	0.0	3.303	2.202	0.000
	0.67	162.00	1	0.0	162.0	2.080	1.387	2.080
	0.67	162.00	3	0.0	486.0	1.193	0.795	3.579
	0.67	162.00	5	0.0	810.0	0.836	0.557	4.180
0.67	162.00	10	0.0	1620.0	0.477	0.318	4.770	
DR=2 SR=2.00	0.50	216.00	-16	3456.0	0.0	0.379	0.190	-6.064
	0.50	216.00	-8	1728.0	0.0	0.828	0.414	-6.624
	0.50	216.00	-5	1080.0	0.0	1.486	0.743	-7.430
	0.50	216.00	-3	648.0	0.0	3.164	1.582	-9.492
	0.50	216.00	-2	432.0	0.0	7.137	3.569	-14.274
	0.50	216.00	-1.5	324.0	0.0	17.415	8.708	-26.123
	0.50	216.00	-1	216.0	0.0	17.831	8.916	-17.831
	0.50	216.00	0	0.0	0.0	4.402	2.201	0.000
	0.50	216.00	1	0.0	216.0	2.472	1.236	2.472
	0.50	216.00	3	0.0	648.0	1.310	0.655	3.930
	0.50	216.00	5	0.0	1080.0	0.893	0.447	4.465
0.50	216.00	10	0.0	2160.0	0.495	0.248	4.950	

Factor of Safety variation with Pressure Ratio, DR = 2



FoS, Critical Strength Ratios and Critical Pressure Ratios for Upper Bound SRM Results, DR = 3								
Blue shading indicates blowout failure.								
Case	SR = ( $\gamma^*D$ )/ (Su) (1)	Su (kPa)	PR= ( $\sigma_s - \sigma_t$ )/ Su (2)	$\sigma_t$ (kPa) fix	$\sigma_s$ (kPa) fix	SRM UB FoS (3)	( $\gamma D$ )* (FoS)/ (Su) when FoS=1 (1)*(3)	PR <sub>c</sub> = ( $\sigma_s - \sigma_t$ )* (FoS)/(Su) when FoS=1 (2)*(3)
DR=3 SR=0.10	10.0	10.8	-16	172.8	0.0	0.325	3.250	-5.200
	10.0	10.8	-8	86.4	0.0	0.233	2.330	-1.864
	10.0	10.8	-5	54.0	0.0	0.210	2.100	-1.050
	10.0	10.8	-3	32.4	0.0	0.197	1.970	-0.591
	10.0	10.8	-2	21.6	0.0	0.191	1.910	-0.382
	10.0	10.8	-1.5	16.2	0.0	0.188	1.880	-0.282
	10.0	10.8	-1	10.8	0.0	0.185	1.850	-0.185
	10.0	10.8	0	0.0	0.0	0.180	1.800	0.000
	10.0	10.8	1	0.0	10.8	0.175	1.750	0.175
	10.0	10.8	3	0.0	32.4	0.166	1.660	0.498
	10.0	10.8	5	0.0	54.0	0.158	1.580	0.790
10.0	10.8	10	0.0	108.0	0.141	1.410	1.410	
DR=3 SR=0.30	3.33	32.4	-16	518.4	0.0	1.382	4.607	-22.112
	3.33	32.4	-8	259.2	0.0	1.612	5.373	-12.896
	3.33	32.4	-5	162.0	0.0	0.932	3.107	-4.660
	3.33	32.4	-3	97.2	0.0	0.724	2.413	-2.172
	3.33	32.4	-2	64.8	0.0	0.650	2.167	-1.300
	3.33	32.4	-1.5	48.6	0.0	0.618	2.060	-0.927
	3.33	32.4	-1	32.4	0.0	0.591	1.970	-0.591
	3.33	32.4	0	0.0	0.0	0.541	1.803	0.000
	3.33	32.4	1	0.0	32.4	0.500	1.667	0.500
	3.33	32.4	3	0.0	97.2	0.433	1.443	1.299
	3.33	32.4	5	0.0	162.0	0.380	1.267	1.900
3.33	32.4	10	0.0	324.0	0.292	0.973	2.920	
DR=3 SR=0.50	2.00	54.00	-16	864.0	0.0	0.704	1.408	-11.264
	2.00	54.00	-8	432.0	0.0	4.489	8.978	-35.912
	2.00	54.00	-5	270.0	0.0	2.925	5.850	-14.625
	2.00	54.00	-3	162.0	0.0	1.553	3.106	-4.659
	2.00	54.00	-2	108.0	0.0	1.252	2.504	-2.504
	2.00	54.00	-1.5	81.0	0.0	1.142	2.284	-1.713
	2.00	54.00	-1	54.0	0.0	1.050	2.100	-1.050
	2.00	54.00	0	0.0	0.0	0.902	1.804	0.000
	2.00	54.00	1	0.0	54.0	0.794	1.588	0.794
	2.00	54.00	3	0.0	162.0	0.633	1.266	1.899
	2.00	54.00	5	0.0	270.0	0.528	1.056	2.640
2.00	54.00	10	0.0	540.0	0.375	0.750	3.750	

DR=3 SR=0.70	1.43	75.60	-16	1209.6	0.0	0.577	0.824	-9.232
	1.43	75.60	-8	604.8	0.0	2.076	2.966	-16.608
	1.43	75.60	-5	378.0	0.0	6.140	8.771	-30.700
	1.43	75.60	-3	226.8	0.0	3.036	4.337	-9.108
	1.43	75.60	-2	151.2	0.0	2.076	2.966	-4.152
	1.43	75.60	-1.5	113.4	0.0	1.788	2.554	-2.682
	1.43	75.60	-1	75.6	0.0	1.571	2.244	-1.571
	1.43	75.60	0	0.0	0.0	1.263	1.804	0.000
	1.43	75.60	1	0.0	75.6	1.055	1.507	1.055
	1.43	75.60	3	0.0	226.8	0.792	1.131	2.376
	1.43	75.60	5	0.0	378.0	0.634	0.906	3.170
	1.43	75.60	10	0.0	756.0	0.424	0.606	4.240
DR=3 SR=0.90	1.11	97.20	-16	1555.2	0.0	0.525	0.583	-8.400
	1.11	97.20	-8	777.6	0.0	1.535	1.706	-12.280
	1.11	97.20	-5	486.0	0.0	5.250	5.833	-26.250
	1.11	97.20	-3	291.6	0.0	6.381	7.090	-19.143
	1.11	97.20	-2	194.4	0.0	3.258	3.620	-6.516
	1.11	97.20	-1.5	145.8	0.0	2.609	2.899	-3.914
	1.11	97.20	-1	97.2	0.0	2.173	2.414	-2.173
	1.11	97.20	0	0.0	0.0	1.624	1.804	0.000
	1.11	97.20	1	0.0	97.2	1.296	1.440	1.296
	1.11	97.20	3	0.0	291.6	0.919	1.021	2.757
	1.11	97.20	5	0.0	486.0	0.714	0.793	3.570
	1.11	97.20	10	0.0	972.0	0.458	0.509	4.580
DR=3 SR=1.10	0.91	118.80	-16	1900.8	0.0	0.496	0.451	-7.936
	0.91	118.80	-8	950.4	0.0	1.316	1.196	-10.528
	0.91	118.80	-5	594.0	0.0	3.412	3.102	-17.060
	0.91	118.80	-3	356.4	0.0	9.679	8.799	-29.037
	0.91	118.80	-2	237.6	0.0	5.095	4.632	-10.190
	0.91	118.80	-1.5	178.2	0.0	3.670	3.336	-5.505
	0.91	118.80	-1	118.8	0.0	2.865	2.605	-2.865
	0.91	118.80	0	0.0	0.0	1.984	1.804	0.000
	0.91	118.80	1	0.0	118.8	1.511	1.374	1.511
	0.91	118.80	3	0.0	356.4	1.027	0.934	3.081
	0.91	118.80	5	0.0	594.0	0.775	0.705	3.875
	0.91	118.80	10	0.0	1188.0	0.481	0.437	4.810
DR=3 SR=1.30	0.77	140.40	-16	2246.4	0.0	0.477	0.367	-7.632
	0.77	140.40	-8	1123.2	0.0	1.195	0.919	-9.560
	0.77	140.40	-5	702.0	0.0	2.729	2.099	-13.645
	0.77	140.40	-3	421.2	0.0	11.415	8.781	-34.245
	0.77	140.40	-2	280.8	0.0	8.322	6.402	-16.644
	0.77	140.40	-1.5	210.6	0.0	5.136	3.951	-7.704
	0.77	140.40	-1	140.4	0.0	3.685	2.835	-3.685
	0.77	140.40	0	0.0	0.0	2.345	1.804	0.000
	0.77	140.40	1	0.0	140.4	1.712	1.317	1.712
	0.77	140.40	3	0.0	421.2	1.115	0.858	3.345
	0.77	140.40	5	0.0	702.0	0.826	0.635	4.130
	0.77	140.40	10	0.0	1404.0	0.501	0.385	5.010

DR=3 SR=1.50	0.67	162.00	-16	2592.0	0.0	0.465	0.310	-7.440
	0.67	162.00	-8	1296.0	0.0	1.122	0.748	-8.976
	0.67	162.00	-5	810.0	0.0	2.367	1.578	-11.835
	0.67	162.00	-3	486.0	0.0	8.736	5.824	-26.208
	0.67	162.00	-2	324.0	0.0	13.221	8.814	-26.442
	0.67	162.00	-1.5	243.0	0.0	7.194	4.796	-10.791
	0.67	162.00	-1	162.0	0.0	4.653	3.102	-4.653
	0.67	162.00	0	0.0	0.0	2.708	1.805	0.000
	0.67	162.00	1	0.0	162.0	1.909	1.273	1.909
	0.67	162.00	3	0.0	486.0	1.189	0.793	3.567
	0.67	162.00	5	0.0	810.0	0.867	0.578	4.335
	0.67	162.00	10	0.0	1620.0	0.516	0.344	5.160
DR=3 SR=2.00	0.50	216.00	-16	3456.0	0.0	0.445	0.223	-7.120
	0.50	216.00	-8	1728.0	0.0	1.018	0.509	-8.144
	0.50	216.00	-5	1080.0	0.0	1.954	0.977	-9.770
	0.50	216.00	-3	648.0	0.0	5.014	2.507	-15.042
	0.50	216.00	-2	432.0	0.0	17.957	8.979	-35.914
	0.50	216.00	-1.5	324.0	0.0	17.506	8.753	-26.259
	0.50	216.00	-1	216.0	0.0	8.138	4.069	-8.138
	0.50	216.00	0	0.0	0.0	3.608	1.804	0.000
	0.50	216.00	1	0.0	216.0	2.302	1.151	2.302
	0.50	216.00	3	0.0	648.0	1.339	0.670	4.017
	0.50	216.00	5	0.0	1080.0	0.940	0.470	4.700
	0.50	216.00	10	0.0	2160.0	0.542	0.271	5.420

